[redacted]

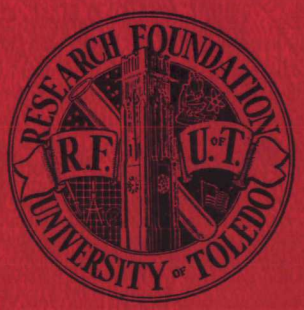

RESEARCH FOUNDATION
The University of Toledo
Toledo, Ohio 43606

DISCLAIMER

AJA

ORO-3822-5
R-6915-1200

INTERACTION BETWEEN SOIL AND NUCLEAR REACTOR FOUNDATIONS DURING EARTHQUAKES

June 10, 1970

Contract No. AT(40-1)-3822

J. Isenberg

Prepared for

THE RESEARCH FOUNDATION OF
THE UNIVERSITY OF TOLEDO
Toledo, Ohio

AGBABIAN-JACOBSEN ASSOCIATES
Los Angeles, California

SUMMARY

The present analysis is one part of a three-part study of the dynamic response of a nuclear reactor structural and surrounding soil that is subjected to earthquake motion. A previous part of the study by IIT Research Institute uses the finite element method to compute the response of a reactor structure whose foundation is on the ground surface. A parallel study of this problem using analytic or closed-form techniques has been performed by the University of Toledo. The present study also considers this problem, but its main subject is the more typical case of a reactor structure whose foundation is embedded below ground surface. The structure and soil are represented by an assembly of two-dimensional finite elements. In some examples, elastic properties are assumed for the soil, and in others, inelastic properties are assumed. The computer programs used to perform the analyses and the version of plasticity theory used to represent inelastic soil properties are described.

The study indicates that the horizontal response of the structure foundation, as measured either by its response spectrum or peak acceleration, is less than the corresponding response at the surface of the free field. The structural response appears to be suppressed by a greater amount if its natural frequencies are about the same as the dominant frequencies of the earthquake input. Suppression is also greater if the stiffness of the soil is decreased. The ratio of horizontal response spectra (foundation response/free field response) varies from about 0.2 to 1.0. A typical suppression ratio for elastic soils in the frequency range of 3 to 5 cps is 0.5, while for inelastic soils it is 0.3. The vertical response spectrum of the foundation is amplified by 1.0 to 1.5 relative to that of the free field at 1 to 3 cps and suppressed by 0.2 to 1.0 at 3 to 8 cps. The scope of the study is too limited, however, to draw broad conclusions on the amount of suppression over a wide range of soils, types of structures, and earthquake motions.

Stresses in the soil adjacent to the structure differ from the stress which would have occurred at the same point in the free field. The horizontal stress beneath the foundation is considerably less than the corresponding free field stress. Also, the stress in the soil adjacent to the structure appears to be uniquely related to the velocity of the structure; however, a quantitative relationship is not established.

Finally, an attempt is made to correlate the translational and rotational response spectra of the foundation to the peak acceleration of the single-degree-of-freedom oscillators representing the containment and internal support structures. Since the peak accelerations of the oscillators are less than the sum of the two response spectra at the appropriate frequencies, it is concluded that rocking and translation are out of phase with each other, and their response spectra should not be superposed.

CONTENTS

CONTENTS (CONTINUED)

ILLUSTRATIONS

ILLUSTRATIONS (CONTINUED)

ILLUSTRATIONS (CONTINUED)

ILLUSTRATIONS (CONTINUED)

TABLES

SECTION 1

INTRODUCTION

This is a theoretical study of the dynamic response of a nuclear reactor power structure subjected to earthquake motions. Dynamic response of the structure is defined here primarily as the motion and frequency response spectra of its foundation. A main purpose of the study is to compare the response of the foundation surrounded by soil with that of the same soil alone when it is subjected to the same earthquake.

Interaction between soil and structure is postulated to influence the response of the structure relative to the response of the free field. The effects of interaction appear as motion of the structure and stresses in the adjacent soil, which differ from motions and stresses at the same points in the free field. Several factors that are presently considered to influence interaction between soil and a partially embedded structure are:

a. Stiffness and strength of soil

b. Presence of two different soils in horizontal layers

c. Frequency content of earthquake input

d. Natural frequencies of structure and its contents

Of several candidate methods of analysis for the present study, the finite element method seems most suitable. The geometry of the embedded structure can be represented by a two-dimensional, plane-strain section. All contributions to interaction, from nearly rigid body response of the foundation to wave effects in the soil, are included.

Since the goal of the present study is insight into interaction, the results of the analysis are frequently presented in the form of a comparison between structural and free-field responses. For example, the

frequency spectra of structural responses are compared with those of the free field to determine whether the presence of a structure suppresses free field spectra locally. By comparing stress in the soil adjacent to the structure with the stress at the same depth when the structure is absent, the influence of the structure on stress in the soil can be examined to see whether the structure tends to promote or retard failure in the adjacent soil. Since this is primarily a study of interaction, the details of superstructure and equipment response are given little attention here. However, an attempt is made below to relate the translation and rotation of the foundation to the translation of elevated parts of the structure where, in an actual structure, equipment might be attached.

It is inevitable that in a limited study such as this some important topics are slighted or omitted altogether. Among these is the question of how best to represent properties of soils. Part of the present analysis represents the soil as being linearly elastic while another part represents it as being elastic/perfectly-plastic. These crude representations are considered to be adequate to show the trends in the response of structures relative to free field. A second important topic which is not investigated is the most representative way to apply earthquake loading to a structure embedded in soil. The present method is to define a region of soil surrounding the structure and to apply uniform earthquake input along one side. This method differs from the commonly used one of shaking the bottom of the soil/structure system to simulate bedrock motions. The reason for choosing the less orthodox method is that it makes best use of available techniques to prevent spurious reflections from artificial boundaries of the finite element grid. The present definition of boundary conditions, like the choice of soil properties, is considered to show trends. Within limits imposed by these assumptions and others discussed below, the present analysis appears to represent correctly interaction between soil and structure.

SECTION 2

PREVIOUS WORK

This section describes briefly some previous studies in the area of soil/structure interaction under earthquake loading. The purpose of the section is to point out a gap in previous work and to identify analytic methods which are available to the present study in trying to fill the gap. For a more complete bibliography (51 references) and review of the literature up to 1968, the reader is directed to References 1 and 2.

The previous work which contributes directly to the present study may be divided into three catagories. The first catagory deals with the analysis of several kinds of structures subjected to earthquake loading. These studies, which are carried out by a variety of analytic techniques, help to identify what is important in analyzing earthquake response of structures. One example is by Housner (Reference 3), in which the behavior of buildings during earthquakes is described by response spectra which show the effect of size and distance of the earthquake and the period and damping of the structure. The analyses are based on lumped-mass and stiffness models of structures whose bases are subjected to motions measured in the basements of actual buildings during earthquakes. In this way the effect of interaction on the base motion of the structure is taken into account, thus allowing upper stories to be analyzed. The article also suggests the idea, which is used in the present analysis, that the area under a response spectrum curve is a measure of the intensity of an earthquake.

In designing a new building or analyzing an existing one where the basement response to earthquake shaking of the surrounding soil is not known, a possible second approach is to apply a known earthquake record to the base of the building. This implies that the foundation medium is rigid, and has been done by several authors for buildings (References 4 and 5) and for earth banks and dams (References 6 and 7). These reports are

useful for theoretical insight into the motions of buildings and stress levels in soil structures. Reference 7 also points out the need to take into account static overburden stresses when analyzing the inelastic response of soils.

A question arising from these analyses is whether taking into account the flexibility of the foundation medium would significantly change the results. In a third type of analysis, Parmelee, et al., (Reference 8) addressed this question by utilizing Bycroft's solution for translation and rotation of a rigid plate on the surface of an infinite half space and subjected to harmonic exciting forces and moments. The results of analyzing single- and multi-story buildings sitting on top of the plate indicate that when the soil medium becomes sufficiently soft or flexible relative to the structure, there is significant interaction. If the soil is relatively stiff (defined in Reference 8 as $C_s \geq 1000$ fps for the example given there), a rigid base analysis would be satisfactory. Scavuzzo, et al., (Reference 9) obtained a solution to the problem of a two-dimensional elastic-half space subjected to a time-dependent uniform shearing stress representing inertia loading by a surface structure. The structure is represented by a large base mass and several single-degree-of-freedom oscillators representing equipment attached to the base. The results show that interaction depends strongly on soil stiffness and on the relationship between frequency of the seismic motion and that of the structure. The magnitude of interaction effects appears large enough to be considered in seismic design of nuclear power plants.

The work of Reference 9 is the starting point of the present study. The finite element method is used here because of its ability to represent embedded structures and inelastic soil properties. The application of the finite element method to problems of earthquake response is illustrated in references cited above. The finite element formulation and computer program for the elastic calculations are due, with modifications described below, to Wilson (Reference 10). The inelastic finite element

computer program was written by making appropriate changes to the program in Reference 10. The model of inelastic soil properties is based on the mathematical theory of plasticity as described in References 11 and 12.

A major difficulty in applying the finite element technique to the present problem is prescribing adequate boundary conditions for the edges of the finite element grid. One of these edges (top) is treated as a free surface which accurately represents the ground surface. The remaining edges of the grid do not correspond to physical boundaries. Inappropriate treatment of these boundaries may distort the solution in the vicinity of the structure. One way to approach this problem is to move the boundaries a considerable distance from the structure (Reference 13). An alternative approach is to regard the motions adjacent to artificial boundaries as being associated with waves which may be reflected back toward the structure. A procedure for absorbing such waves at artificial boundaries using damping has been proposed (Reference 14). The procedure adopted in the present work takes the wave propagation point of view, but uses an alternative to the damping method of Reference 14 to prevent unwanted reflections.

SECTION 3

ANALYTIC METHOD

The main technique of analysis used in the present study is the finite element method adapted to dynamic loading under plane strain conditions. Both linear elastic and inelastic representations of the soil are used. It is inconvenient to write a single computer program to perform both types of computations. Hence, a very efficient computer program capable of representing only elastic materials is used whenever possible in the study, and a second program capable of representing both elastic and inelastic properties is used in the remainder. The purpose of this section is to describe the main features of the two computer programs.

ELASTIC FINITE ELEMENT PROGRAM

An elastic finite element computer program due to Wilson (Reference 10) is used for calculations where both soil and structure are linearly elastic. The force equilibrium equations for the linear elastic finite element system are expressed by the following matrix equations:

$$[M]\{\ddot{u}_t\} + [C]\{\dot{u}_t\} + [K]\{\ddot{u}_t\} = \{P_t\} \qquad (3\text{-}1)$$

where

$\{\ddot{u}_t\}, \{\dot{u}_t\}, \{u_t\}$ = Nodal point displacements, velocities and accelerations at time t

P_t = Nodal point forces at time t

$[M], [C], [K]$ = Global mass, damping and stiffness matrices

The stiffness matrix [K] used in Equation 3-1 is formed only once during the calculation. The type of element used is a quadrilateral composed of two triangular elements. Within each triangular element,

Figure 3-1, the assumed displacement field forces a linear and compatible variation of displacements along sides 1-2, 2-3, 3-4, and 4-1. The displacements along line 1-5-3 vary parabolically; compatibility is maintained since each of these points is forced to have the same displacement as the corresponding points of the second triangle. Each of the five nodal points has two degrees of freedom, making a total of ten for the quadrilateral element and leading to a 10 x 10 element stiffness matrix. The unknown displacements associated with point 5 are then expressed in terms of those at points 1 through 4, and eliminated from the system. The remaining 8 x 8 element stiffness matrices are combined by direct stiffness procedures to form the global stiffness matrix [K]. The program also includes constant strain triangles and bar elements. These may be attached to the corner points of the quadrilaterals or to each other.

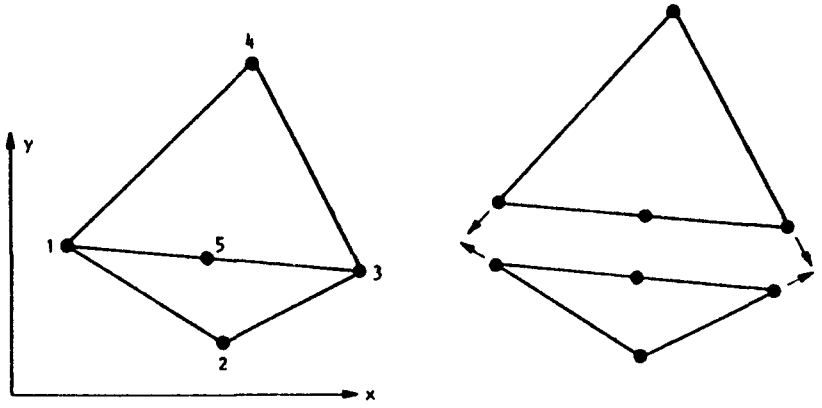

FIGURE 3-1. LINEAR STRAIN QUADRILATERAL ELEMENT (WILSON, REFERENCE 10)

The global mass matrix [M] is based on a lumped mass approximation in which one-fourth of the mass of each quadrilateral (one-third of each constant strain triangle and one-half of each bar element) is assumed to be concentrated at the corner points. This leads to a diagonal mass matrix.

Wilson's program has available a form of viscous damping in which the damping matrix [C] is proportional to [M] and [K]. For reasons explained in Section 4, damping is not used in this study.

A step-by-step procedure developed by Wilson is used to integrate Equation 3-1. It is assumed that the acceleration varies linearly over the interval $2\Delta t$, where Δt is the integration time step. Then, from the previous solution at $t - \Delta t$ and the new solution at the end of the increment $2\Delta t$, $t + \Delta t$, the desired displacement, velocity and acceleration at t are found by interpolation. This technique is remarkably stable, and relaxes the restriction imposed by many other techniques that Δt must be less than the least transit time of a compression wave across any element in the assemblage. This results in considerable economy by permitting Δt to be greater than other integration techniques would allow. There is some numerical damping associated with this technique which, though uncontrollable, does not appear harmful in the present calculation.

Two important features have been added to the computer program given in Reference 10. One is a kinematic boundary condition in which the input may be prescribed as a velocity/time history at selected nodal points. This feature is used to apply earthquake input to one edge of the finite element assemblage. The method consists of constructing an effective load vector from the prescribed motion and stiffness properties of the assemblage, and then solving the system of equations in the usual way. Details of the technique are described in Appendix A.

The second feature which has been added is called a "quiet boundary" technique. In the present calculations, the earthquake motions are propagated as waves throughout the assemblage. Eventually they encounter artificial boundaries from which, if no steps were taken to prevent it, they would be reflected back toward the structure and other points of engineering interest. These reflected waves would distort the calculated response of the structure. In some studies it is possible to make the finite element grid so large that reflections do not reach the structure during the time

of interest. In the present case, this is impractical because the duration of the loading is long and the distance over which unwanted reflections can propagate is very great.

A quiet boundary technique has been incorporated into the program for the purpose of reducing unwanted reflections from boundaries to negligible amplitudes. The underlying idea is to compute the motion which a nodal point on the boundary of the finite element grid would have if there were no boundary--that is, the motion which the same point would have in an infinite continuum--and to force the point to have that velocity. Some readers may find it easier to conceive of this as anticipating a reflection and cancelling it as it occurs by superposing a signal of equal magnitude and opposite sign. The technique is exact for one-dimensional wave propagation, and has given satisfactory results in the type of two-dimensional calculations performed in the present study. The method is described in Appendix B.

INELASTIC FINITE ELEMENT PROGRAM

The inelastic finite element formulation is adapted from Wilson's elastic formulation. The adaptations include:

a. Replacing elastic stress/strain properties by elastic/perfectly-plastic relations for use in formulating the stiffness matrix and in expressing the strain/displacement relation for calculating stresses.

b. Replacing the integration technique which incorporates interpolation by a straightforward one-step linear acceleration technique.

The subjects of this section are the definition of inelastic material properties in the program, incorporation of these properties into the stiffness matrix and formulation of the integration procedure together with some of its implications.

MATERIAL PROPERTY REPRESENTATION

The present definition of inelastic material properties is based in part on flow or incremental theories of plasticity in which the strain increments $(d\varepsilon_{ij})$ may be expressed in terms of the current stresses (σ_{ij}) and the stress increments $(d\sigma_{ij})$. The superiority of incremental theories over deformation or total strain formulations appears to be established (Reference 11) and the latter were not seriously considered for the present purpose.

The flow theory of plasticity incorporates a yield criterion which is convex with respect to the origin in stress space and a rule of plastic flow by which the plastic part of the strain increment is related to the stress and stress increment (References 15 and 16). The yield criterion for an isotropic material whose properties are insensitive to temperature and strain rate may be expressed in terms of stress increments

$$f(J_1, J_2, J_3) = 0 \qquad (3\text{-}2)$$

where J_1, J_2, J_3 = invarients of the stress tensor. Equation 3-2 represents the yield criterion for an ideally plastic material since the criterion is a permanent property of the material and does not change with loading history. Work hardening and strain hardening extensions to flow theories are available (References 11 and 17) but are not incorporated into the present work.

The objective of the following derivation is an incremental stress/strain relation for an elastic-plastic material undergoing small strains and small displacements. The starting point is Hooke's law for small strains.

$$d\sigma_{ij} = \lambda\left(de^{e}_{kk}\right)\left(\delta_{ij}\right) + 2G\left(de^{e}_{ij}\right) \qquad (3\text{-}3)$$

where

λ = Lame's parameter $B - \frac{2}{3} G$

B, G = Bulk modulus, shear modulus

δ_{ij} = Kronecker delta (= 1 if $i = j$, = 0 if $i \neq j$)

If the state of stress

$$\left(\sigma_{ij}\right)_{new} = \left(\sigma_{ij}\right)_{old} + d\sigma_{ij} \tag{3-4}$$

does not satisfy the yield criterion

$$f < 0 \tag{3-5}$$

Equation 3-3 correctly gives the stress increment. If the new state of stress, considered as a trial state, exceeds the yield criterion

$$f \geq 0 \tag{3-6}$$

further computations are necessary.

Defining the elastic strain increment as the difference between the plastic strain increment, de^P_{ij}, and the total strain increment, de_{ij}, a definition which is meaningful for small strain (Reference 18), Equation 3-3 may be rewritten as follows:

$$d\sigma_{ij} = \lambda\left(de_{kk} - de^P_{kk}\right) \delta_{ij} + 2G \left(de_{ij} - de^P_{ij}\right) \tag{3-7}$$

Regarding the yield function f in Equation 3-2 as a potential function and expressing the plastic strain increment as follows

$$de^P_{ij} = \Lambda \frac{\partial f}{\partial \sigma_{ij}} \tag{3-8}$$

insures uniqueness (Reference 19) and is called a plastic potential flow rule.

From the assumption of no work or strain hardening, it follows that there is no change in the yield function during plastic flow. A statement of this is

$$d\left(f(\sigma_{ij})\right) = 0 \tag{3-9a}$$

or

$$\frac{\partial f}{\partial \sigma_{ij}} d\sigma_{ij} \equiv f_{ij}\, d\sigma_{ij} = 0 \tag{3-9b}$$

Substituting Equation 3-7 into Equation 3-9b and making use of Equation 3-8 leads to the following expression

$$\lambda\left(de_{kk} - \Lambda f_{kk}\right)\delta_{ij} f_{ij} + 2G\left(de_{ij} - \Lambda f_{ij}\right) f_{ij} = 0 \tag{3-10}$$

Equation 3-10 may be solved for the scalar quantity Λ

$$\Lambda = \frac{\lambda de_{kk}\, f_{\ell\ell} + 2G(de_{ij})(f_{ij})}{\lambda f_{kk}\, f_{\ell\ell} + 2G\, f_{ij}\, f_{ij}} \tag{3-11}$$

Making use of Equation 3-11 in Equation 3-8 and substituting the result into Equation 3-7, the stress increment is expressed explicitly in terms of the total strain increment and the total stresses. This is the desired result.

The remaining task is to express the relationship between $\{d\sigma_{ij}\}$ and $\{de_{ij}\}$ as a matrix of coefficients $[C]$ such that

$$\{d\sigma\} = [C]\,\{de\} \tag{3-12}$$

where for the plane strain case

$$\{d\sigma\} = < d\sigma_{xx} \; d\sigma_{yy} \; d\sigma_{zz} \; d\sigma_{xy} >^T$$

$$\{de\} \quad < de_{xx} \; de_{yy} \; de_{zz} \; d\sigma_{xy} >^T$$

The engineering definition of shear strain is used.

$$d\gamma_{xy} = \frac{\partial U_x}{\partial y} + \frac{\partial U_y}{\partial x}$$

where U_x and U_y are displacements in x and y directions, respectively.

[C] is given in the following table.

$$C = \begin{bmatrix} \lambda + 2G - \dfrac{\lambda F + 2Gf_x}{\lambda F^2 + 2Gx} & \lambda - \dfrac{(\lambda F + 2Gf_y)(\lambda F + 2Gf_x)}{\lambda F^2 + 2Gx} & \lambda - \dfrac{(\lambda F + 2Gf_z)(\lambda F + 2Gf_x)}{\lambda F^2 + 2Gx} & -2Gf_{xy}\dfrac{\lambda F + 2Gf_x}{\lambda F^2 + 2Gx} \\ & \lambda + 2G - \dfrac{(\lambda F + 2Gf_y)^2}{\lambda F^2 + 2Gx} & \lambda - \dfrac{(\lambda F + 2Gf_y)(\lambda F + 2Gf_z)}{\lambda F^2 + 2Gx} & -2Gf_{xy}\dfrac{\lambda F + 2Gf_y}{\lambda F^2 + 2Gx} \\ \text{Symmetrical} & & \lambda + 2G - \dfrac{(\lambda F + 2Gf_z)^2}{\lambda F^2 + 2Gx} & -2Gf_{xy}\dfrac{\lambda F + 2Gf_z}{\lambda F^2 + 2Gx} \\ & & & G - \dfrac{4G^2 f_{xy}^2}{LF^2 + 2Gx} \end{bmatrix}$$

where

$$F = f_x + f_y + f_z$$

$$x = f_x^2 + f_y^2 + f_z^2 + 2f_{xy}^2$$

f_x, etc. = Derivatives of the yield function f with respect to stress components (plastic potential flow rule). Subscripts x, y and z indicate differentiation with respect to x, y and z components of stress while subscript xy indicates differentiation with respect to shear stress.

ELEMENT STIFFNESS MATRIX

The following derivation shows that the procedure for evaluating an inelastic element stiffness matrix is the same as for an elastic stiffness matrix if the linear stress/strain relations for the elastic material are replaced by the local tangents to the stress/strain curves. The local tangents are represented by [C], Equation 3-12.

The equations for the inelastic element stiffness matrix are derived by equating the increment in complementary strain energy to the amount of complementary work done by external loads acting through virtual displacements.

$$\int_{Vol} < e > \{d\sigma\} dV = < u > \{dp\} \qquad (3\text{-}13)$$

where

$< e >$ = Element strain

$\{d\sigma\}$ = Element stress increment

$< u >$ = Virtual displacement on surface

$\{dp\}$ = Increment of external load

Expressing the strain by

$$\{e\} = [A] \{u\}$$

and

$$\{de\} = [A]\{du\}$$

and the stress increment by

$$\{d\sigma\} = [C]\{de\}$$

Equation 3-12 may be rewritten as

$$< u > \int_{Vol} [A]^T [C] [A] \, dV \{du\} = < u > \{dp\} \qquad (3\text{-}14)$$

The expression

$$\left(\int_{Vol} [A]^T [C] [A] \, dV \right) \{du\} = \{dp\} \qquad (3\text{-}15)$$

is a statement of equilibrium in which the integral represents the stiffness matrix. It is the same as the expression for an elastic finite element with the understanding that [C] is the tangent stress/strain relation. As a result, the element stiffness formulation in the elastic computer program can be used merely by replacing the original elastic stress/strain relations by [C] on p. 14.

The element stiffness matrices are reformed at every time step using a condensed (3x3) form of [C], in which the third row and column, corresponding to direct stresses and strains in the direction of zero strain, are eliminated. The full [C] matrix is required for the computation of stresses, however. At every time step for every element a test is made to determine whether the element is elastic or inelastic. If it is elastic, elastic coefficients are used in the [C] matrix; if it is plastic, the elastic-plastic coefficients are used. The appropriate coefficients are substituted into the expressions for deriving the element stiffness matrix in Reference 10).

In the present work, the yield criterion is assumed to be of the form

$$f = \sqrt{J_2'} - \alpha J_1 - C \qquad (3\text{-}16)$$

where

J_2' = Second invariant of stress deviator

$= \frac{1}{2}\left(\sigma_{ij} - \frac{1}{3}\delta_{ij}\sigma_{kk}\right)^2$

J_1 = First stress invariant

$= \sigma_{kk}$

α = A parameter, to be determined experimentally, which governs the dependence of shear strength on confining pressure. Similar to angle of internal friction.

C = An experimental parameter. Similar to cohesion.

Equation 3-16 is applied such that

$f < 0$ deformation is elastic

$f = 0$ deformation is inelastic

States of stress for which

$f > 0$

are not permitted.

INTEGRATION TECHNIQUE

A step-by-step method is used to integrate the following incremental equation of motion.

$$[M]\{\delta\ddot{u}_t\} + [C]\{\delta\dot{u}_t\} + [K]\{\delta u_t\} = \{\delta P_t\} \qquad (3\text{-}17)$$

where the subscript t on an incremental quantity indicates the change from $t - \Delta t$ to t. The acceleration is assumed to vary linearly during the time step Δt. Integrating directly from $t - \Delta t$ to t the acceleration, velocity and displacement at t may be expressed in terms of known quantities at $t - \Delta t$ and unknown displacement and acceleration at t, u_t and $\ddot{u}_t$.

$$\ddot{u}_t = \frac{6\,u_t}{\Delta t^2} - \frac{6\,u_{t-\Delta t}}{\Delta t^2} - \frac{6\,\dot{u}_{t-\Delta t}}{\Delta t} - 2\,\ddot{u}_{t-\Delta t} \tag{3-18}$$

$$\dot{u}_t = \dot{u}_{t-\Delta t} + \ddot{u}_{t-\Delta t}\Delta t + \frac{\ddot{u}_t - \ddot{u}_{t-\Delta t}}{2}\Delta t \tag{3-19}$$

$$u_t = u_{t-\Delta t} + \dot{u}_{t-\Delta t}\Delta t + \frac{\ddot{u}_t - \ddot{u}_{t-\Delta t}}{6}(\Delta t)^2 + \frac{\ddot{u}_{t-\Delta t}(\Delta t)^2}{2} \tag{3-20}$$

The incremental velocity and acceleration may be expressed in terms of the incremental displacement as follows:

$$\delta\ddot{u}_t = \frac{6\,\delta u_t}{\Delta t^2} - \frac{6\,\dot{u}_{t-\Delta t}}{\Delta t} - 3\,\ddot{u}_{t-\Delta t} \tag{3-21}$$

$$\delta\dot{u}_t = \frac{3\,\delta u_t}{\Delta t} - 3\,\dot{u}_{t-\Delta t} - \frac{\ddot{u}_{t-\Delta t}}{2}\Delta t \tag{3-22}$$

When Equations 3-21 and 3-22 are substituted into Equation 3-15, a reduced equation of motion may be written.

$$[\bar{K}]\,\{\delta u_t\} = \{\bar{\delta P}\} \tag{3-23}$$

where

$$[\bar{K}] = \frac{6}{\Delta t^2}[M] + \frac{3}{\Delta t}[C] + [K]$$

$$\{\bar{\delta P}\} = [M]\{A_{t-\Delta t}\} + [C]\{B_{t-\Delta t}\} + \{\delta P\}$$

$$A_{t-\Delta t} = \frac{6\,\dot{u}_{t-\Delta t}}{\Delta t} + 3\,\ddot{u}_{t-\Delta t}$$

$$B_{t-\Delta t} = 3\,\dot{u}_{t-\Delta t} + 0.5\,(\ddot{u}_{t-\Delta t})\Delta t$$

The damping matrix [C] is assumed to be of the form

$$[C] = \xi[M] + \zeta[K] \qquad (3\text{-}24)$$

where

ξ, ζ = Damping coefficients

Substitution of Equation 3-24 into Equation 3-21 allows computation of the incremental displacements, from which the incremental velocities and acceleration may be obtained. The new total displacement, velocity and acceleration is obtained by adding the incremental values to the previous total values.

This integration procedure is stable and convergent so long as Δt is small in comparison with the natural periods of the system. An investigation which is reported in Appendix C indicates that satisfactory results will be obtained so long as Δt is less than the p-wave transit time across an element. This is a much more stringent requirement than that imposed by the integration technique of Reference 10, which is incorporated into the elastic version of the program.

DEMONSTRATION

Several example problems for which exact or approximate closed-form solutions are available were solved to demonstrate that the inelastic finite element computer program is working properly. The problems used are as follows:

a. Plane, one-dimensional wave propagation in an elastic rod.

b. Plane, one-dimensional wave propagation in an elastic-plastic rod.

c. Superseismic air-blast (pressure) waving at constant speed over the surface of air elastic half-space. Reference 20.

d. Cylindrical wave propagation in an elastic-plastic medium.

The solutions to these problems, which are given in Appendix D, illustrate that the present program approaches the correct answers.

SECTION 4

SOIL/STRUCTURE INTERACTION STUDIES

This section summarizes the soil/structure interaction calculations in terms of the following parameters:

a. Finite element representations of free field and of various structures surrounded by soil

b. Soil properties

c. Input and boundary conditions

The present studies of interaction are summarized in Table 4-1. Other studies performed under the present contract, which demonstrate the validity of analysis techniques, are mentioned in Appendices.

Three different types of analyses are made. The first (Case 1) is a finite element analog of a highly-simplified, closed-form analysis by Scavuzzo (Reference 21) which represents the structure by a cantilever and the soil medium by a narrow strip of material which supports the cantilever. The second (Case 2) considers a slab (the reactor foundation) which supports transverse oscillators (superstructure and equipment) and which rests on the surface of a linearly elastic soil. These two analyses are idealized to an unnecessary extent, and are performed only to compare with previous work (References 9, 21, and 22). The third type of analysis (Cases 3 through 6, I-1 and I-3), which is the major part of the present study, considers a reactor-type structure embedded in the ground with transverse oscillators representing superstructure and equipment. Both elastic and inelastic properties are assumed for the soil.

In Cases 3 through 6 and I-1 through I-3, soil properties and input motions are parameters which are varied one at a time so that the effect on interaction of changing them may be studied. Case 3 differs from Case 6 only in the dominant frequency content of input motion, which is

TABLE 4-1. SUMMARY OF INTERACTION STUDIES

Case	Type of Structure	Input	Soil Properties
1	Cantilever	Harmonic (1 cps)	Homogeneous elastic C_p = 10,750 fps C_s = 5,375 fps
2	Surface reactor	Harmonic (5 cps)	Homogeneous elastic C_p = 1,400 fps C_s = 800 fps
3	Embedded reactor	Golden Gate S80E (0-4 sec)	Homogeneous elastic C_p = 1,510 fps C_s = 875 fps
4	Embedded reactor	Golden Gate S80E (0-4 sec)	Layered elastic C_p = 1,510 fps C_s = 875 fps (surface to 45 ft) C_p = 2,500 fps C_s = 1,440 fps (below 45 ft)
5	Embedded reactor	Golden Gate S80E (0-4 sec)	Homogeneous elastic C_p = 2,500 fps C_s = 1,440 fps
6	Embedded reactor	0.2 x Olympia N10W (7-11 sec)	Homogeneous elastic C_p = 1,510 fps C_s = 875 fps
1-1	Embedded reactor	3 x Golden Gate S80E (0-3 sec)	Homogeneous (except for overburden, which increases with depth); elastic-plastic; same elastic properties as Case 3.
1-2	Embedded reactor	2 x Olympia N10W (7-10 sec)	Same as Case 1-1
1-3	Embedded reactor	3 x Golden Gate S80E (0-3 sec)	Same as Case 1-1 until t = 0.5 sec, when shear strength is abruptly reduced by a factor of 12.

2.5 to 5 cps in Case 3 and 1 to 2 cps in Case 6. Case 3 differs from Case 5 only in soil stiffness, which is greater in Case 5 than in Case 3. The effect of a soft soil overlying a stiffer one may be studied by comparing Case 4 with the uniform sites of Cases 3 and 5. The effect of allowing plastic deformation to occur during a high-frequency earthquake may be studied by comparing Case 3 with Case 1-1. The effect of allowing plastic deformation to occur during a lower-frequency earthquake may be studied by comparing Case 6 with Case 1-2.* The effect of an abrupt decrease in shear strength, such as might occur during liquefaction of the soil, may be studied by comparing Case 1-1 with Case 1-3. These studies cover a range of possible soil properties and input motions within which significant interaction effects seem to occur. Further study is required to define interaction effects under conditions outside this range.

The method of input and boundary conditions follow from the present assumption that earthquake loading may be regarded as a train of waves which propagate through soil and engulf a structure. The input is applied as horizontal velocity to one edge of the mesh and the waves which encounter other artificial boundaries of the finite element mesh are transmitted through the boundary by the quiet boundary procedure described in Section 3.

---

*Before comparing results, output from Case 3 (elastic soil) is multiplied by a factor of 3.0 and that from Case 6 (elastic soil) by a factor of 2.0 to account for difference in input intensity between Cases 3 and 6 and their companion Cases 1-1 and 1-2.

MODELS OF FREE-FIELD AND SOIL/STRUCTURE INTERACTION

The finite element representation of Case 1 in which the cantilever structure is embedded in a strip of soil (Reference 21) is shown in Figure 4-1. The properties of the structure and soil correspond to $\alpha = 2$ in the analysis of Reference 21. Input and quiet boundary points are indicated in the figure.

The representation for Case 2 is adapted from design drawings of a possible nuclear reactor structure, in which the three main elements are the circular foundation slab, the containment structure and the internal support structure. A simplified view of the three-dimensional structure and its present two-dimensional representation are shown in Figure 4-2. To obtain the two-dimensional model, the circular mat is first represented as an equivalent rectangular slab of the same area.

$$\pi R^2 = \text{Length x width of equivalent slab}$$

Defining the length of the rectangular slab to be the same as the diameter $2R$ of the circular slab, the width of the rectangular slab is

$$\frac{\pi R}{2} \cong 110 \text{ ft}$$

To obtain a representative slice of the structure suitable for plane strain analysis, the masses of the foundation, containment structure, and internal support structure are reduced by an appropriate factor. In the present analysis, this is assumed to be $\frac{1}{110 \times 12}$ for a 1-in.-thick slice. This is illustrated in Figure 4-2. For computational economy and to try to take into account the fact that 140 ft is too large to be a representative length for an equivalent rectangle, the plane strain model in the present analysis has a length of only 120 ft.

	Element No.	ν	E, psi	ρ (lb-sec^2/in.^{4})	C_p, fps	C_s, fps
Foundation	1-10, 18-22	0	41,600	0.000025	10,750	5,375
Structure	12-17	0	416,000	0.000025	--	--
Concentrated Mass			4,160,000	0.008625	--	--

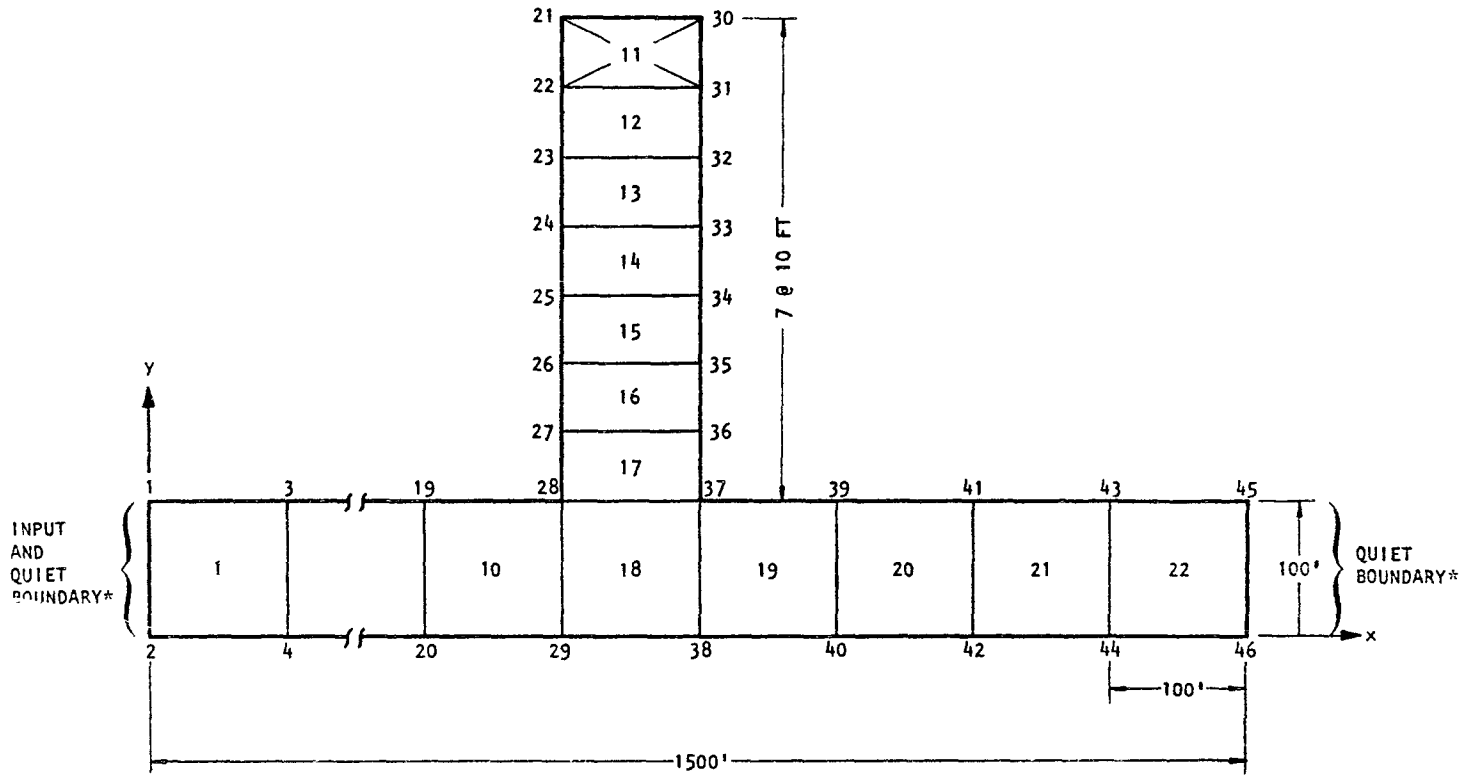

FIGURE 4-1. FINITE ELEMENT GRID (WITH STRUCTURE) USED IN CASE 1

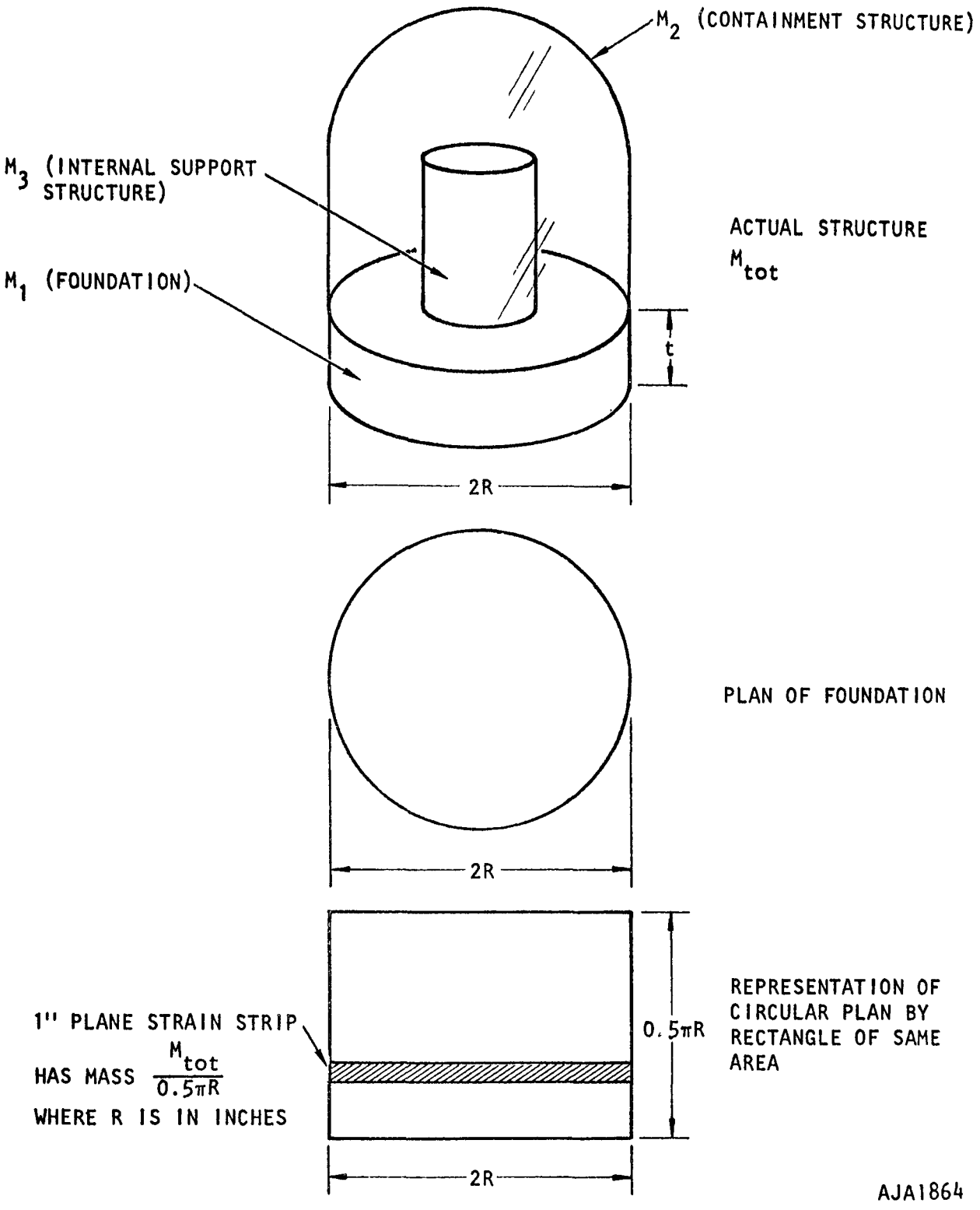

FIGURE 4-2. PLANE STRAIN REPRESENTATION OF THREE-DIMENSIONAL REACTOR STRUCTURE (PRESENT ANALYSIS USES LENGTH SLIGHTLY LESS THAN 2R)

The containment and support structures are represented as cantilevers fastened to the upper surface of the slab. Their fundamental frequencies, 4 cps and 5 cps respectively, are the same as those presently being used for a candidate design. The cantilevers have a concentrated mass at the top equal to the total mass of the actual structure times the plane strain scale factor $\frac{1}{110 \times 12}$. The meshes for free-field and interaction cases and the properties for the various elements are shown in Figure 4-3. The free vibrational responses of the cantilevers are shown in Figures 4-4 and 4-5.

The structural model for Cases 3 through 6 (elastic soil) which is shown in Figure 4-6 is an extension of the model for Case 2. Instead of being on the surface, the bottom of the foundation slab is 55 ft below the surface. The walls are 4.5 ft thick, which is assumed to be a typical thickness for an actual reactor structure, and they are assumed to have the properties of plain concrete. The foundation slab is 10 ft thick and in Cases 3 through 5 it is also assumed to have the properties of plain concrete. These cases show appreciable local distortion of the slab at points where the 4 cps and 5 cps oscillators are attached, and this interferes with interpreting effects of rocking of the foundation. In Case 6, the present investigator decided to prevent local distortion of the slab in order to clarify interpretation of rocking effects. The only means available within the present computer program is to increase the Young's modulus of the foundation material over the value in Cases 3 through 5. The foundation Young's modulus in Case 6 is 80 times greater than that in the previous cases, which effectively prevents local distortion and permits a meaningful analysis of rocking to be made. Since the stiffner of the structure foundation in all Cases (1 through 6 and 1-1 through 1-3) is much greater than that of the soil, increasing the foundation stiffness in Case 6 has negligible effect on interaction between soil and structure.

The present analysis of a plane strain section implies that the structure is a trench of infinite length. The walls of this idealized structure are more flexible with respect to lateral load than the actual cylindrical structure, and hence, the lateral stiffness of the present model needs to be

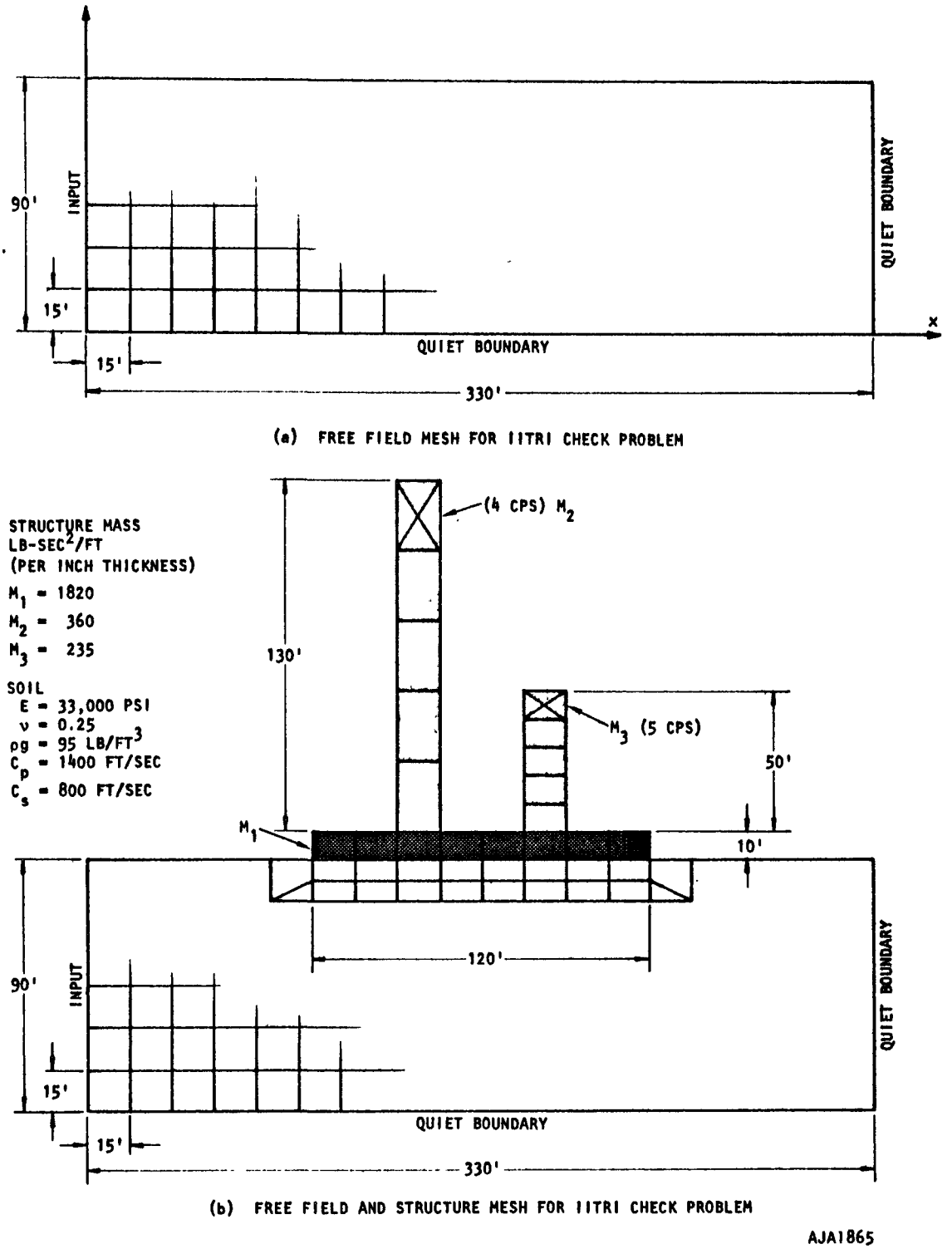

FIGURE 4-3. FINITE ELEMENT MESHES FOR IITRI CHECK PROBLEM, CASE 2 (REFERENCE 21)

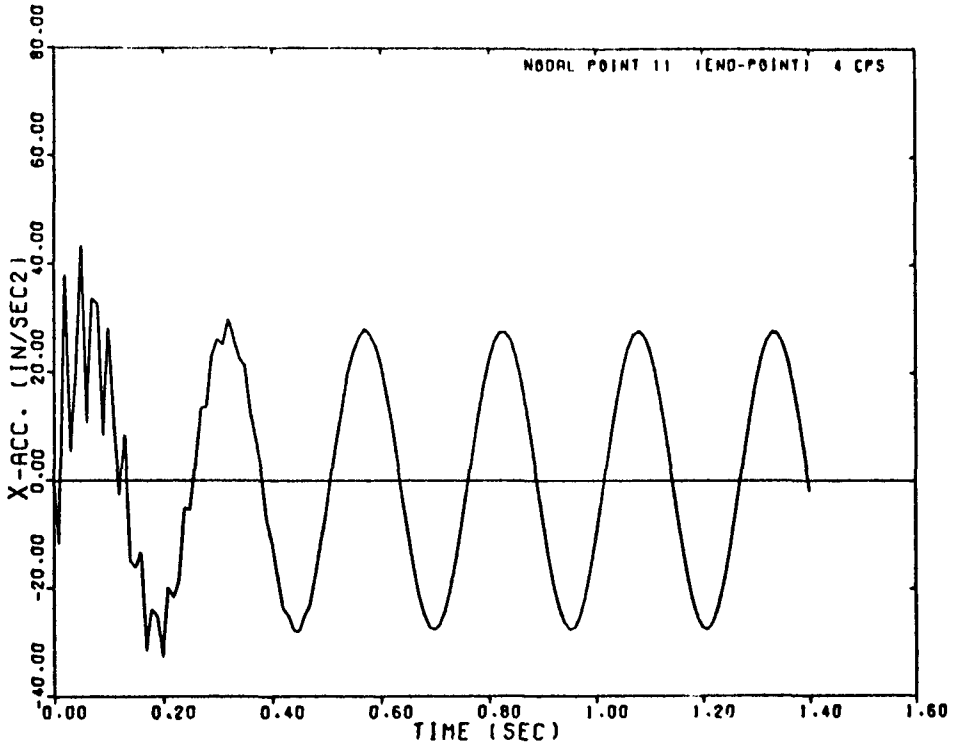

FIGURE 4-4. FREE VIBRATIONS OF 4 CPS OSCILLATOR (REPRESENTS CONTAINMENT STRUCTURE)

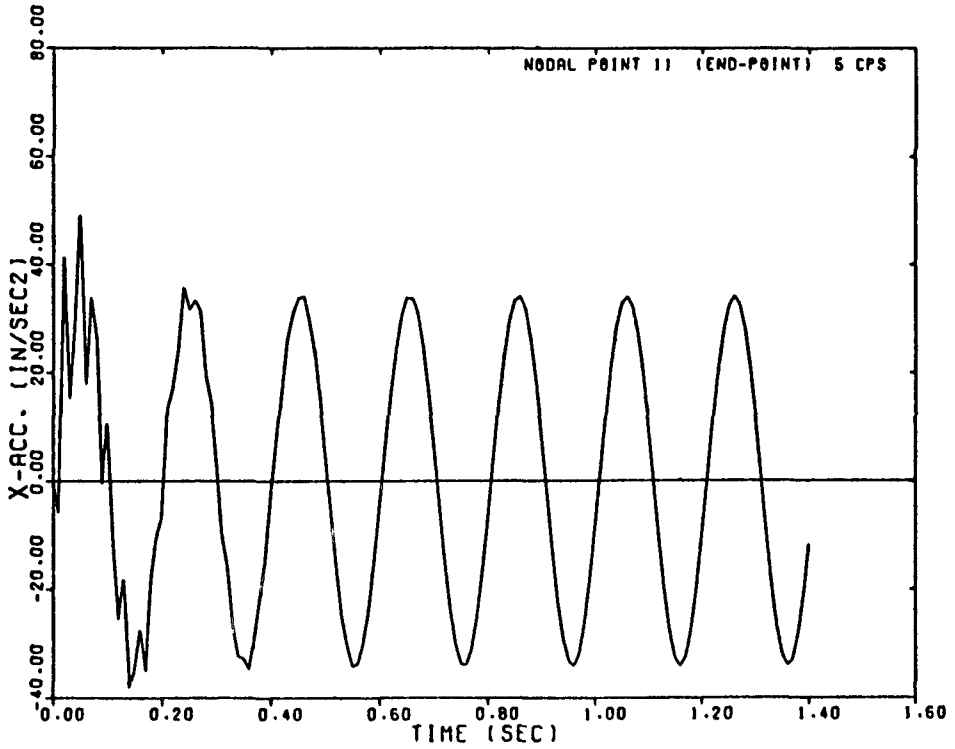

FIGURE 4-5. FREE VIBRATIONS OF 5 CPS OSCILLATOR (REPRESENTS INTERNAL SUPPORT STRUCTURE)

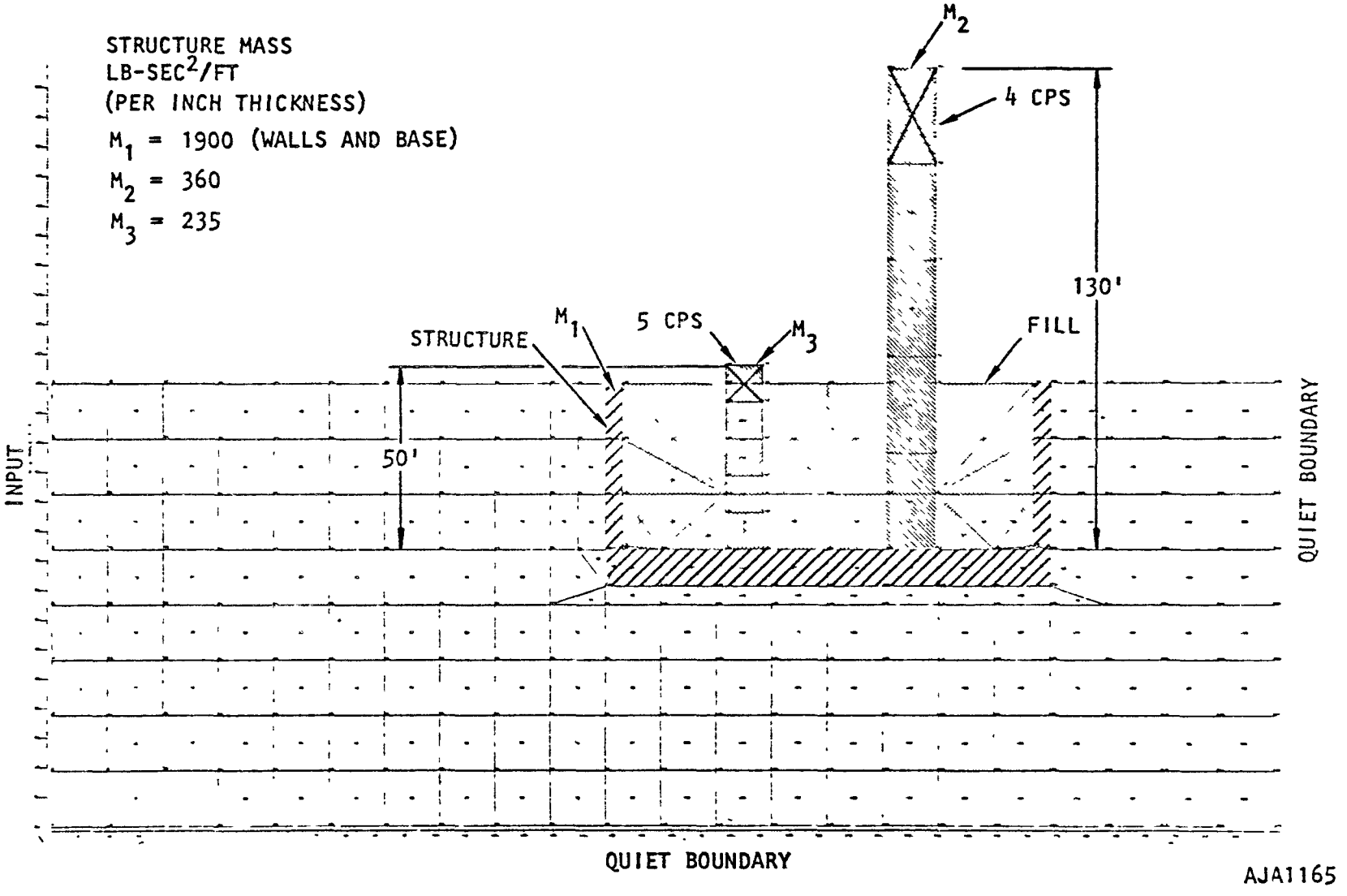

FIGURE 4-6. FINITE ELEMENT REPRESENTATION OF EMBEDDED NUCLEAR REACTOR STRUCTURE FOR CASES 3 THROUGH 6

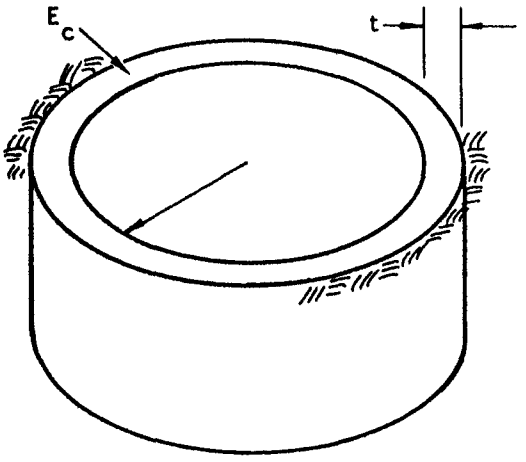

(a) EMBEDDED PORTION OF CYLINDRICAL CONTAINMENT STRUCTURE

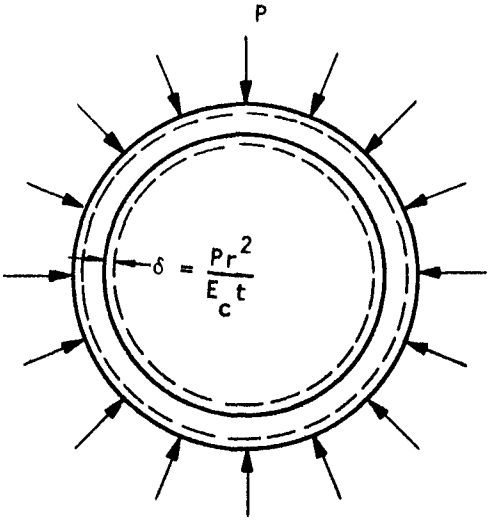

(b) DEFLECTION OF STRUCTURE SUBJECTED TO IDEALIZED SOIL PRESSURE (MEMBRANE EFFECT OF FOUNDATION NEGLECTED)

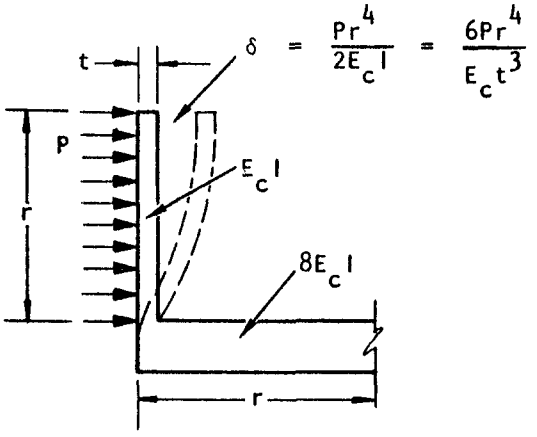

(c) DEFLECTION OF WALL IN PLANE STRAIN IDEALIZATION WITHOUT FILL

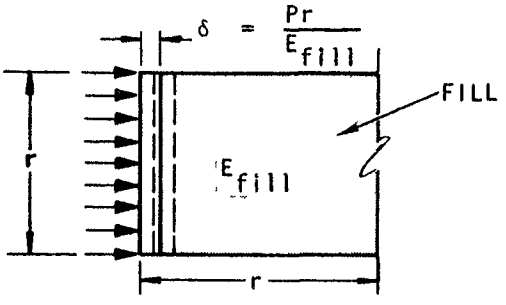

(d) DEFLECTION OF WALL IN PLANE STRAIN IDEALIZATION WITH FILL (EFFECT OF FOUNDATION NEGLECTED)

AJA2063

FIGURE 4-7. PLANE STRAIN IDEALIZATION OF EMBEDDED CYLINDRICAL STRUCTURE

enhanced. Figure 4-7b and c illustrate that, for a fixed soil pressure p, the deflection of the trench is

$$\frac{\delta_{trench}}{\delta_{cyl}} = \frac{6pr^4/E_c t^3}{pr^2/E_c t} = 6\left(\frac{r}{t}\right)^2 \qquad (4\text{-}1)$$

$$\delta_{trench} \simeq 80\,\delta_{cyl} \qquad (4\text{-}2)$$

(for present conditions)

about 80 times greater than that of the cylinder. Including the membrane effect of the foundation on stiffness of the cylinder would make the ratio even greater than 80.

One way to stiffen the walls in the present analyses is to increase their Young's modulus E_c. This approach was rejected because it would make the shock impedance (ρc) of the wall unrealistically high. Instead, the trench is filled with material (labelled Fill in Figures 4-6 and 4-7d) whose Young's modulus E_{fill} provides a lateral stiffness which is roughly the same as the cylindrical structure in Figure 4-7b. Assuming that, for a fixed soil pressure, the deflection δ in Figures 4-7b and d are equal

$$\delta_{cyl} = \delta_{trench} = \frac{Pr^2}{E_c t} = \frac{Pr}{E_{fill}} \qquad (4\text{-}3)$$

or

$$E_{fill} = \frac{t}{r} E_c \qquad (4\text{-}4)$$

$$E_{fill} \simeq E_c/13 \qquad (4\text{-}5)$$

(for present conditions)

In writing Equations 4-3 through 4-5, the influence of the foundation on stiffness of the wall and the resulting variation of wall deflections as a function of height are neglected. Fill stiffness could be computed according to more accurate assumptions about shell stiffness, but this is not considered to be justified.

The fill has negligible mass and is attached to the walls and foundation at nodal points. It is not attached to upper parts of the 4 cps and 5 cps oscillators and does not interfere with their responses.

The soil properties for Cases 3 through 6 for both structures embedded in elastic soil and elastic free-field are given in Table 4-2. Each of the four cases required calculation of free-field response and a second calculation of response of embedded structure. The soil is homogeneous in all cases except Case 4, in which a horizontal layer 45 ft deep overlies an infinite medium of stiffer material.

Damping, which is often used to dissipate energy in elastic computation, is omitted from the present model of soil. This is due to a limitation in the present computer program, which uses the same damping coefficients ξ and η in all equations of motion regardless of whether they apply to soil or structure. Although it might be possible to choose ξ and η such that appreciable damping is applied to the soil and negligible damping is applied to the structure, this is considered to be an undesirable complication. The goal of the present work is to study trends in interaction phenomena. So long as assumptions about damping are held fixed while other parameters are varied, it is expected that the trends obtained will also be found when suitable damping models become available. Radiation damping, whereby energy associated with the earthquake motions is allowed to pass out of the finite element grid, is accounted for by means of the quiet boundary technique.

The structural and free-field models for Cases I-1 through I-3 (inelastic soil) which are shown in Figures 4-8 and 4-9 are very similar to the model in Figure 4-6 and its corresponding free-field model. In preparing the finite element grid for the inelastic calculations, however, several important changes from the elastic calculations are made. First, some of the elements in the foundation and in other stiff members are made larger. This reduces the natural frequencies of the system and permits a larger integration time step and more economical calculation. Second, backfill material having virtually no tensile strength is introduced next to the structure wall. This represents normal poor contact between structure wall and backfill material

and improves the representation of soil properties in Cases 1-1 through 1-3 over those in Cases 1 through 6. Third, the structure is at the center with respect to the sides of the grid. This change was made because it was expected that inelastic deformation would occur primarily in the vicinity of the structure. It is better for operation of the quiet boundary procedure to move the inelastic zone as far from the boundary as possible. The reason for this is explained below. This reasoning was later somewhat undermined by the finding during actual calculations that the inelastic zone is less concentrated at the structure than expected.

The properties used to represent inelasticity in the soil are defined below in Table 4-3 and Figure 4-10. In Case 1-3, the shear strength of the soil is abruptly decreased to represent liquefaction. This change of properties is illustrated in Figure 4-11.

TABLE 4-2. MATERIAL PROPERTIES FOR CASES 3 THROUGH 6, STRUCTURE EMBEDDED IN ELASTIC SOIL

Case	G, psi	B, psi	ρ, #-Sec^2/in.^{4}	C_p, fps	C_s, fps
3 (homogeneous)	1.98×10^4	3.3×10^4	0.00018	1510	875
4 Surface to 45 ft	1.98×10^4	3.3×10^4	0.00018	1510	875
4 Below 45 ft	5.4×10^4	9×10^4	0.00018	2500	1440
5 (homogeneous)	5.4×10^4	9×10^4	0.00018	2500	1440
6 (homogeneous)	1.98×10^4	3.3×10^4	0.00018	1510	1440

where

G = Shear modulus

B = Bulk modulus

ρ = Density

C_p = Dilitation wave speed

C_s = Shear wave speed

In each case, a calculation of free-field response and a calculation of interaction response were made.

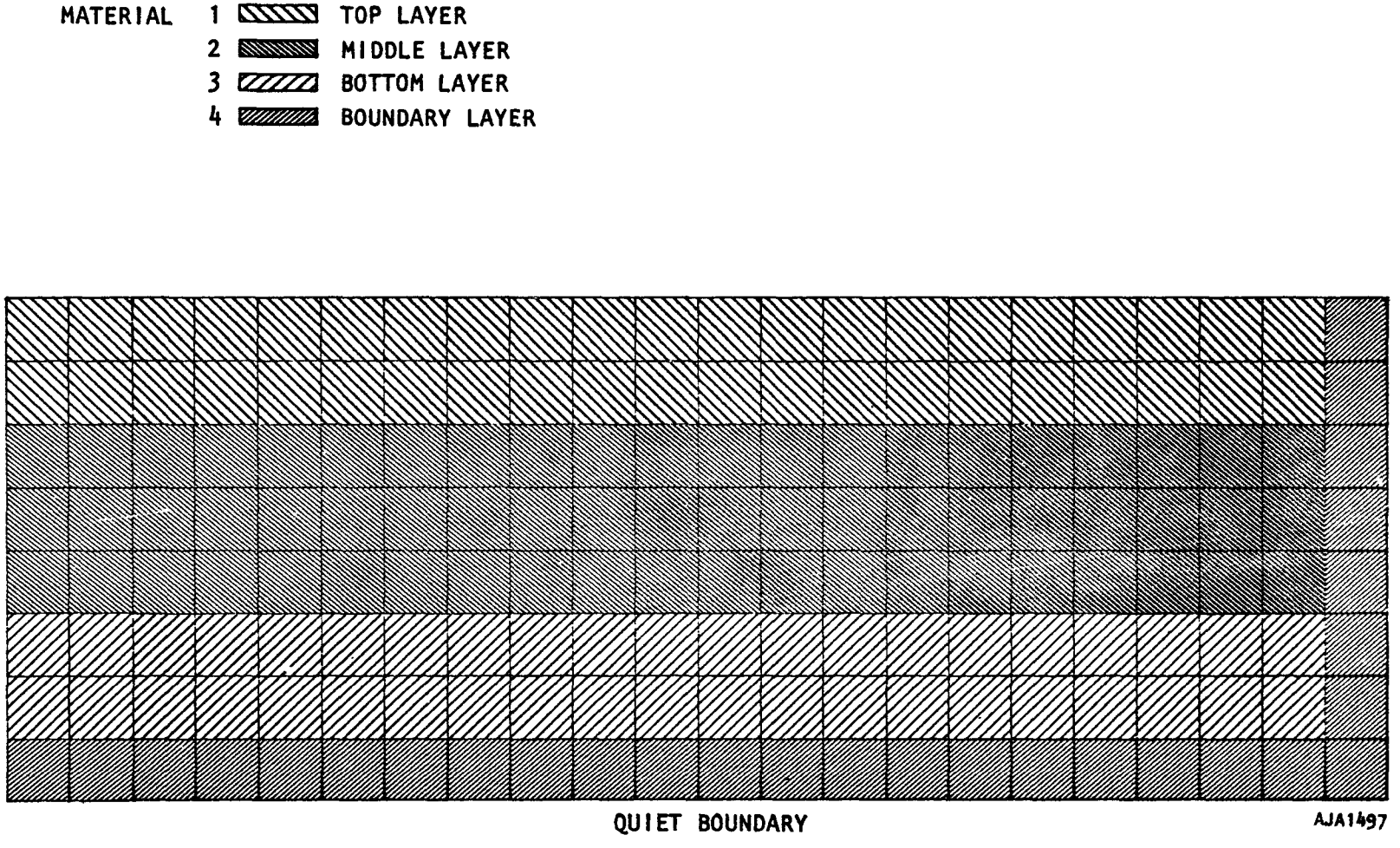

FIGURE 4-8. FINITE ELEMENT REPRESENTATION OF FREE FIELD FOR CASES 1-1, 1-2 (FREE-FIELD CALCULATION NOT PERFORMED FOR CASE 1-3)

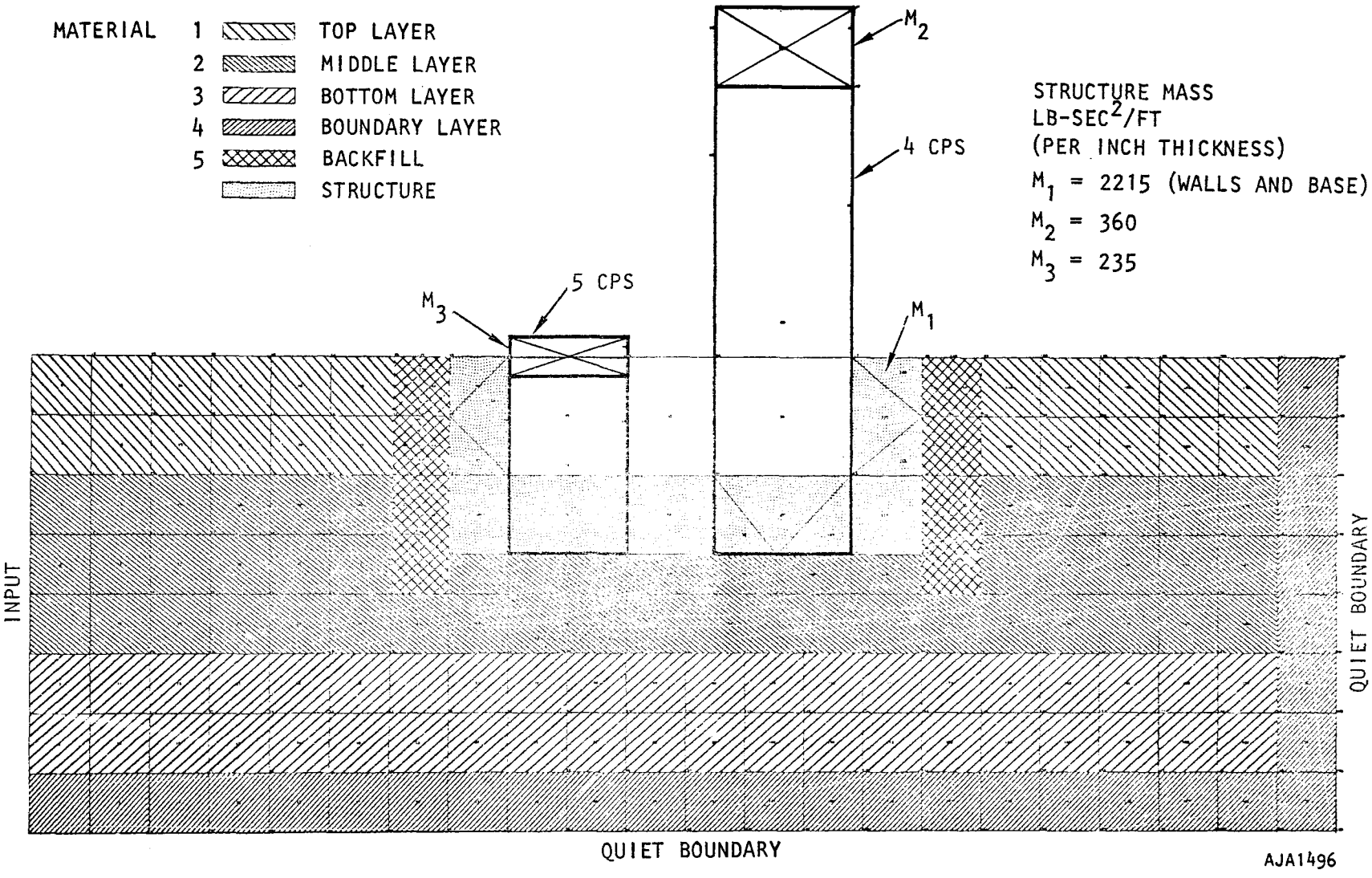

FIGURE 4-9. FINITE ELEMENT REPRESENTATION OF EMBEDDED NUCLEAR REACTOR STRUCTURE, CASES I-1, I-2, I-3

TABLE 4-3. MATERIAL PROPERTIES FOR INELASTIC SOIL

(a) CASE I-1

Material Type	Region	Overburden, psi	G, psi	B, psi	ρ, lb-sec^2/in.^{4}	C_p, fps	C_s, fps	α_1,	C_1, psi	α_2	C_2, psi	J_1', psi
1	Top layer	-10	19800	33000	0.00018	1510	875	-0.42	15	0	3.5	+27.4
2	Middle layer	-50	19800	33000	0.00018	1510	875	0	3.5	0	3.5	--
3	Bottom layer	-90	19800	33000	0.00018	1510	875	0	3.5	0	3.5	--
4	Boundary layer	0	19800	33000	0.00018	1510	875	does not yield				
5	Backfill	0	19800	33000	0.00018	1510	875	-0.42	2.4	0	3.5	-2.4

*Applies to cases with structure only

where

- G = Shear modulus
- B = Bulk modulus
- ρ = Density
- C_p = Dilitation wave speed (elastic)
- C_s = Shear wave speed (elastic)
- α_1, α_2 = Coefficients of friction
- C_1, C_2 = Cohesion
- J_1 = Mean stress at which yield criterion changes from (α_1, C_1) to (α_2, C_2)

For illustration of the meaning of yield criteria, see Figure 4-10.

(b) CASE I-2

Material Type	Region	Overburden, psi	G, psi	B, psi	ρ, lb-sec^2/in.^{4}	C_p, fps	C_s, fps	α_1,	C_1, psi	α_2	C_2, psi	J_1', psi
1	Top layer	-10	19800	33000	0.00018	1510	875	-0.42	15	0	29	-33.3
2	Middle layer	-50	19800	33000	0.00018	1510	875	-0.42	65.5	0	29	87.0
3	Bottom layer	-90	19800	33000	0.00018	1510	875	0	29	0	29	0
4	Boundary layer	0	19800	33000	0.00018	1510	875	does not yield				
5	Backfill	0	19800	33000	0.00018	1510	875	-0.42	2.5	0	29	-63.0

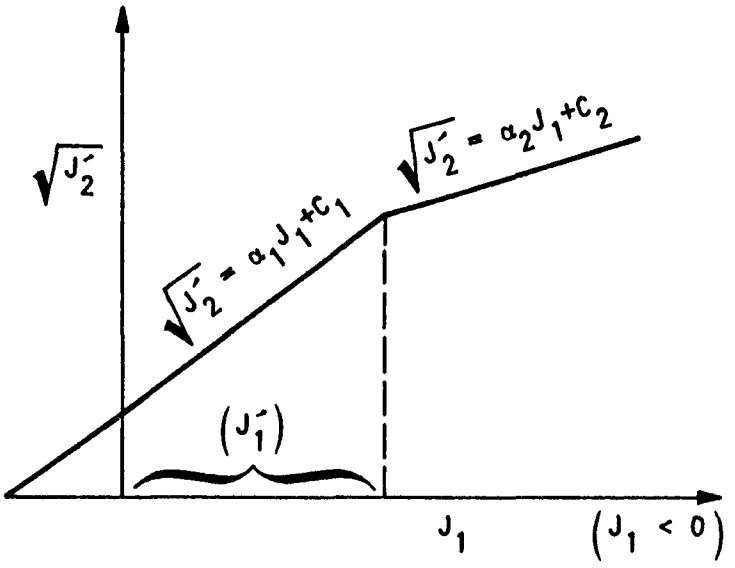

Where

$$J_1 = \sigma_{11} + \sigma_{22} + \sigma_{33}$$

$$J_2' = \left\{\frac{1}{6}\left[(\sigma_{11} - \sigma_{22})^2 + (\sigma_{33} - \sigma_{22})^2 + (\sigma_{33} - \sigma_{11})^2\right]\right\}^{1/2}$$

FIGURE 4-10. DEFINITION OF YIELD COEFFICIENTS

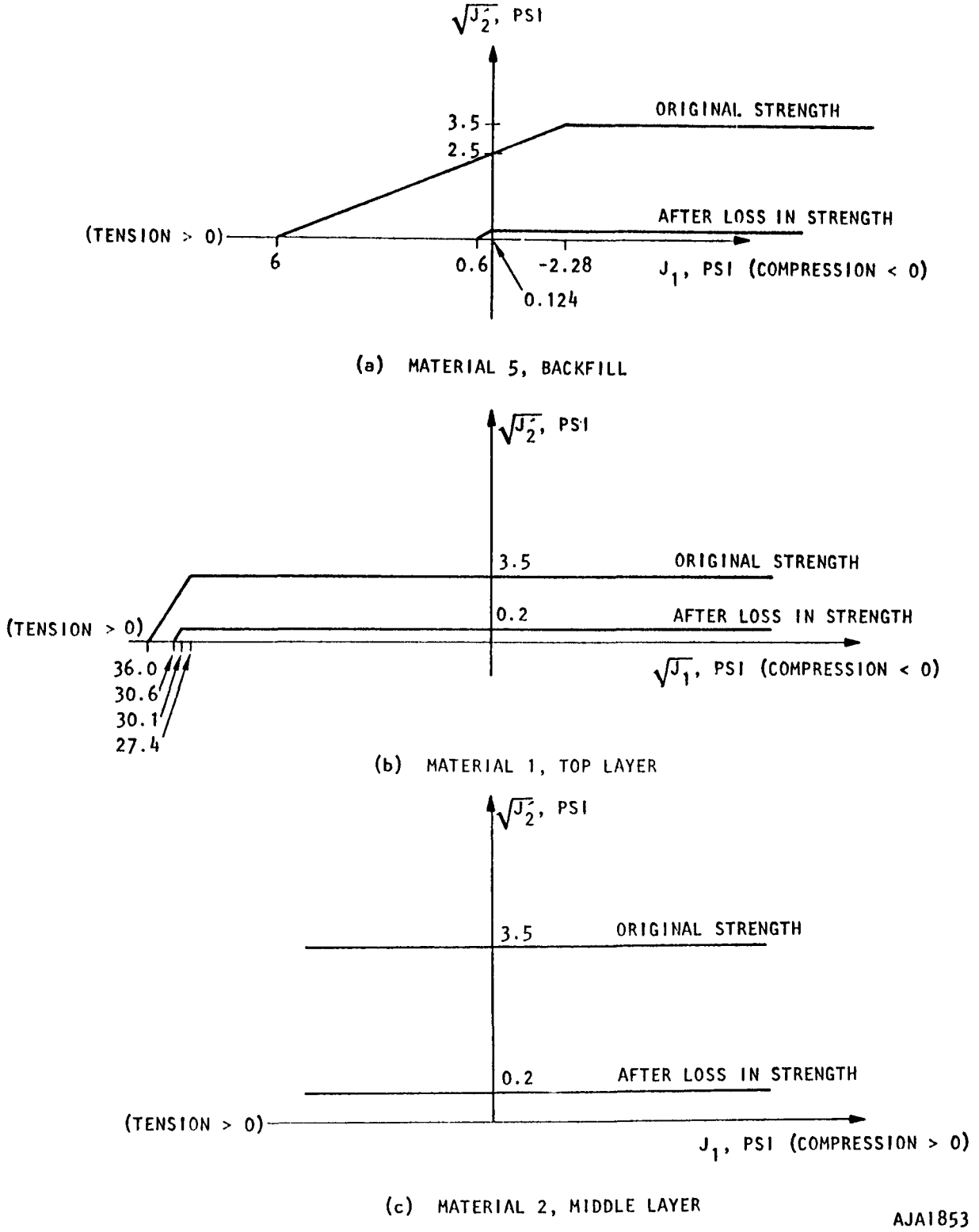

FIGURE 4-11. SOIL STRENGTH BEFORE AND AFTER ONSET OF INSTABILITY, CASE 1-3

Inelastic material properties depend on the state of stress, which includes the overburden stress. The state of overburden stress could be prescribed element by element as initial conditions for the dynamic solution. However, it is difficult to know what the overburden stresses are, especially when the overburden is great enough to produce inelasticity. The present approach is to estimate the overburden stress in terms of stress invariants and to reflect this in the inelastic properties. Several layers of soil are defined to share a common overburden stress and a common yield criterion which takes into account the confining effects of the average overburden stress within that layer. Evidently, a site which appears to be homogeneous will have some features of a layered site.

BOUNDARY CONDITIONS

The present technique of applying input motion to the site of the finite element grid and using a quiet boundary method to prevent reflections from the bottom and from the opposite side is based on a view of earthquake motions as a train of waves, Figure 4-12. If a wave train, having interacted with the structure or bypassed it through the surrounding soil, subsequently encounters a boundary of the grid which has no physical counterpart, it will be reflected back into the grid, Figure 4-12(b). Each time such a reflection encounters the structure, its influence is superposed on that of the basic input motion and that of all previous reflections. Eventually, the reflections can distort the response of the structure. The best solution to this problem available in the present computer program is shown in Figure 4-12(c) where the quiet boundary technique is used to prevent reflections from two of the three artificial boundaries of the grid.

The reason for using an elastic boundary layer in Cases I-1 through I-3 is that the present quiet boundary procedure has a theoretical basis for materials in which the dilatation and shear wave speeds are constant. The wave speeds in inelastic materials depend on the stress intensity in the material. A simple example of this is illustrated in Appendix D where the elastic and plastic dilatation wave speeds differ from

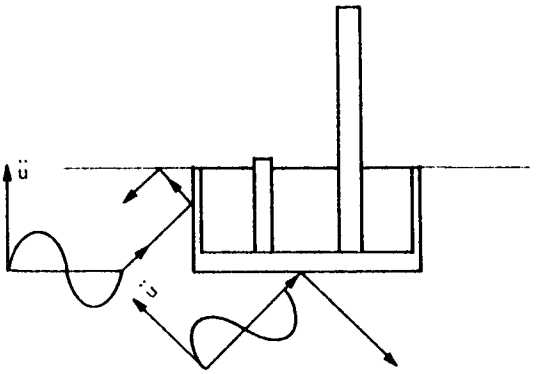

(a) WAVE TRAIN APPROACHING STRUCTURE THROUGH INFINITE MEDIUM

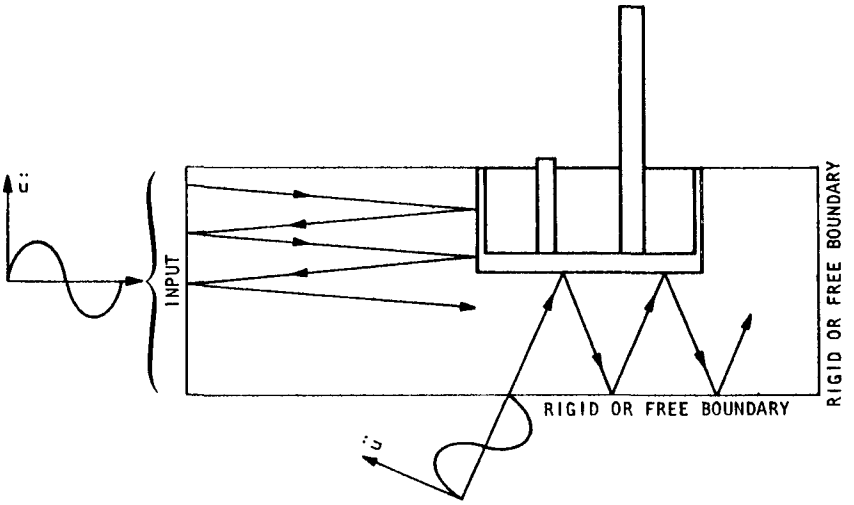

(b) WAVE TRAIN APPROACHING STRUCTURE IN A FINITE ELEMENT GRID WHERE BOUNDARY REFLECTIONS OCCUR

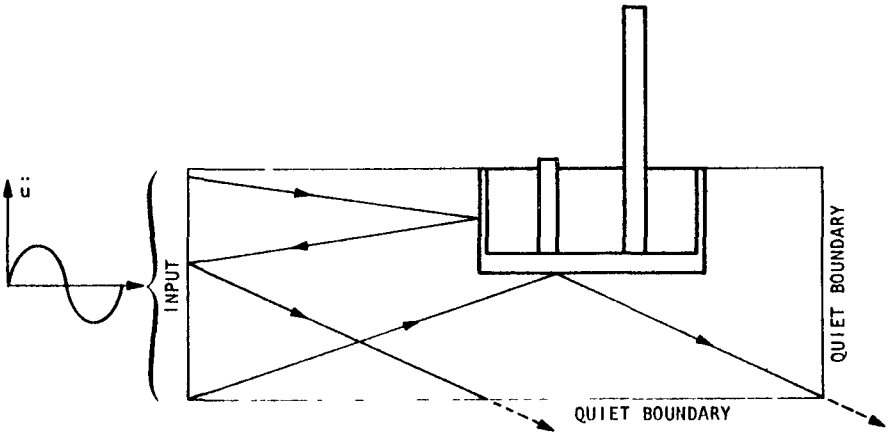

(c) EARTHQUAKE WAVE TRAIN APPROACHING STRUCTURE IN A FINITE ELEMENT GRID WHERE BOUNDARY REFLECTIONS OCCUR ONLY ON THE INPUT BOUNDARY--PRESENT PROCEDURE

AJA1868

FIGURE 4-12. USE OF QUIET BOUNDARY TECHNIQUE IN PRESENT ANALYSIS

each other. In an attempt to overcome this problem, the material between sensor and corrector points in the quiet boundary technique (points j and j-1 of Figure B-3, Appendix B) is required to remain elastic and hence to have constant wave speeds. An undesirable side effect of this procedure is to introduce an artificial boundary between two layers having somewhat different shock impedances. This is unavoidable with present techniques. The effects on the solution are neglected. In the present series of calculations, the assumptions of the quiet boundary procedure are met by requiring that the elements adjacent to the boundaries to be quieted remain elastic. The error committed in following this procedure lies in creating an impedance mismatch between the boundary elements and adjacent interior ones when the interior ones are inelastic. This is considered to be preferable to allowing the boundary elements to become plastic while using the quiet boundary procedure as if they were elastic.

As an alternative to using a quiet boundary technique, it is common (for example, see Reference 12) to use either zero displacement (fixed) or zero stress (free) boundary conditions for the sides of the grid and to apply earthquake shaking to the bottom of the grid. The bottom then behaves as a rigid boundary with respect to waves. This appears to be satisfactory so long as periods of the wave motion are long enough that wave effects are negligible. The present study uses the spatial gradient of motion as a criterion to determine the importance of wave effects. If the minimum rise time of periods of interest is t_r and the shear wave speed is C_s, the rise is spread over a distance L

$$L = C_s \times t_r$$

If L is greater than the characteristic distance of the structure there is some justification for neglecting wave effects and using the fixed or free boundaries described above. In the present study, L is typically 40 ft while the base of the structure is 120 ft. On this basis, it appears that wave effects may not be neglected in the present study, and that a quiet boundary procedure is needed.

INPUT

In all cases, the input is applied as a horizontal velocity/time history. The input vertical velocity is zero. Table 4-4 indicates the input conditions for all cases.

The Golden Gate and 0.2 x Olympia records are shown in Figures 4-13 and 4-14. Their pseudovelocity spectra are shown in Figure 4-15. The reason for applying the scale factor 0.2 to the Olympia record is to make the areas under their respective pseudovelocity versus period curves, Figure 4-16, about the same. According to Reference 2, this means that the intensities of the Golden Gate and 0.2 x Olympia records are about the same. Hence, the structural responses to two earthquakes of about the same intensity but with different frequency contents, may be compared.

The reason for selecting the Golden Gate record is that it has dominant motions in the frequency range 2.5 cps to 5 cps, which covers the range of the containment vessel and the internal support structure. According to Reference 8, such a situation may be expected to produce maximum interaction effects. The reason for selecting the Olympia record is to study the effect of a strong motion earthquake whose dominant frequency range is lower than that of structural components.

The calculations with inelastic soil were performed with 3 x Golden Gate and 2 x Olympia records. The effect of allowing plastic deformation of the soil may be determined by scaling up the results of purely elastic calculations and comparing with the companion inelastic cases.

TABLE 4-4. INPUT CONDITIONS, ALL CASES

Case	Input
Elastic Soil	
1	$V_x = (60.5)\ \{1 - \frac{e^{0.6t}}{2\pi}\ (0.6 \sin 2\pi t + 0.2 \cos \pi t)\}$ (in./sec)
2	$0 < t < 0.8$ sec: $V_x = (1/16\pi)\ [-t \cos 10\pi t + (1/10\pi) \sin 10\pi t]$ (in./sec) $0.8 < t < 2$ sec: $V_x = (1/14\pi)\ \{-\cos 10\pi t + 0.5\ [t \cos 10\pi t - (1/10\pi)]\} \sin 10\pi t$ (in./sec) $t > 2$ sec: $V_x = 0$
3	V_x = Golden Gate S80E, 0-4 sec
4	V_x = Golden Gate S80E, 0-4 sec
5	V_x = Golden Gate S80E, 0-4 sec
6	V_x = 0.2 x Olympia N10W, 7-11 sec
Inelastic Soil	
I-1	V_x = 3 x Golden Gate S80E, 0-3 sec
I-2	V_x = 2 x Olympia N10W, 7-10 sec
I-3	V_x = 3 x Golden Gate S80E, 0-1.8 sec

In all cases, input vertical velocity $V_y = 0$.

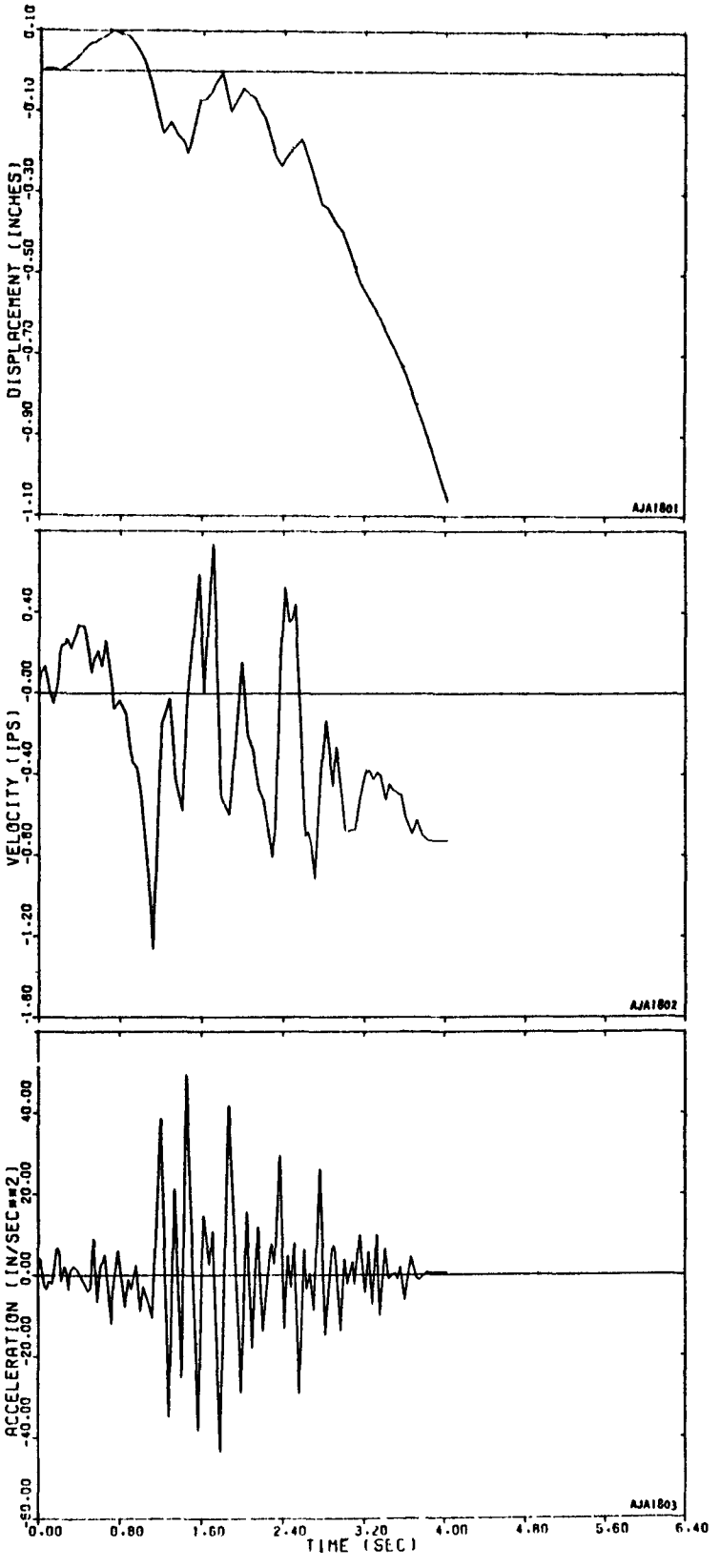

FIGURE 4-13. GOLDEN GATE E-W (0.4 SEC), INPUT TO CASES 3-5 (ELASTIC SOIL) TO OBTAIN INPUT TO CASES 1-1, 1-3, MULTIPLY ORDINATES BY 3

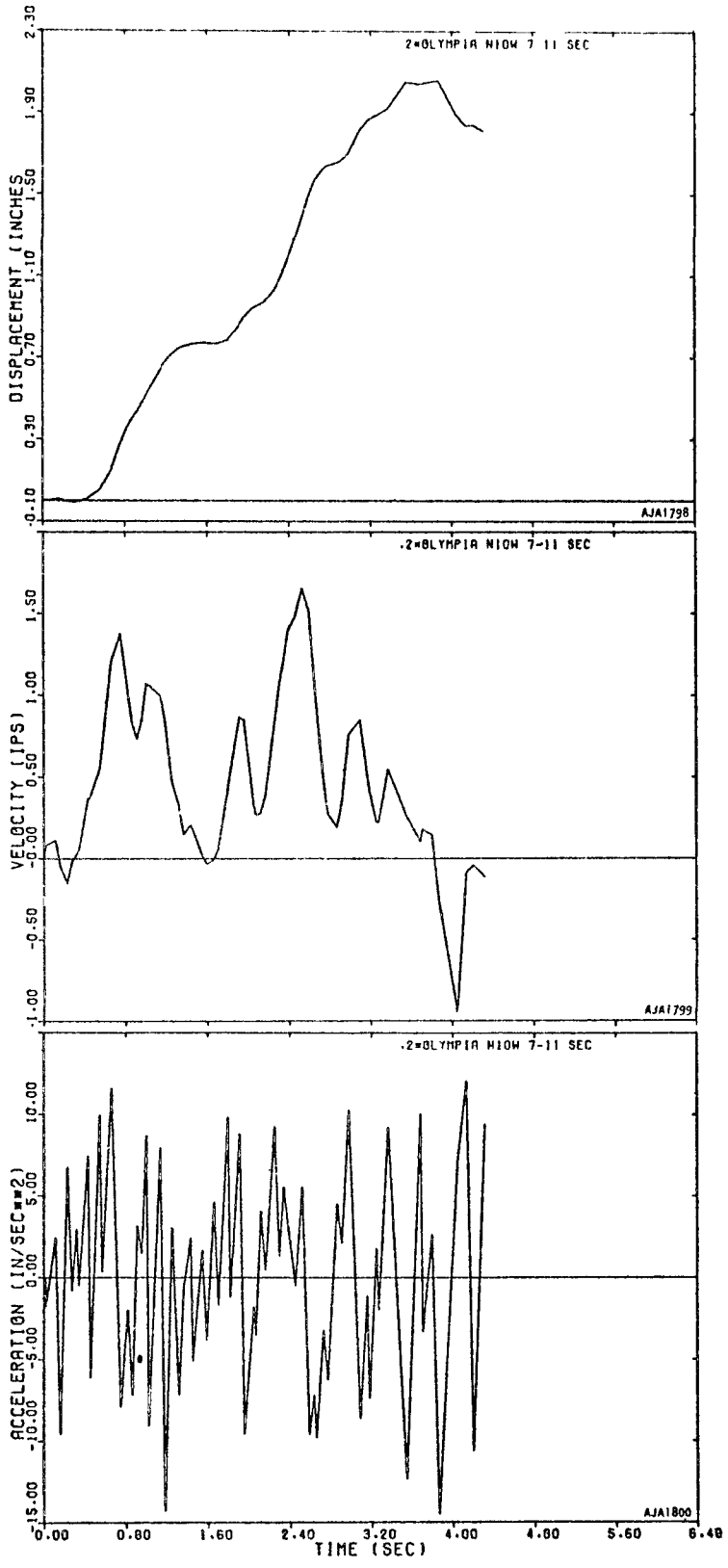

FIGURE 4-14. 0.2X OLYMPIA N10W (7-11 SEC), INPUT TO CASE 6 (ELASTIC SOIL)

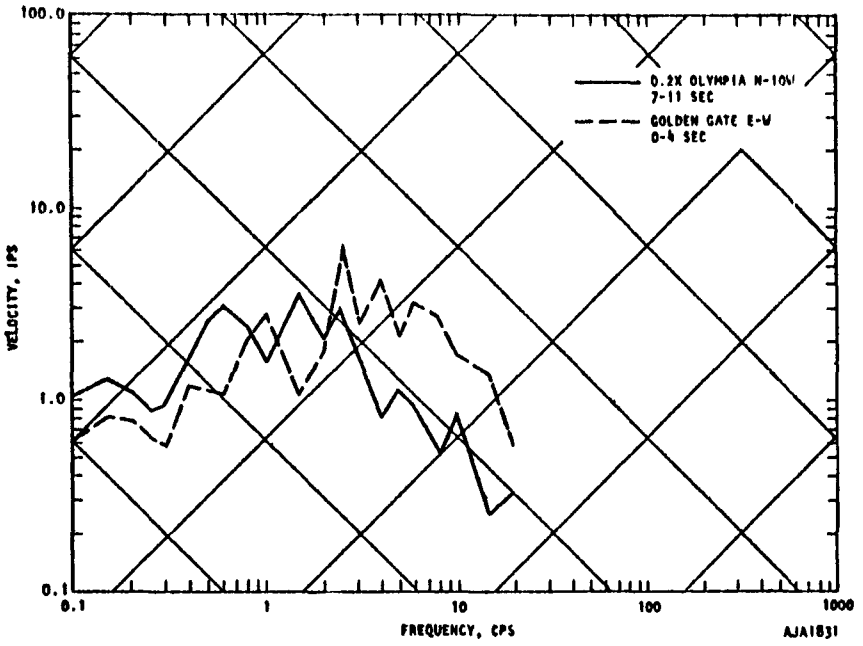

FIGURE 4-15. RESPONSE SPECTRA FOR EARTHQUAKE INPUTS

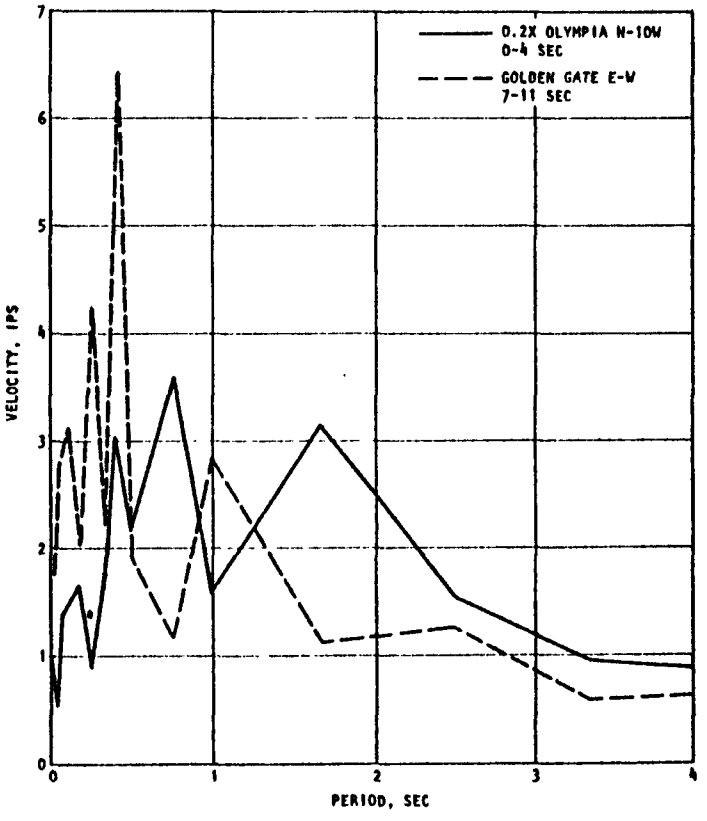

FIGURE 4-16. RESPONSE SPECTRA FOR EARTHQUAKE INPUTS

SECTION 5

RESULTS

The present analytic results are used to study three main subjects. The first subject is the relation between motion of the foundation and that of the free-field. Also studied are the influence of soil stiffness, including plasticity, and the frequency content of earthquake input relative to frequency of the structure. The second subject is the relation between stresses in the soil adjacent to the structure and those at corresponding points in the free-field. The influence of plasticity on this relation is also studied. The third major subject is the relationship between the motion of the foundation and that of the 4-cps oscillator representing the superstructure. These findings are drawn from studies summarized in Table 4-1.

RELATION BETWEEN MOTIONS OF FOUNDATION AND FREE FIELD

The ratios of acceleration spectra at the foundation to spectra at the surface of the free field are shown for all embedded structure cases in Tables 5-1 and 5-2. To illustrate the findings more clearly, the pseudo-velocity response spectra for Cases 3 and 6 are plotted in Figures 5-1 through 5-4. Ratios of structural to free-field spectral response, where the free-field response is measured at the level of the foundation, are given in Appendix E.* These results are consistent with the results of Cases 1 and 2, Appendix F.

These data clearly indicate that the horizontal response of the foundation is less than that of the free field. The amount of suppression in the horizontal direction is greatest when the free-field response is defined at the surface. The trend in the vertical response is less clear.

*Present design procedures that are based either on response spectrum curves or on time-dependent ground motions use recorded surface motions as input to foundation analyses. Thus, in the present analysis, emphasis is given to the ratio of foundation response to free-field surface response (Tables 5-1 and 5-2). For completeness, ratios of spectra at the foundation to spectra at the same depth in the free field are given in Appendix E.

TABLE 5-1. HORIZONTAL ACCELERATION SPECTRA $\left(\frac{\text{STRUCTURE (FOUNDATION)}}{\text{FREE-FIELD (SURFACE)}}\right)$

Frequency, cps	Case					
	3	4	5	6	I-1	I-2
1	1.06	1.05	1.09	1.04	0.63	0.67
2	0.73	0.91	1.09	0.65	0.59	0.42
2.5	0.54	0.63	0.76	0.45	0.32	0.25
3	0.51	0.55	0.76	0.39	0.25	0.24
4	0.50	0.34	0.59	0.55	0.23	0.26
5	0.63	0.44	0.51	0.72	0.31	0.42
6	0.51	0.61	0.61	0.43	0.28	0.34
8	0.48	0.29	0.84	0.50	0.33	0.41
10	0.65	0.31	0.50	0.58	0.20	0.84

TABLE 5-2. VERTICAL ACCELERATION SPECTRA $\left(\frac{\text{STRUCTURE (FOUNDATION)}}{\text{FREE-FIELD (SURFACE)}}\right)$

Frequency, cps	Case					
	3	4	5	6	I-1	I-2
1	1.20	1.00	1.06	0.99	1.45	1.40
2	0.75	1.42	1.67	0.84	2.34	0.70
2.5	0.66	1.29	1.55	0.79	1.93	0.93
3	0.97	0.89	1.30	0.82	1.10	0.68
4	0.42	0.43	0.92	0.60	1.94	0.35
5	0.24	0.30	1.44	0.26	0.92	0.48
6	0.19	0.14	1.03	0.36	0.94	0.79
8	0.11	0.17	0.62	0.51	0.61	0.67
10	0.68	0.21	0.29	1.07	0.19	0.61

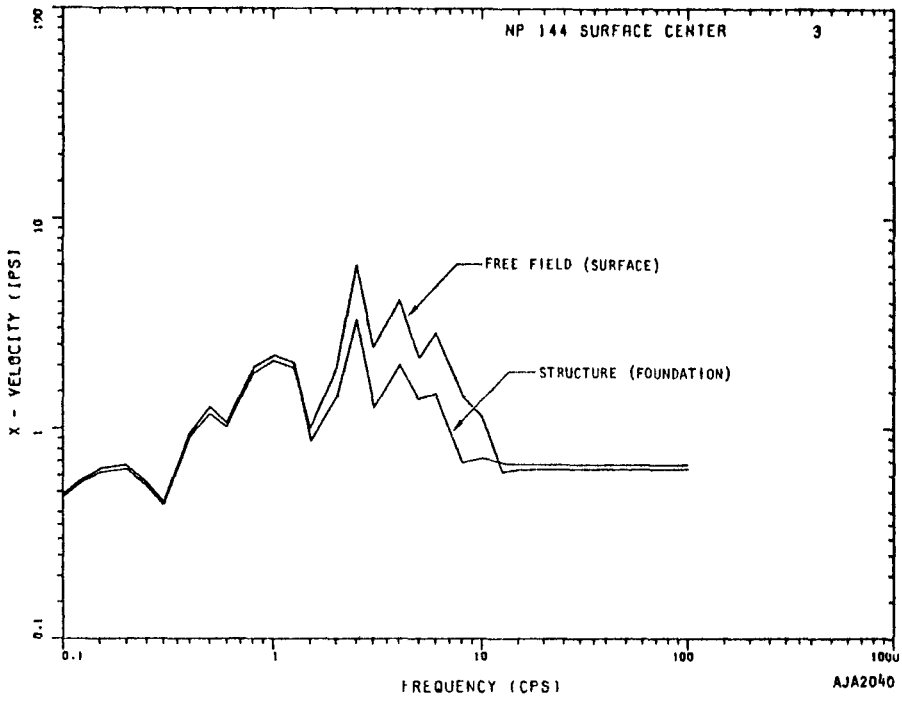

FIGURE 5-1. HORIZONTAL RESPONSE SPECTRA, CASE 3

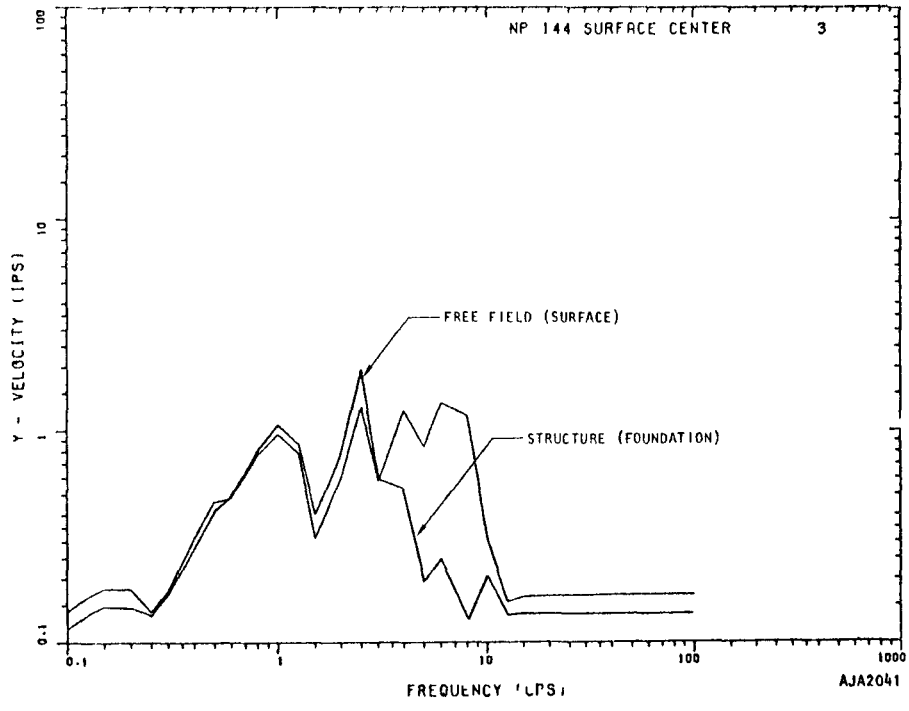

FIGURE 5-2. VERTICAL RESPONSE SPECTRA, CASE 3

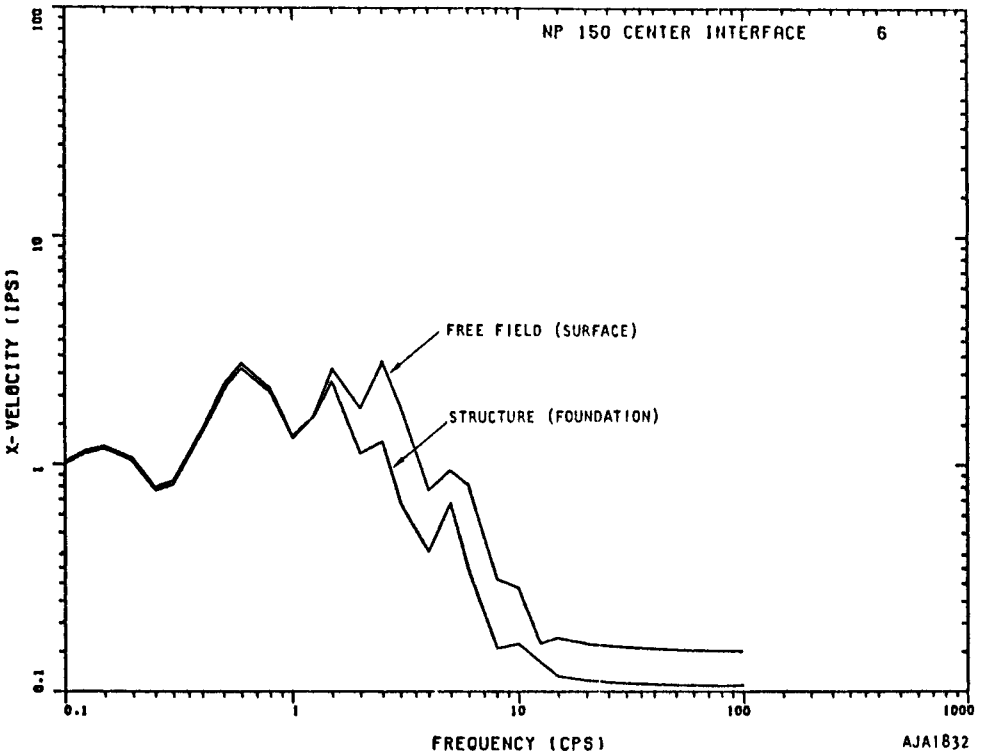

FIGURE 5-3. HORIZONTAL RESPONSE SPECTRA, CASE 6

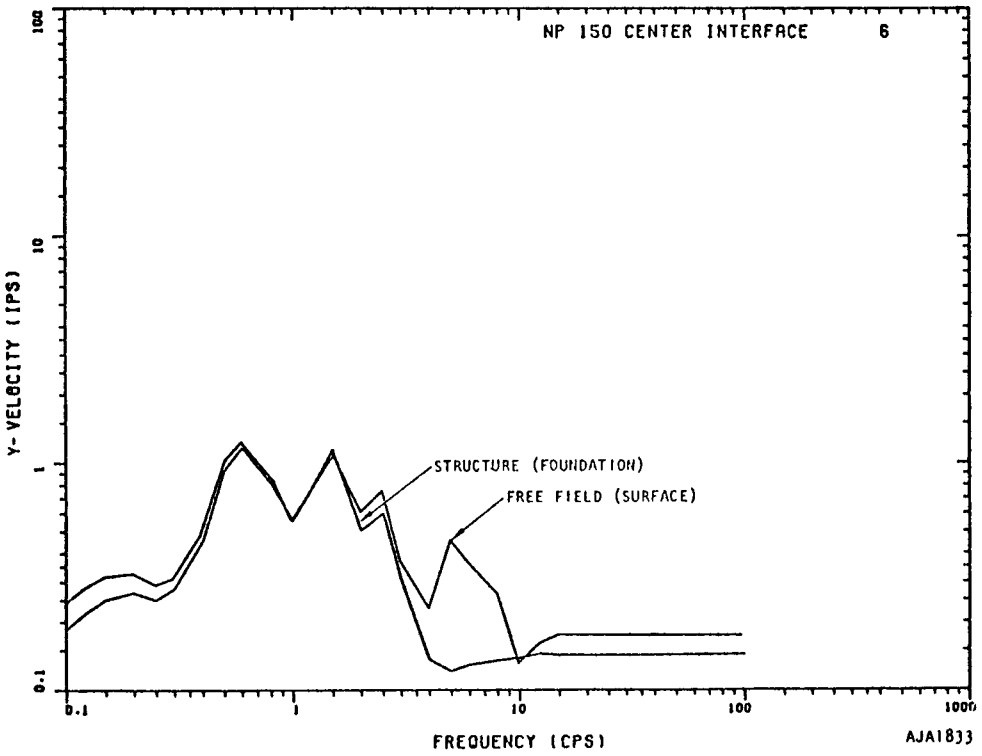

FIGURE 5-4. VERTICAL RESPONSE SPECTRA, CASE 6

Some cases indicate amplification in the 1 to 3 cps frequency range. The reason for this in the inelastic Cases I-1 and I-3 is discussed in the section on interaction stresses.

The peak accelerations and velocities of the foundation relative to the free field are summarized in Table 5-3 for Cases 3 through 6 and I-1 and I-2. The peak horizontal acceleration is suppressed by a factor of 0.4 to 0.7, while the velocity is suppressed by a factor of 0.5 to 1.0.

The horizontal accelerations of the free field and foundation for Cases 3, 6, and I-1, Figures 5-5 through 5-10, also illustrate the findings summarized in Table 5-3. The suppression of foundation response relative to free-field response is greater in Cases 3 and I-1 than in Case 6. The reason for this is suggested by closed-form analyses, which indicate that maximum suppression occurs when the dominant frequencies of of the input are in the same range as the frequencies of the structure. In Case 6, the dominant frequency of input is 1 to 2 cps, whereas in

TABLE 5-3. PEAK ACCELERATIONS AND VELOCITIES OF FOUNDATION RELATIVE TO THE FREE FIELD

Case	Peak Motion $\frac{\text{Structure (foundation)}}{\text{Free-Field (surface)}}$					
	3	4	5	6	I-1	I-2
Peak Acceleration						
Horizontal	0.57	0.38	0.58	0.72	0.50	0.53
Vertical	--	0.40	0.84	0.89	0.60	0.75
Peak Velocity						
Horizontal	0.87	0.86	0.91	0.97	0.48	0.59
Vertical	1.06	0.96	1.12	1.10	1.15	1.14

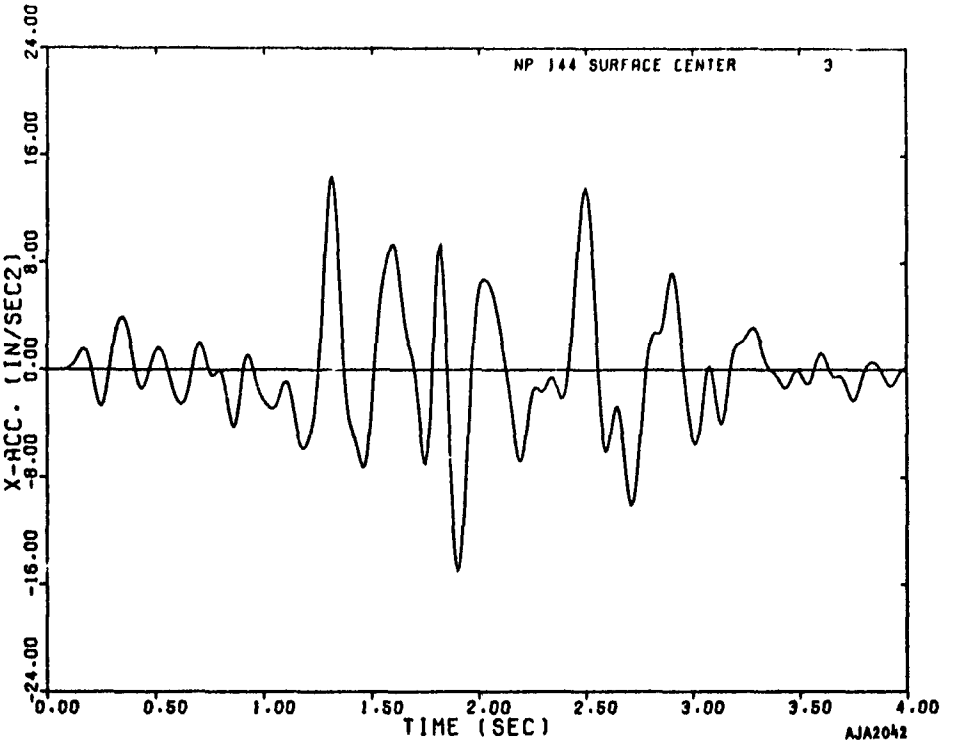

FIGURE 5-5. HORIZONTAL ACCELERATION OF FREE-FIELD SURFACE, CASE 3

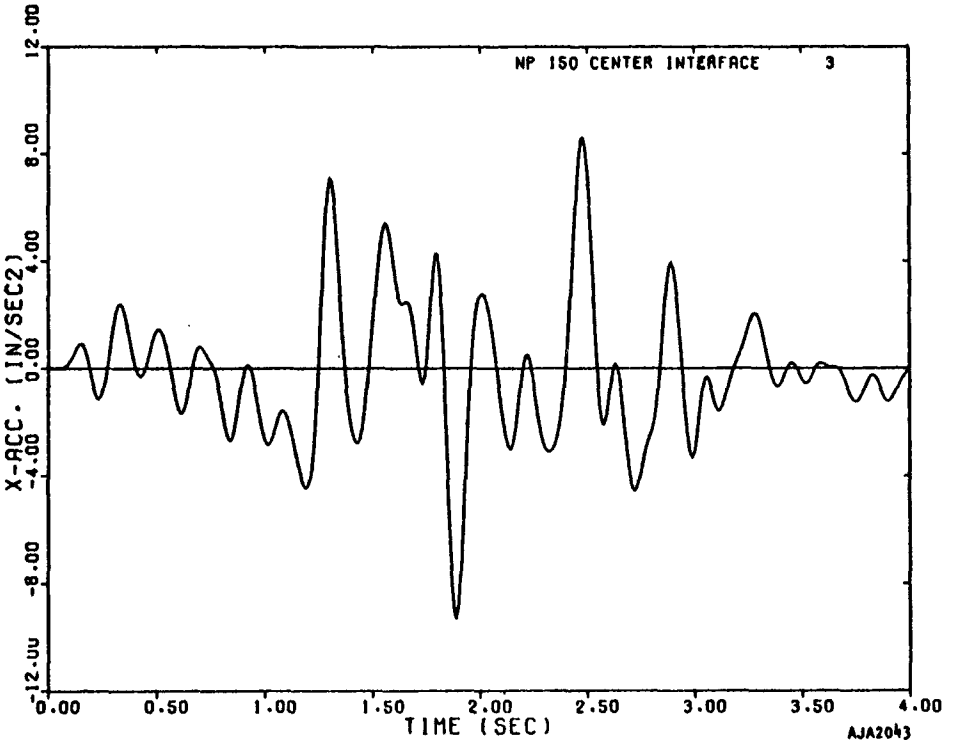

FIGURE 5-6. HORIZONTAL ACCELERATION OF STRUCTURE FOUNDATION, CASE 3

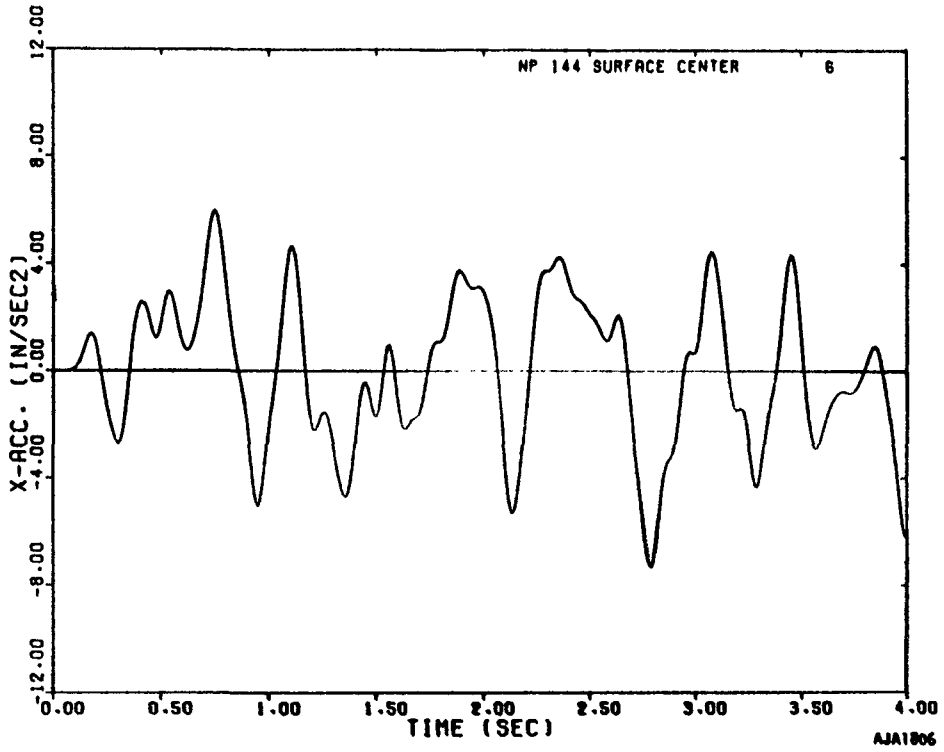

FIGURE 5-7. HORIZONTAL ACCELERATION, SURFACE OF FREE FIELD, CASE 6

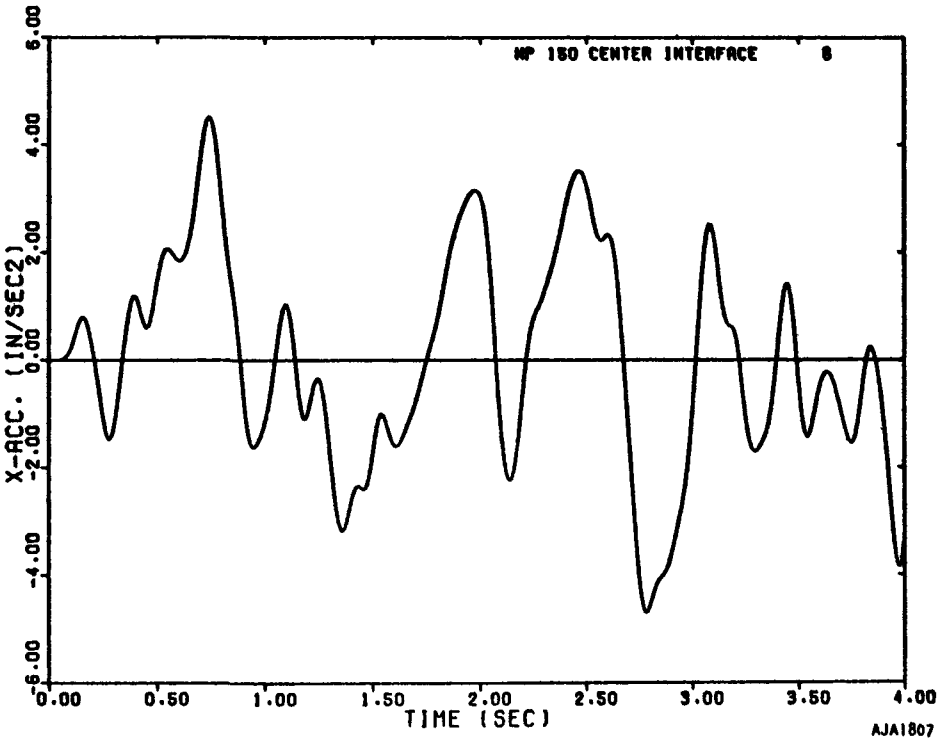

FIGURE 5-8. HORIZONTAL ACCELERATION OF FOUNDATION, CASE 6

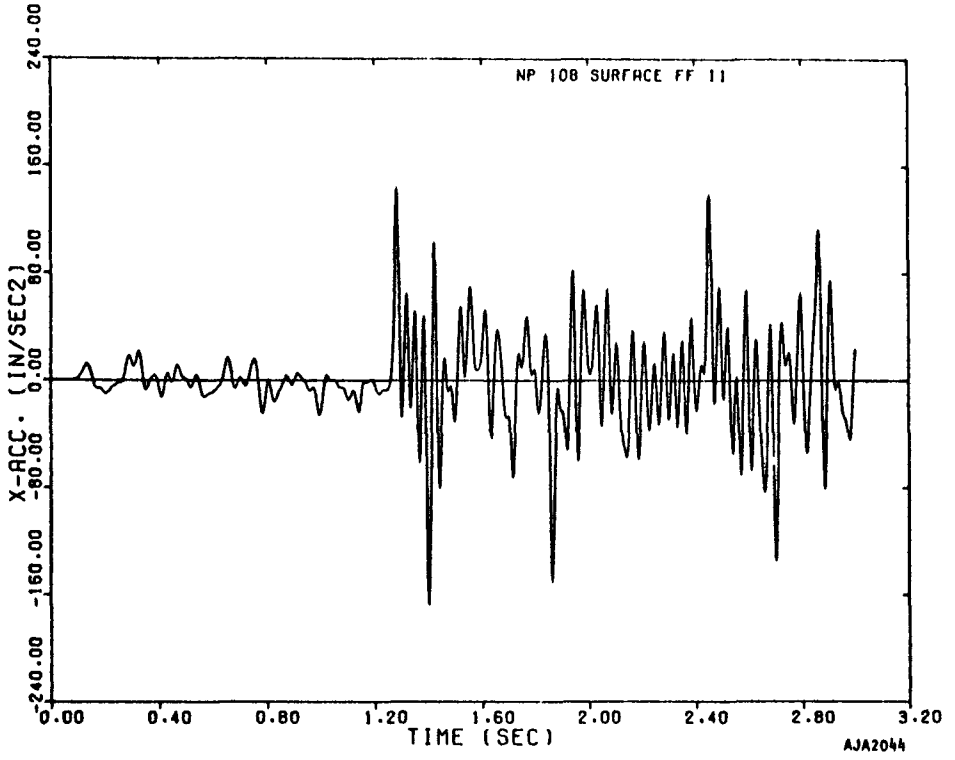

FIGURE 5-9. HORIZONTAL ACCELERATION, SURFACE, FREE FIELD, CASE I-1

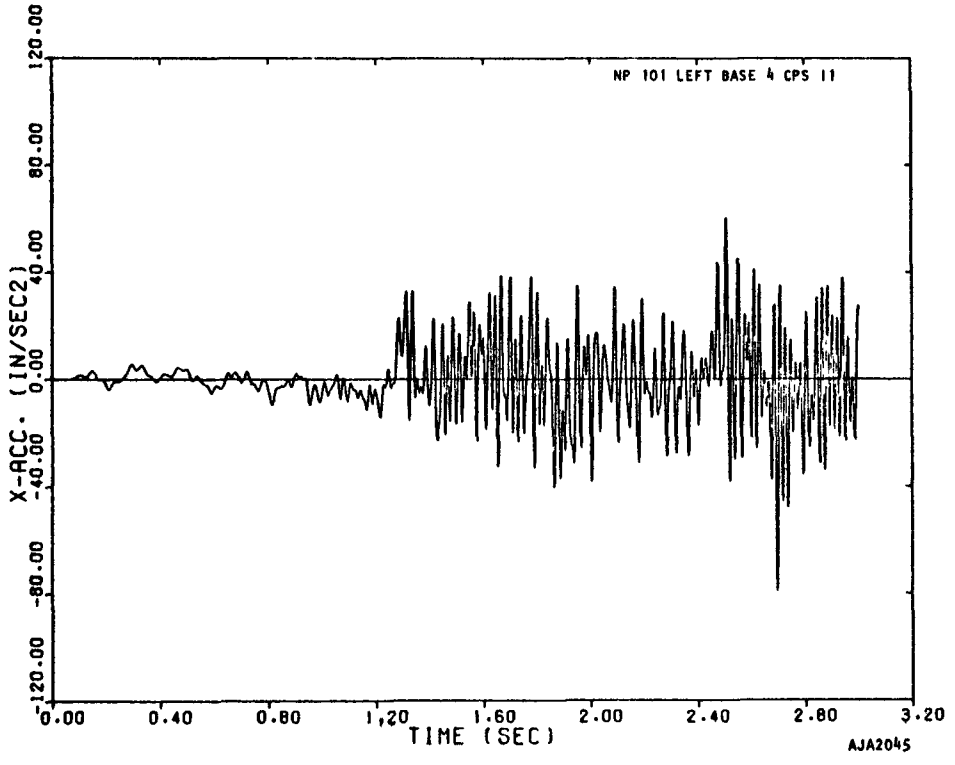

FIGURE 5-10. HORIZONTAL ACCELERATION, FOUNDATION OF STRUCTURE, CASE I-1

Cases 3 and I-1, the dominant frequency is 4 to 6 cps. Since the oscillators give the structure significant frequency response in the range 3 to 5 cps, greater interaction and hence suppression of structural response is expected and observed in Cases 3 and I-1 than in Case 6.

This finding is modified when the soil is made softer. As shown in Table 5-3, the amount of suppression is increased significantly when plastic deformation occurs in the soil. This is illustrated by comparing Cases 6 and I-1.

Numerical oscillations induced by the integration technique in the present inelastic finite-element program interfere with interpreting response at frequencies higher than 6 to 8 cps. Accelerations from Case I-1, Figures 5-9 and 5-10, illustrate the problem. A significant part of the foundation response, Figure 5-10, is in the frequency range 10 to 30 cps, which is too high for the present finite-element mesh to represent accurately. The corresponding velocities, Figures 5-11 and 5-12, show the high-frequency accelerations to be merely small perturbations superposed on the main structural response. In order to present a true picture of the acceleration responses in Table 5-3, an attempt was made to separate the true acceleration pulse from the superposed high-frequency numerical noise. Figures 5-11 and 5-12 and similar figures for other cases were used to guide the interpolation of computed accelerations, such as Figures 5-9 and 5-10. A more objective way of obtaining accelerations would be to filter the velocity/time histories and then perform numerical differentiation. This is beyond the scope of the present work, however.

The following summarizes present findings regarding horizontal motion of the foundation relative to the free field:

a. The horizontal response spectra of the foundation are suppressed relative to the free field. The suppression factor varies from about 0.2 to 1.0 in most cases. A typical suppression ratio for elastic soils in the frequency range 3 to 5 cps is 0.5, while for inelastic soils, it is 0.3.

b. The suppression is greater (ratio is smaller) when the structure has natural frequencies in the same range as the frequencies of

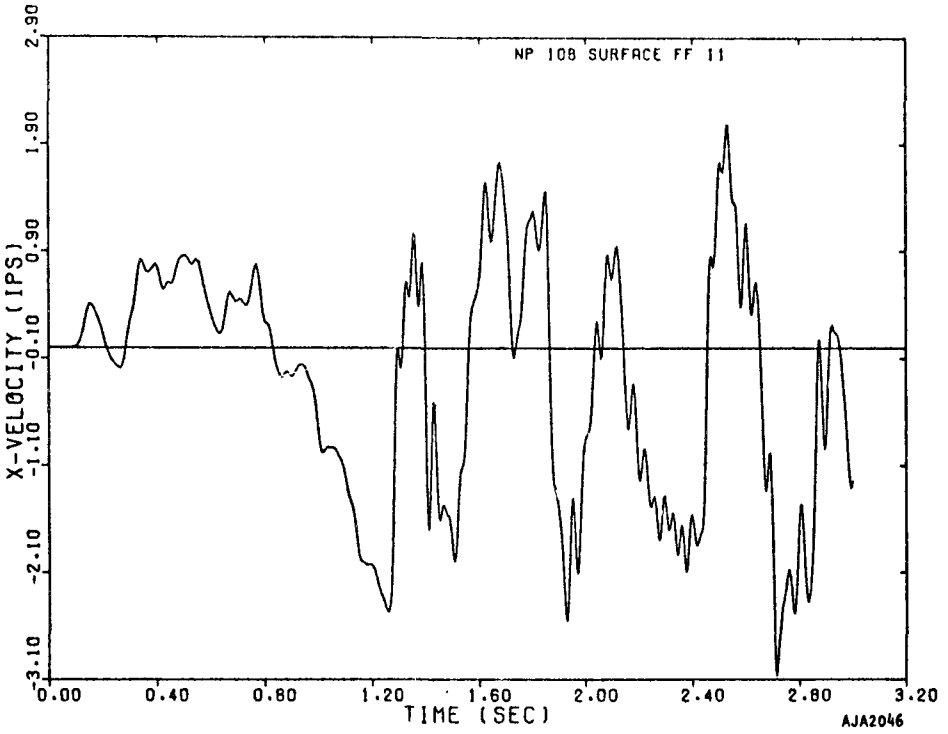

FIGURE 5-11. HORIZONTAL VELOCITY, SURFACE OF FREE FIELD, CASE I-1

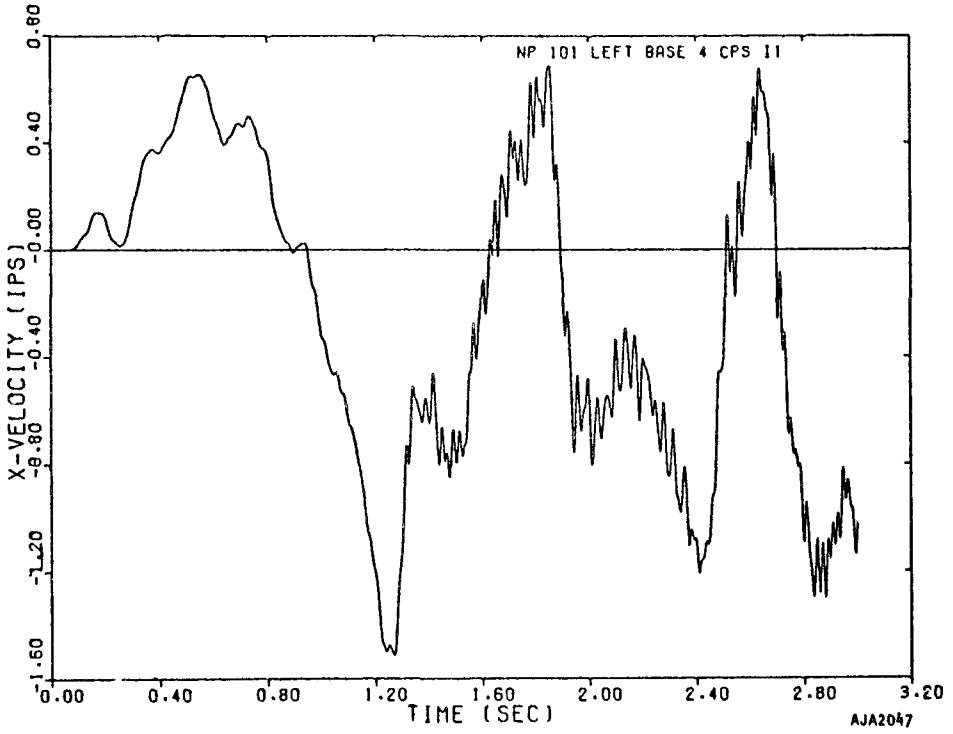

FIGURE 5-12. HORIZONTAL VELOCITY, FOUNDATION OF STRUCTURE, CASE I-1

the input. Suppression may occur over a wide range of frequencies, but tends to be maximum (ratio is minimum) near natural frequencies of the structure. (Greatest suppression of foundation spectra occurs in Cases 3, 4, and 5 at 2.5 to 5 cps, which is the frequency range where input and structural response overlap. Suppression of foundation spectra is more nearly uniform in Case 6, where the dominant input frequencies (1 to 2 cps) do not overlap the structural frequencies (2.5 to 5 cps)).

c. Horizontal response spectra of the foundation are suppressed more in softer soils than in stiffer soils. (Cases 3, 4, and I-1 relative to Case 5; Case I-2 relative to Case 6.)

d. The peak horizontal accelerations of the foundation are suppressed relative to the peak free-field surface accelerations by factors of 0.4 to 0.7. Peak foundation velocities are suppressed by factors of 0.5 to 1.0.

e. The present inelastic finite-element computer program tends to generate high-frequency accelerations, which complicates interpreting acceleration/time histories. This difficulty can be overcome by filtering the acceleration response; smoothing the velocity/time histories and redifferentiating appears to be a practical method.

The vertical response of the structure occurs at predominantly lower frequencies than that of the corresponding free field, as Figures 5-13 through 5-16 illustrate. This frequency shift appears in the spectra (Table 5-3, Figures 5-2 and 5-4) as amplification of foundation response over that of the free field at low frequency and suppression at higher frequencies. This trend is clearly shown in Table 5-3 where the peak accelerations (high frequency) are amplified and the peak velocities (lower frequency) are suppressed. This frequency shift is not related to vertical vibration of the oscillators, since the fundamental frequencies of these are 24 cps for the taller and 32 cps for the shorter. Probably the shift

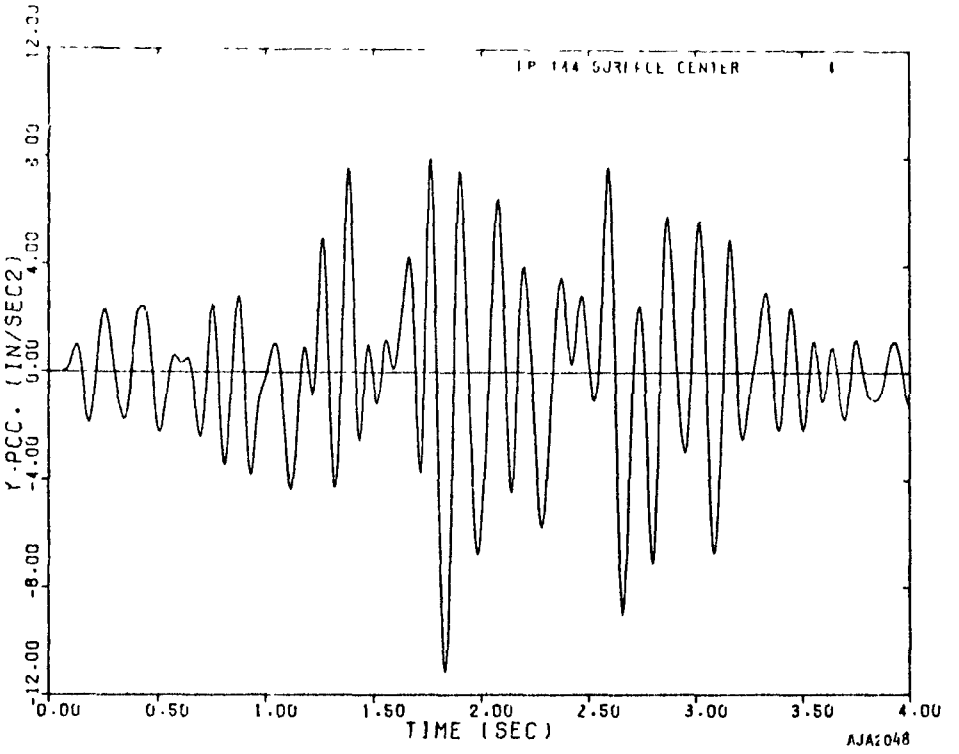

FIGURE 5-13. VERTICAL ACCELERATION OF FREE FIELD SURFACE, CASE 4

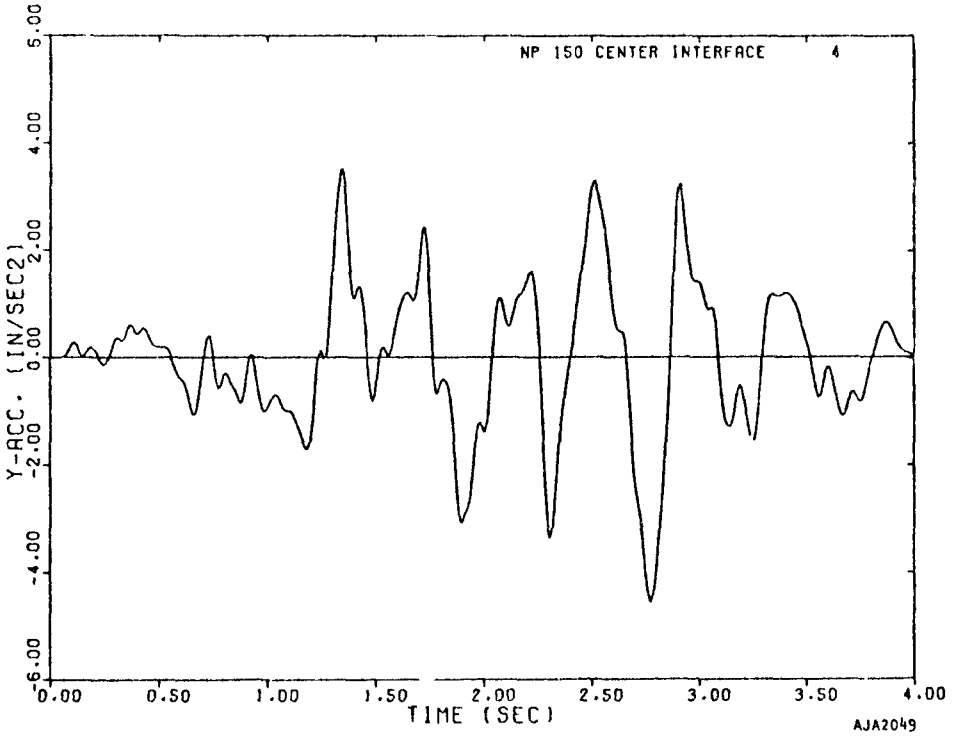

FIGURE 5-14. VERTICAL ACCELERATION OF STRUCTURE FOUNDATION, CASE 4

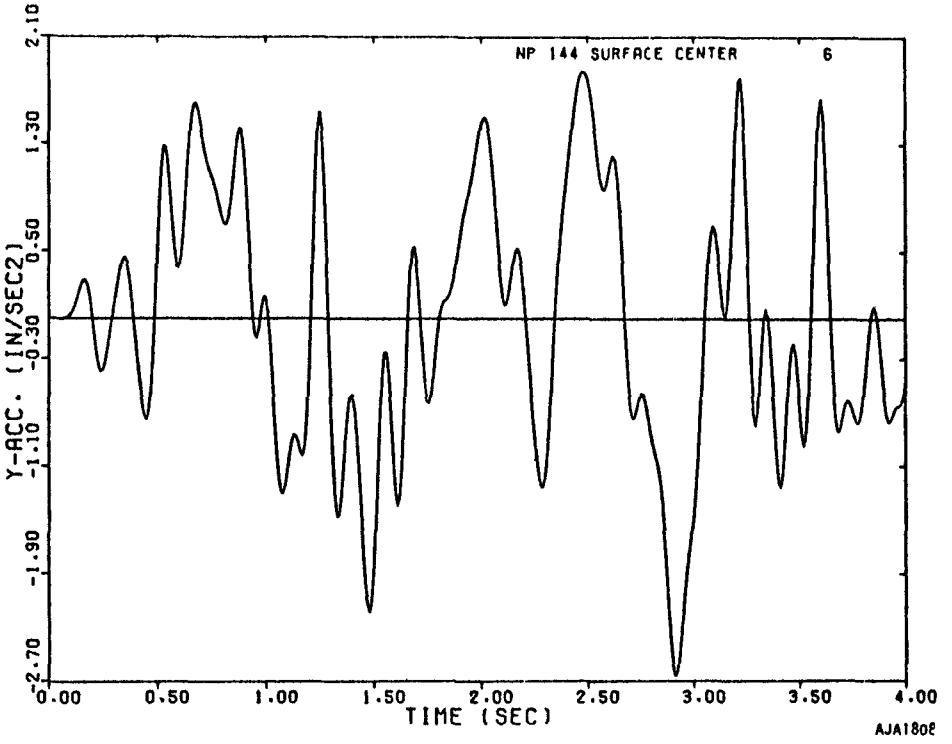

FIGURE 5-15. VERTICAL ACCELERATION, SURFACE OF FREE FIELD, CASE 6

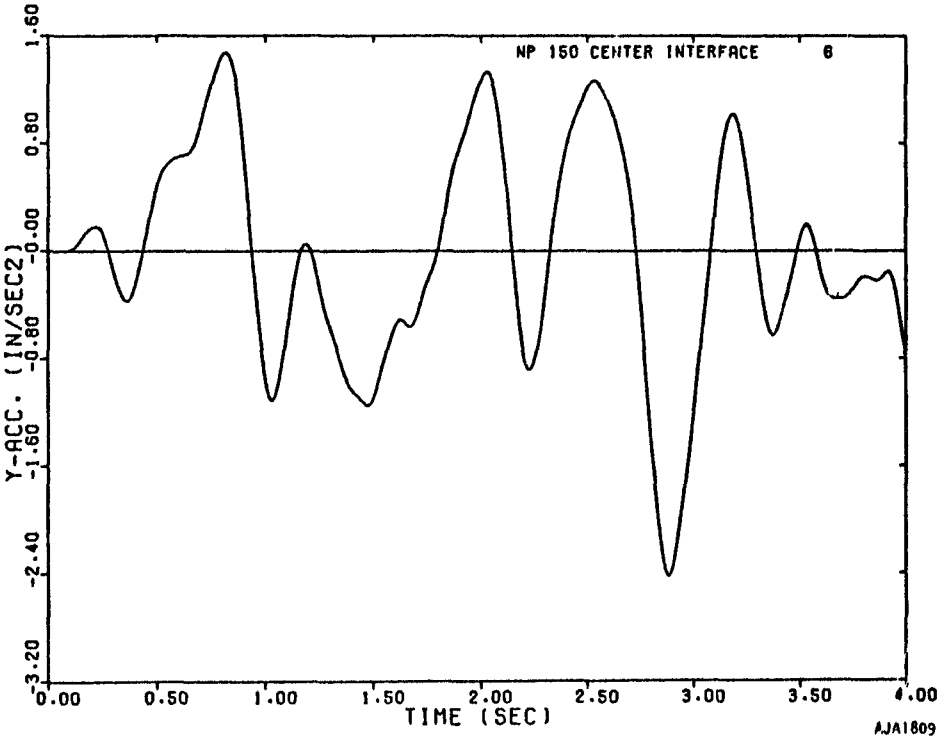

FIGURE 5-16. VERTICAL ACCELERATION OF FOUNDATION, CASE 6

in frequency is due to vertical interaction, which is controlled by the fundamental frequency of the entire embedded structure. The fundamental frequency was not determined in the present study, but it appears likely to be in the range of 1 to 5 cps.

RELATION BETWEEN STRESS IN FREE FIELD AND STRESS ADJACENT TO STRUCTURE

The present study indicates that stresses in the soil adjacent to the structure in general differ from the stress which would develop at the same point in the soil if the structure were not present. One general finding is that the horizontal stress in the soil beneath the foundation is less than the corresponding free-field stress. This appears to be due to the stiffness of the foundation being much greater than that of the soil and attracting load to itself. This is illustrated in Figures 5-17 through 5-20.

A second finding is that the interaction stress appears to be uniquely related to the velocity of the structure. This is illustrated in Figures 5-21 through 5-26, where the shapes of the structural-velocity/time history and the interaction-stress/time histories correlate with each other but do not correlate with the free-field stress/time history.

The extent of inelastic deformation in the soil surrounding the structure is compared with that in the free field for Cases I-1 and I-3 at selected instants of time in Figures 5-27 through 5-30. Figure 5-27(a) shows the areas of inelasticity surrounding the structure in Cases I-1 and I-3 at $t = 0.498$ sec (there is no inelasticity in the corresponding free field at this time). Figure 5-27(b) illustrates the instantaneous growth of the inelastic zone surrounding the structure in Case I-3 when the shear strength of the soil is abruptly decreased to represent liquefaction. Figures 5-28(a) and (b) show the inelastic zones in the free field and near the structure in Case I-1 at $t = 1.2$ sec. The extent of inelastic deformation in the free field of Case I-1 is unusual. The effect of the structure as indicated in Figure 5-28(b) is to stiffen the soil and reduce the extent of inelastic deformation. Figure 5-28(c) shows how reducing the shear strength of the soil greatly increases the extent of

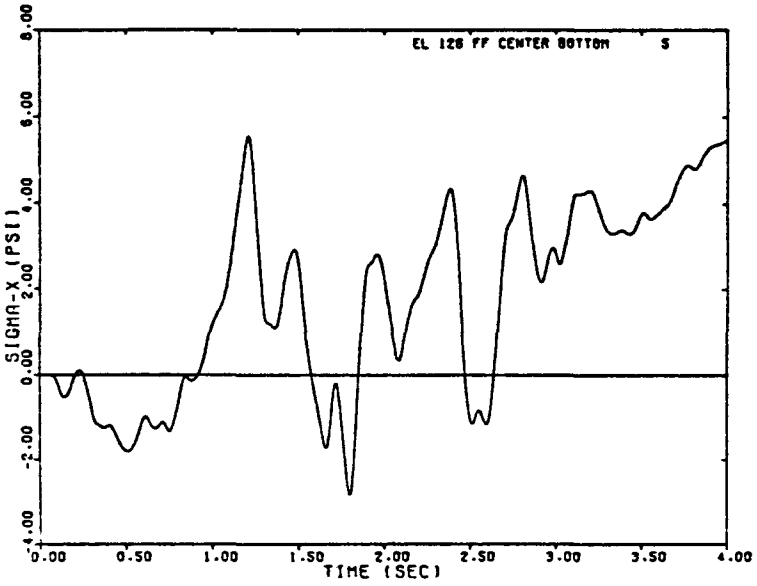

FIGURE 5-17. HORIZONTAL STRESS IN FREE FIELD, CORRESPONDING TO MIDPOINT OF FOUNDATION, CASE 5

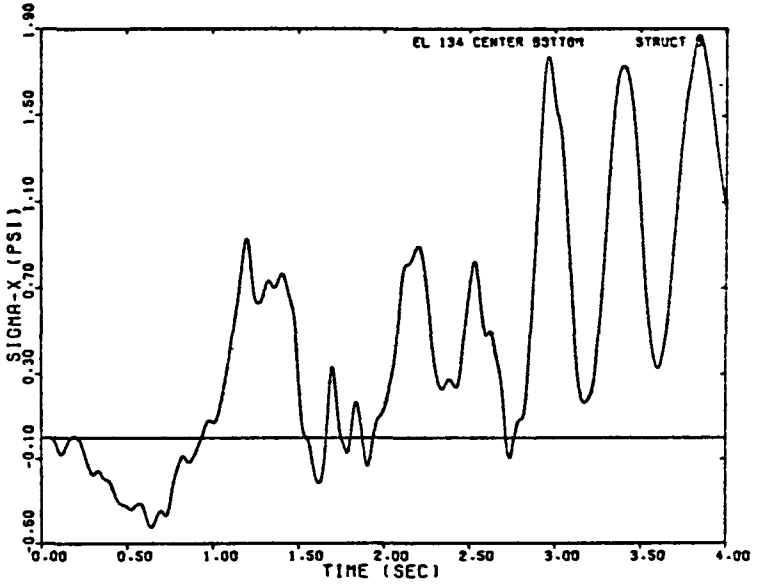

FIGURE 5-18. HORIZONTAL STRESS IN SOIL BENEATH MIDPOINT OF FOUNDATION, CASE 5

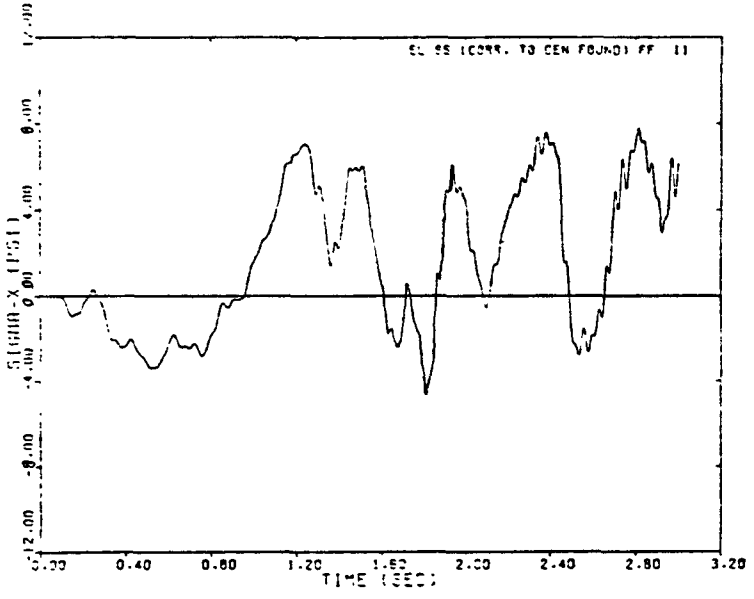

FIGURE 5-19. HORIZONTAL STRESS IN FREE FIELD CORRESPONDING TO MIDPOINT OF FOUNDATION, CASE 1-1

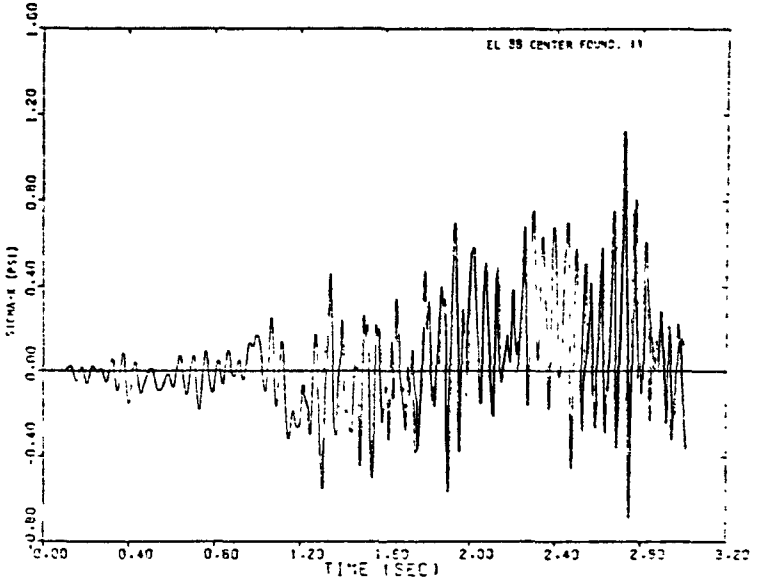

FIGURE 5-20. HORIZONTAL STRESS IN SOIL BENEATH MIDPOINT OF FOUNDATION, CASE 1-1

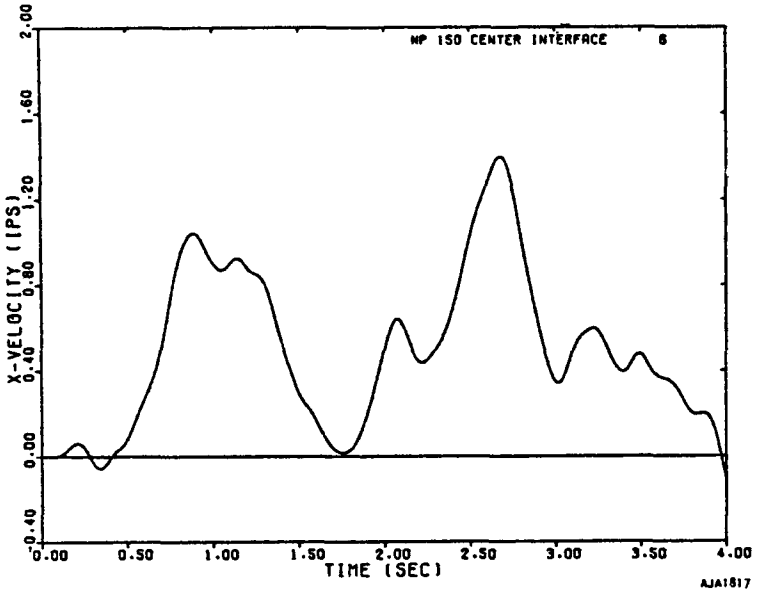

FIGURE 5-21. HORIZONTAL VELOCITY OF FOUNDATION

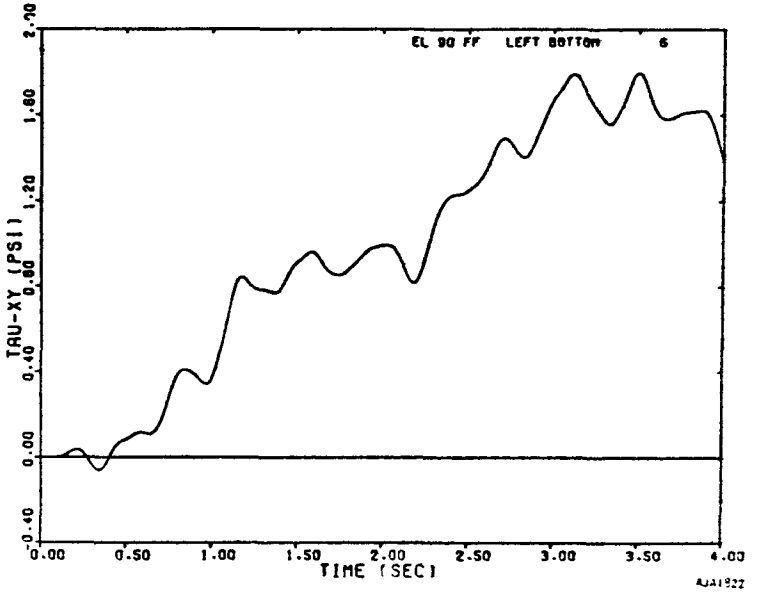

FIGURE 5-22. SHEAR STRESS IN FREE FIELD AT POINT CORRESPONDING TO LOWER LEFT CORNER OF FOUNDATION

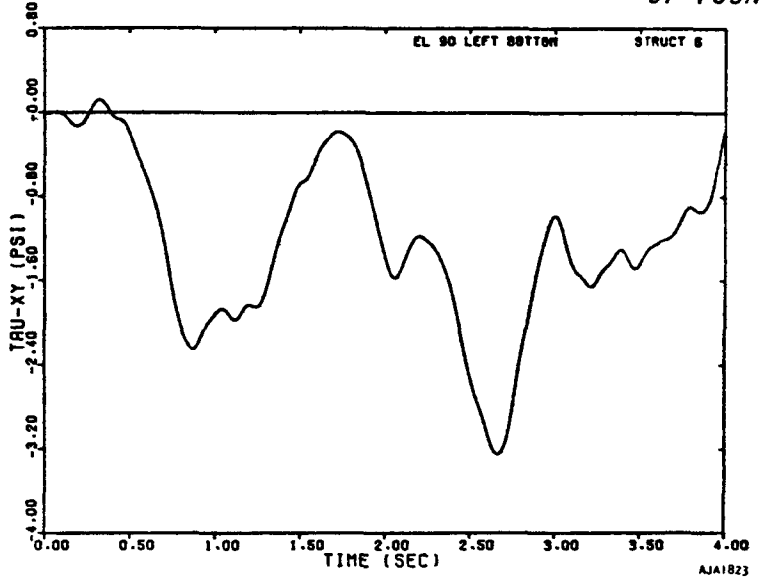

FIGURE 5-23. SHEAR STRESS IN SOIL BELOW LEFT CORNER OF FOUNDATION

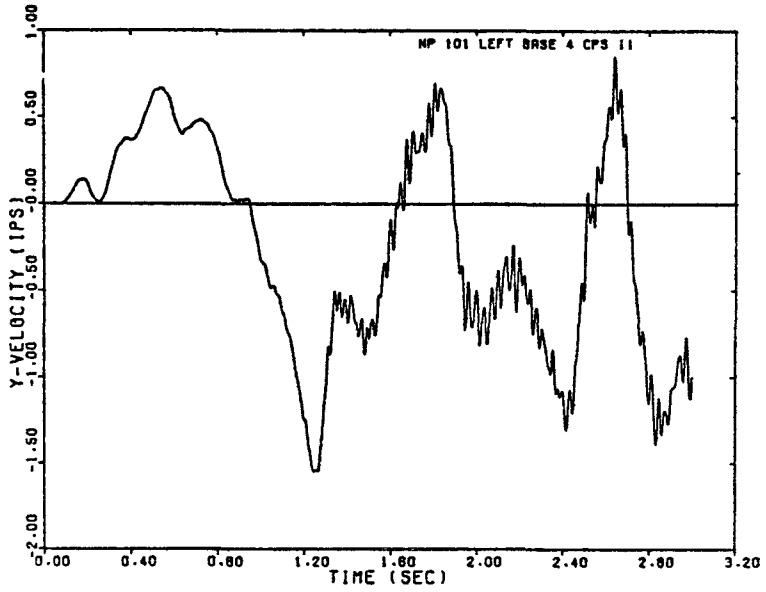

FIGURE 5-24. VERTICAL VELOCITY OF FOUNDATION

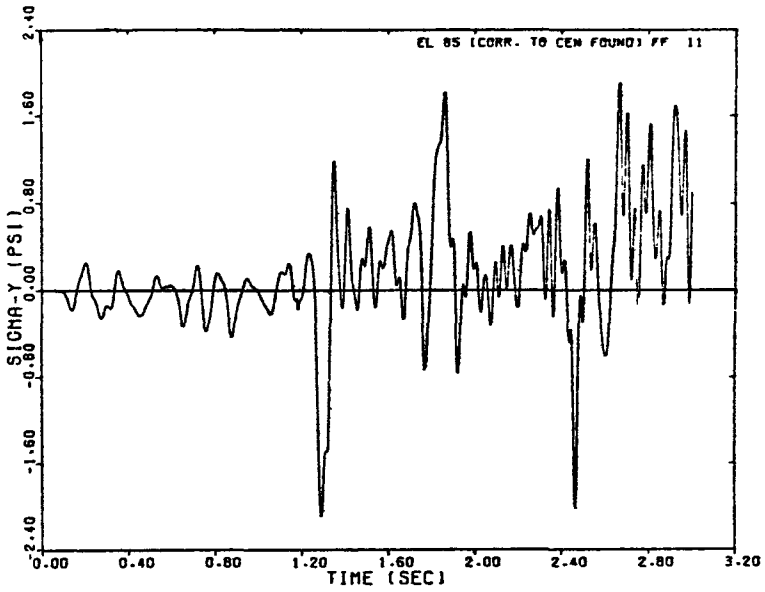

FIGURE 5-25. VERTICAL STRESS IN FREE FIELD CORRESPONDING TO MIDPOINT OF FOUNDATION, CASE I-1

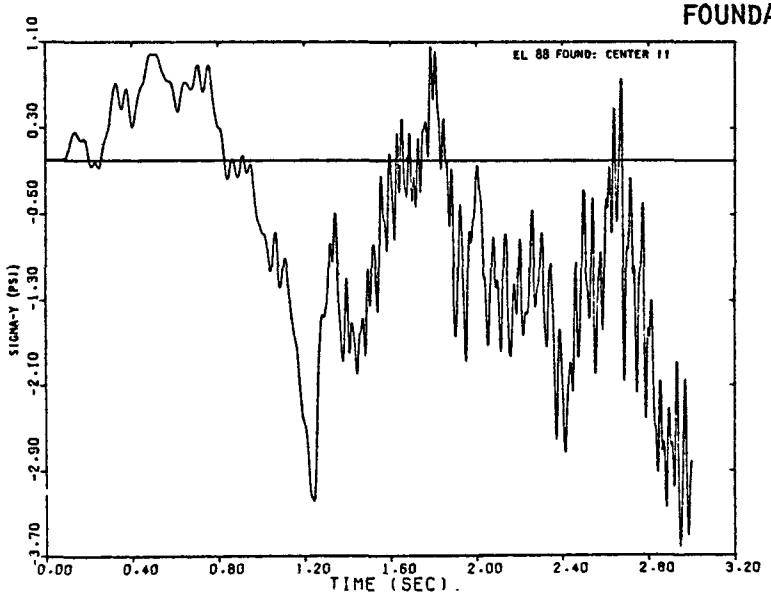

FIGURE 5-26. VERTICAL STRESS IN SOIL BENEATH MIDPOINT OF FOUNDATION, CASE I-1

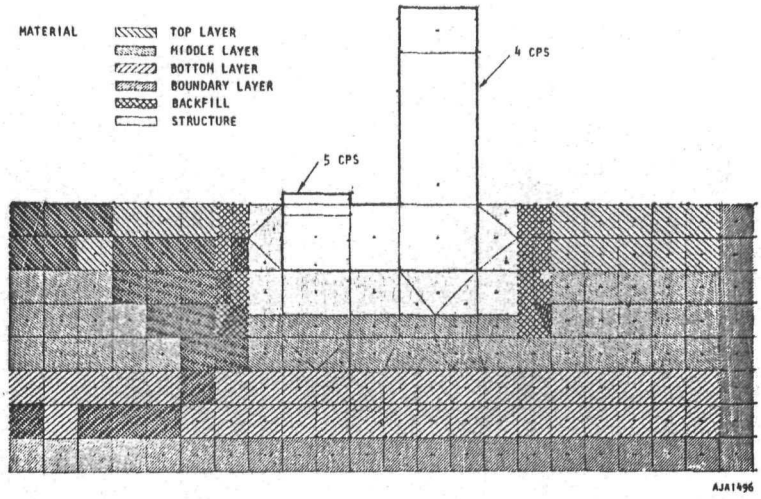

(a) INELASTIC ZONES AT t = 0.498 SEC (LAST STEP USING ORIGINAL STRENGTH) CASES I-1 AND I-3

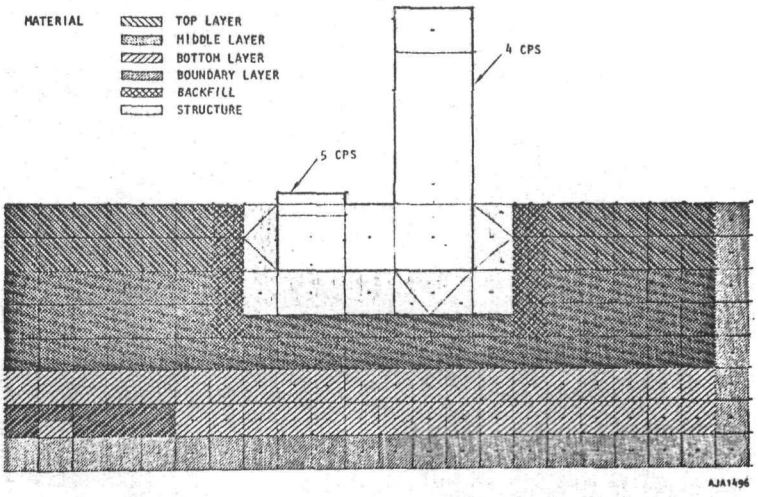

(b) INELASTIC ZONES AT t = 0.501 SEC (FIRST STEP USING DECREASED STRENGTH), CASE I-3

FIGURE 5-27. DEVELOPMENT OF PLASTICITY DUE TO ABRUPT DECREASE STRENGTH OF SOIL; ALSO EXTENT OF PLASTICITY IN CASE I-1 AT 5 = 0.498 SEC

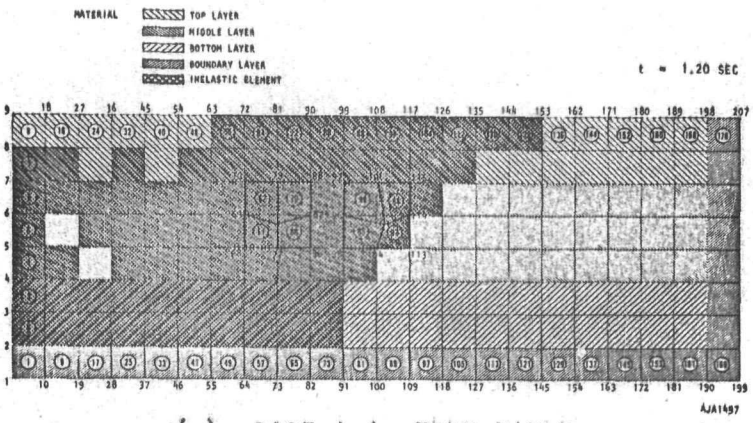

(a) CASE I-1, FREE FIELD

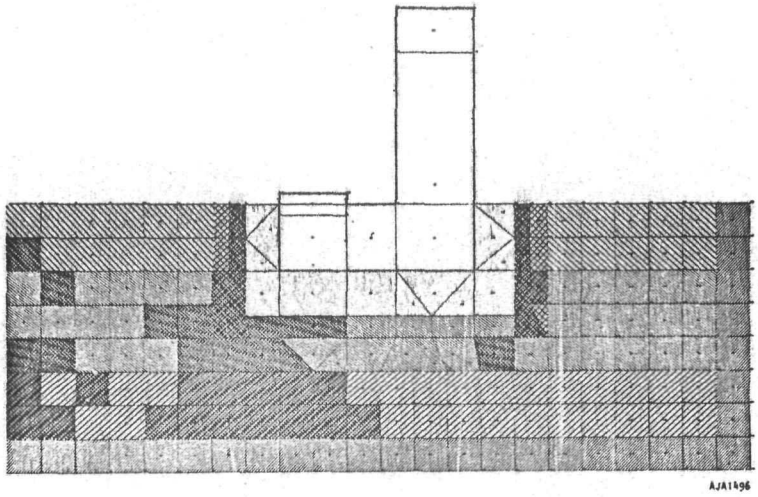

(b) CASE I-1, WITH STRUCTURE

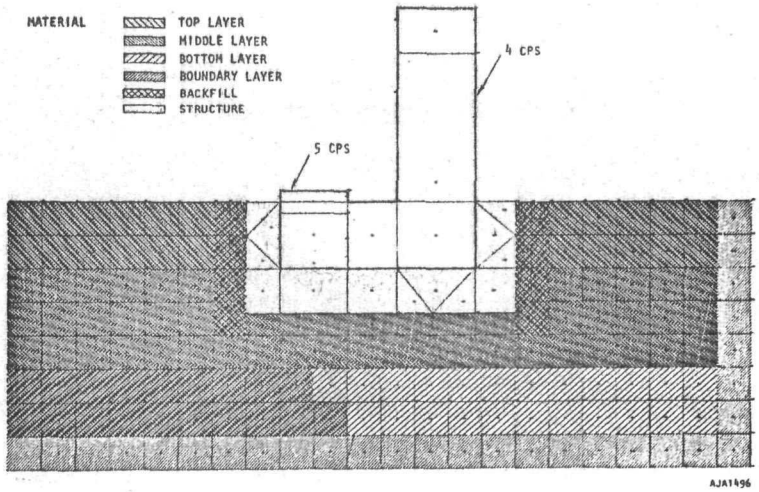

(c) CASE I-3, WITH STRUCTURE

FIGURE 5-28. INELASTIC ELEMENTS IN FREE FIELD AND INTERACTION ZONE AT t = 1.20 SEC, CASES I-1 AND I-3

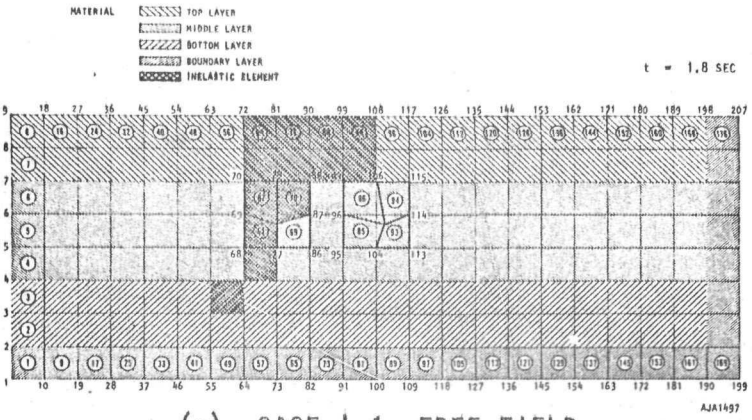

(a) CASE I-1, FREE FIELD

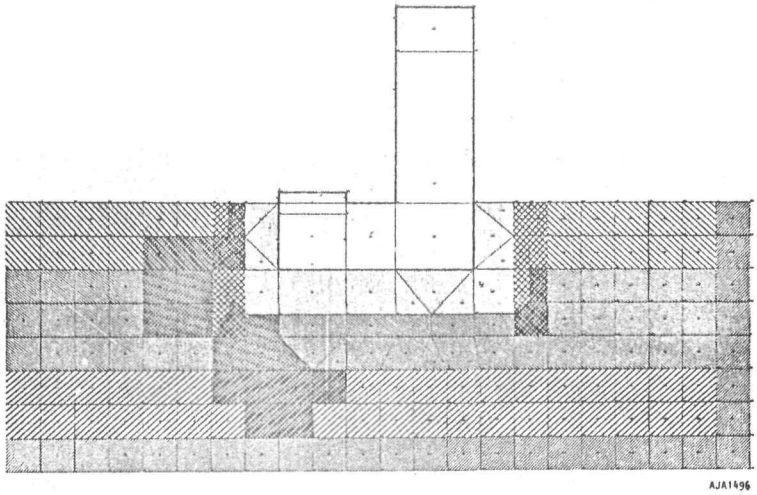

(b) CASE I-1, WITH STRUCTURE

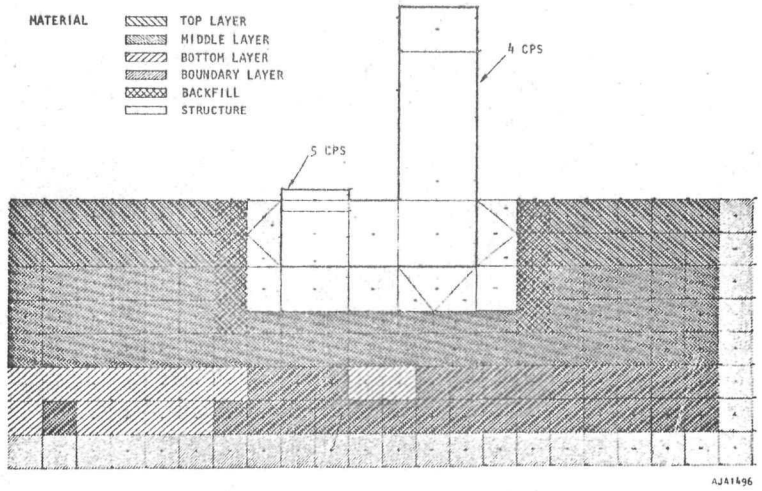

(c) CASE I-3, WITH STRUCTURE

FIGURE 5-29. INELASTIC ELEMENTS IN FREE FIELD AND INTERACTION ZONE AT t = 1.8 SEC, CASES I-1 AND I-3

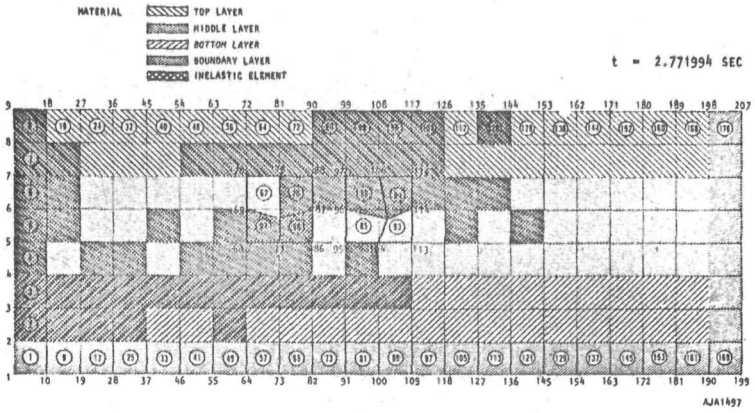

(a) CASE I-1, FREE FIELD

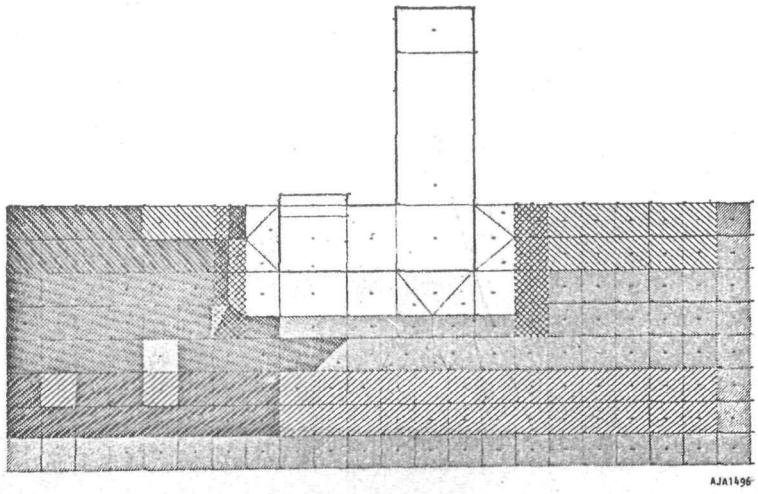

(b) CASE I-1, WITH STRUCTURE

FIGURE 5-30. INELASTIC ELEMENTS IN FREE FIELD AND INTERACTION ZONE AT t = 2.772 SEC, CASE I-1

inelasticity. Figure 5-29 shows the same type of information as is in Figure 5-28 at $t = 1.8$ sec. Inelasticity in the free field of Case I-1, Figure 5-29(a), is in a limited zone which appears to be migrating toward the right. Inelasticity is concentrated on the left (input) side of the structure in Case I-1, Figure 5-29(b). This is because the leftward displacement of the input induces tensile stresses in the soil between the left boundary and the left wall of the structure. Since the soil is assumed to have little tensile strength, this is a favored region for inelasticity. The soil between the right wall of the structure and the right boundary is somewhat shielded from this effect by the inertia of the structure. Figure 5-29(c) shows the zones of inelasticity for Case I-3, where liquefaction of the soil is assumed. Figure 5-30 shows inelasticity in the soil in Case I-1 at $t = 2.77$ sec. The effect of leftward displacement which induces tensile stress in the soil dominates the response.

The wide extent of plastic deformation in Case I-1 and especially I-3 suggests that large displacements would occur.

Case I-3 attempts to create a situation in which exceptionally large displacements, comparable to the original dimensions of an element can occur. Since the coordinates of nodal points are defined as their original coordinates plus their current displacements, the elements were expected to become greatly distorted which would lead eventually to negative area for one of the elements and to terminating execution. This is not the familiar definition of instability in terms of rate of strain energy release, but is an attempt to calculate onset of large displacements.

Horizontal displacement is about the same in Cases I-1 and I-3 (Figure 5-31) because the dominant force applied by the soil to the structure is by direct stresses on the structure walls. The soil adjacent to the walls is plastic in both cases beginning at early times, and hence, the structure is subjected to about the same net horizontal force in both cases. The difference in horizontal displacements between Cases I-1 and I-3 is probably due to a wider extent of plastic deformation in the soil in Case I-3 with resulting increases in flexibility and natural periods of the system.

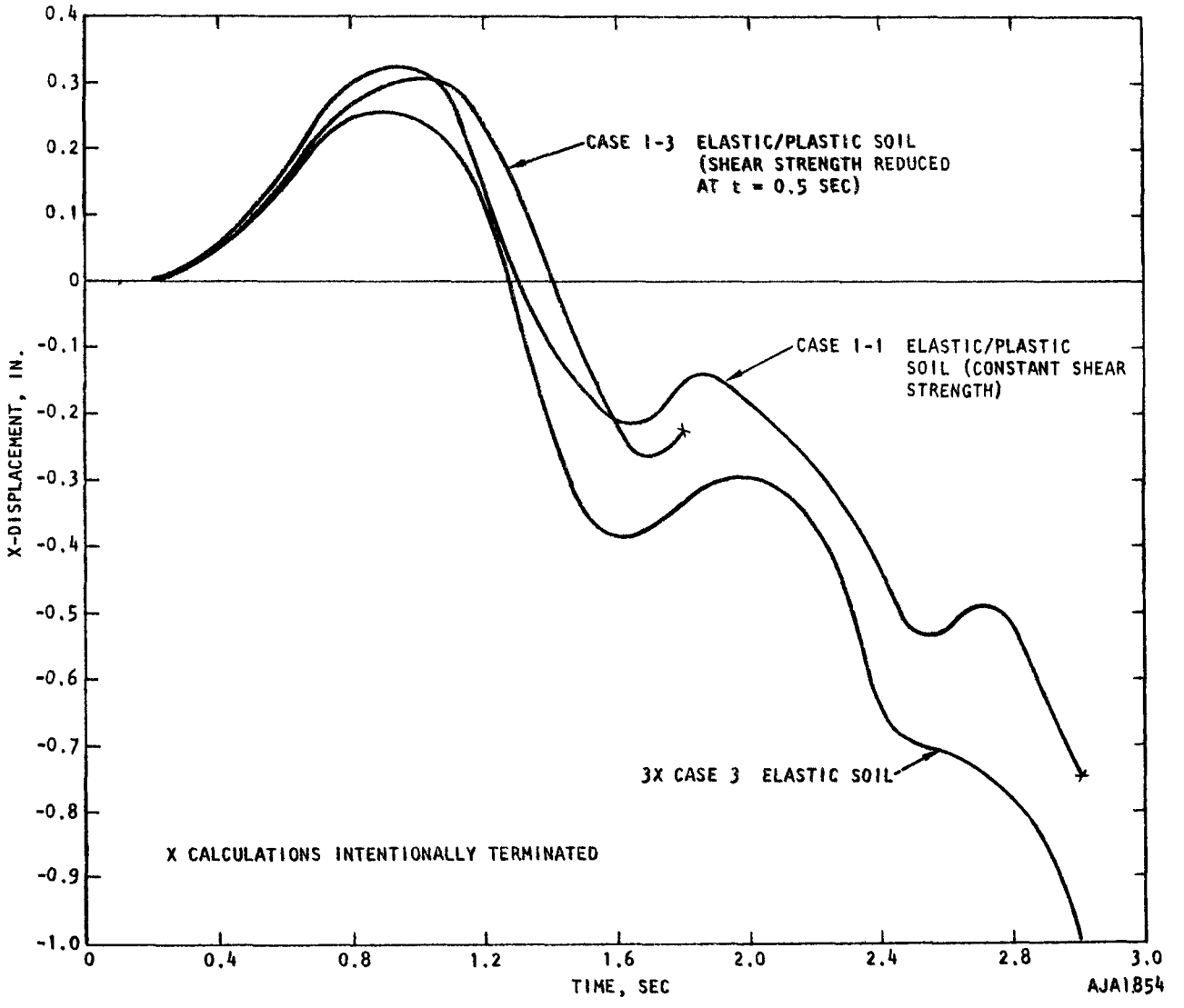

FIGURE 5-31. HORIZONTAL DISPLACEMENT OF FOUNDATION, CASES 3, 1-1, 1-3

The surprising result of the calculations is that the scaled displacements in Case 3 (Input to Case 3 was 1 x Golden Gate; Input to Cases 1-1 and 1-3 was 3 x Golden Gate) are greater than those in both Cases 1-1 and 1-3. The result is apparently related to attenuation of displacements due to energy dissipation in the soil. Apparently the

effects of energy dissipation overcome the effects of increased flexibility of the soil. This result would be very difficult to accept if it were not for the fact that the horizontal force of the soil on the structure is governed by direct stress on the walls rather than by shear stresses on the foundation. The direct stress/strain relationship for plastic deformation under uniaxial strain is only about two times less stiff for the soil of Cases I-1 and I-3 than for the perfectly elastic soil of Case 3. Of course, the shear-stress/strain relation is vastly more flexible in Cases I-1 and I-3 than in Case 3; but since shear stress on the foundation bottom has little effect on the motion, reducing the shear stress by reducing strength also has little effect. (The elastic and elastic/plastic stress/strain relationships are illustrated in Figure 5-32.)

The influence of plasticity on the interaction forces seems to be more important, relative to energy dissipation, for vertical displacements than it is for horizontal displacements. This is illustrated in Figure 5-33. In Case 3, the main interaction force at $t > 0.8$ sec is provided by shear stresses acting on the vertical walls of the structure. If the soil adjacent to the walls is allowed to become plastic, as in Cases I-1 and I-3, larger vertical displacements are expected. Figure 5-33 shows that the vertical displacements are 2.5 to 3 times greater in the cases with inelastic soil than in the case with elastic soil. It might be expected that the computed vertical displacements in Case I-3 would be even larger due to the fact that the maximum shear force available for resisting vertical structural motion is very small. This result has not definitely been explained in terms of the present mathematical model, but it seems related to the fact that there is only a small upward force acting from beneath the foundation, which arises from confined compression of the soil. Including a vertical component of earthquake motion might change the outcome of the calculations considerably. In addition to considering a vertical component of earthquake input, future calculations should account for the weight of the structure, which may affect vertical displacements as much as any factor considered in the present calculations.

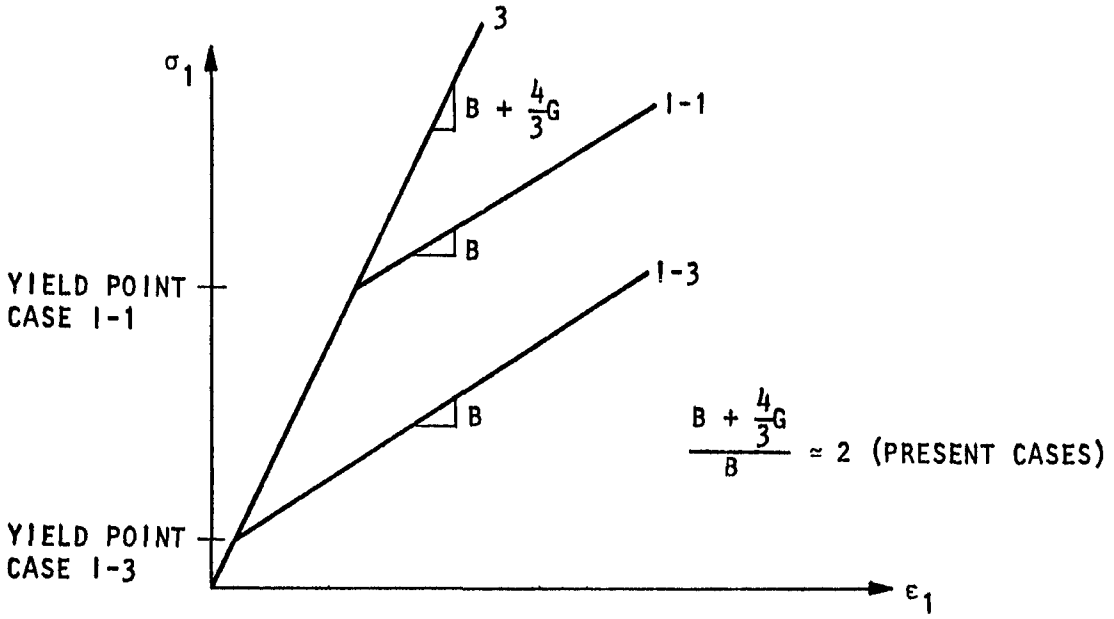

(a) DIRECT-STRESS/STRAIN RELATIONSHIP, UNIAXIAL STRAIN (POSTYIELDING STIFFNESS GOVERNS HORIZONTAL INTERACTION FORCE ON WALLS OF STRUCTURE)

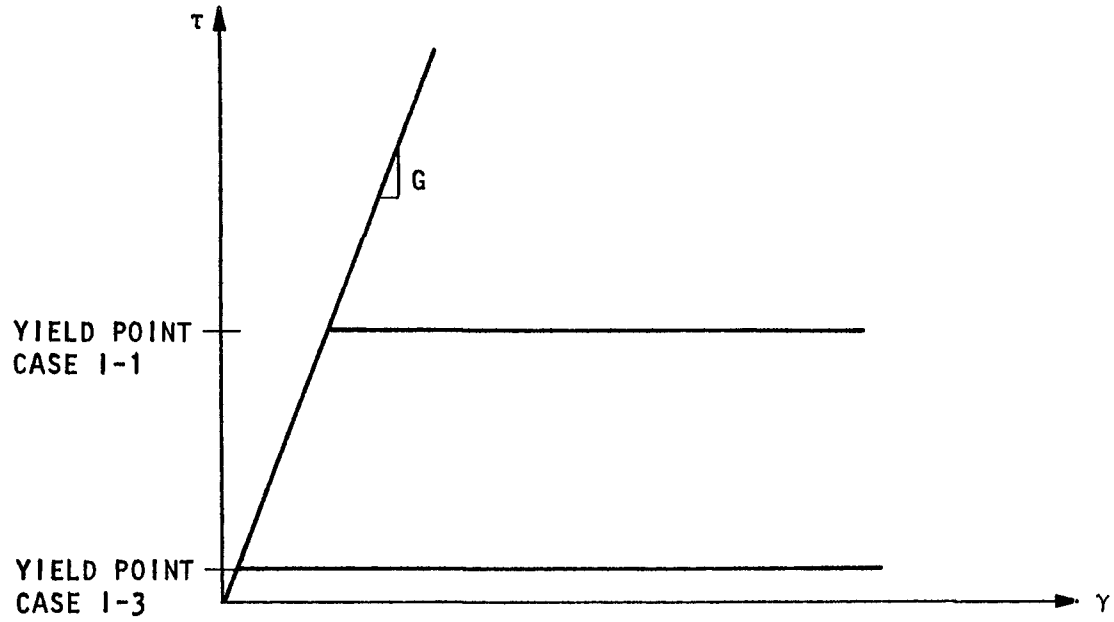

(b) SHEAR-STRESS/STRAIN RELATIONSHIP (POSTYIELDING STIFFNESS GOVERNS TANGENTIAL INTERACTION FORCE ON FOUNDATION)

AJA1851

FIGURE 5-32. STRESS/STRAIN RELATIONS IN SOIL PERTAINING TO INTERACTION

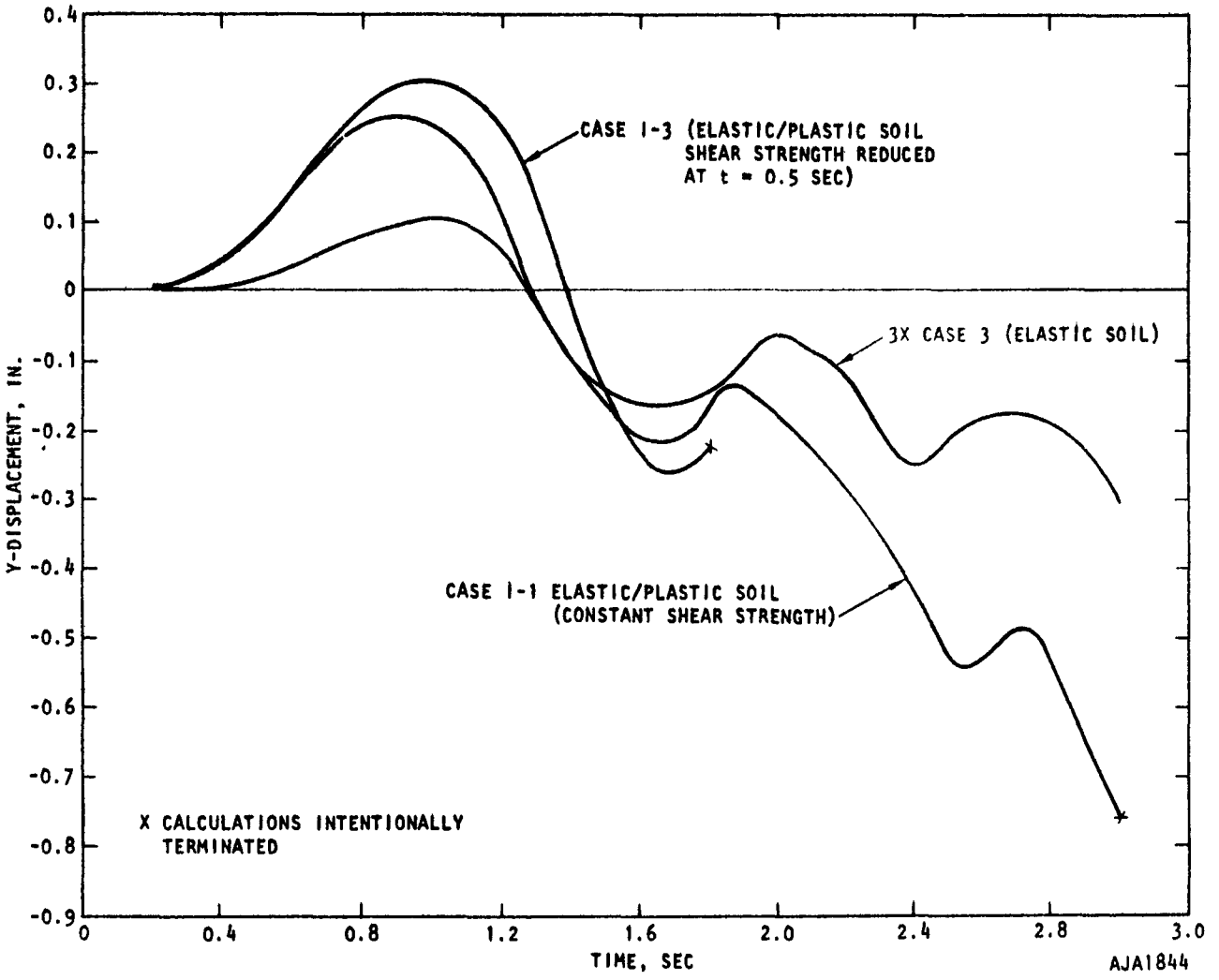

FIGURE 5-33. VERTICAL DISPLACEMENT OF FOUNDATION, CASES 3, I-1, I-3

RELATION BETWEEN RESPONSES OF FOUNDATION AND SUPERSTRUCTURE

The containment and internal support structures are represented in the present analysis by the 4-cps and 5-cps oscillators, respectively. Their response is governed by the translation and rotation of the foundation. It would be useful if the response of these structures and of equipment attached to them could be related in a simple way to the motion of the foundation. The following analysis investigates this relationship.

The time-varying response of each single-degree-of-freedom oscillator may be computed from the translation and projected rotation of the foundation as follows (derivation given in Appendix G):

$$\ddot{x} = \omega \int_0^t \ddot{u}(\tau) \sin [\omega(t - \tau)] d\tau$$

$$+ \omega \int_0^t L\ddot{\theta}(\tau) \sin [\omega(t - \tau)] d\tau \qquad (5\text{-}1)$$

where

$\ddot{u}$, $\ddot{\theta}$ = Time histories of horizontal acceleration and rotation of foundation

t = Interval of time over which $\ddot{u}$ and $\ddot{\theta}$ are given

τ = Variable in convolution integral

ω = Natural frequency of the oscillator

L = Height of top of oscillator above foundation

The maximum value $(\ddot{x})_{max}$ occurring during the interval $0 - t$ is the sum of the two terms in Equation 5-1 and is the spectral acceleration at the frequency ω.

$$(\ddot{x})_{max} = (\text{translation} + \text{projected rotation})_{max} \qquad (5\text{-}1a)$$

Equations 5-1 and 5-1a were verified by performing the indicated integration and comparing with $\ddot{x}$ at the tops of the oscillators. The next step is to determine whether the translational and rotational spectra can be superposed without regard to phase of $\ddot{u}(t)$ and $\ddot{\theta}(t)$. That is

$$(\ddot{x})_{max} \stackrel{?}{=} \left(\omega\int_0^t \ddot{u}(\tau)\ \sin\ [\omega(t-\tau)]d\tau\right)_{max} \left(\omega\int_0^t L\ddot{\theta}(\tau)\ \sin\ [\omega(t-\tau)]d\tau\right)_{max} \qquad (5\text{-}2)$$

The translational acceleration/time history, $\ddot{u}(t)$, and its response spectra, $(\text{translation})_{max}$, are shown in Figures 5-34 and 5-35 for Case 6. The rotational acceleration/time history, $\ddot{\theta}(t)$, and its response spectra, $(\text{rotation})_{max}$, are shown in Figures 5-36 and 5-37 for Case 6. The horizontal acceleration/time history $\ddot{x}(t)$ for the 4-cps oscillator in Case 6 is shown in Figure 5-38. Following Equation 5-2, $(\text{translation})_{max} + L(\text{rotation})_{max}$, at the appropriate frequencies, is compared with the peak acceleration $(\ddot{x})_{max}$ of the 4-cps and 5-cps oscillators. Table 5-4 summarizes the results of this comparison over a range of frequencies 2.5 to 5 cps to allow for the possibility that the natural frequencies of the oscillators are a little lower than the nominal values of 4 cps and 5 cps.

The results indicate that the peak response of oscillators representing the containment and support structures cannot be determined by simply adding the spectra of the two contributory motions at the foundation. It appears that the phase relation between these two motions is unfavorable for superposition of maximum amplitudes.

The response of light equipment attached to the containment structure (4-cps oscillator) may be represented by response spectra at various elevations on the structure. The responses in the range of 1 to 6 cps are shown in Figure 5-39 as ratios to the response of the foundation.

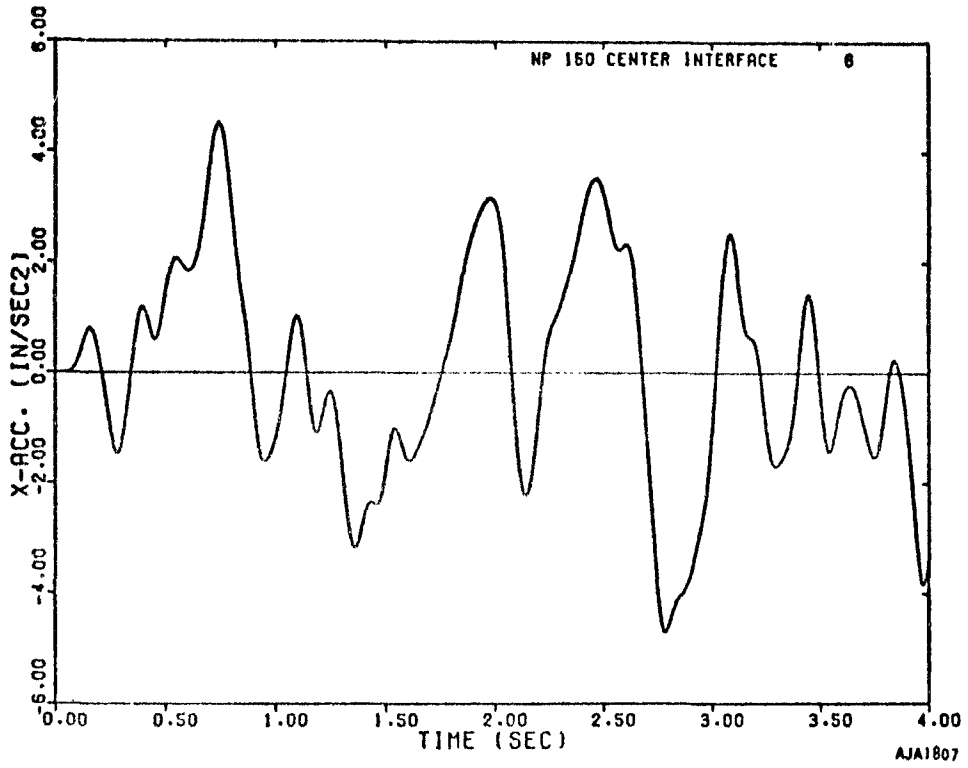

FIGURE 5-34. HORIZONTAL ACCELERATION OF FOUNDATION, CASE 6

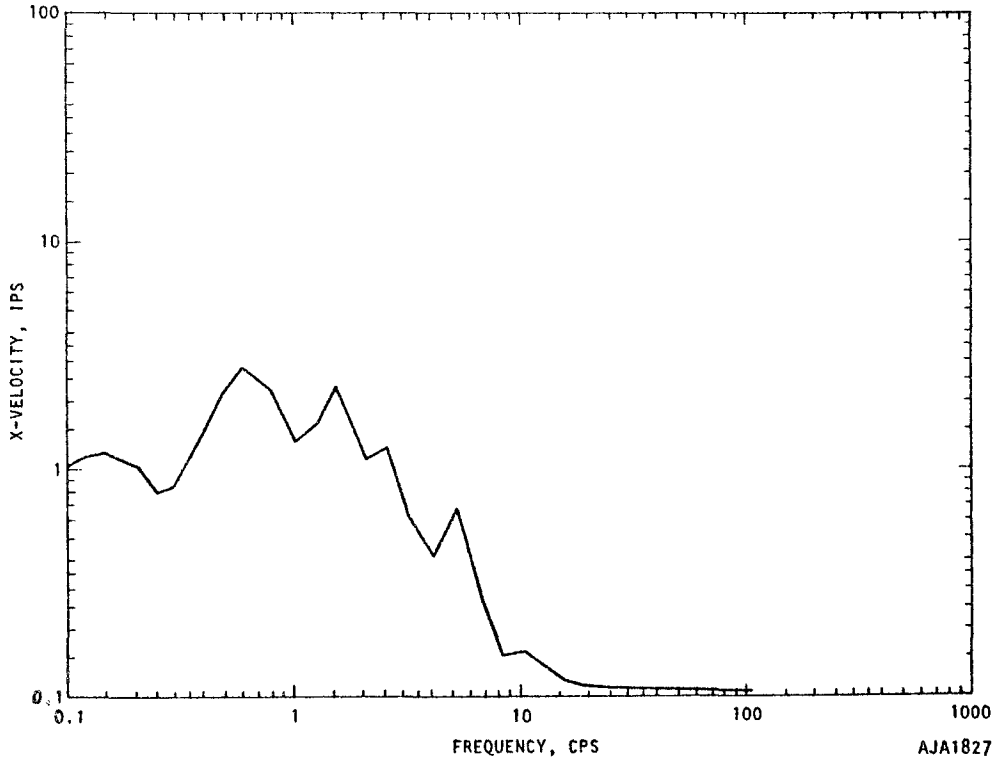

FIGURE 5-35. HORIZONTAL SPECTRA OF FOUNDATION, CASE 6

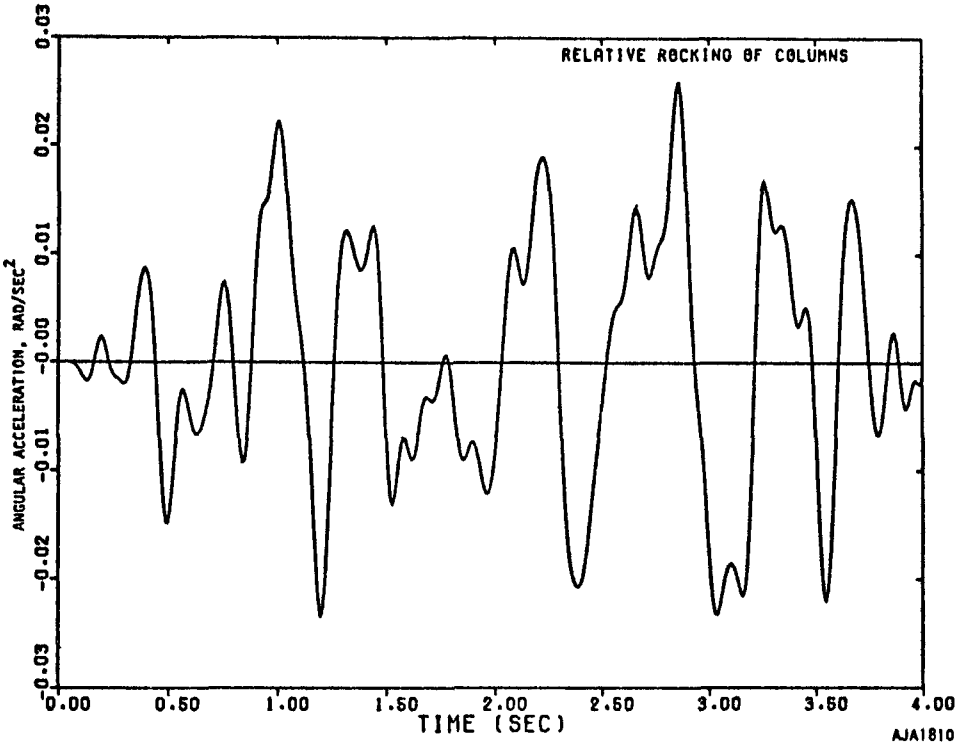

FIGURE 5-36. ANGULAR ACCELERATION/TIME HISTORY OF FOUNDATION, CASE 6

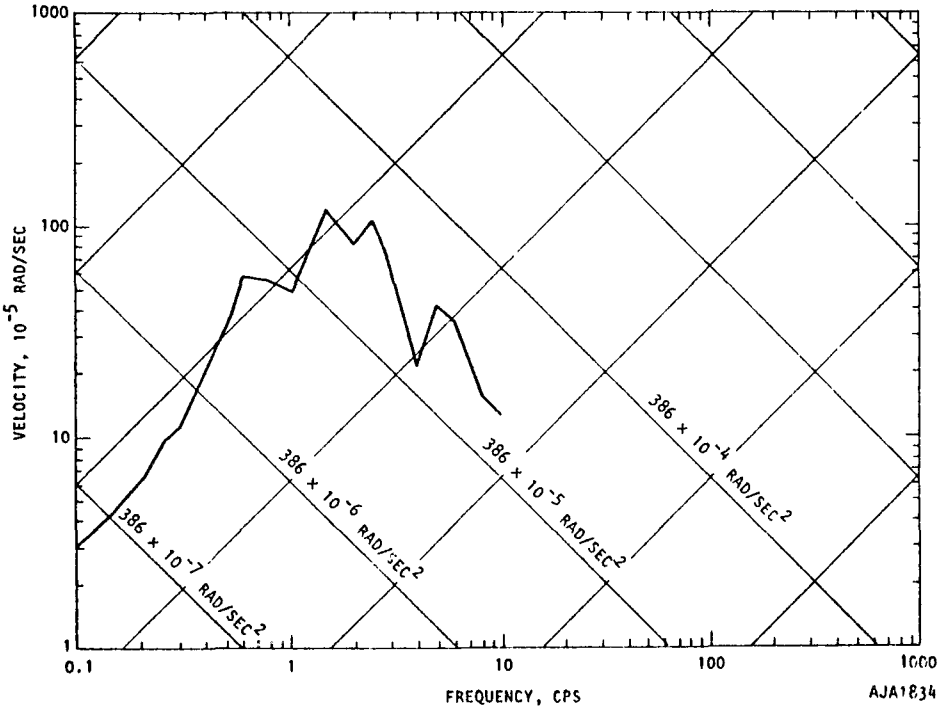

FIGURE 5-37. ANGULAR PSEUDO-VELOCITY SPECTRA, CASE 6

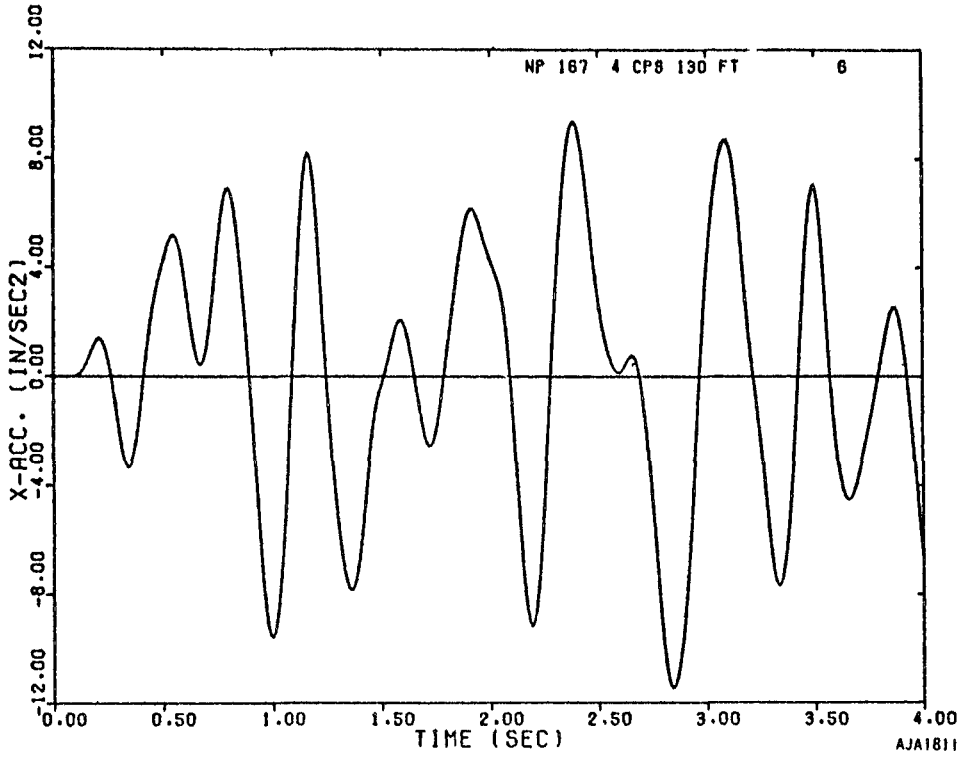

FIGURE 5-38. HORIZONTAL ACCELERATION, TOP OF 4 CPS OSCILLATOR, CASE 6

TABLE 5-4. RESPONSE OF OSCILLATORS RELATIVE TO ROTATION OF FOUNDATION, CASE 6

f, cps	Spectral Acceleration (base)		Total (base), g
	$(translation)_{max}$, g	$Lx(rotation)_{max}$, g	
2.5	0.051	0.072	0.123
3	0.033	0.051	0.084
4	0.027	0.022	0.049
5	0.055	0.056	0.111

Peak Acceleration

4 cps oscillator - 0.030 g

5 cps oscillator - 0.027 g

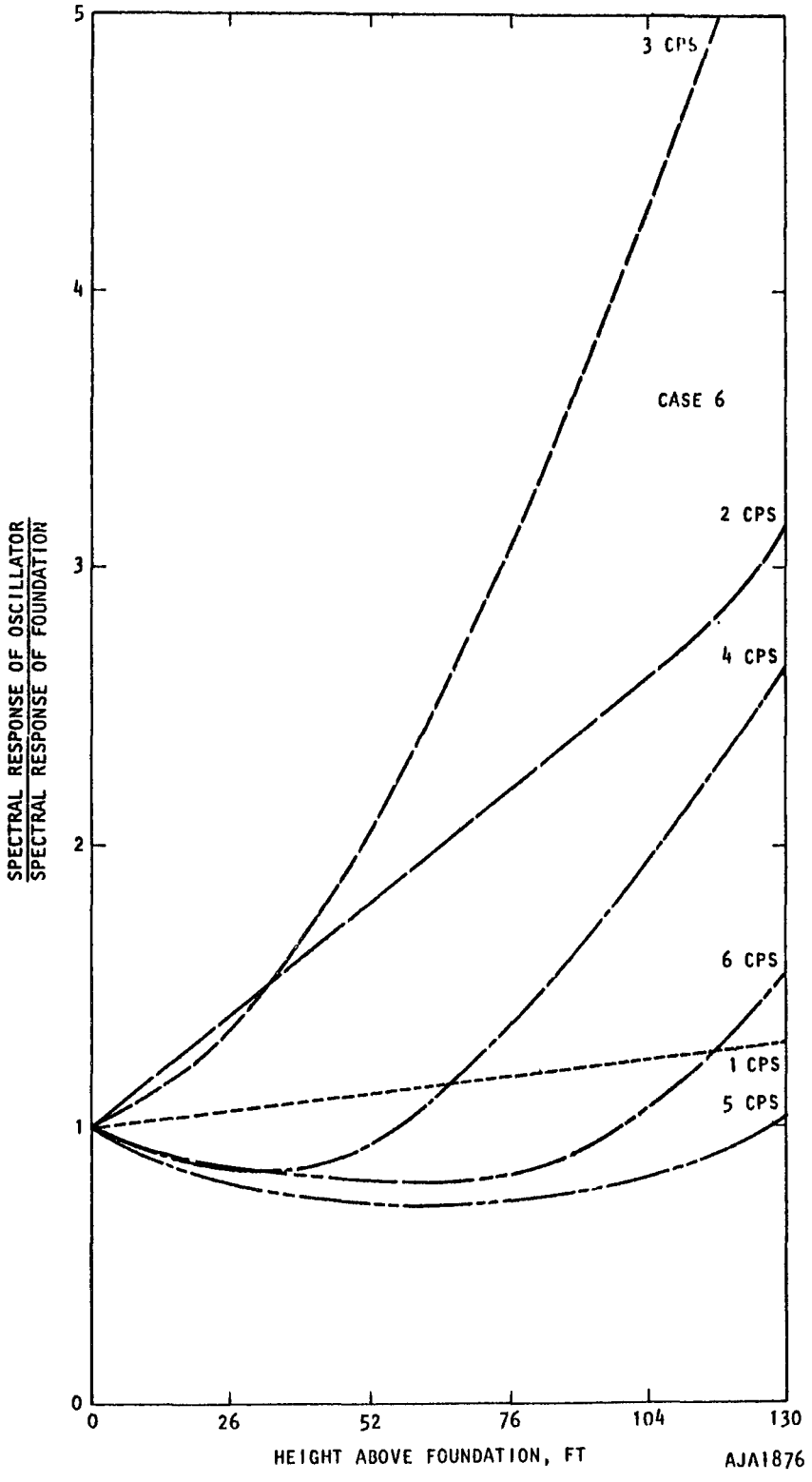

FIGURE 5-39. HORIZONTAL RESPONSE SPECTRA AT VARIOUS ELEVATIONS ON 4-CPS OSCILLATOR RELATIVE TO FOUNDATION RESPONSE, CASE 6

In the frequency range of 1 to 3 cps, the response increases with height. A more complicated relation exists for higher frequencies.

The results indicate that there is no simple relation between response spectra at the base and spectra at higher elevations. The reason is probably related to the finding that rocking and translation of the base are out of phase, or have different dominant frequencies.

EXAMPLE OF COMPLETE ANALYSIS

To economize on the length of the present report, only the most important aspects of the structural and free-field responses have been summarized, illustrated, and discussed above. The complete results of a typical elastic analysis (Case 5) are given in Appendix I as a further illustration.

SECTION 6

CONCLUSIONS BASED ON PRESENT STUDY

The following conclusions are based on the analyses described in the previous sections. The conclusions may need to be modified for earthquake inputs having different frequency contents or longer durations, for different soil properties, and for structures with different natural frequencies. However, input motions, soil properties, and structural response frequencies cover a wide enough range that the present trends appear to be valid and they may also occur under conditions differing from those studied here. How strongly the trends persist under other conditions requires further study.

a. Horizontal response spectra of an embedded structure foundation are suppressed relative to the free field by a factor of 0.2 to 1.0. A typical suppression ratio for elastic soils in the frequency range of 3 to 5 cps is 0.5, while for inelastic soils it is 0.3. This appears to be large enough to consider in seismic design.

b. Suppression of horizontal response spectra relative to the free field tends to be maximum at frequencies near the natural response frequencies of the structure.

c. Suppression is greater in softer soils than in stiffer soils.

d. The peak horizontal accelerations and velocities of the foundation are suppressed relative to the peak free field accelerations. The amount of suppression is somewhat less than for the response spectra in the range of 3 to 5 cps. This finding is probably influenced more than other findings by the particular choice of input and structural response frequencies.

e. The vertical response spectrum of the foundation is amplified by 1.0 to 1.5 relative to that of the free field at 1 to 3 cps and suppressed by 0.2 to 1.0 at 3 to 8 cps.

f. The horizontal stress in the soil beneath the foundation is 0.2 to 0.3 times the corresponding free-field stress.

g. The main horizontal interaction force on the embedded reactor structure is provided by direct stresses on the walls of the structure. Shear stresses on the bottom of the foundation do not contribute significantly. The vertical interaction force is provided in approximately equal parts by vertical direct stresses on the foundation and shear stresses on the walls.

h. The interaction stresses appear to be uniquely related to the velocity of the structure.

i. There is no simple relation between response spectra at the base and either the maximum acceleration or the response spectra at higher elevations. This is apparently due to rocking and translation modes of foundation response being out of phase.

REFERENCES

1. Scavuzzo, R. J. and D. Raftopoulas, *Literature Review of Structure-Foundation Interaction*, Technical Report No. 1, Univ. of Toledo, The Research Foundation, AEC Contract No. AT-(40-1)-3822, October 1968.

2. Werner, S. D., *A Study of Earthquake Input Motions for Seismic Design*, AJA R-6914-925, Agbabian-Jacobsen Associates, AEC Contract No. AT(49-5)-3012, June 1970.

3. Housner, G. W., "Behavior of Structures During Earthquakes," *J. of Eng. Mech. Div., Proc. ASCE*, Vol. 85, No. EM4, October 1959.

4. Clough, R. W., "Dynamic Effects of Earthquakes Transactions," *Proc. ASCE*, Vol. 126, Part II, 1961, pp. 847-876.

5. Penzien, J., "Elasto-Plastic Response of Idealized Multi-Story Structures Subject to Strong Earthquake Motion," *Proc. 2nd World Conference on Earthquake Engineering*, Japan, 1960, pp. 739-760.

6. Clough, R. W. and A. K. Chopra, "Earthquake Stress Analysis in Earth Dams," *J. of Eng. Mech. Div., Proc. ASCE*, Vol. 92, No. EM2, April 1966, pp. 197-211.

7. Dibaj, M. and J. Penzien, *Nonlinear Seismic Response of Earth Structures*, Report No. EERC 69-2, Univ. of California, Berkeley, Earthquake Engineering Research Center, January, 1969.

8. Parmelee, R. A., et al., "Seismic Response of Structure-Foundation Systems," *J. of the Eng. Mech. Div., Proc. ASCE*, Vol. 94, No. EM6, December 1968, pp. 1295-1315.

9. Scavuzzo, et al., *Lateral Structure-Foundation Interaction of Nuclear Power Plants with Large Base Masses*, Technical Report No. 3, Univ. of Toledo, The Research Foundation, AEC Contract No. AT-(40-1)-3822, September 1969.

10. Wilson, E. L., *A Computer Program for the Dynamic Stress Analysis of Underground Structures*, Univ. of California, Berkeley, Contract DACA 39-67-C-0020, January 1968.

11. Hill, R., *The Mathematical Theory of Plasticity*, Oxford University Press, 1950.

12. Drucker, D. C. and W. Prager, "Soil Mechanics and Plastic Limit Analysis or Limit Design," *Quart. Appl. Math.*, Vol. X, No. 2, July 1952, pp. 157-165.

13. Idriss, I. M., "Finite Element Analysis for the Seismic Response of Earth Banks," *J. of the Soil Mech. and Found. Div., Proc. ASCE*, Vol. 94, No. SM3, May 1968, pp. 617-636.

14. Lysmer, J. and R. L. Kuhlemeyer, "Finite Dynamic Model for Infinite Media," *J. of Eng. Mech. Div., Proc. ASCE*, Vol. 95, No. EM4, August 1969, pp. 859-877.

15. Drucker, D. C., "A More Fundamental Approach to Stress-Strain Relations," *Proc. of U. S. Congr. Appl. Mech., ASME*, 1950, pp. 487-491.

16. Drucker, D. C., "Some Implications of Work-Hardening and Ideal Plasticity," *Quart. Appl. Math.*, Vol. 7, 1950, pp. 411-418.

17. Prager, W., "A New Method of Analyzing Stresses and Strains in Work-Hardening Plastic Solids," Paper No. 56, APM-34, National Conf. of Appl. Mech. Div. ASME, June 1956.

18. Lee, E. H., "Elastic Plastic Deformation at Finite Strains," *J. of Appl. Mech.*, March 1969, Paper No. 69-APM-1.

19. Drucker, D. C., "On Uniqueness in the Theory of Plasticity," *Quart. Appl. Math.*, Vol. 14, 1956, pp. 35-42.

20. Cole, J. D. and J. H. Huth, "Elastic Stresses Produced in a Half Plane by Steadily Moving Loads," *J. Appl. Mech.*, Vol. 25, December 1958.

21. Scavuzzo, R. J., "Foundation-Structure Interaction in the Analysis of Wave Motions," *Bull. of the Seismological Society of America*, Vol. 57, No. 4, pp. 735-746.

22. Chiapetta, R., *Effect of Soil-Structure Interaction on the Response of Reactor Structures to Seismic Ground Motion*, IIT Research Institute, AEC Contract AT-(40-1)-3822, Subcontract 1, July 1969.

23. Mehta, P. K., "Cylindrical and Spherical Elastoplastic Stress Waves by a Unified Direct Analysis Method," *AIAA Journal*, Vol. 5, No. 12, December 1967, pp. 2242-2248.

APPENDIX A

METHOD OF APPLYING PRESCRIBED MOTIONS AS INPUT

This Appendix describes the matrix operations used to apply velocity input to a finite element grid.

THEORETICAL OUTLINE OF THE METHOD

The equations of motion are:

$$[M]\{\ddot{u}\} + [C]\{\dot{u}\} + [K]\{u\} = \{P(t)\} \qquad \text{(A-1)}$$

where $[M]$ = Mass matrix (a diagonal matrix resulting from lumped mass idealization)

$[C]$ = Damping matrix

$[K]$ = Stiffness matrix (derived using the finite element method)

$\{P(t)\}$ = Load vector

and $\{u\}$, $\{\dot{u}\}$ and $\{\ddot{u}\}$ are the displacement, velocity, and acceleration vectors, respectively.

Suppose $u_i = u_{io}$, $\dot{u}_i = \dot{u}_{io}$, and $\ddot{u}_i = \ddot{u}_{io}$ are known motions at the i^{th} node for all time $t \geq 0$. (The procedure is outlined for the i^{th} component and can be extended easily to include a finite number of such components.) Equation A-1 can be written in the expanded form as

$$\begin{bmatrix} m_1 & & & & & & \\ & m_2 & & & & & \\ & & \ddots & & & & \\ & & & m_{i-1} & & & \\ & & & & m_i & & \\ & & & & & m_{i+1} & \\ & & & & & & \ddots \\ & & & & & & & m_n \end{bmatrix} \begin{Bmatrix} \ddot{u}_1 \\ \ddot{u}_2 \\ \vdots \\ \ddot{u}_{i-1} \\ \ddot{u}_i \\ \ddot{u}_{i+1} \\ \vdots \\ \ddot{u}_n \end{Bmatrix} + \begin{bmatrix} c_{11} & c_{12} & \cdots & c_{1,i-1} & c_{1,i} & c_{1,i+1} & \cdots & c_{1n} \\ c_{21} & c_{22} & \cdots & c_{2,i-1} & c_{2,i} & c_{2,i+1} & \cdots & c_{2n} \\ \vdots & \vdots & & \vdots & \vdots & \vdots & & \vdots \\ c_{i-1,1} & c_{i-1,2} & \cdots & c_{i-1,i-1} & c_{i-1,i} & c_{i-1,i+1} & \cdots & c_{i-1,n} \\ c_{i,1} & c_{i,2} & \cdots & c_{i,i-1} & c_{ii} & c_{i,i+1} & \cdots & c_{in} \\ c_{i+1,1} & c_{i+1,2} & \cdots & c_{i+1,i-1} & c_{i+1,i} & c_{i+1,i+1} & \cdots & c_{i+1,n} \\ \vdots & \vdots & & \vdots & \vdots & \vdots & & \vdots \\ c_{n1} & c_{n2} & \cdots & c_{n,i-1} & c_{ni} & c_{n,i+1} & \cdots & c_{nn} \end{bmatrix} \begin{Bmatrix} \dot{u}_1 \\ \dot{u}_2 \\ \vdots \\ \dot{u}_{i-1} \\ \dot{u}_i \\ \dot{u}_{i+1} \\ \vdots \\ \dot{u}_n \end{Bmatrix}$$

$$+\begin{bmatrix} k_{11} & k_{12} & \cdots & k_{1,i-1} & k_{1i} & k_{1,i+1} & \cdots & k_{1n} \\ k_{21} & k_{22} & \cdots & k_{2,i-1} & k_{2i} & k_{2,i+1} & \cdots & k_{2n} \\ \vdots & \vdots & & \vdots & \vdots & \vdots & & \vdots \\ k_{i-1,1} & k_{i-1,2} & \cdots & k_{i-1,i-1} & k_{i-1,i} & k_{i-1,i+1} & \cdots & k_{i-1,n} \\ k_{i1} & k_{i2} & \cdots & k_{i,i-1} & k_{ii} & k_{i,i+1} & \cdots & k_{in} \\ k_{i+1,1} & k_{i+1,2} & \cdots & k_{i+1,i-1} & k_{i+1,i} & k_{i+1,i+1} & \cdots & k_{i+1,n} \\ \vdots & \vdots & & \vdots & \vdots & \vdots & & \vdots \\ k_{n1} & k_{n2} & \cdots & k_{n,i-1} & k_{ni} & k_{n,i+1} & \cdots & k_{nn} \end{bmatrix} \begin{Bmatrix} u_1 \\ u_2 \\ \vdots \\ u_{i-1} \\ u_i \\ u_{i+1} \\ \vdots \\ u_n \end{Bmatrix} = \begin{Bmatrix} P_1 \\ P_2 \\ \vdots \\ P_{i-1} \\ P_i \\ P_{i+1} \\ \vdots \\ P_n \end{Bmatrix} \qquad \text{(A-2)}$$

Imposing the motion constraints $u_i = u_{i0}$, $\dot{u}_i = \dot{u}_{i0}$, and $\ddot{u}_i = \ddot{u}_{i0}$, Equation A-2 can be written as

$$\begin{bmatrix} m_1 & & & & & & \\ & m_2 & & & & & \\ & & \ddots & & & & \\ & & & m_{i-1} & & & \\ & & & & m_i & & \\ & & & & & m_{i+1} & \\ & & & & & & \ddots \\ & & & & & & & m_n \end{bmatrix} \begin{Bmatrix} \ddot{u}_1 \\ \ddot{u}_2 \\ \vdots \\ \ddot{u}_{i-1} \\ \ddot{u}_{i0} \\ \ddot{u}_{i+1} \\ \vdots \\ \ddot{u}_n \end{Bmatrix} + \begin{bmatrix} c_{11} & c_{12} & \cdots & c_{1,i-1} & 0 & c_{1,i+1} & \cdots & c_{1n} \\ c_{21} & c_{22} & \cdots & c_{2,i-1} & 0 & c_{2,i+1} & \cdots & c_{2n} \\ \vdots & \vdots & & \vdots & \vdots & \vdots & & \vdots \\ c_{i-1,2} & c_{i-1,2} & \cdots & c_{i-1,i-1} & 0 & c_{i-1,i+1} & \cdots & c_{i-1,n} \\ 0 & 0 & \cdots & 0 & c_{ii} & 0 & \cdots & 0 \\ c_{i+1,1} & c_{i+2,} & \cdots & c_{i+1,i-1} & 0 & c_{i+1,i+1} & \cdots & c_{i+1,n} \\ \vdots & \vdots & & \vdots & \vdots & \vdots & & \vdots \\ c_{n1} & c_{n2} & \cdots & c_{n,i-1} & 0 & c_{n,i+1} & \cdots & c_{nn} \end{bmatrix} \begin{Bmatrix} \dot{u}_1 \\ \dot{u}_2 \\ \vdots \\ \dot{u}_{i-1} \\ \dot{u}_{i0} \\ \dot{u}_{i+1} \\ \vdots \\ \dot{u}_n \end{Bmatrix}$$

$$+\begin{bmatrix} k_{11} & k_{12} & \cdots & k_{1,i-1} & 0 & k_{1,i+1} & \cdots & k_{1n} \\ k_{21} & k_{22} & \cdots & k_{2,i-1} & 0 & k_{2,i+1} & \cdots & k_{2n} \\ \vdots & \vdots & & \vdots & \vdots & \vdots & & \vdots \\ k_{i-1,1} & k_{i-1,2} & \cdots & k_{i-1,i-1} & 0 & k_{i-1,i+1} & \cdots & k_{i-1,n} \\ 0 & 0 & \cdots & 0 & k_{ii} & 0 & \cdots & 0 \\ k_{i+1,1} & k_{i+1,2} & \cdots & k_{i+1,i-1} & 0 & k_{i+1,i+1} & \cdots & k_{i+1,n} \\ \vdots & \vdots & & \vdots & \vdots & \vdots & & \vdots \\ k_{n1} & k_{n2} & \cdots & k_{n,i-1} & 0 & k_{n,i+1} & \cdots & k_{nn} \end{bmatrix} \begin{Bmatrix} u_1 \\ u_2 \\ \vdots \\ u_{i-1} \\ u_{i0} \\ u_{i+1} \\ \vdots \\ u_n \end{Bmatrix} = \begin{Bmatrix} P_1 - c_{11}\dot{u}_{i0} - k_{11}u_{i0} \\ P_2 - c_{2i}\dot{u}_{i0} - k_{2i}u_{i0} \\ \vdots \\ P_{i-1} - c_{i-1,i}\dot{u}_{i0} - k_{i-1,i}u_{i0} \\ m_i\ddot{u}_{i0} + c_{ii}\dot{u}_{i0} + k_{ii}u_{i0} \\ P_{i+1} - c_{i+1,i}\dot{u}_{i0} - k_{i+1,i}u_{i0} \\ \vdots \\ P_n - c_{ni}\dot{u}_{i0} - k_{ni}u_{i0} \end{Bmatrix} \qquad \text{(A-3)}$$

Equation A-3 can be solved for the displacements, velocities, and accelerations by any convenient method. The linear acceleration method will be emphasized in the discussion that follows, since this method has been utilized in the DEPS Code.

LINEAR ACCELERATION METHOD

Assuming the acceleration vector (including $\ddot{u}_{io}$) to be linear within a small time step of Δt, Equation A-3 takes the form

$$[\bar{K}]\{\bar{u}_t\} + \{\bar{P}_t\} \tag{A-4}$$

where $[\bar{K}] = [K] + C_2[M]$; $[K]$ and $[M]$ are defined in Equation A-3, and the remaining variables are defined as follows:

$$\{\bar{u}_t\} = \frac{1}{C_1}\{u_t\} - \beta\{B_t\}$$

$$\{\bar{P}_t\} = \{P\} + [M]\left(\{A_t\} + C_3\{B_t\}\right) - \begin{Bmatrix} k_{1i} \\ k_{2i} \\ \vdots \\ k_{ni} \end{Bmatrix}\bar{u}_i \quad \text{except} \quad \bar{P}_i$$

$$\text{and} \quad \bar{P}_i = \left(k_{ii} + C_2 m_i\right)\bar{u}_i$$

$$C_0 = \frac{3\alpha}{\Delta t} + \frac{6}{\Delta t^2}$$

$$C_1 = \frac{1}{1 + \frac{3}{\Delta t}\beta}$$

$$C_2 = C_0 C_1$$

$$C_3 = \alpha - C_2\beta$$

$$[C] = \alpha[M] + \beta[K]; \ \alpha \text{ and } \beta \text{ are damping constants}$$

$$\{\ddot{u}_t\} = \frac{6}{\Delta t^2}\{u_t\} - \{A_t\}; \quad \{A_t\} = \frac{6}{\Delta t^2}\{u_{t-\Delta t}\} + \frac{6}{\Delta t}\{\dot{u}_{t-\Delta t}\} + 2\{\ddot{u}_{t-\Delta t}\}$$

$$\{\dot{u}_t\} = \frac{3}{\Delta t}\{u_t\} - \{B_t\}; \quad \{B_t\} = \frac{3}{\Delta t}\{u_{t-\Delta t}\} + 2\{\dot{u}_{t-\Delta t}\} + \frac{\Delta t}{2}\{\ddot{u}_{t-\Delta t}\}$$

Equation 4-15 can be written as

$$\begin{bmatrix} (k_{11}+C_2m_1) & k_{12} & \cdot & \cdot & k_{1,i-1} & 0 & k_{1,i+1} & \cdot & \cdot & k_{1n} \\ k_{21} & (k_{22}+C_2m_2) & \cdot & \cdot & k_{2,i-1} & 0 & k_{2,i+1} & \cdot & \cdot & k_{2n} \\ \cdot & \cdot & \cdot & \cdot & \cdot & \cdot & \cdot & \cdot & \cdot & \cdot \\ \cdot & \cdot & \cdot & \cdot & \cdot & \cdot & \cdot & \cdot & \cdot & \cdot \\ k_{i-1,1} & k_{i-1,2} & \cdot & \cdot & (k_{i-1,i-1}+C_2m_{i-1}) & 0 & k_{i-1,i+1} & \cdot & \cdot & k_{i-1,n} \\ 0 & 0 & \cdot & \cdot & 0 & (k_{ii}+C_2m_i) & 0 & \cdot & \cdot & 0 \\ k_{i+1,1} & k_{i+1,2} & \cdot & \cdot & k_{i+1,i-1} & 0 & (k_{i+1,i+1}+C_2m_{i+1}) & \cdot & \cdot & k_{i+1,n} \\ \cdot & \cdot & \cdot & \cdot & \cdot & \cdot & \cdot & \cdot & \cdot & \cdot \\ \cdot & \cdot & \cdot & \cdot & \cdot & \cdot & \cdot & \cdot & \cdot & \cdot \\ k_{n1} & k_{n2} & \cdot & \cdot & k_{n,i-1} & 0 & k_{n,i+1} & \cdot & \cdot & (k_{nn}+C_2m_n) \end{bmatrix} \begin{Bmatrix} \bar{u}_1 \\ \bar{u}_2 \\ \cdot \\ \cdot \\ \bar{u}_{i-1} \\ \bar{u}_i \\ \bar{u}_{i+1} \\ \cdot \\ \cdot \\ \bar{u}_n \end{Bmatrix} = \begin{Bmatrix} \bar{P}_1 \\ \bar{P}_2 \\ \cdot \\ \cdot \\ \bar{P}_{i-1} \\ \bar{P}_i \\ \bar{P}_{i+1} \\ \cdot \\ \cdot \\ \bar{P}_n \end{Bmatrix} \quad \text{(A-5)}$$

where $\{\bar{u}_t\} = \frac{1}{C_1}\{u_t\} - \beta\{B_t\}$

and $\{\bar{P}_t\} = \{P_t\} + [M]\left(\{A_t\} + C_3\{B_t\}\right) - \begin{Bmatrix} k_{1i} \\ k_{2i} \\ \vdots \\ k_{ni} \end{Bmatrix} \bar{u}_i$ except $\bar{P}_i$, where $\bar{P}_i = (k_{ii} + C_2m_i)\bar{u}_i$

$\bar{u}_t$ can be solved from Equation A-5 as.

$$\{\bar{u}_t\} = [K]^{-1} \{\bar{P}_t\} \tag{A-6}$$

and then the displacements $\{u_t\}$, velocities $\{\dot{u}_t\}$ and accelerations $\{\ddot{u}_t\}$ are determined from the expressions given in Equation A-4.

PRACTICAL IMPLEMENTATION

The present program accepts velocity boundary. Tabular values of velocities are input as functions of time using time increments. The velocities at actual time of computation are found by linear interpolation of the input values. The appropriate columns of the stiffness matrix (only the nonzero elements) are stored separately for the purpose of modifying the load vector. The effective displacements of the boundary nodal points are determined from the input velocities and used to modify the load vector before each time step. Then, the solution of Equation A-5 results in the effective displacements of all the nodal points, from which the response quantities can be determined.

APPENDIX B

METHOD OF PREVENTING UNWANTED REFLECTIONS FROM ARTIFICIAL BOUNDARIES

The present quiet boundary technique is most clearly illustrated in the one-dimensional wave-propagation case. This is shown in Figure B-1 with the aid of the common conception of real and "phantom" waves. A dilatation wave (p-wave) is shown traveling in a finite element rod from the left toward a fixed boundary. This wave has a partner "phantom" wave traveling from the right. As these waves meet each other at the boundary, they superpose to produce zero particle velocity at the boundary. At later times, the incident wave has traveled out of the finite element grid and has become a "phantom" wave, while the original "phantom" wave has entered the grid and has become a reflected wave which may interfere with the response calculations within the grid. The aim of the quiet boundary technique is to minimize or prevent boundary reflections. The analytical technique used is to calculate the motion of the boundary surface as it would occur if the rod were continuous. The computer then imposes this motion on the boundary. Inputs to the calculation are the velocity-time history of the incoming wave and the material properties of the rod. The calculation is based on the solution to the wave equation in one-dimension.

The effect of the quiet boundary technique is illustrated in Figure B-2. It may be considered that the reflection occurs, but that it is exactly cancelled by a wave of equal magnitude and opposite sign. Hence, the problem in the quiet boundary technique becomes one of defining the amplitude of the correction wave and its phasing relative to the reflected wave.

To illustrate the application of the quiet boundary technique, let us first consider the problem of representing an infinitely long one-dimensional continuum by an elastic rod of finite length. In this, it is desired to determine the boundary conditions at the far end of the rod, such that the response in the interior of the rod corresponds to that for the infinitely long continuum.

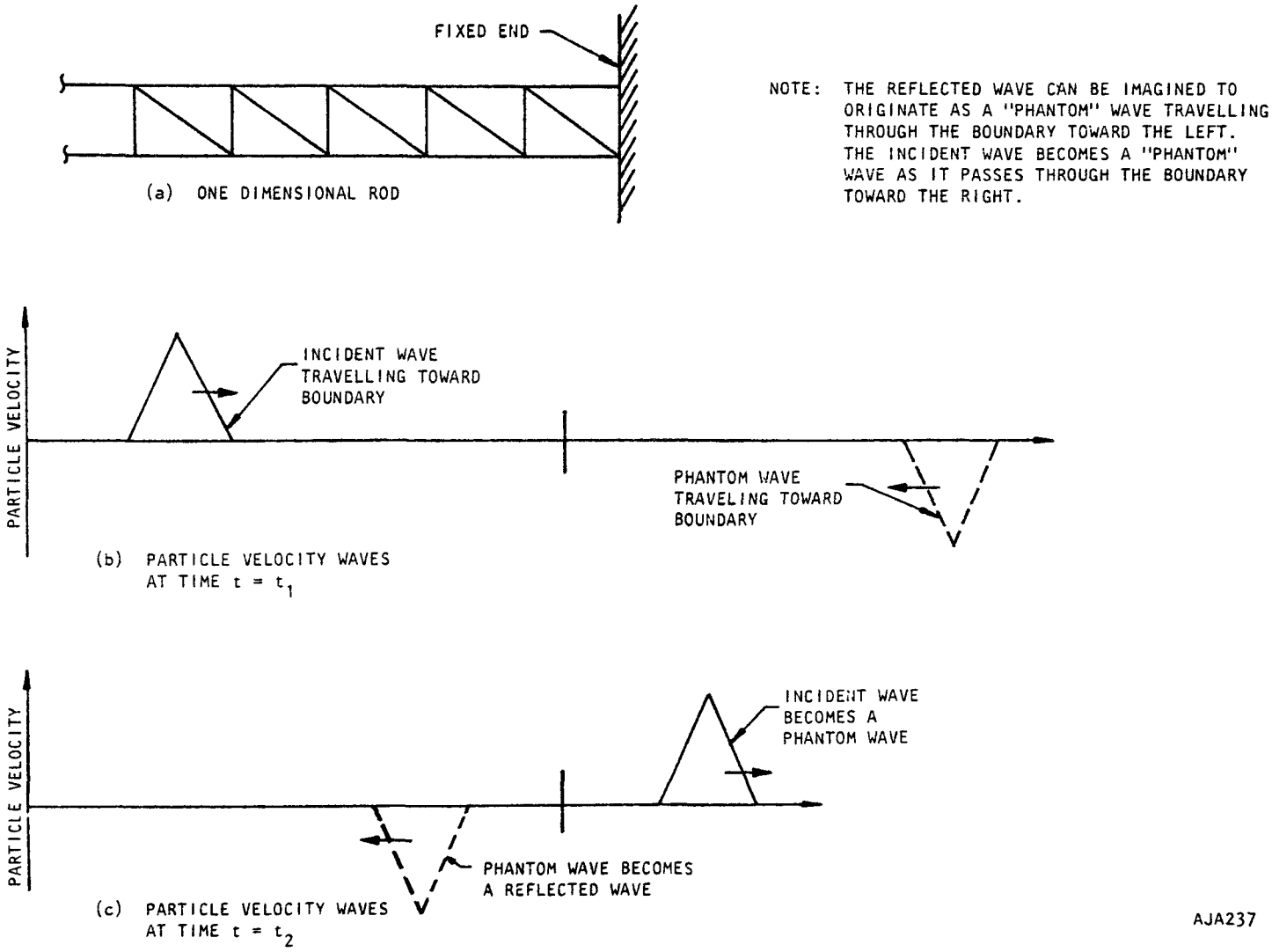

FIGURE B-1. REFLECTION OF WAVE AT FIXED END OF ONE-DIMENSIONAL ROD

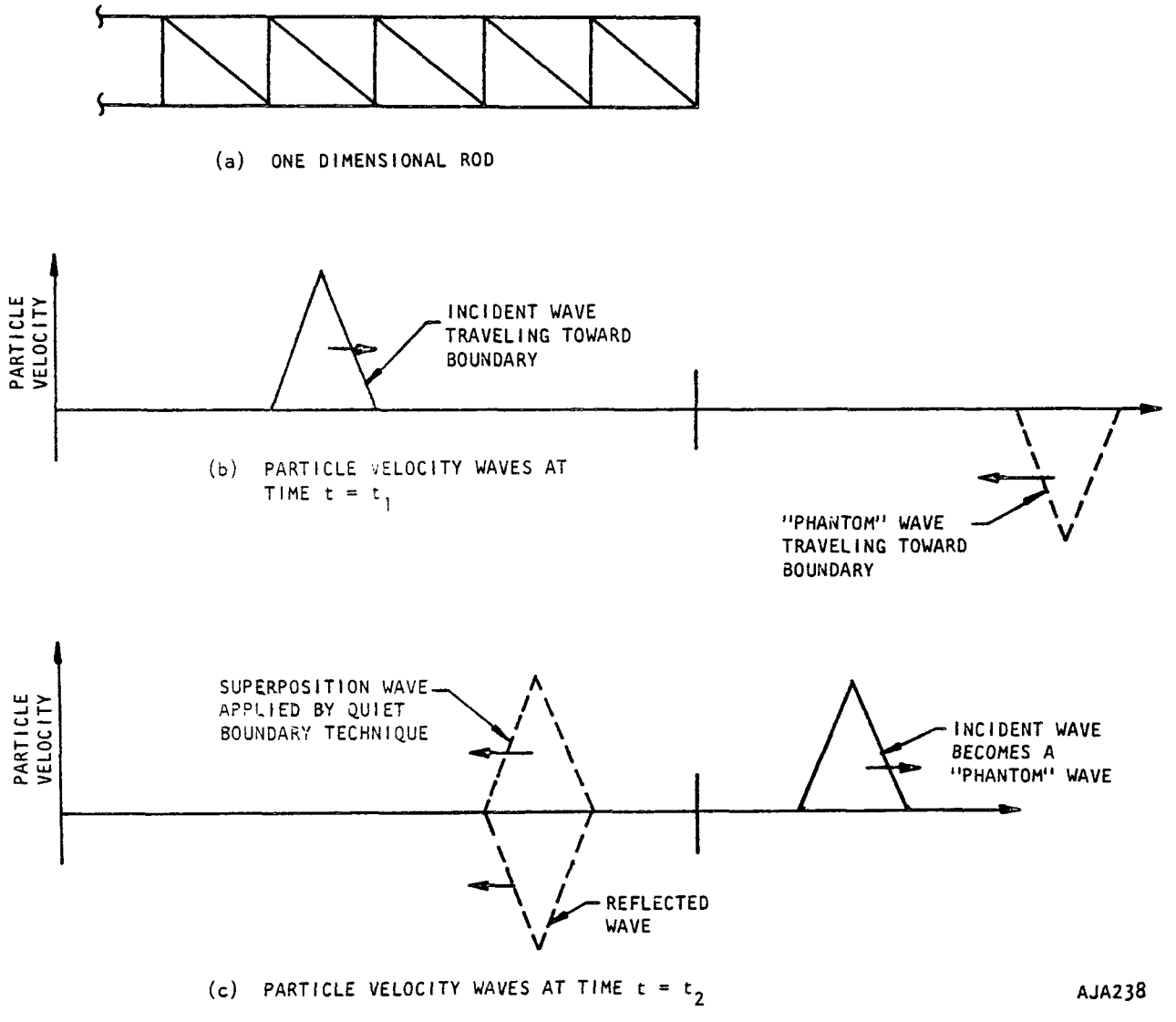

FIGURE B-2. ILLUSTRATION OF QUIET BOUNDARY TECHNIQUE

In this problem, it is assumed that at time $t = t_0$ the particle velocities at points j and j-1 in Figure B-3 are known, where point j is the far boundary point of the rod and point j-1 is located adjacent to point j, a distance Δx away. These velocities are denoted by

$V_{j-1}(t_0)$ = Particle velocity at point j-1 and time $t = t_0$,

$V_j(t_0)$ = Particle velocity at point j and time $t = t_0$.

The solution to the wave equation in one dimension gives the particle velocity at j at time $t = t_0 + \frac{\Delta x}{C_p}$ as

$$V_j\left(t_0 + \frac{\Delta x}{C_p}\right) = V_{j-1}(t_0) \tag{B-1}$$

where C_p is the p-wave propagation velocity of the rod material. The integration scheme used in the finite element code requires the determination of velocity V_j at time $t = t_0 + 2\Delta t$, where Δt is the integration time step. This is found by linear interpolation, using the expression

$$V_j(t_0 + 2\Delta t) = \frac{V_j(t_0)\left\{\frac{\Delta x}{C_p} - 2\Delta t\right\} + V_j\left(t_0 + \frac{\Delta x}{C_p}\right)\left\{2\Delta t\right\}}{\left(\frac{\Delta x}{C_p}\right)} \tag{B-2}$$

where, for this to be a solution to the wave equation

$$2\Delta t \leq \frac{\Delta x}{C_p} \tag{B-3}$$

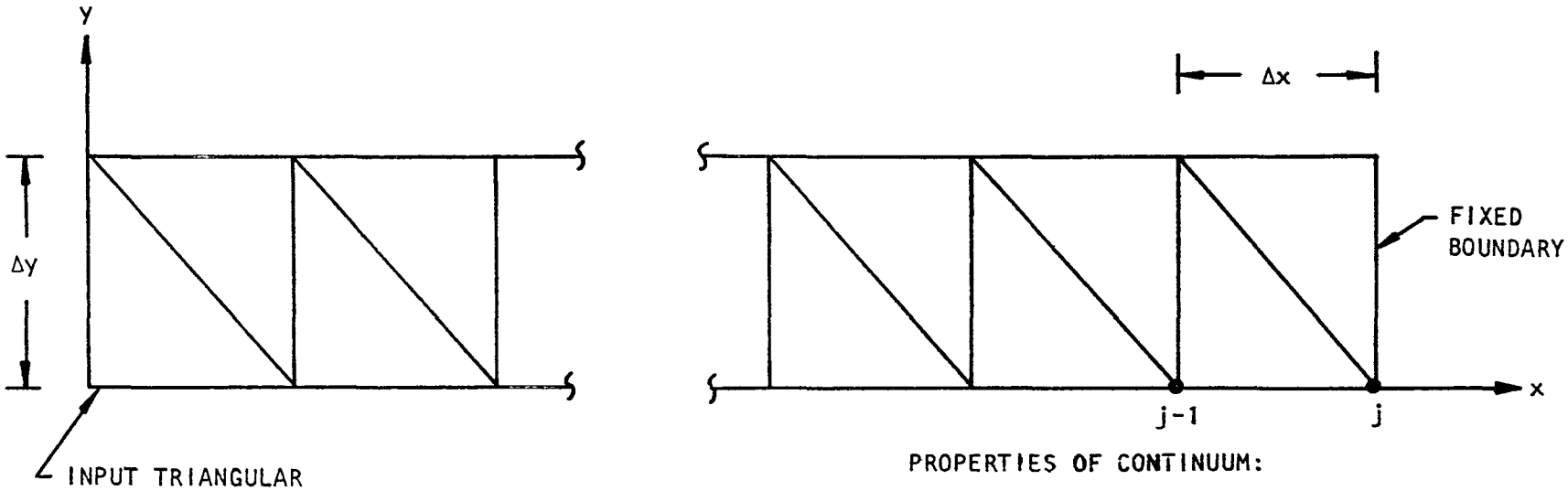

PROPERTIES OF CONTINUUM:

E	= 33,460 PSI	Δx	= 120 IN.
ν	= 0.25	Δy	= 480 IN.
ρ	= 0.0001423 $\frac{\text{LB-SEC}^2}{\text{FT}^4}$		

FIGURE B-3. REPRESENTATION OF AN INFINITELY LONG ONE DIMENSIONAL CONTINUUM BY A ROD OF FINITE LENGTH

At every time step, $V_j(t_0 + 2\Delta t)$ is computed and applied to the boundary nodal points, where it is regarded as a prescribed velocity at time $t = t_0 + 2\Delta t$.

The results of applying this technique to the rod geometry of Figure B-3 are illustrated in Figure B-4. In this figure, the motion of a nodal point in the center of the rod when the quiet boundary technique is not applied is compared to the motion of the same point when the quiet boundary technique is applied. This comparison illustrates the effectiveness of this technique in canceling the reflected wave.

Another example of the application of the quiet boundary technique is that of a one-dimensional rod which contains an impedance mismatch (corresponding to the insertion of a structure) at the midlength of the rod. In this, it is assumed that kinematic boundary conditions, corresponding to the response of the rod without the structure, have been prescribed at both ends of the rod. The problem here is to alter these boundary conditions so that the reflections at the boundary that arise from the presence of the structure are prevented.

In the discussion that follows, the term "boundary" velocity will represent the prescribed input motion which is computed prior to the finite element calculation. The term "scattered" velocity will represent the motion arising due to interaction with the structure in the middle of the grid, and which must be canceled to avoid unwanted reflections. The velocities are identified in the following equations by superscripts b and s for boundary and scattered velocities respectively.

At node point $j-1$ in Figure B-3, the particle velocity at time $t = t_0$ is composed of boundary and scattered velocities, as indicated below.

$$V_{j-1}(t_0) = V^b_{j-1}(t_0) + V^s_{j-1}(t_0) \qquad \text{(B-4)}$$

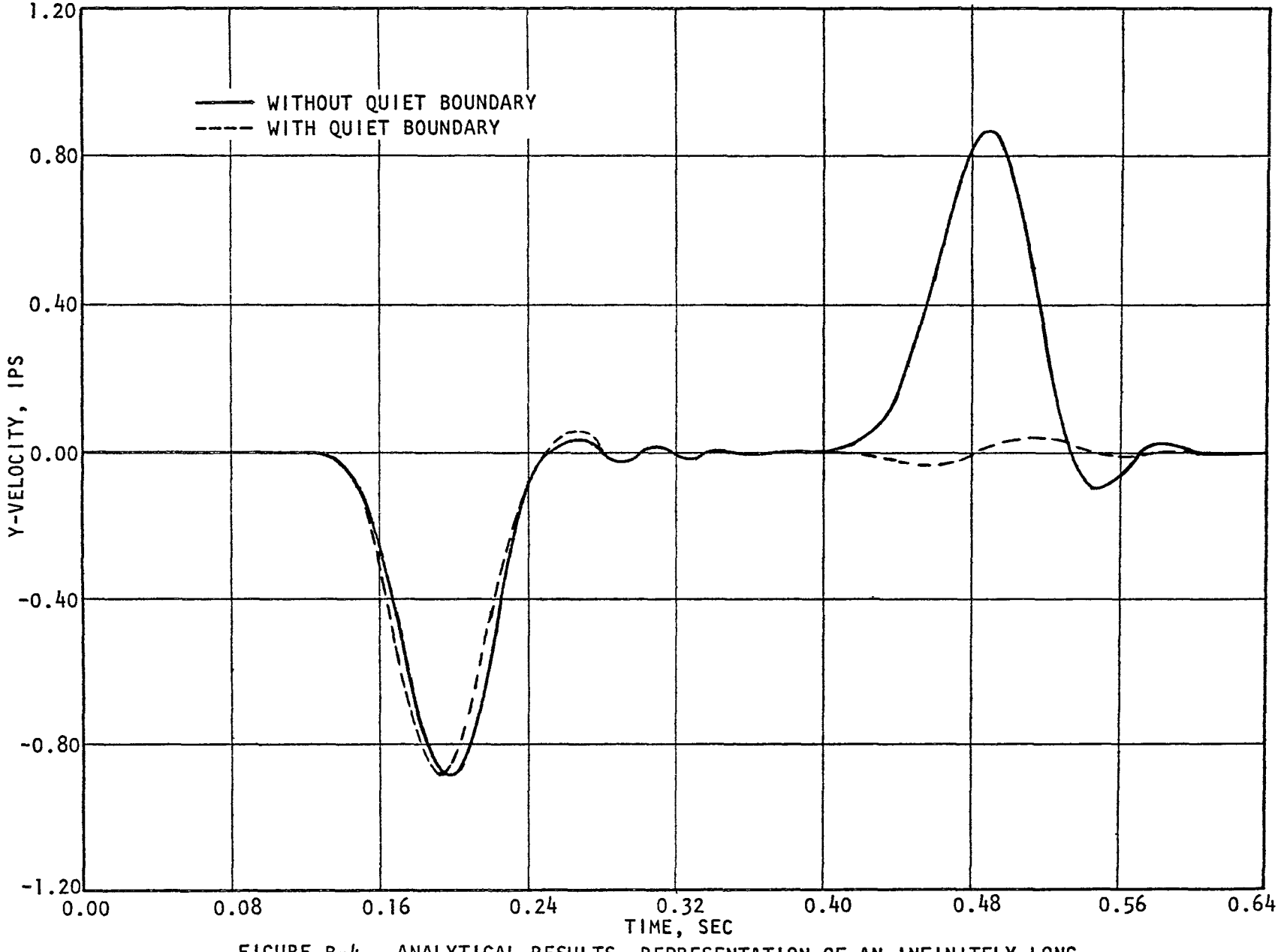

FIGURE B-4. ANALYTICAL RESULTS, REPRESENTATION OF AN INFINITELY LONG ONE-DIMENSIONAL CONTINUUM BY A ROD OF FINITE LENGTH

AJA

R-6915-1200

$V^b_{j-1}(t_0)$ is found from V^b_j, which is known for all time, as indicated by the expression

$$V^b_{j-1}(t_0) = V^b_j\left(t_0 - \frac{\Delta x}{C_p}\right) \tag{B-5}$$

Thus, the scattered motion propagating toward the boundary at point j-1 and time $t = t_0$ is

$$V^s_{j-1}(t_0) = V_{j-1}(t_0) - V^b_j\left(t_0 - \frac{\Delta x}{C_p}\right) \tag{B-6}$$

Employing the wave equation to find the scattered wave velocity at point j and time $t = t_0 + \frac{\Delta x}{C_p}$ gives

$$V^s_j\left(t_0 + \frac{\Delta x}{C_p}\right) = V^s_{j-1}(t_0) \tag{B-7}$$

or

$$V^s_j\left(t_0 + \frac{\Delta x}{C_p}\right) = V_{j-1}(t_0) - V^b_j\left(t_0 - \frac{\Delta x}{C_p}\right) \tag{B-8}$$

The correction to be made to the prescribed boundary velocity at time $t = t_0 + 2\Delta t$ in order to prevent reflection of the scattered wave is:

$$V^s_j\left(t_0 + 2\Delta t\right) = \frac{V^s_j(t_0)\left\{\frac{\Delta x}{C_p} - 2\Delta t\right\} + V^s_j\left(t_0 + \frac{\Delta x}{C_p}\right)\left\{2\Delta t\right\}}{\left(\frac{\Delta x}{C_p}\right)} \tag{B-9}$$

The adjusted boundary condition at time $t = t_0 + 2\Delta t$ then becomes

$$\bar{V}^b_j\left(t_0 + 2\Delta t\right) = V^b_j\left(t_0 + 2\Delta t\right) + V^s_j\left(t_0 + 2\Delta t\right) \tag{B-10}$$

In the above discussion, the quiet boundary technique is applied to incoming p dilatational waves. The technique applies equally well to s shear waves. The scattered s-wave is given by the following equation which is analogous to Equation B-9.

$$V_j^s\left(t_0 + 2\Delta t\right) = \frac{V_j^s\left(t_0\right)\left\{\frac{\Delta x}{C_s} - 2\Delta t\right\} + V_j^s\left(t_0 + \frac{\Delta x}{C_s}\right)\left\{2\Delta t\right\}}{\left(\frac{\Delta x}{C_s}\right)} \qquad \text{(B-11)}$$

In Figure B-3, V_j^s is the y-component of the scattered velocity at point j.

If both p and s waves are present in the rod, the correction calculated by Equation B-9 is applied to the x-component of velocity while that calculated by Equation B-11 is applied to the y-component of velocity.

The equations above give exactly the desired result for one-dimensional wave propagation. The same equations are used in cases of two-dimensional wave propagation to give an approximation to a quiet boundary. The technique described above was used to quiet the boundaries of the air-blast-induced ground-shock problem pictured in Figure B-5. The resulting stress/time histories for a selected element are shown in Figures B-6 through B-8 and are compared to the analytic solutions due to Cole-Huth (Reference 20). The comparison shows that the initial peaks calculated by the finite element method are virtually unaffected by incomplete canceling of reflections. However, reflections of about 20 percent of the peak signal appear in the finite element solution following the initial peak. These reflections are complicated signals containing at least two P-waves and two S-waves. The maximum amplitude of any of these waves is governed by the maximum amplitude of the incident P-wave, which is 83.3 psi. Hence, a 20 percent reflection means that some of the reflected waves could have amplitudes up to about 17 psi. Hence, it is not surprising that the shear stresses in Element 64 which are associated with reflected waves have amplitudes of about 6 psi.

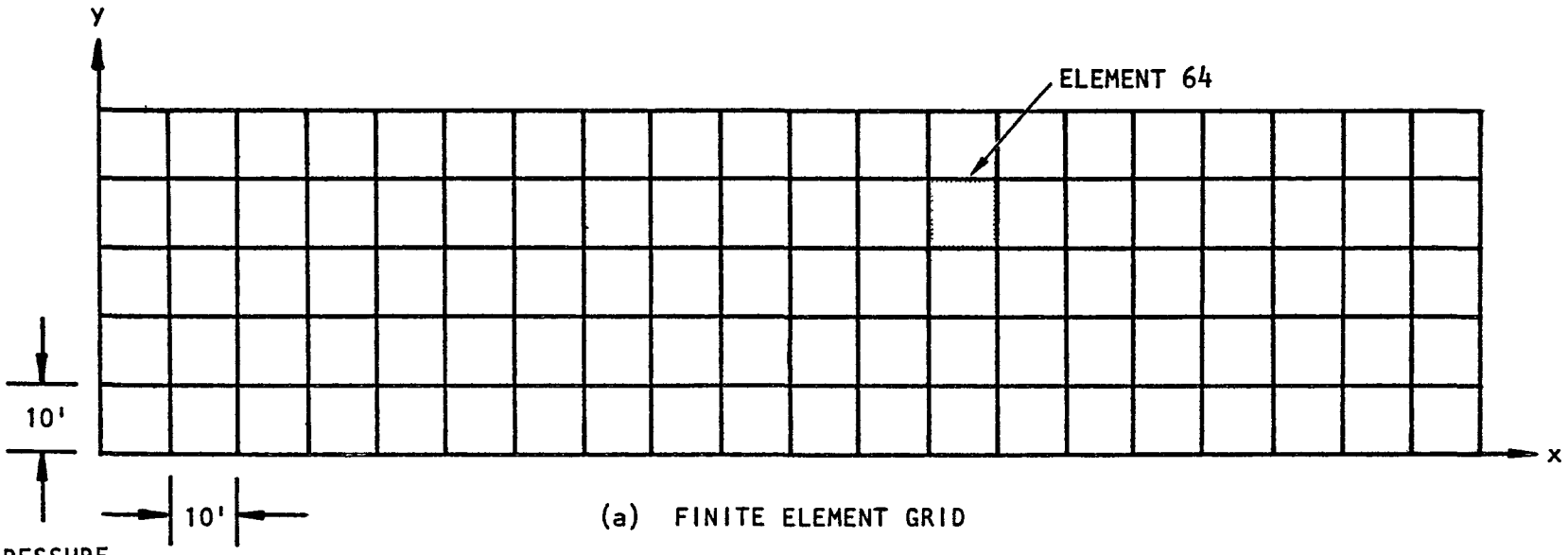

(a) FINITE ELEMENT GRID

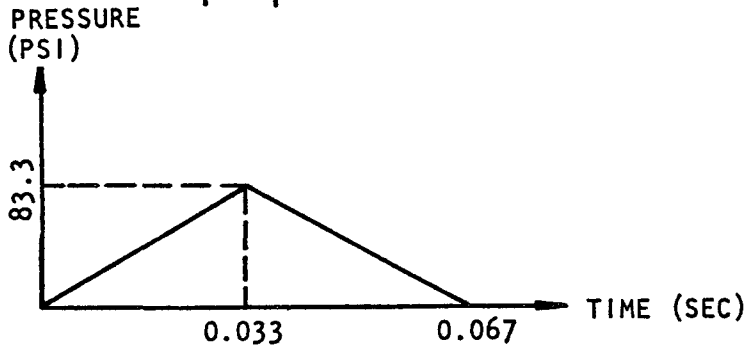

AIR BLAST SPEED = 3000 FPS

(b) INPUT PULSE

PROPOGATION VELOCITIES THROUGH MEDIUM:

C_p = 1000 FPS

C_s = 630 FPS

NOTE: STRESSES IN ELEMENT NO. 64 WERE MONITORED AND ARE SHOWN IN FIGURES B-6 THROUGH B-8.

FIGURE B-5. CHECK PROBLEM UTILIZING TWO-DIMENSIONAL QUIET BOUNDARY TECHNIQUE

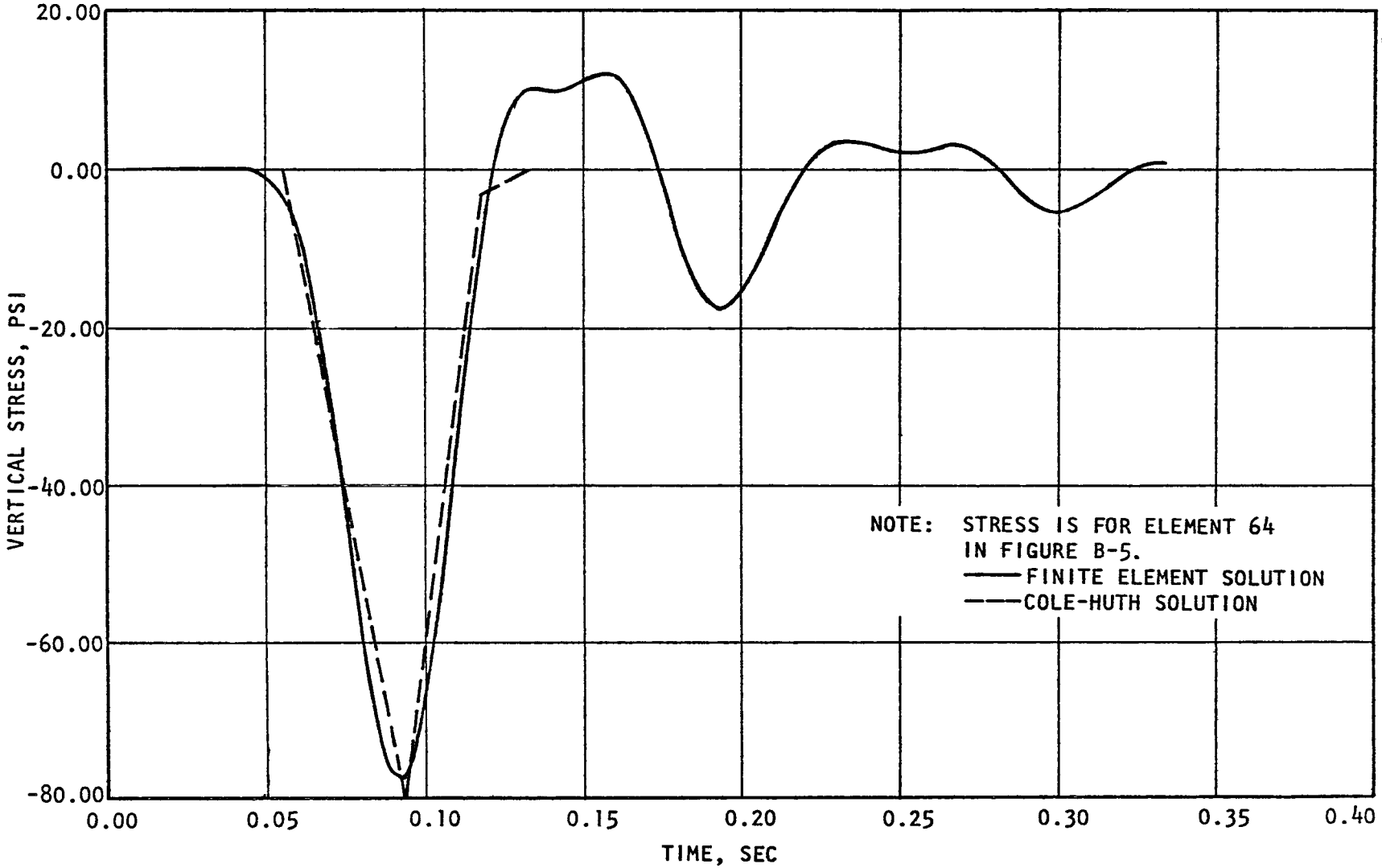

FIGURE B-6. VERTICAL STRESS VS TIME, TWO-DIMENSIONAL QUIET BOUNDRY CHECK PROBLEM

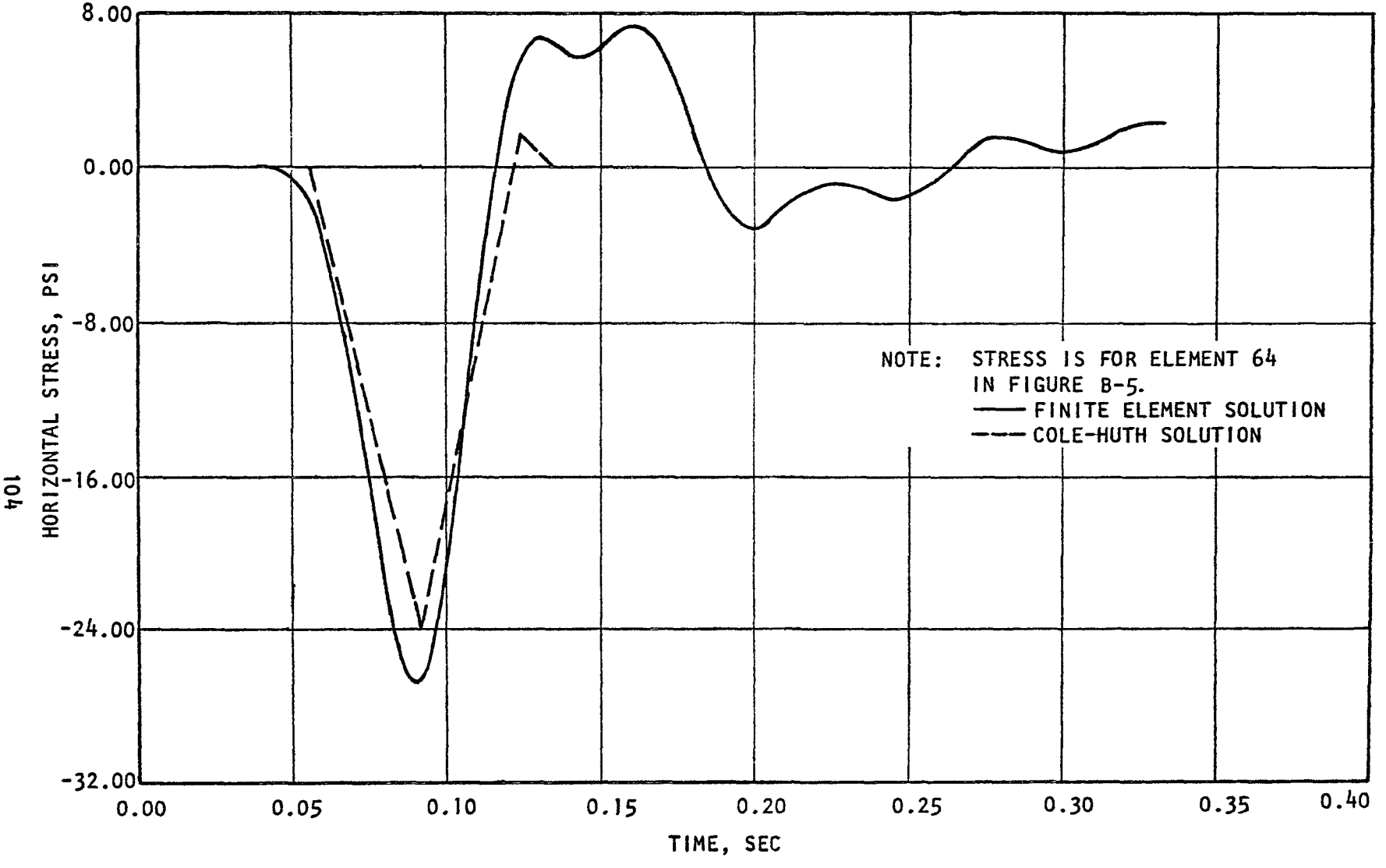

FIGURE B-7. HORIZONTAL STRESS VS TIME, TWO-DIMENSIONAL QUIET BOUNDARY CHECK PROBLEM

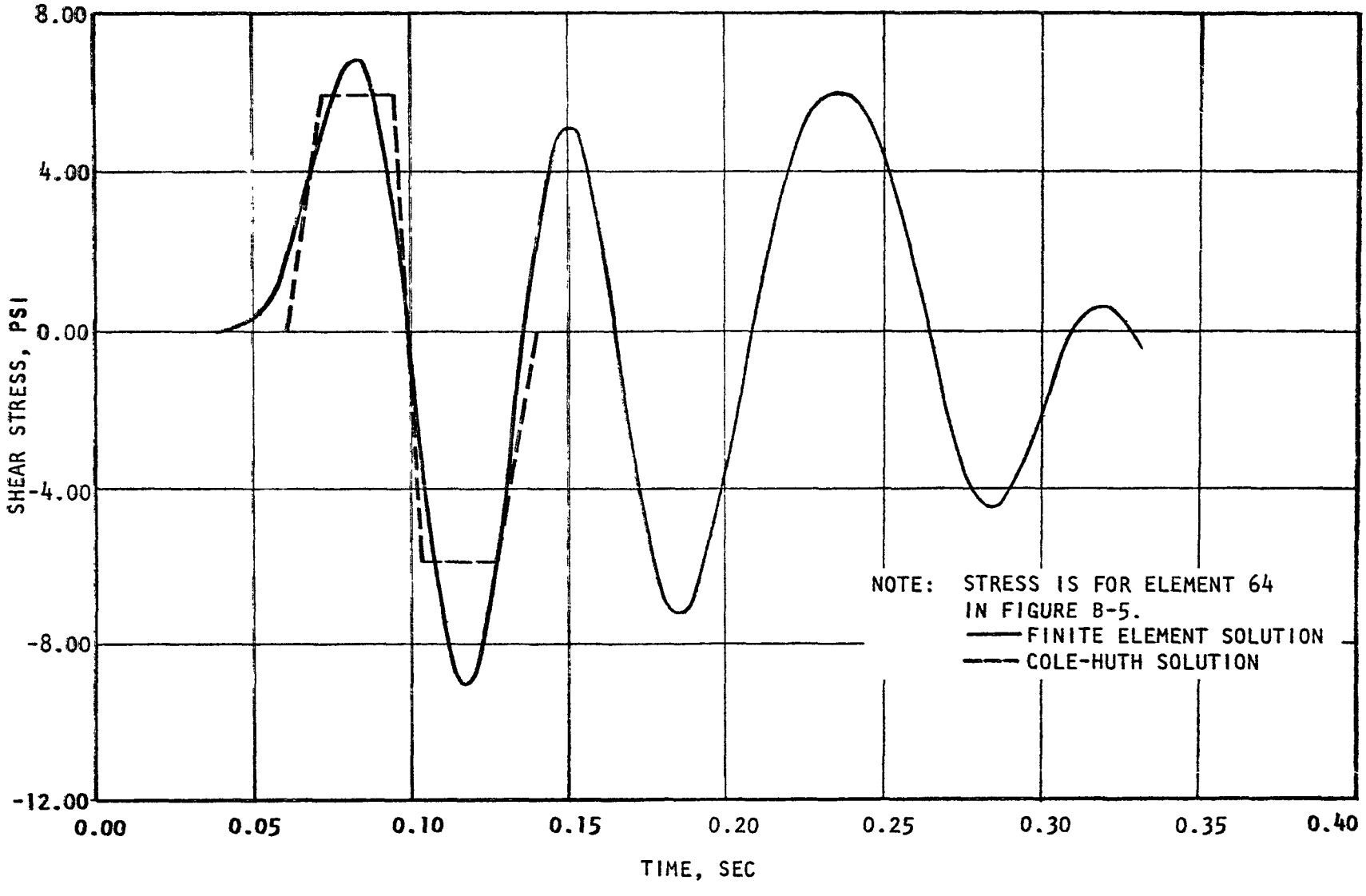

FIGURE B-8. SHEAR STRESS VS TIME, TWO-DIMENSIONAL QUIET BOUNDRY CHECK PROBLEM

APPENDIX C

STABILITY OF SOLUTION FROM INELASTIC FINITE ELEMENT COMPUTER PROGRAM

STABILITY STUDIES

The term stability is used here to mean that oscillations about a true solution, which are present to some extent in all numerical calculations, have a small amplitude relative to the true solution. An unstable solution may diverge rapidly from the true solution by undergoing oscillations whose amplitude increases with time.

The problem of stability arises in using INDEPS because the incremental equations of motion are integrated using the linear acceleration method to obtain a solution at $t + \delta t$ from a known solution at t. Unless δt, the integration time step, is kept small relative to the shortest natural period in the finite element system, divergence and instability may occur. This difficulty is avoided in the elastic finite element program, used in Task I of the present contract, by using the linear acceleration method to interpolate between t and $t + 2\delta t$ for the total solution, rather than the incremental solution, at $t + \delta t$ (Reference 10).

A study was conducted to explore conditions under which instability in INDEPS develops. The study concentrates on the problem of a small number of stiff elements embedded in a large number of more flexible ones. This situation is similar to a concrete structure embedded in soil. The objective is to determine whether the integration time step must be based on the natural period of the stiffest elements even though they are few and are surrounded by a greater mass of flexible ones. The outcome of the study bears directly on the economy of the inelastic finite element calculations to be conducted under Task II of the present contract.

Each of the five problems comprising the stability study, whose identification numbers are unrelated to the 2-D cases, involved triangular pulse propagating in a one-dimensional rod. The P-wave transit times for

various elements in the rod were chosen in each case to bear a certain relation to the integration time step. The cases are summarized in Table C-1. The results show that whenever the transit time was less than the integration time step, instability resulted. The results are described in detail below.

TABLE C-1.

Case	Number of Elements			Result
	Total	$T < \delta t$	$T \geq \delta t$	
1	25	0	25	Stable
2	25	25	0	Unstable
3	25	4	21	Unstable
4	25	0	25	Stable
5	25	2	23	Unstable

δt = Integration time step

T = P-wave transit time across an element

The geometry and loading condition for the rod in each of the five cases are shown in Figure C-1. In Case 1, the properties of the rod were homogeneous such that the p-wave transit time across each element was $T = 0.001$ sec. The time step δt was also 0.001 sec. The stress/time histories at Elements 5, 7, and 15, shown in Figure C-2, indicate that the solution is stable and converges about as well as when $\delta t = T/4$ (not shown).

The properties of the rod in Case 2 were the same as in Case 1, but $\delta t = 0.003$ sec $= 3T$. The results in Figure C-3 show that the solution is unstable.

Cases 3 and 4 anticipate problems of soil-structure/interaction in which stiff material (the structure) is surrounded by more flexible material (the soil). In Case 3, $\delta t = 0.001$ sec $= T$ for soil elements

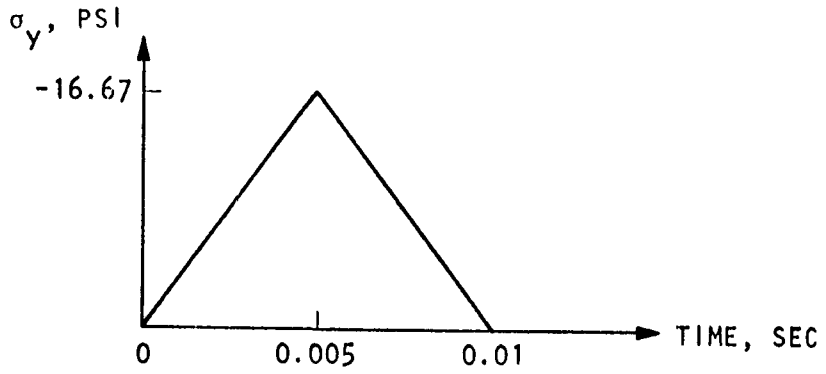

(a) LOAD

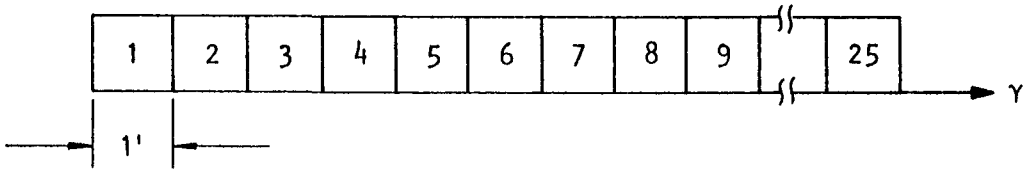

(b) HOMOGENEOUS BAR, c_p = 1000 FPS, CASES 1 AND 2

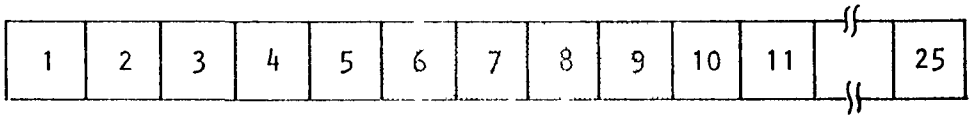

(c) INHOMOGENEOUS BAR, c_p = 1000 FPS (1-5, 10-15), c_p = 3000 FPS (6-9), CASES 3 AND 4

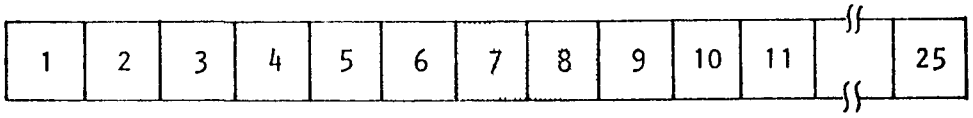

(d) INHOMOGENEOUS BAR, c_p = 1000 FPS (1-6, 9-25), c_p = 3000 FPS (7,8), CASE 5

AJA1326

FIGURE C-1. LOADING AND GEOMETRY FOR STABILITY STUDIES

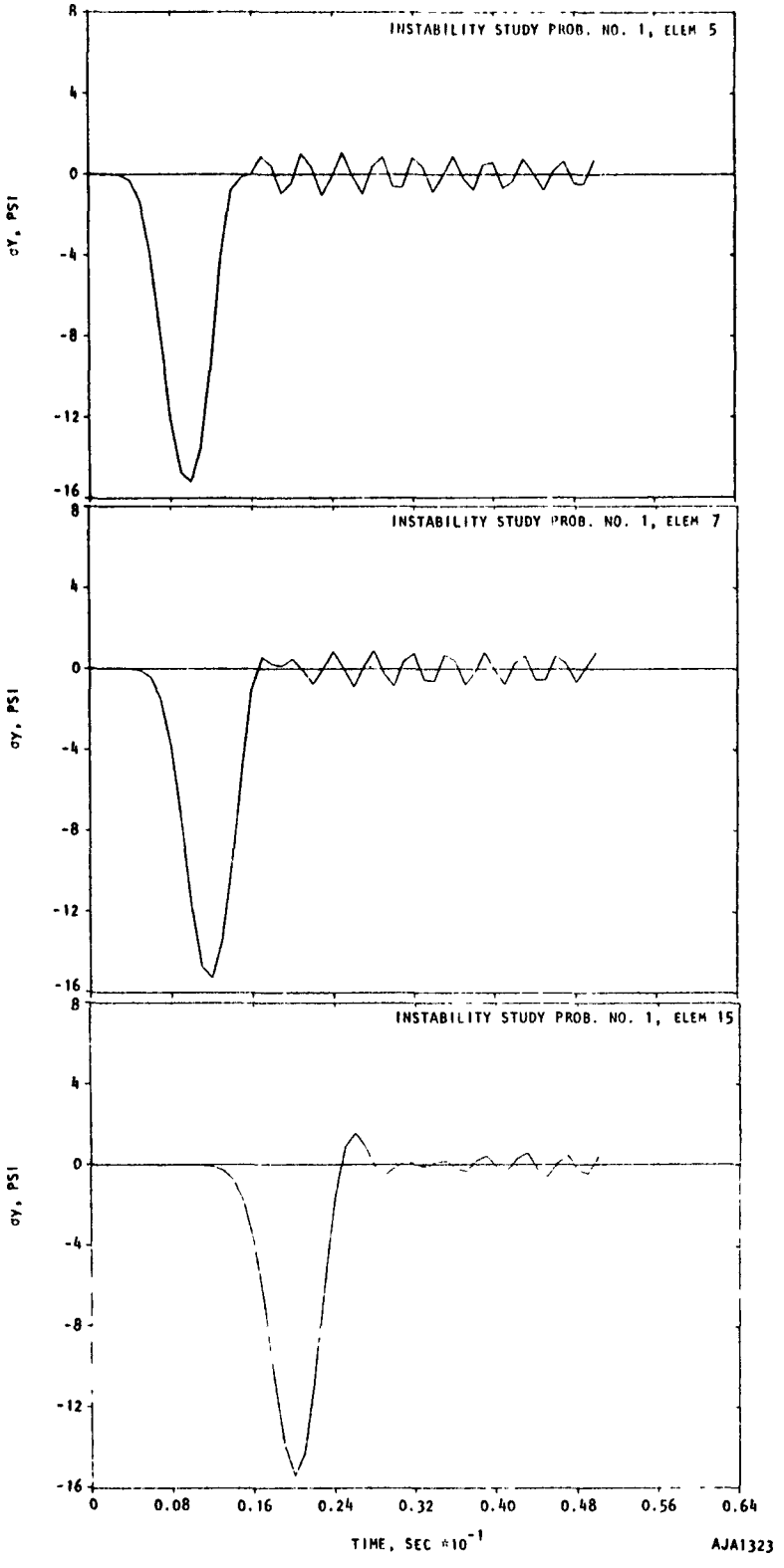

FIGURE C-2. INSTABILITY STUDY, CASE 1

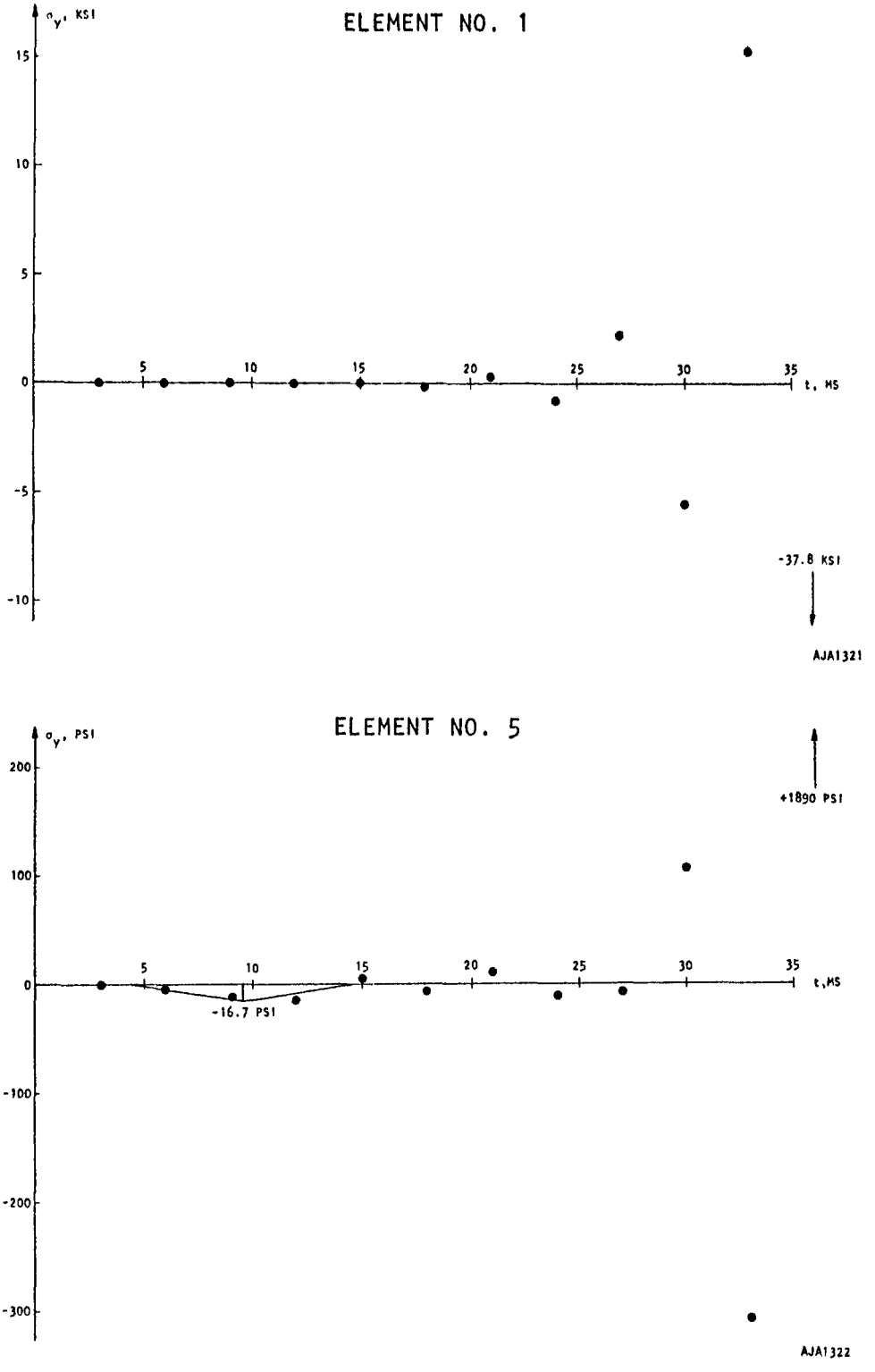

FIGURE C-3. INSTABILITY STUDY, CASE 2

and $3T$ for structure elements. The result was instability of the type found in Case 2. In Case 4, $\delta t = 0.000333$ sec $= T/3$ for soil elements and T for structure elements. The solution is difficult to interpret due to multiple reflections from boundaries between regions of different shock impedance, but it seems to be stable.

Case 5 is very similar to Case 3. The time step is equal to T for soil elements and $3T$ for structure elements. The point being investigated in Case 5 is that if the mass of elements in which $\delta t > T$ is small enough relative to the mass of the entire system, instability may be suppressed. This apparently is not the case, because instability of the same type found in Case 3 developed in Case 5.

The present stability study points to the conclusion that the integration time step must be less than the least transit time in the entire finite element grid. This appears to be due entirely to the choice of integration methods used here. It has unfavorable implications for the economy of inelastic finite element calculations involving interaction between soft soil and concrete structures. Further work is needed to find an economical incremental integration method.

APPENDIX D

COMPARISON BETWEEN INELASTIC FINITE ELEMENT AND CLOSED FORM SOLUTIONS

CONVERGENCE STUDIES

The term convergence is used here to denote the tendency for a solution obtained by INDEPS to approach the exact solution obtained by closed form methods. The problems used to illustrate convergence are as follows:

1. Plane, one-dimensional wave propagation in an elastic rod.
2. Plane, one-dimensional wave propagation in an inelastic rod.
3. Superseismic air blast (pressure) moving at constant speed over the surface of an elastic half-space.
4. Cylindrical wave propagation in an inelastic medium.

PLANE, ONE-DIMENSIONAL WAVE

The case of a plane, one-dimensional wave propagating in an elastic bar is illustrated in Figure D-1. The stress profiles calculated by INDEPS at various times are compared with the exact solution. The quiet boundary procedure is used in INDEPS to absorb the wave at the bottom boundary. The purpose of this procedure is to cause the rod to appear infinitely long, and its effectiveness is demonstrated by the apparent absence of reflections at $t = 0.03$ sec.

Two similar problems involving inelastic deformation of the rod are illustrated in Figures D-2 and D-3. The INDEPS solution for the triangular input pulse represents reasonably well the loading phase of the pulse, including the elastic precursor. The unloading phase is represented less

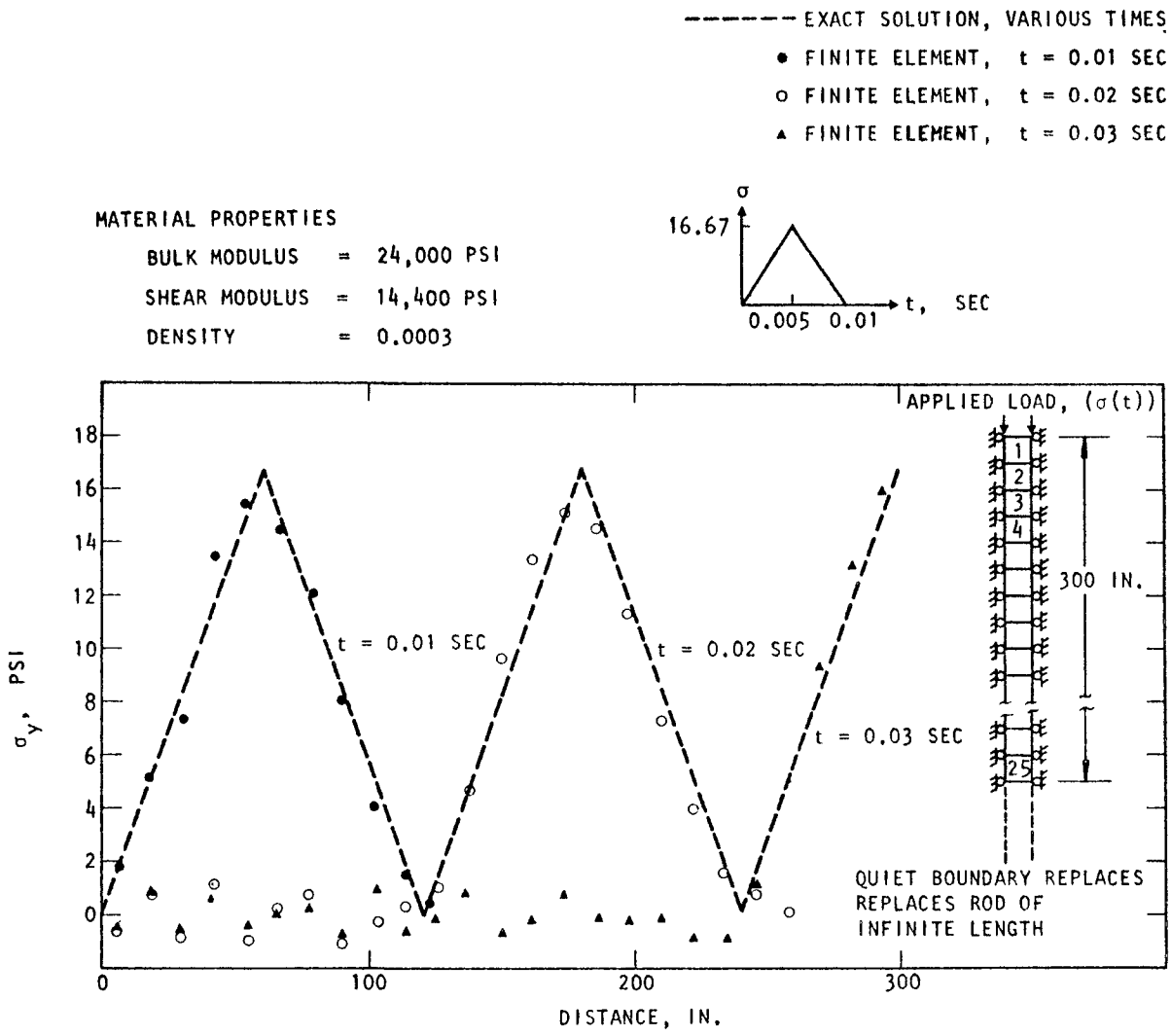

FIGURE D-1. PLANE, ONE-DIMENSIONAL WAVE PROPAGATION

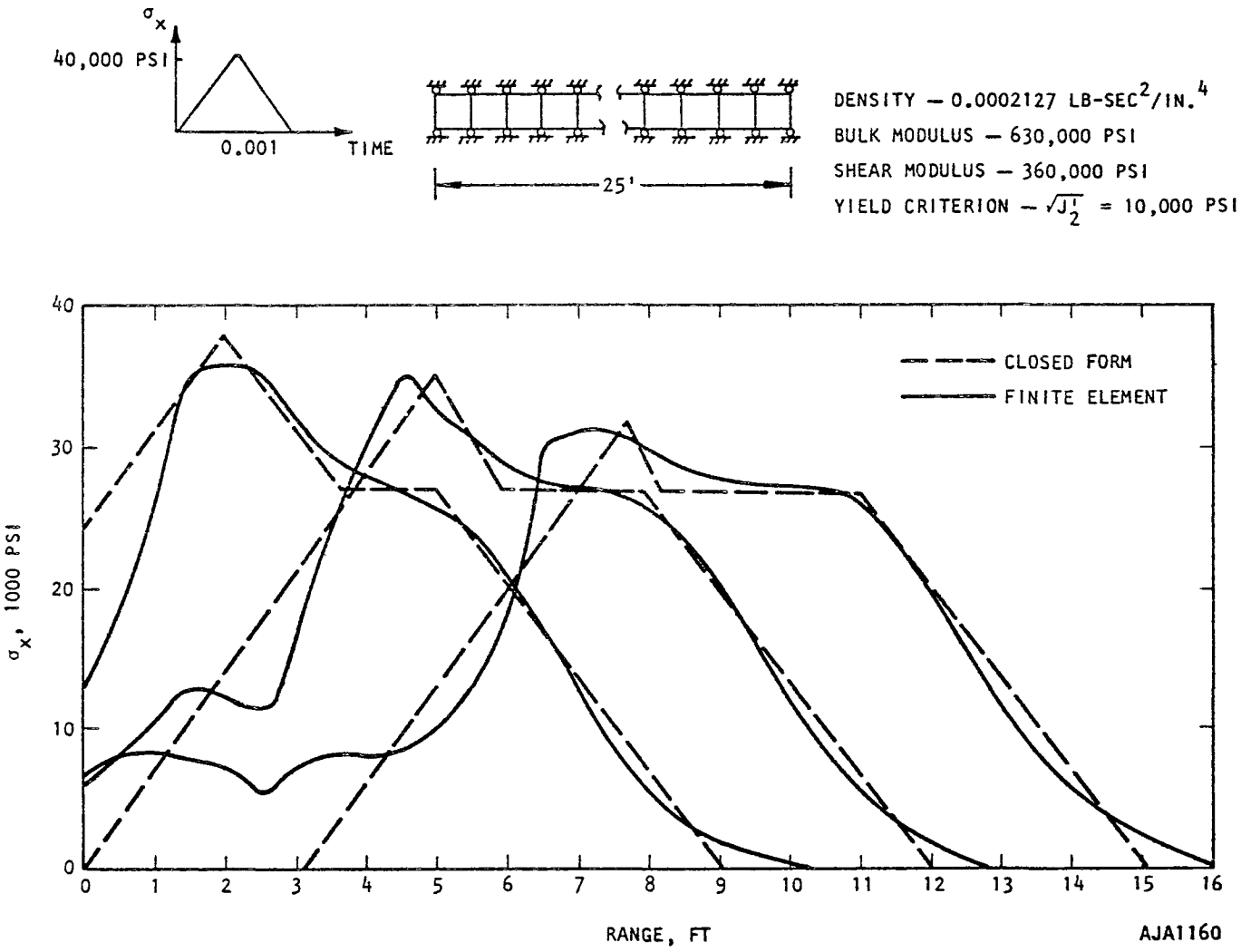

FIGURE D-2. AXIAL STRESS VERSUS RANGE, INELASTIC WAVE PROPAGATION

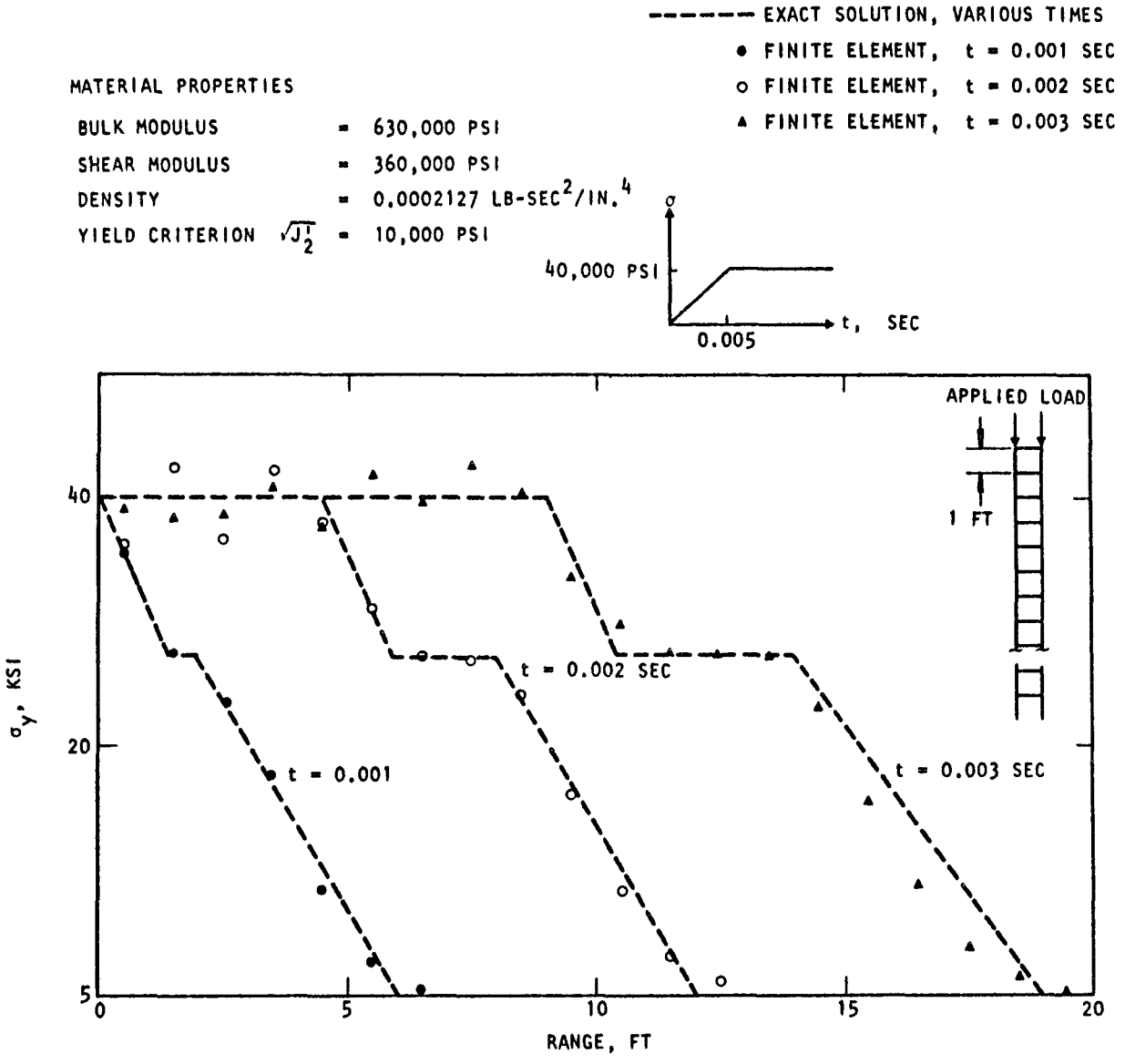

FIGURE D-3. PLANE, ONE-DIMENSIONAL ELASTIC-PLASTIC WAVE PROPAGATION

well. The quiet boundary procedure was not used in this calculation, which was stopped before reflections reached the stations shown in Figure D-2. An attempt was made to reduce or eliminate the oscillations in the unloading portion of the finite element solution by reducing the time step, but no appreciable improvement resulted. It was tentatively concluded that the mesh size would have to be reduced in order to improve agreement with the exact solution.

The INDEPS solution for a ramp load followed by a constant load is shown in Figure D-3. As in the case of the triangular pulse, the loading phase is accurately represented.

CYLINDRICALLY DIVERGING, INELASTIC WAVE

Although there are a few two-dimensional problems for which analytic or semi-analytic solutions exist, these problems are not well suited to checking out INDEPS in its present form. These solutions are for air-blast/induced ground motion, where the air blast is assumed to have zero rise time. It would not be possible to provide a sufficiently refined mesh to approximate a zero rise time without using peripheral storage, which INDEPS is presently unable to do.

Instead, a one-dimensional inelastic wave-propagation problem, for which an approximate solution exists, was solved as a two-dimensional problem. The geometry, loading, and material properties for this problem are shown in Figure D-4. The equations of motion are solved by the present finite element code for the x and y directions (global coordinates). The stresses and motions so obtained may be referred to a cylindrical coordinate system whose origin coincides with the origin in the x-y frame (Figure D-4). By representing the results in this one-dimensional form, comparison may be made with an existing semi-analytic solution (Reference 23). This solution is for a step load, and must be adapted for a ramp load which can be accommodated by the present finite element program. The results of Reference 23 were adapted using the method of characteristics and interpolation. The

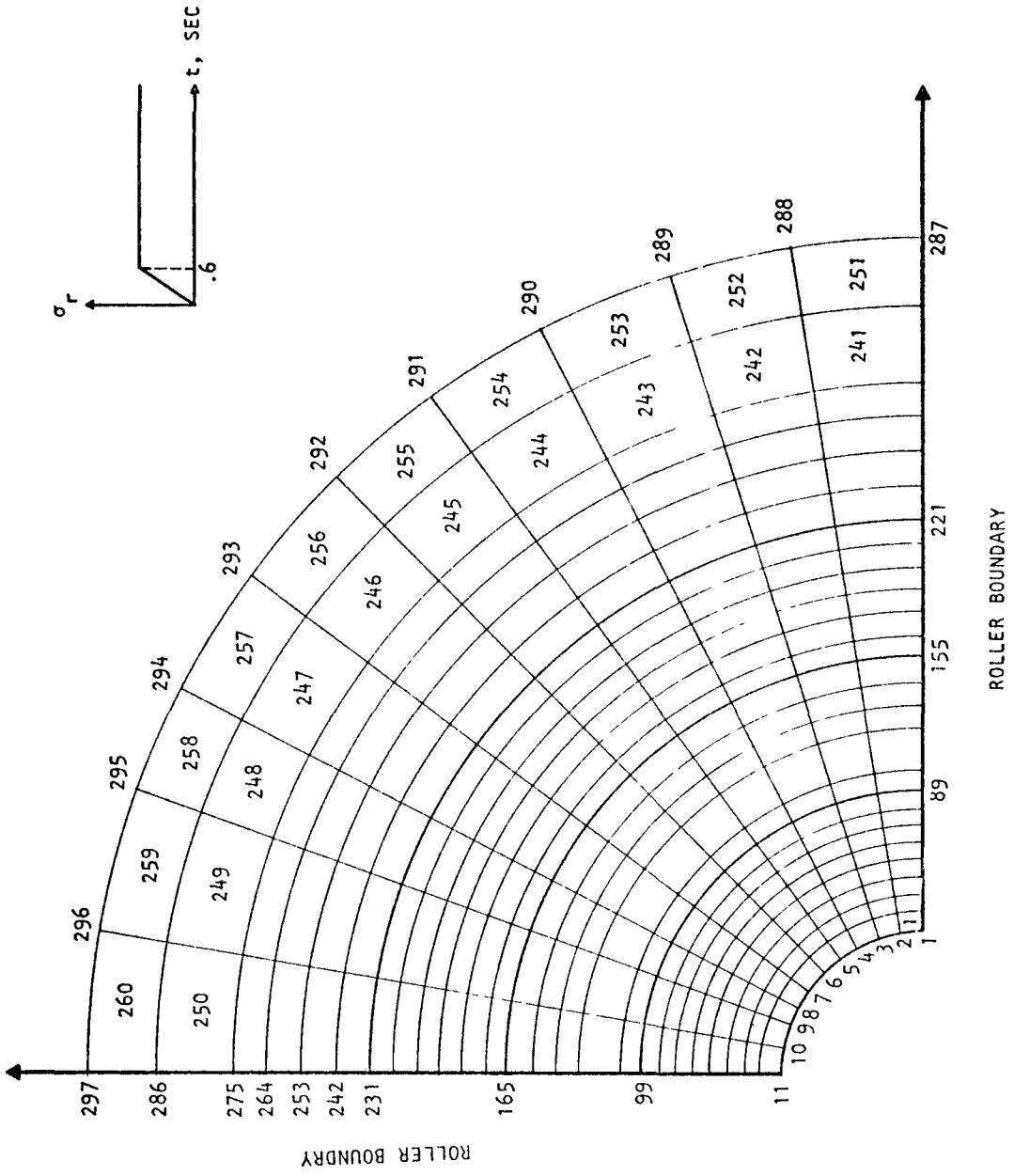

FIGURE D-4. CYLINDRICALLY DIVERGING, ELASTIC-PLASTIC WAVE

characteristics and method of interpolation are illustrated in Figures D-5 and D-6. The adapted results are shown in terms of radial stress σ_r versus range at several instants of time in Figure D-7. The regions where the adaptation is accurate are shown as solid lines and the regions of uncertainty are shown as broken lines. The present finite element results are also plotted in the figure. Agreement is best where the mesh is finest.

TWO-DIMENSIONAL ELASTIC WAVE

The response of a two-dimensional elastic half-space subjected to an air blast pulse of constant shape and amplitude and traveling at constant speed is available in closed form (Reference 20). An example problem which allows comparison to be made between the closed form and the present finite element method is illustrated in Figure D-8. The comparison is valid during the interval between $t = 0$ and $t = 0.092$ sec, after which a signal from the left hand boundary arrives at the target point. The comparison is made in terms of stress and velocity components at points down to 15 ft below the surface.

The results are shown in Figures D-9 through D-18. The comparison is most favorable for vertical components of stress and particle velocity, which is due partly to the highly superseismic (Mach 3.0) nature of this specific example. The comparison is least favorable for shear stresses, which is due partly to the fact that they are small relative to the vertical and horizontal stresses. Hence, a small percentage error in calculating horizontal or vertical stress is a large percentage error in shear stress.

1 ELASTIC TOP BREAKS OUT AT $\sigma_r/Y = 2$ AT $\bar{t} = 0.3$ SEC.

2 PLASTIC FRONT BREAKS OUT AT SAME TIME AS 1 BUT TRAVELS AT C_p = a/SEC RATHER THAN C_e = 1.2a/SEC.

3 SHOWS $X/\bar{t}$ FOR SIGNAL CORRESPONDING TO THE FIRST APPLICATION OF σ_r/Y TO CAVITY SURFACE (PLASTIC).

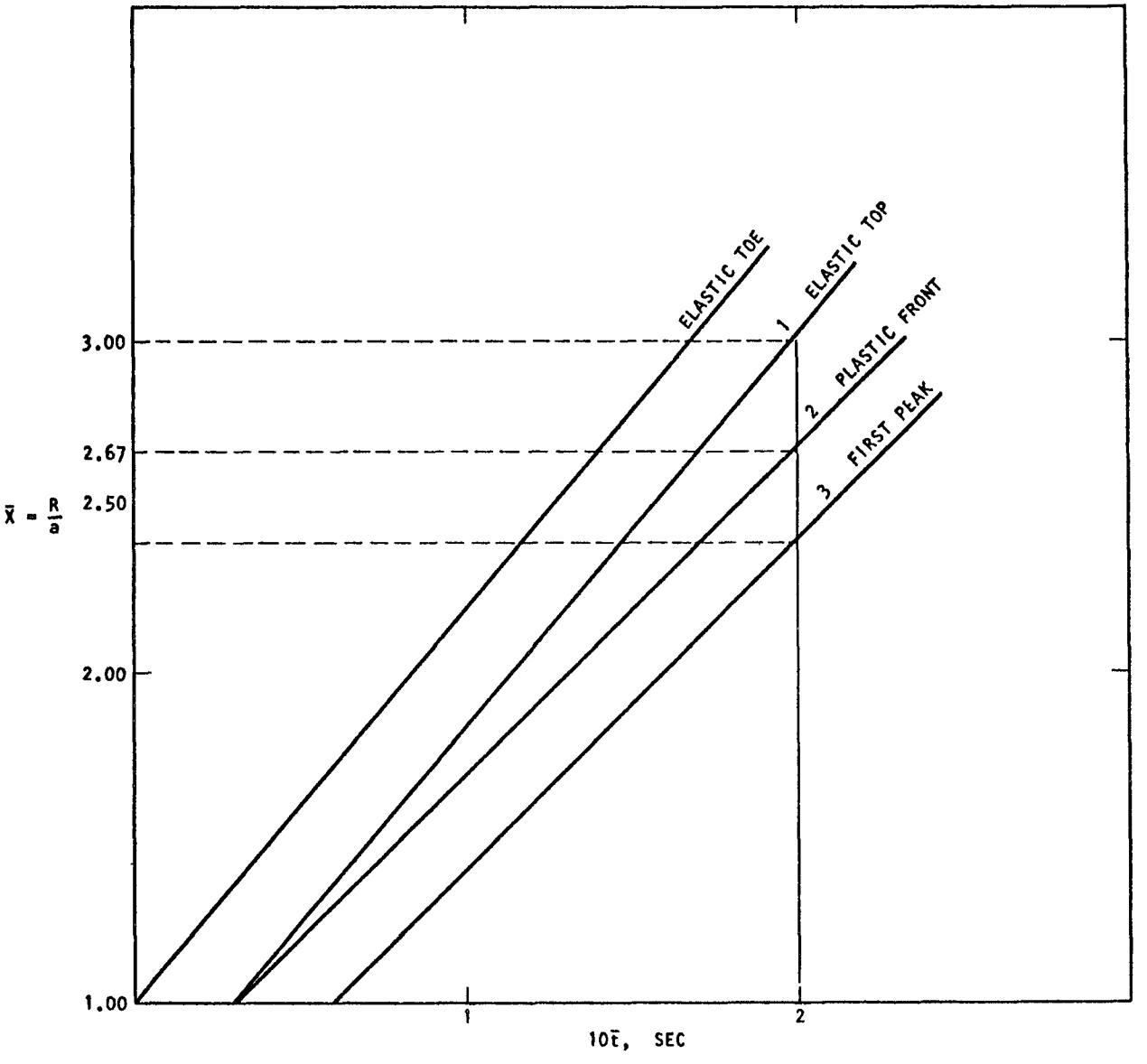

FIGURE D-5. CHARACTERISTICS FOR CYLINDRICAL WAVE SOLUTION

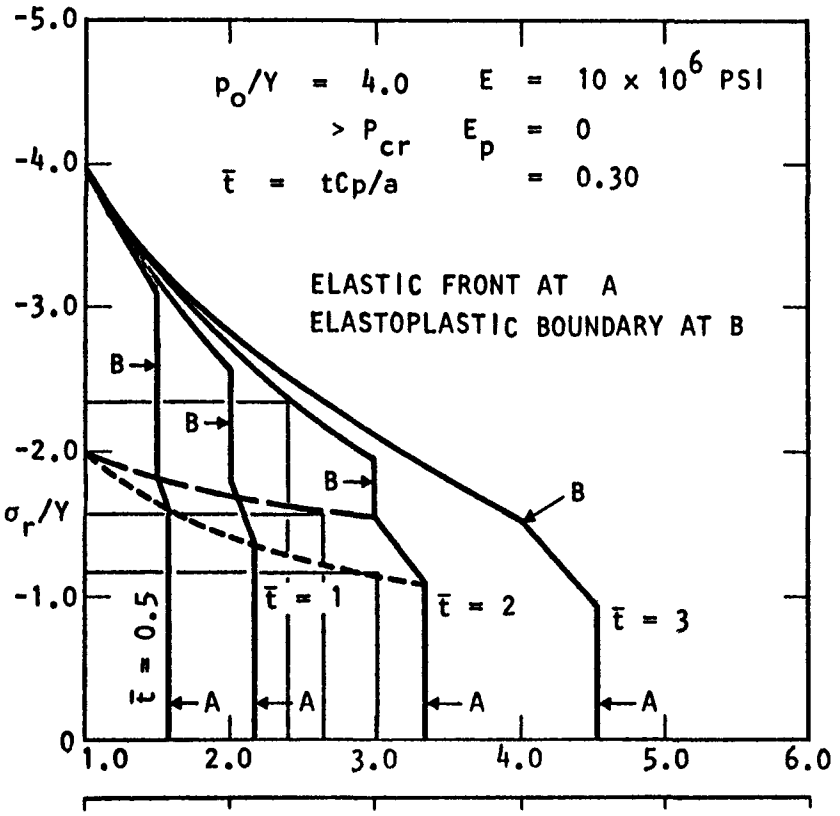

FIGURE D-6. EXAMPLE SHOWING HOW CHARACTERISTICS ARE USED TO ESTIMATE SOLUTION FOR $\bar{t}$ = 2 FOR RAMP INPUT

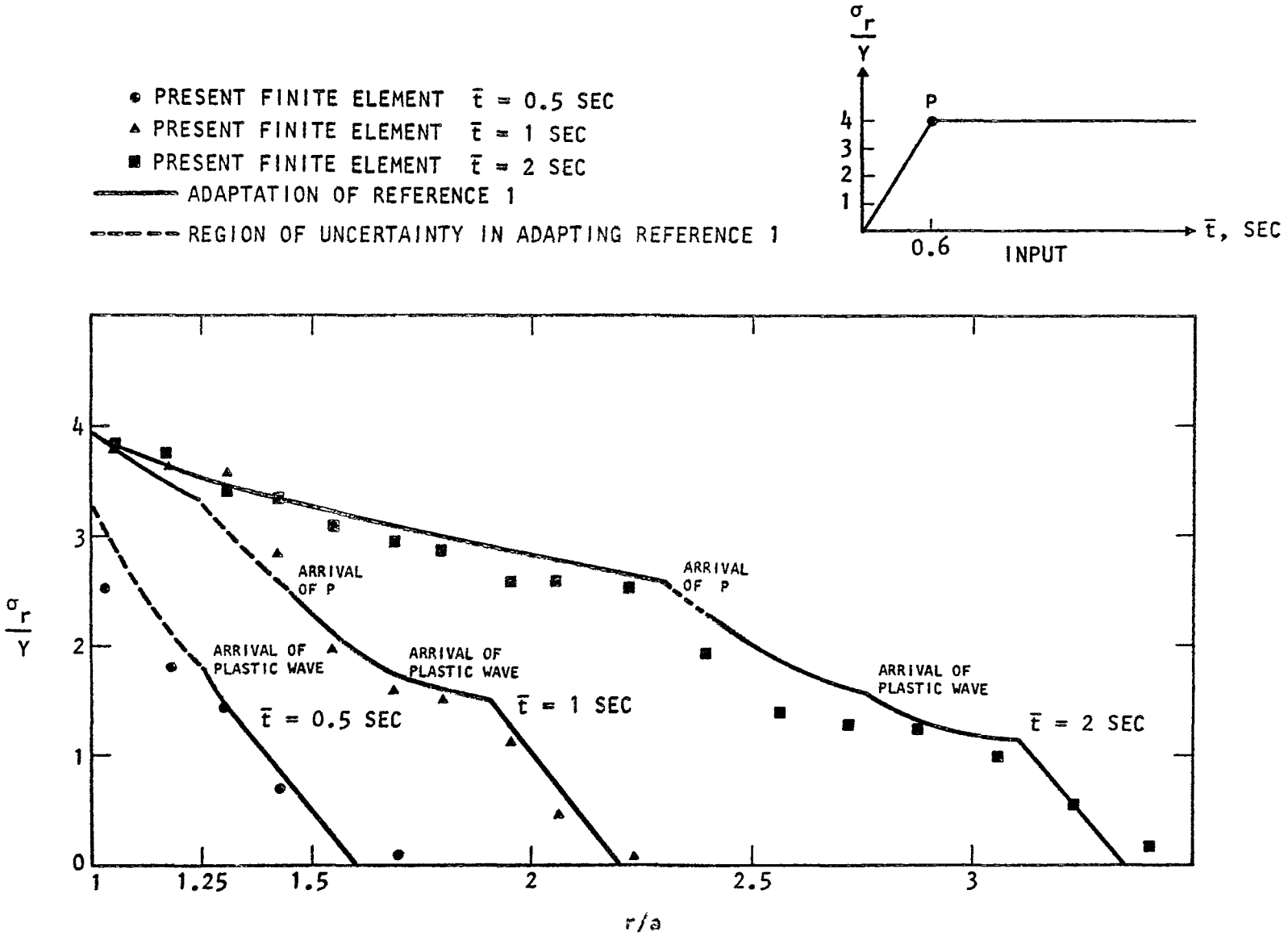

FIGURE D-7. COMPARISON OF PRESENT FINITE ELEMENT WITH ADAPTATION OF CLOSED FORM SOLUTION FOR CYLINDRICAL WAVE PROPAGATION

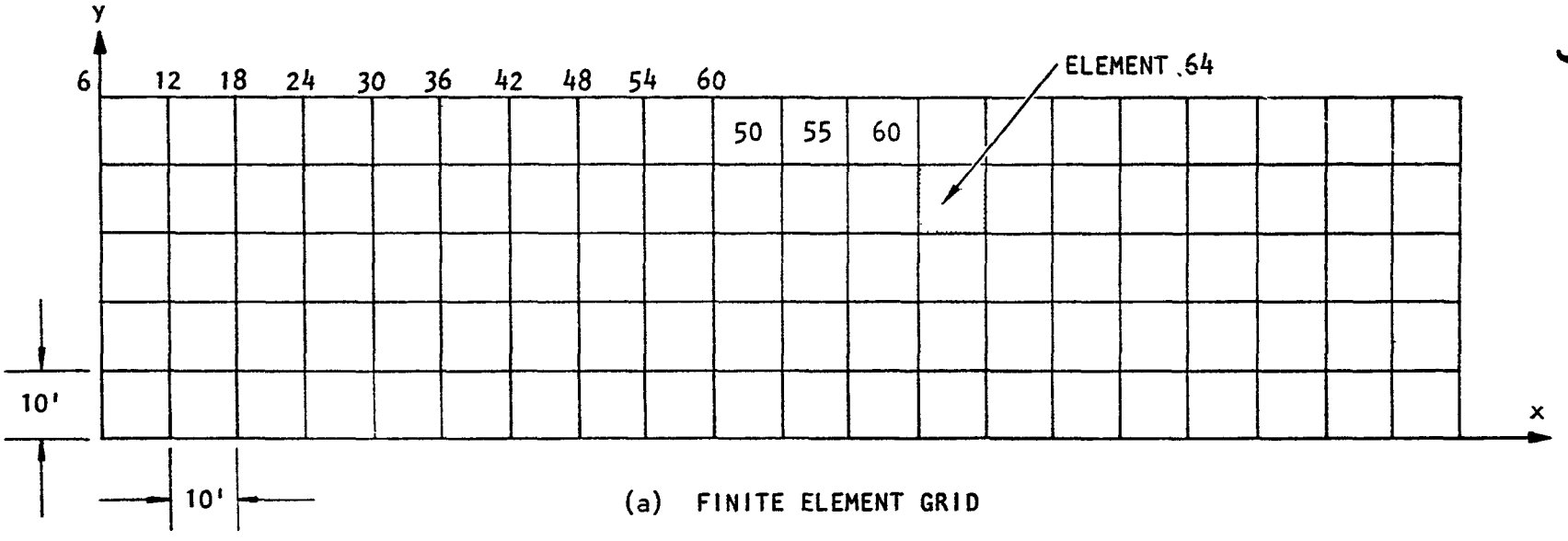

(a) FINITE ELEMENT GRID

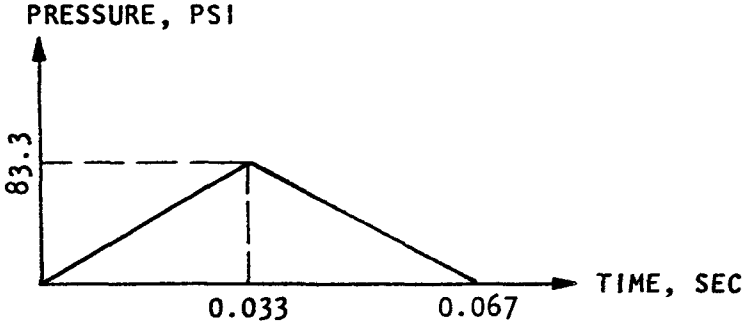

PROPOGATION VELOCITIES THROUGH MEDIUM:

C_p = 1000 FPS

C_s = 570 FPS

AIR BLAST SPEED = 3000 FPS

(b) INPUT PULSE

AJA1325

FIGURE D-8. GEOMETRY AND AIR BLAST LOADING FOR COMPARISON BETWEEN PRESENT FINITE ELEMENT AND COLE-HUTH SOLUTIONS

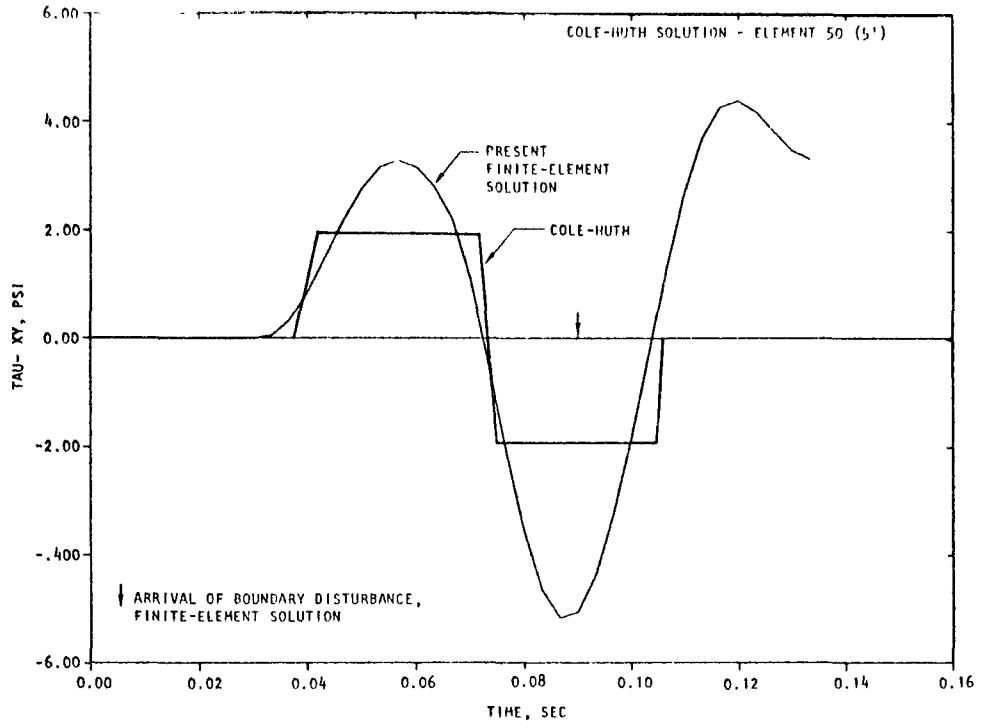

FIGURE D-9. COMPARISON OF PRESENT FINITE-ELEMENT SOLUTION WITH COLE-HUTH

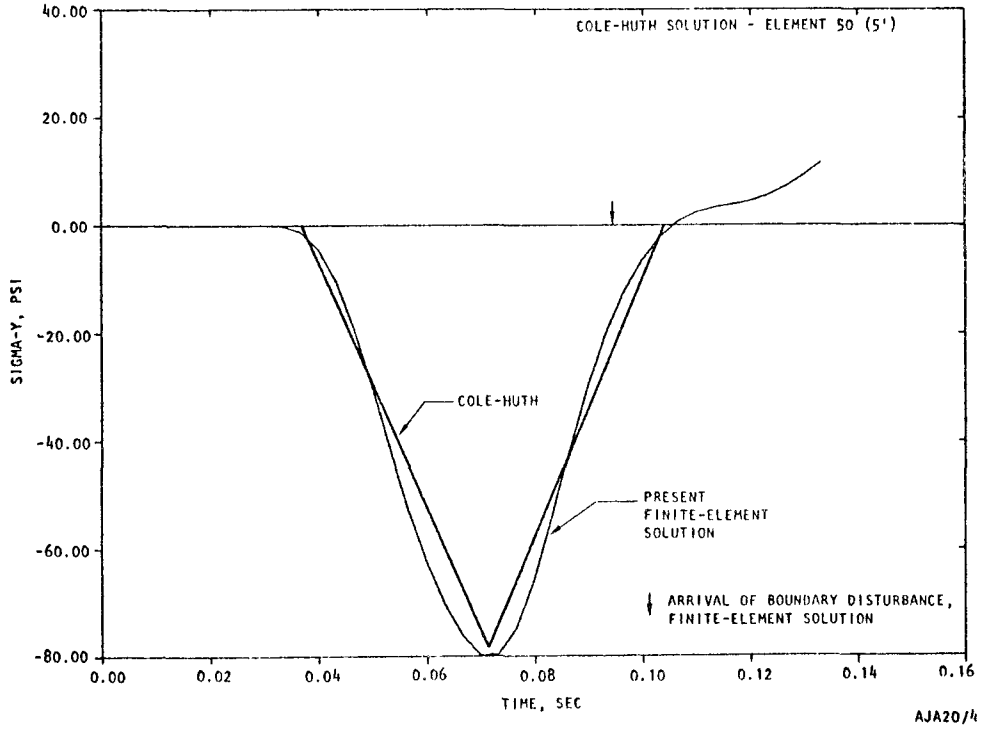

FIGURE D-10. COMPARISON OF PRESENT FINITE-ELEMENT SOLUTION WITH COLE-HUTH

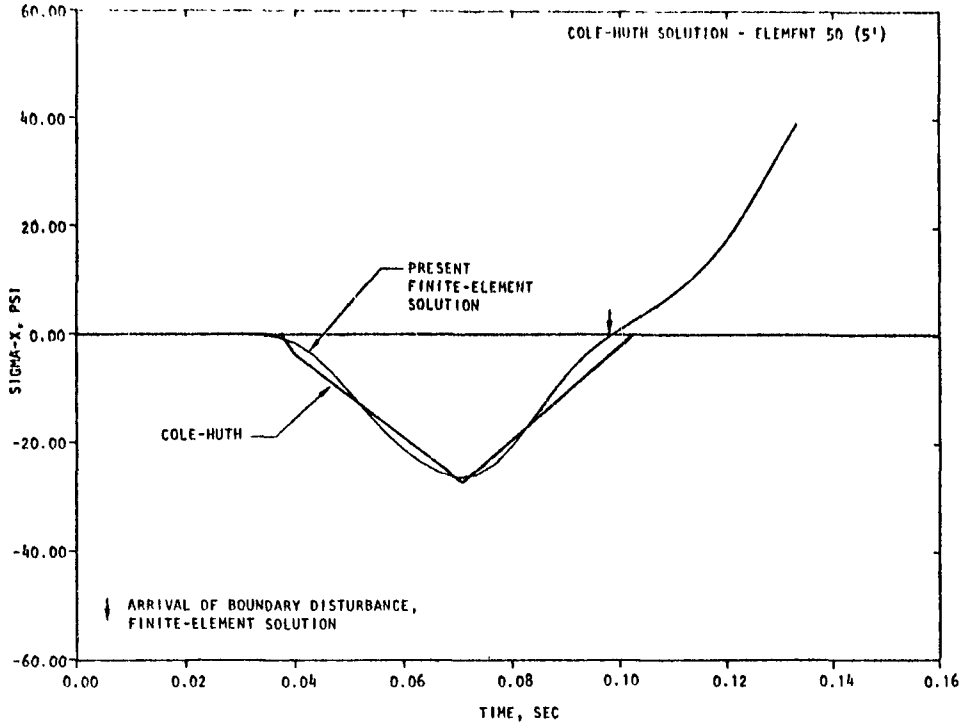

FIGURE D-11. COMPARISON OF PRESENT FINITE-ELEMENT SOLUTION WITH COLE-HUTH

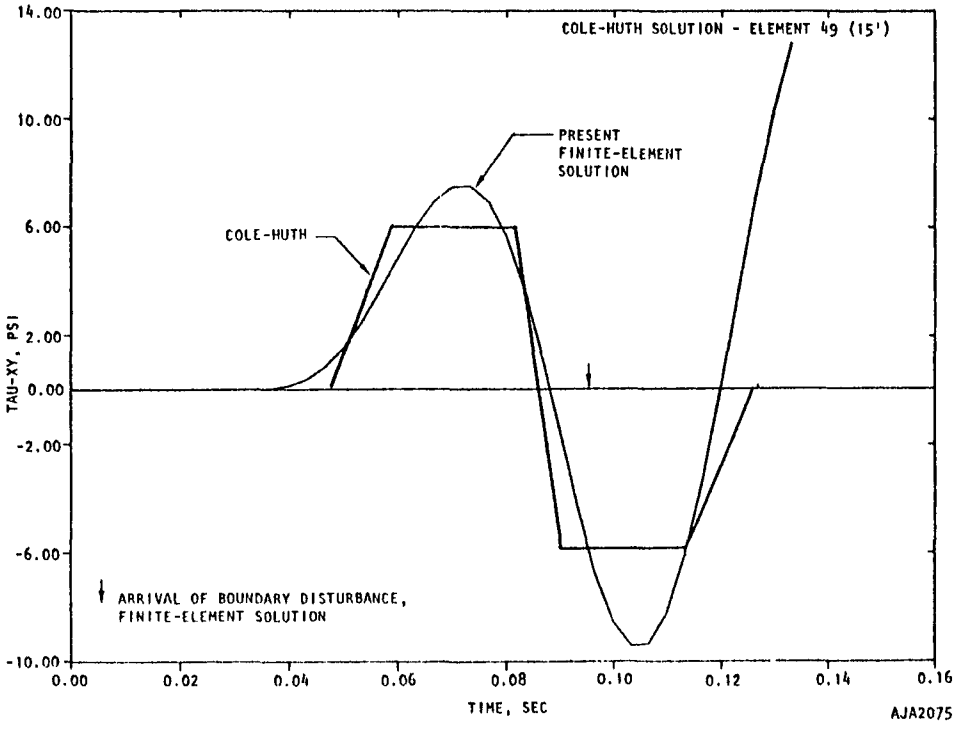

FIGURE D-12. COMPARISON OF PRESENT FINITE-ELEMENT SOLUTION WITH COLE-HUTH

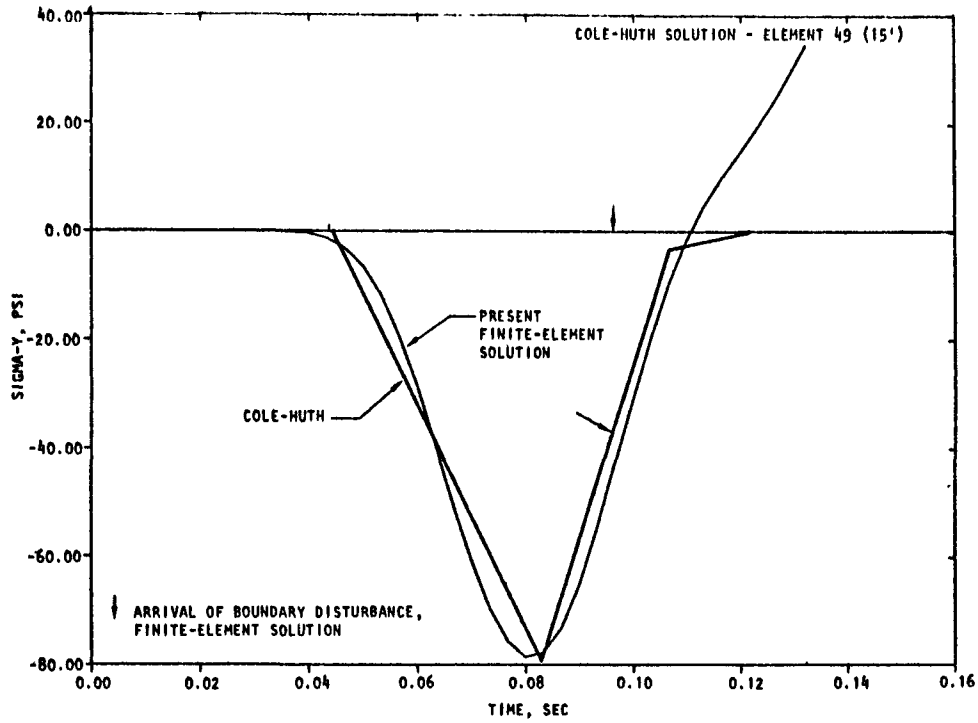

FIGURE D-13. COMPARISON OF PRESENT FINITE-ELEMENT SOLUTION WITH COLE-HUTH

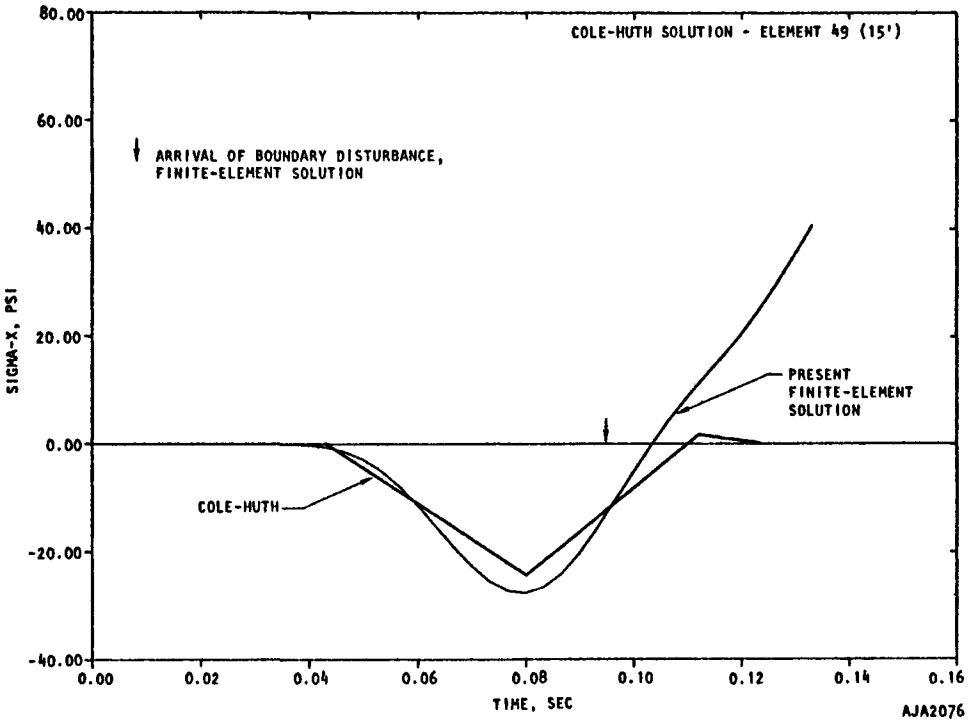

FIGURE D-14. COMPARISON OF PRESENT FINITE-ELEMENT SOLUTION WITH COLE-HUTH

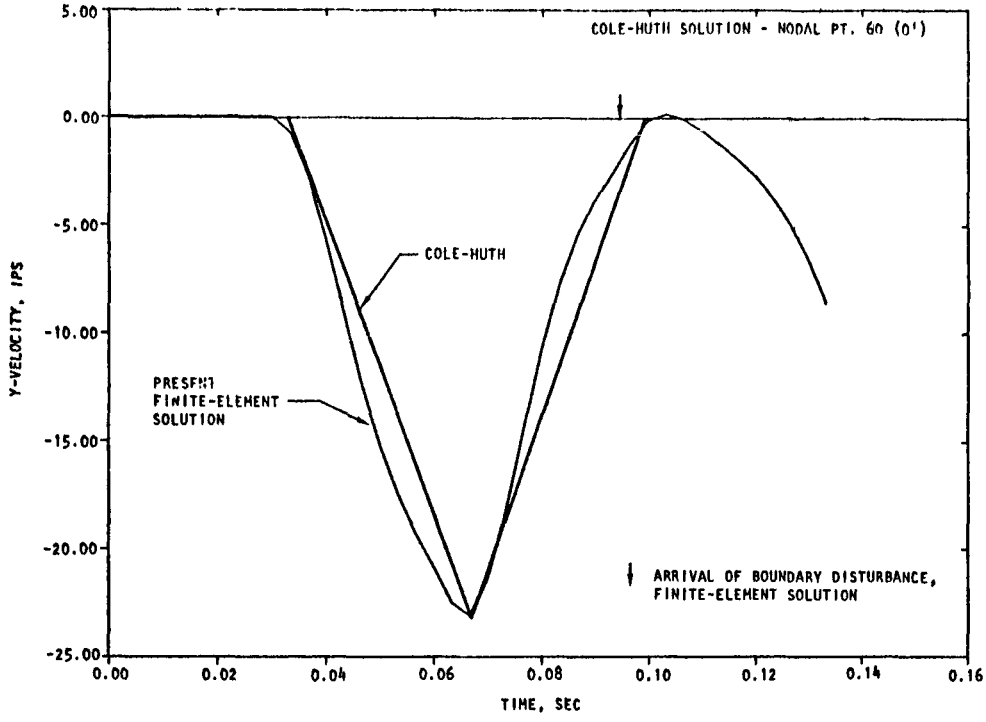

FIGURE D-15. COMPARISON OF PRESENT FINITE-ELEMENT SOLUTION WITH COLE-HUTH

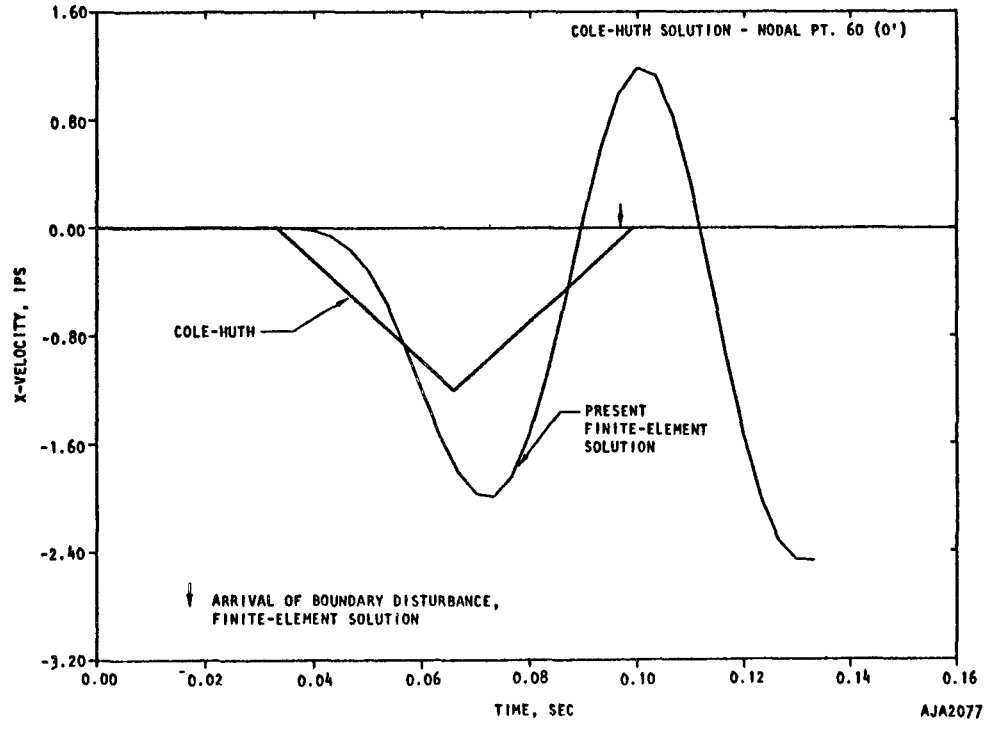

FIGURE D-16. COMPARISON OF PRESENT FINITE-ELEMENT SOLUTION WITH COLE-HUTH

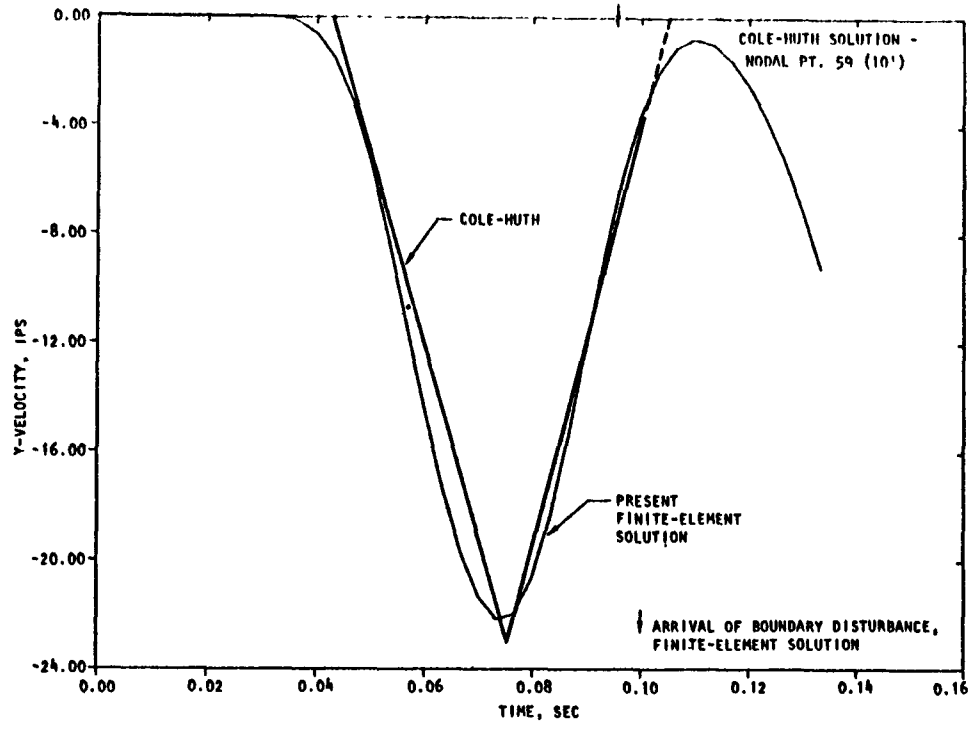

FIGURE D-17. COMPARISON OF PRESENT FINITE-ELEMENT SOLUTION WITH COLE-HUTH

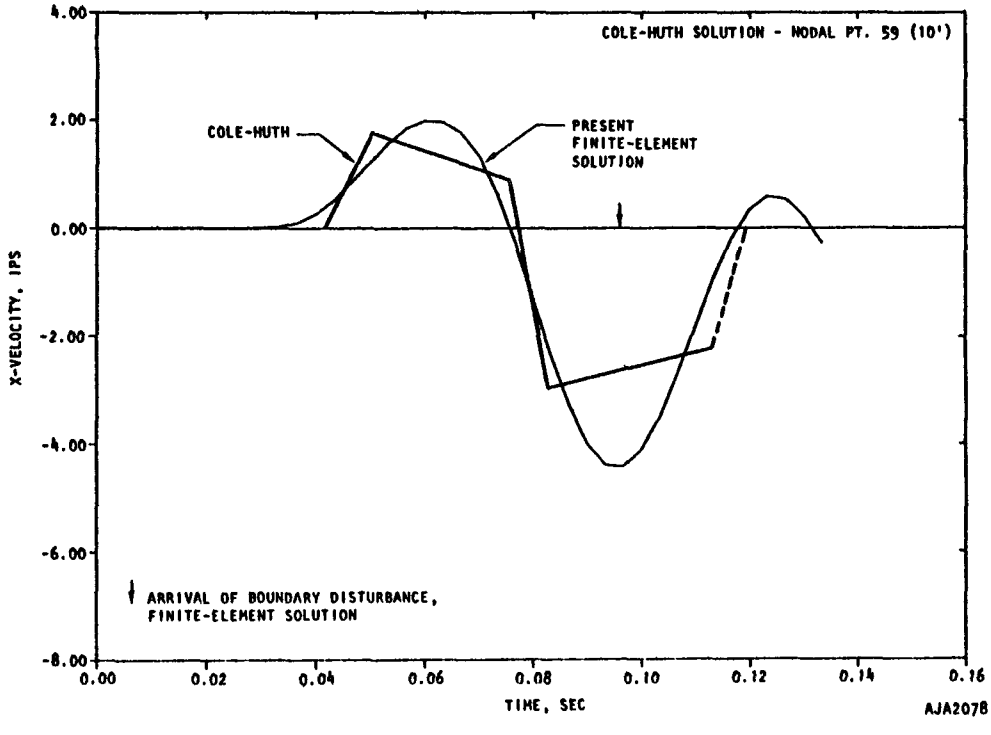

FIGURE D-18. COMPARISON OF PRESENT FINITE-ELEMENT SOLUTION WITH COLE-HUTH

APPENDIX E

ADDITIONAL RESULTS OF INTERACTION STUDIES

Tables E-1 and E-2 compare response at the foundation of the structure with the free-field response at the same elevation. This differs from the comparison in Table 5-2 and 5-3, where the free-field response is defined at the surface. The trend is the same in both instances, although suppression due to the presence of the structure is less when the free-field motion is defined as in Tables E-1 and E-2.

TABLE E-1. HORIZONTAL ACCELERATION SPECTRA $\left(\frac{\text{STRUCTURE (FOUNDATION)}}{\text{FREE-FIELD (55 FT)}}\right)$

Frequency, cps	Case					
	3	4	5	6	1-1	1-2
1	1.2	1.12	1.09	1.10	0.73	0.74
2	0.87	1.04	1.12	0.85	0.76	0.69
2.5	0.69	0.89	0.89	0.62	0.44	0.31
3	0.67	0.83	0.95	0.52	0.37	0.38
4	0.59	0.63	0.74	0.67	0.34	0.31
5	0.73	1.00	0.66	0.87	0.45	0.48
6	0.74	2.2	0.73	0.69	0.47	0.40
8	0.92	1.7	0.97	0.93	0.64	0.52
10	0.8	0.67	0.7	1.03	0.54	0.50

TABLE E-2. VERTICAL ACCELERATION SPECTRA $\left(\frac{\text{STRUCTURE (FOUNDATION)}}{\text{FREE-FIELD (55 FT)}}\right)$

Frequency, cps	Case					
	3	4	5	6	1-1	1-2
1	1.14	1.00	1.00	0.91	NOT OBTAINED	1.27
2	1.0	1.28	1.48	0.63		1.50
2.5	0.85	0.98	1.25	0.49		0.95
3	0.69	0.78	0.95	0.50		0.73
4	0.57	0.26	0.48	0.67		0.95
5	0.53	0.51	0.67	0.84		0.62
6	0.42	0.63	0.99	0.67		0.48
8	0.23	0.94	1.41	1.01		0.36
10	1.06	0.93	0.56			0.56

APPENDIX F

COMPARISON OF FINITE ELEMENT SOLUTIONS WITH CLOSED FORM SOLUTIONS

Two attempts, identified as Cases 1 and 2, were made to compare the present methods of computing interaction effects with those of previous investigators. Case 1 considers a cantilever structure embedded in a strip of soil, Figure 4-1, and is reported by Scavuzzo in Reference 21. The present results are compared with those of Reference 21 in Figure F-1.

Comparison is made in Figures F-2 and F-3 between the present results and those reported in Reference 22 for Case 2. The comparison is qualitatively favorable. Quantitative differences are due partly to distortion of the input in the analysis of Reference 22. Whereas the input is 5-cps harmonic motion and the present analysis faithfully preserves this, the analysis of Reference 22 distorts the input to predominately 4-cps motion by using excessively large elements in the soil. This data is also presented in Table F-1.

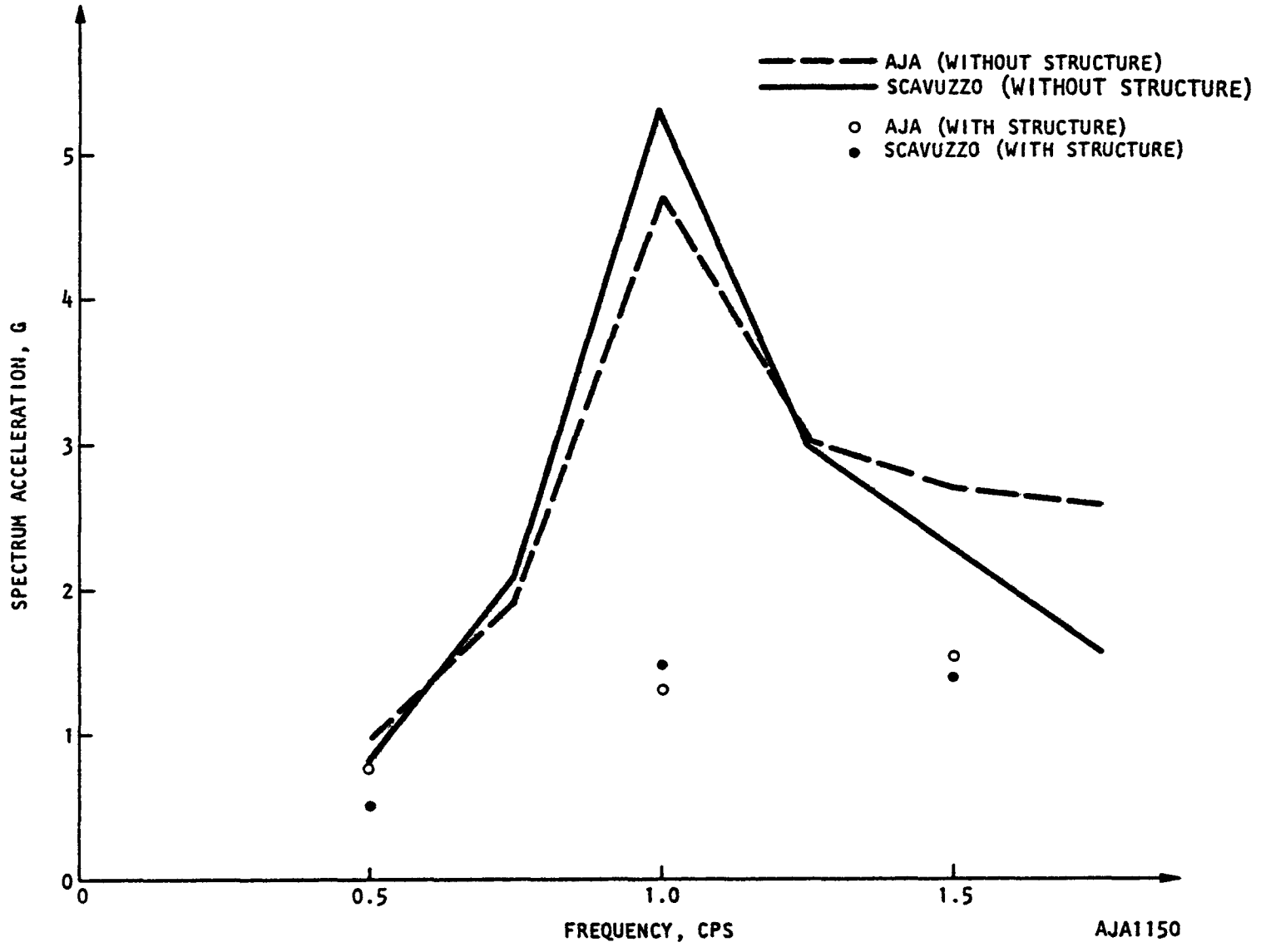

FIGURE F-1. SPECTRUM ACCELERATION VS FREQUENCY, $\lambda = 2$

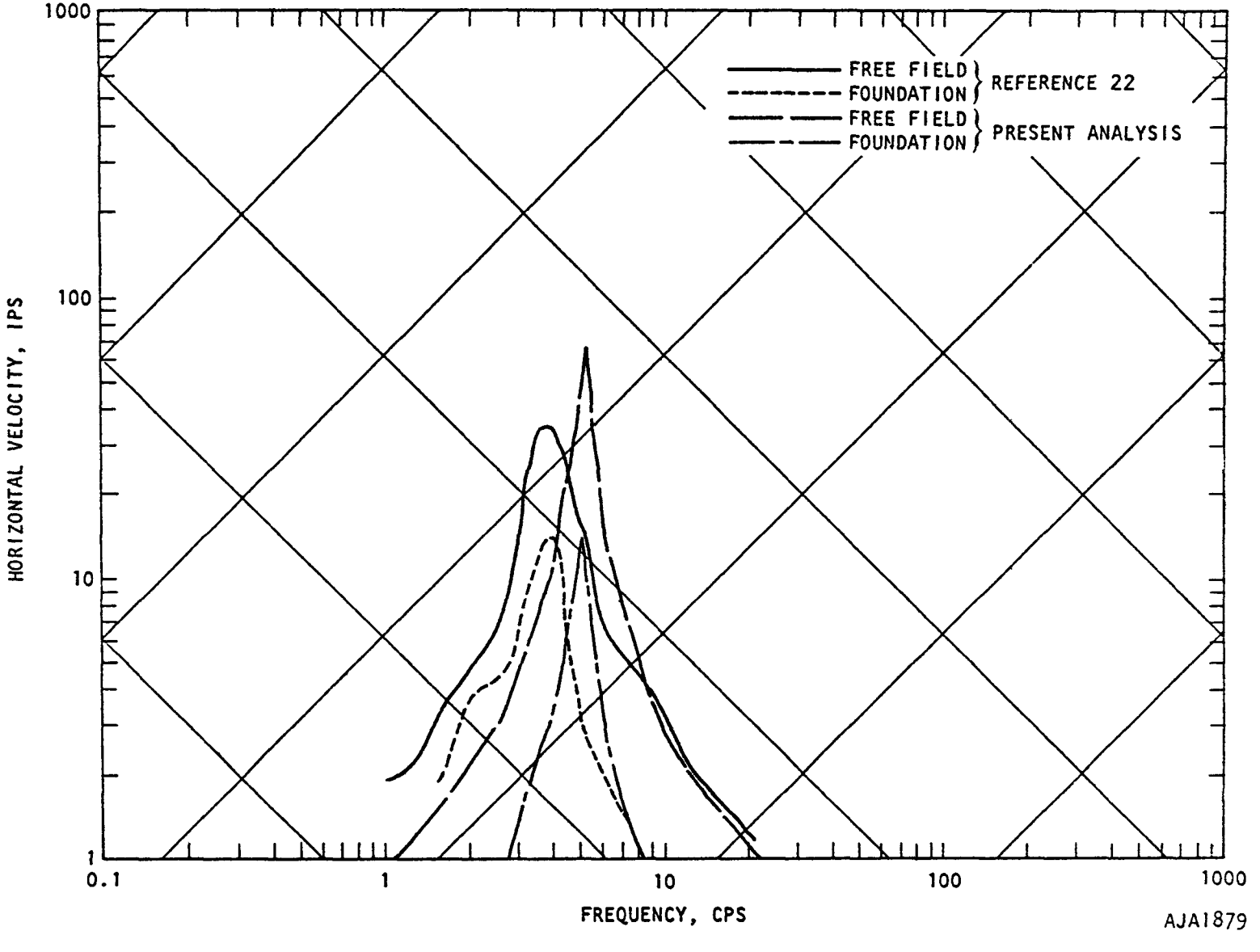

FIGURE F-2. HORIZONTAL RESPONSE SPECTRA, CASE 2

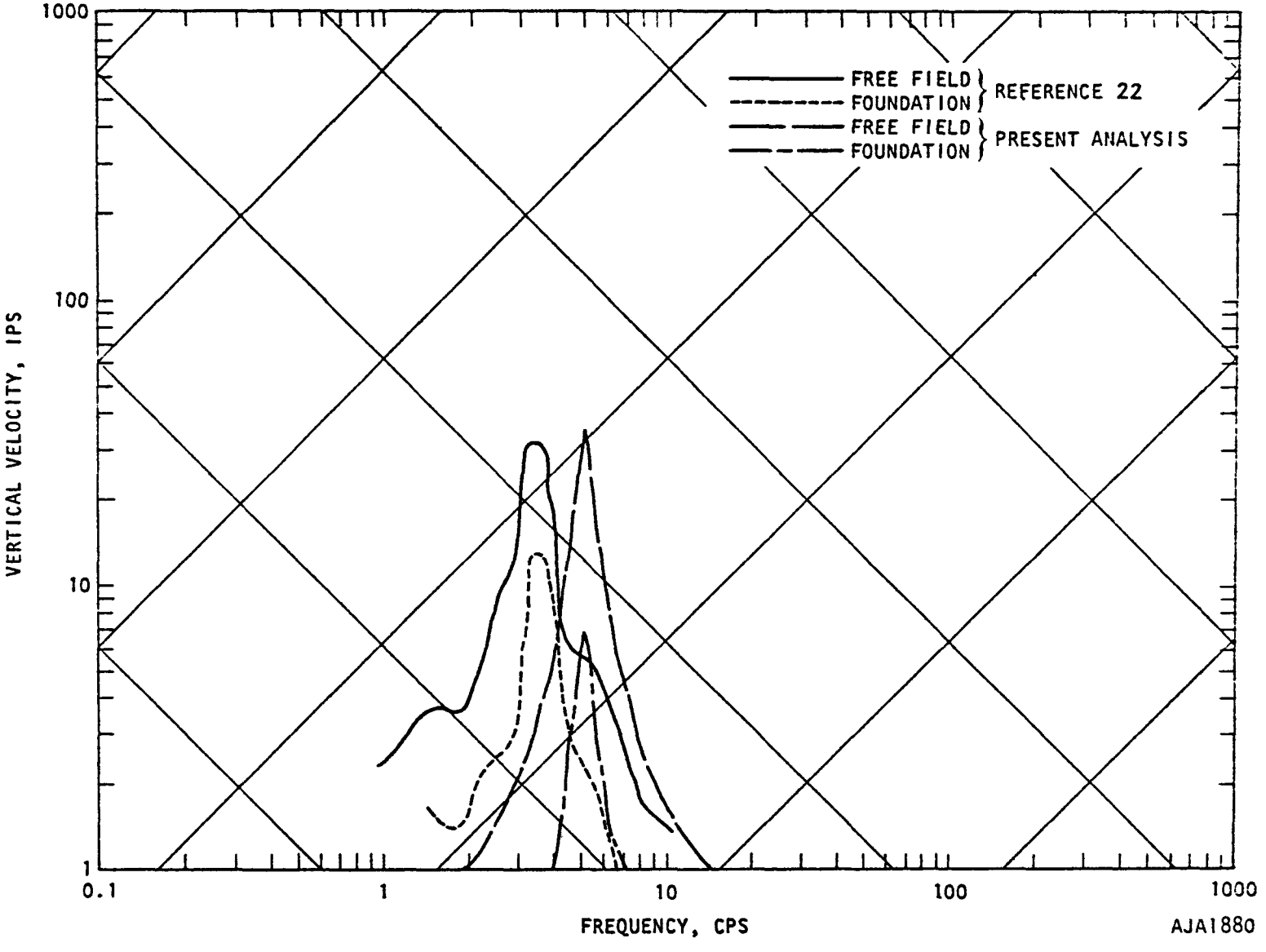

FIGURE F-3. VERTICAL RESPONSE SPECTRA, CASE 1

TABLE F-1. VELOCITY RESPONSE SPECTRA $\left(\frac{\text{FOUNDATION}}{\text{FREE FIELD (SURFACE)}}\right)$

Frequency, cps	Case 2			
	Horizontal		Vertical	
	AJA	Reference 22	AJA	Reference 22
1	0.23	0.71	0.28	0.45
2	0.37	0.81	0.22	0.39
2.5	0.26	0.63	0.22	0.42
3	0.28	0.4	0.21	0.28
4	0.28	0.39	0.19	0.44
5	0.20	0.16	0.20	0.44
6	0.19	0.25	0.18	0.36
8	0.2	0.2	0.19	0.32

A second comparison with the present Case 2 was performed by Scavuzzo, who used the closed form methods in Reference 21. Scavuzzo's analysis represents the horizontal translational degrees of freedom of the base mass and of the 4-cps and 5-cps oscillators. His analysis differs from the present Case 2 in that he omits rocking of the foundation and wave propagation underneath the foundation. The input to Scavuzzo's analysis was the 5-cps harmonic motion defined in Table 4-4. This motion has a peak acceleration (180/138) times greater than that computed at the surface by the present Case 2 free field analysis. The difference is due to numerical distortion by the finite element grid and to part of the momentum being changed from all horizontal to part horizontal and part vertical as the input motion propagates through the grid. To compare the two methods, the differences in input motion must be taken into account when the output is evaluated. This is done by scaling upward the foundation response spectra of the present Case 2 by (180/138). Figure F-4 and Table F-2, which include this scaling factor, indicate that the two methods give similar results, especially at the fixed base frequencies of the internal support structure and containment vessel (4 to 5 cps).

TABLE F-2. VELOCITY RESPONSE SPECTRA (FOUNDATION)

Frequency	Case 1, ips	Reference 21, ips
1	0.28	1.35
2	1.11	2.35
3	1.83	2.88
4	4.80	4.82
5	17.73	18.51
6	3.56	8.82
8	1.23	2.09

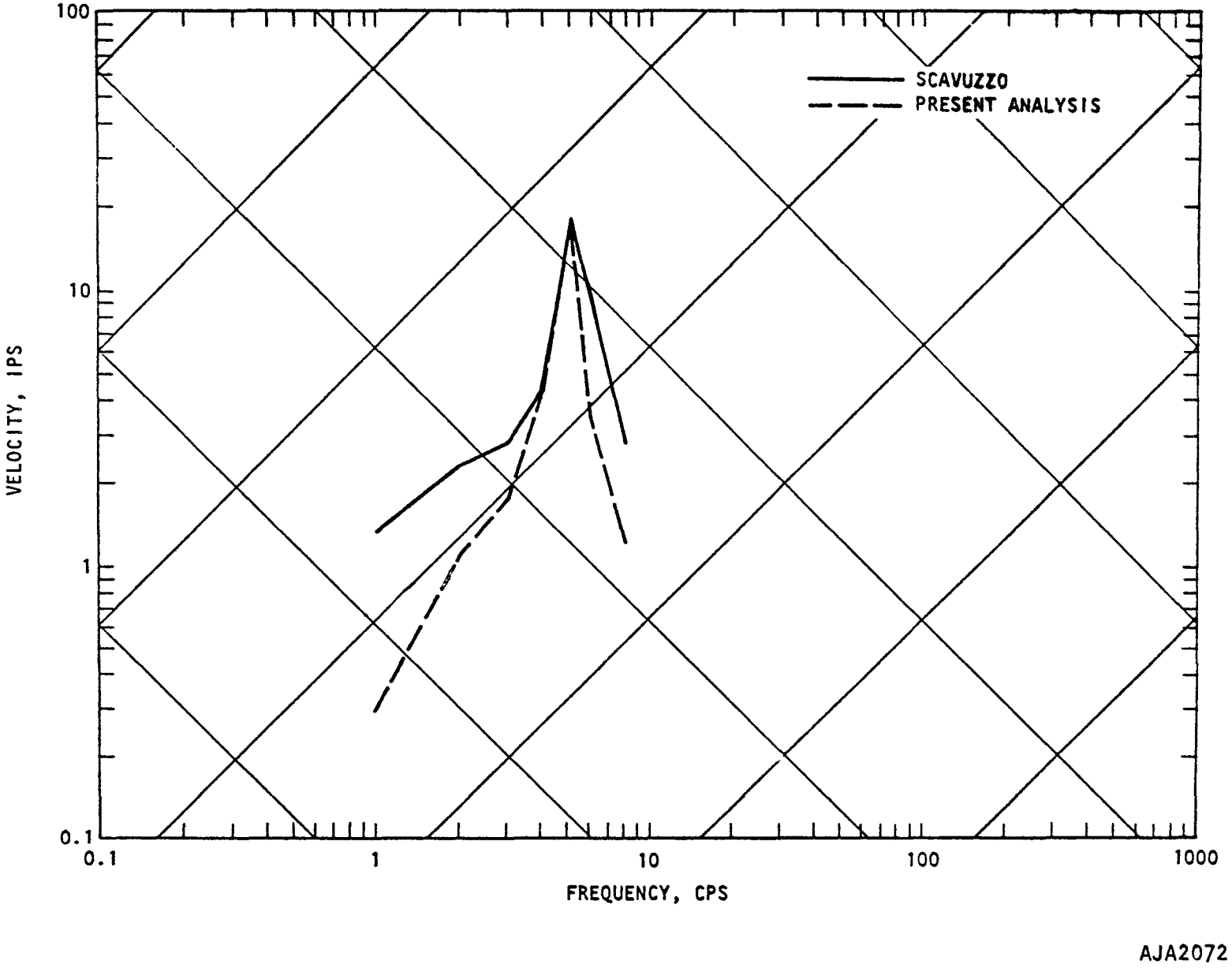

FIGURE F-4. HORIZONTAL RESPONSE SPECTRA FOR FOUNDATION

APPENDIX G

CONTRIBUTION OF ROCKING TO RESPONSE SPECTRA

The relation between the motion of the mass of a single degree of freedom oscillator and the translation and rotation of its base is derived below with the aid of a convolution integral. The geometry of the oscillator is shown in Figure G-1..

The equation of motion for the mass subjected to base motions $u(t)$ and $\theta(t)$ is

$$m\ddot{x} + k\left(x - (u+\theta L)\right) = 0 \qquad \text{(G-1)}$$

or

$$\ddot{x} + \omega^2\left(x - (u+\theta L)\right) = 0 \qquad \text{(G-1a)}$$

letting

$$x - (u+\theta L) = z \qquad \text{(G-2)}$$

$$\ddot{x} - (\ddot{u}+\ddot{\theta}L) = \ddot{z} \qquad \text{(G-3)}$$

$$\ddot{u} = \ddot{z} + \ddot{u} + \ddot{\theta}L \qquad \text{(G-4)}$$

Substituting Equations G-4 and G-2 into G-1a leads to

$$\ddot{z} + \omega^2 z = -(\ddot{u}+\ddot{\theta}L) \qquad \text{(G-5)}$$

$z(t)$ can be expressed as a function of the excitation $\ddot{u}(t)$, $\ddot{\theta}(t)$ and the impulsive response $h(t)$ by means of a convolution integral.

$$z(t) = \int_o^t -\left[\ddot{u}(\tau) + L\ddot{\theta}(\tau)\right] h(t-\tau)\, d\tau \qquad \text{(G-6)}$$

$h(t)$ is the solution to the equation

$$\ddot{z} + \omega^2 z = 1 \qquad \text{(G-7)}$$

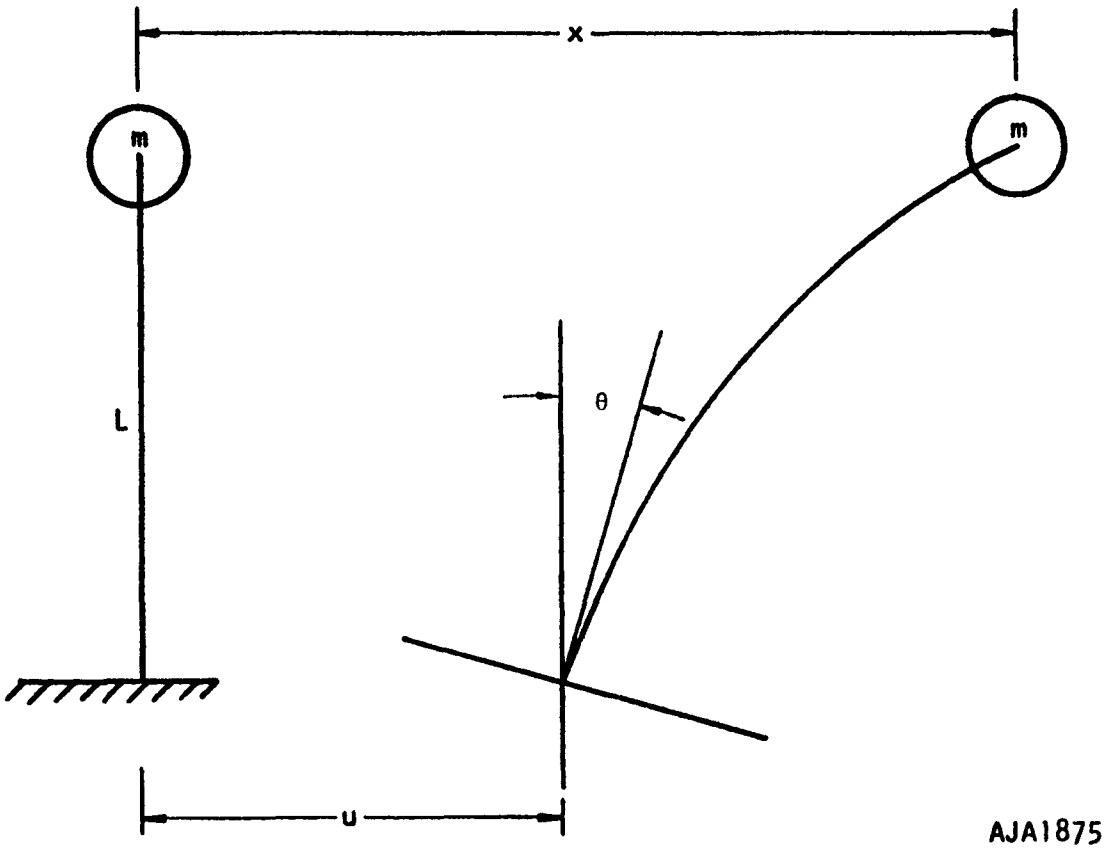

FIGURE G-1. SINGLE-DEGREE-OF-FREEDOM OSCILLATOR SUBJECTED TO TRANSLATION AND ROTATION OF BASE

The Laplace transform of Equation (G-7) is

$$s^2\,\bar{z}(s) + \omega^2\bar{z}(s) = \frac{1}{s} \tag{G-8}$$

or

$$\bar{z}(s) = \frac{1}{s}\left(\frac{1}{s^2+\omega^2}\right) \tag{G-9}$$

The inverse transform is:

$$z(t) = L(t) = \frac{1}{\omega}\sin\omega t \tag{G-10}$$

Substituting G-10 into G-6

$$z(t) = \int_o^t - \left[u(\tau) + L\theta(t)\right]\frac{1}{\omega}\sin\left[\omega(t-\tau)\right]d\tau \tag{G-11}$$

and noting from Equations G-2 and G-1a that

$$z = -\frac{\ddot{x}}{\omega^2} \tag{G-12}$$

it follows that

$$-\frac{\ddot{x}}{\omega^2} = \frac{1}{\omega}\int_o^t - \ddot{u}(\tau)\sin\left[\omega(t-\tau)\right]\,d\tau + \frac{1}{\omega}\int_o^t - L\theta(\tau)\sin\left[\omega(t-\tau)\right]d\tau \tag{G-13}$$

Given L, $\ddot{\theta}(t)$, $\ddot{u}(t)$, the maximum response $\ddot{x}$ at a given frequency ω over the interval t can be found. An array of such responses for a range of ω is the response spectrum.

APPENDIX H

DEFINITION OF INPUT FOR INDEPS CODE

Card Group	No. of Cards	Data and Definitions	Fortran Format
1	1	INTRY, KARD, (HED(I), I=1,12) INTRY = A numeric flag informing the computer as to whether or not there is another problem following the problem being read in. = 1 for a single problem or the last in a series of problems included in the run. = 0 when subsequent problems follow. KARD = * If this variable is different, than an asterisk (*), card will continue to be read until this flag is found. HED = A 72 column label of alphanumeric characters used to identify each problem. This label will appear at the top of each printed output page.	(I1,A1, 12A6)
2	1	JPT, JPL JPT = Total number of nodal points whose displacements, velocities or accelerations are to be saved for subsequent processing (i.e., plotting) JPL = Total number of displacements, velocities, and/or accelerations saved.	(2I3)

AJA FORM NO. 1075

DEFINITION OF INPUT FOR
INDEPS CODE

Card Group	No. of Cards	Data and Definitions	Fortran Format
3**	JPT	((JPLOT(I,J), J=1,7), I=1,JPT) JPLOT(I,1) = Nodal point number of a point for which displacement, velocity, or acceleration data is to be saved. JPLOT(I,2) = Horizontal displacement flag.* JPLOT(I,3) = Vertical displacement flag.* JPLOT(I,4) = Horizontal velocity flag.* JPLOT(I,5) = Vertical velocity flag.* JPLOT(I,6) = Horizontal acceleration flag.* JPLOT(I,7) = Vertical acceleration flag.* The total number of nonzero columns in JPLOT(I,2) through JPLOT(I,7) for all I must equal to JPL. * In columns 5 through 10 a 1 is punched to identify the quantities whose time histories are to be plotted. **No cards needed in this card group if JPT = 0	(I3,1X,6I1)

DEFINITION OF INPUT FOR
INDEPS CODE

Card Group	No. of Cards	Data and Definitions	Fortran Format
4*	= JPT	(JCOMNT(I),I=1,JCO) JCO = 6 * JPT ∿ Comment cards are supplied for only those points for which plots are requested (1 card per Nodal point) JCOMNT = A 36 column label of alphanumeric characters which is to be written toward the upper right-hand corner of all the plots pertaining to the corresponding nodal point.	(6A6)
5	1	KEL = Total number of elements whose stresses are to be saved for subsequent processing (I.e., plotting) KPL = Total number of stresses saved	(2I3)

* No cards needed if JPT = 0

AJA FORM NO. 1075

DEFINITION OF INPUT FOR
INDEPS CODE

Card Group	No. of Cards	Data and Definitions	Fortran Format
6	KEL	((KPLOT(I,J),6,I=1,KEL) KPLOT(I,1) = Element number of the elements for which stresses are to be saved. KPLOT(I,2) = Horizontal normal stress flag.* KPLOT(I,3) = Vertical normal stress flag.* KPLOT(I,4) = Horizontal or vertical shearing stress flag.* KPLOT(I,5) = Max. prinicpal stress flag.* KPLOT(I,6) = Min. principal stress flag.* The total number of nonzero columns in KPLOT(I,2) through KPLOT(I,6) for all I must be equal to KPL. * In columns 5 through 9 a 1 is punched to identify the quantities whose time histories are to be plotted.	(I3,1X, 5I1)

AJA FORM NO. 1075

DEFINITION OF INPUT FOR
INDEPS CODE

Card Group	No. of Cards	Data and Definitions	Fortran Format
7*	= KEL	(KCOMNT(I),I=1,KCO) (KCO = 6 * KEL) ∿ Comment cards are supplied for only those elements which are to be plotted, (1 card per element). KCOMNT =A 36 column label of alphanumeric characters which is to be written toward the upper right hand corner of all the plots pertaining to the corresponding element.	(6A6)
8	1	NUMNP, NUMEL, NUMMAT, NT, NPRINT, NP, ALFA, BETA, DELT NUMNP = Total number of nodal points in the finite element mesh. NUMEL = Total number of elements in the mesh - including all the quadrilateral, triangular, and "one-dimensional" elements. NUMMAT = Total number of different materials included in the finite element mesh. NT = Total number of integration cycles to be performed.	(615, 3F10.0)

*No cards needed if KEL = 0

AJA FORM NO. 1075

DEFINITION OF INPUT FOR
INDEPS CODE

Card Group	No. of Cards	Data and Definitions	Fortran Format
8 Contd.		NPRINT = Printing interval in cycles for the nodal point displacements velocities, accelerations and element stresses. NP = The number of cards used to specify the two histories involved in a pressure set. (See card group 11). ALFA = α BETA = β The damping coefficients involved in the expression: $[C] = \alpha[M] + \beta[K]$ The units of α and β are $\frac{1}{sec}$ and sec, respectively. DELT = Step size, in seconds, used in the numerical integration.	

DEFINITION OF INPUT FOR
INDEPS CODE

Card Group	No. of Cards	Data and Definitions	Fortran Format
9	2	I, BLK(I), SHR(I), RO(I), ALPHA(I), CELL(I)	(I5,5F15.0)
		I = Material identification number.	
		BLK(I) = Bulk modulus	
		SHR(I) = Shear modulus	
		RO(I) = Density	
		ALPHA(I) = Angle of friction	
		CELL(I) = Cohesion	
		I, B11(I), B22(I), B33(I), V11(I), V22(I)	(I5,5F15.0)
		Bulk modulus parameters.	

DEFINITION OF INPUT FOR
INDEPS CODE

Card Group	No. of Cards	Data and Definitions	Fortran Format
10	Variable depending upon the number of nodal points to be generated automatically by the Code.	N, KODE(N), R(N), Z(N), CH(N), CV(N), T(N), Q(N) N = Nodal point number. KODE(N) = Boundary condition code. = 01 for a horizontal roller. = 10 for a vertical roller. = 11 for a pinned nodal point, i.e., both horizontal and vertical constraint. = 0, or left blank, for a free nodal point, a point with velocity input, or a point to be quieted. R(N) = X coordinate in feet. The positive X axis is usually taken to be directed toward the right. Z(N) = Y coordinate in feet. The positive Y axis is usually taken to be directed upward.	(2I5,6F10.0)

AJA FORM NO. 1075

DEFINITION OF INPUT FOR
INDEPS CODE

Card Group	No. of Cards	Data and Definitions	Fortran Format
10 Contd.		CH(N)* = The vertical "tributary length" in feet. In the Code, this number is first multiplied by 12* and then multiplied by the associated horizontal pressure to get the horizontal force acting at the nodal point. CV(N)* = The horizontal "tributary length" in feet for the vertical force acting at the point. CH and CV are all necessarily zero for a point which is not loaded. T(N) = Arrival time in seconds of the associated pressures at the nodal point. Q(N) = 0, INITIAL Velocity, displacement=0. ≠ 0, INITIAL Velocity, displacement to be specified. *Note: Since the thickness of the finite element system (in the direction perpendicular to the mesh) is taken as 1 inch in the code, the "tributary length" in inches is numerically equal to the tributary area in square inches.	

AJA FORM NO. 1075

DEFINITION OF INPUT FOR
INDEPS CODE

Card Group	No. of Cards	Data and Definitions	Fortran Format
10a	1 for each of the nodal points with nonzero initial conditions.	XO(2 *N-1), XO(2 *N), XI(2 *N-1), XI(2 * N) XO(2 *N-1) = Initial horizontal displacement in inches. XO(2 * N) = Initial vertical displacement in inches. XI(2 *N-1) = Initial horizontal velocity in in/sec. XI(2 * N) = Initial vertical velocity in in/sec. All these quantities are considered positive when directed in the direction of the positive coordinate axis.	(4E20.10)
11	NP	((P(K,M),K = 1,3), M = 1,NP) P(1,M) = Time at which load is specified (sec) P(2,M) = Horizontal load (lb/in.) P(3,M) = Vertical load (lb/in.)	(3F10.1)

AJA FORM NO. 1075

DEFINITION OF INPUT FOR
INDEPS CODE

Card Group	No. of Cards	Data and Definitions	Fortran Format
12		M, (IX(M,I), I=1,5)	(615)

M = Element number

IX(M,1) =
IX(M,2) =
IX(M,3) =
IX(M,4) =

} Nodal point numbers of the corner points. IJKL in the case of a quadrilaterial,* IJKK in the case of a triangle, and IJJI in the case of a one-dimensional element.** In the case of a quadrilateral or a triangle, the nodal points must be read in counter-clockwise order.

IX(M,5) = Material number

NOTE: If element cards are missing in card group 12, automatic element generation will occur. This generation takes place by incrementing the values of the element and nodal point numbers in the IX array by 1 (e.g. (IX(M,J),J=1,4) = (IX (M-1,J), J=1,4) +1). The material number (IX(M,5)) is set to the value on the last input card.

Element generation only fills in any skipped element numbers and does not extrapolate. This requires that the last element card of a mesh must always be supplied.

*NOTE: When a quadrilateral is concave (not recommended), the entrant corner must be either J or K. For example the concave quadrilateral shown below must be numbered in one of the two ways shown.

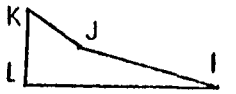

Entrant Corner "J"

or

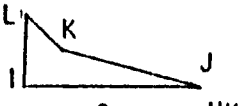

Entrant Corner "K"

**NOTE: One-dimensional element have elastic properties only.

DEFINITION OF INPUT FOR
INDEPS CODE

Card Group	No. of Cards	Data and Definitions	Fortran Format
13	1	KBP Number of nodal points where there are kinematic (velocity) inputs. These nodal points include those which are to be quieted. If there is no kinematic input, a blank card is supplied and all the following cards are omitted.	(13)
14	KBP	(KBNP(I),I=1,KBP) Nodal point numbers with kinematic input. If the nodal point does not share the user-prescribed velocity/time history (i.e. node points which are quieted and which do not have velocity input prescribed), the nodal point number is preceded by a minus sign.	(1015)
15	1	NTIME Number of discrete times at which input velocities are specified. If there are no velocities to be specified, a blank card is supplied.	(13)
16	NTIME	((V(I,J),J=1,3),I=1,NTIME) V(I,1) = Time at which velocity is specified (sec) V(I,2) = Horizontal velocity (in./sec) V(I,3) = Vertical velocity (in./sec)	(3E20.0)

AJA FORM NO. 1075

DEFINITION OF INPUT FOR

INDEPS CODE

Card Group	No. of Cards	Data and Definitions	Fortran Format
17	1	NQ Number of nodal points to be quieted. If no points are quieted, a blank card is supplied.	(I3)
18	NQ	((IQ(I,J),J=1,5),I=1,NQ) IQ(I,1) = Type of boundary. = 1 if boundary vertical = 2 if boundary horizontal IQ(I,2) = Node point number of corrector IQ(I,3) = Node point number if sensor IQ(I,4) = Material property index IQ(I,5) = Sequence number of the point in the KBNP array	(5I5)

AJA FORM NO. 1075

```
C      PROGRAM INDEPS (INPUT,OUTPUT,PLOT,TAPE5=INPUT,TAPE6=OUTPUT,TAPE10
      1=PLOT)
       REAL MASS
       COMMON ALFA,BETA,DELT,MBAND,N,NEQ,NNN,NP,NT,NUMNP,NUMEL,NUMMAT,
      1 TT,VOL,DUMMY(5),A(550,36),SIG(250,7),B(550),B0(550),CC(1500),
      2 C(3,3),CH(275),CV(275),EPS(250,4),H(6000),IX(250,5),KODE(275),
      3 MASS(275),P(3,50),R(275),Z(275),S(10,10),T(275),X0(550),X1(550),
      4 X2(550)
       COMMON/MATARG/BLK(12),SHR(12),RO(12),ALPHA(12),CELL(12),B11(12),
      1 B22(12),B33(12),U11(12),U22(12)
       COMMON/PLDATA/PLD(50,51),JKPL1,KEL,LSHIFT,NTAPE
       COMMON/KINBC/KBP,KBNP(60),NTIME,NQ,IQ(60,5),DV(120),V(150,3),
      1 IV(60)
       DIMENSION NAMEX(3),NAMEY(34),JPLOT(50,7),JCOMNT(300),KPLOT(50,6),
      1 KCOMNT(300)
       DIMENSION AJA(9),HED(12),XC(250),YC(250)
       EQUIVALENCE (B(1),NAMEX(1)),(B(4),NAMEY(1)),(B(38),JCOMNT(1)),
      1 (B(338),KCOMNT(1)),(A(1,1),XC(1)),(A(1,2),YC(1))
       DATA (AJA(I), I=1,9)/6HA G B ,6HA B I ,6HA N - ,6HJ A C ,6HO B S ,
      1 6HE N  A,6H S S O,6H C I A,6H T E S/
       DATA (NAMEX(I), I=1,3)/2, 12H TIME (SEC) /
       DATA (NAMEY(I), I=1,34)/3, 18H   X-DISPL. (IN)   ,
      1 18H   Y-DISPL. (IN)   , 18H X-VELOCITY (IPS) ,
      2 18H Y-VELOCITY (IPS) , 18H X-ACC. (IN/SEC2) ,
      3 18H Y-ACC. (IN/SEC2) , 18H   SIGMA-X (PSI)   ,
      4 18H   SIGMA-Y (PSI)   , 18H   TAU-XY (PSI)    ,
      5 18H SIGMA-MAX. (PSI) , 18H SIGMA-MIN. (PSI) /
       DATA INTRY,MARK/0,1H*/
       DATA NTAPE/7/
C
C      READ AND PRINT OF CONTROL INFORMATION AND MATERIAL PROPERTIES
C
   50 IF(INTRY.EQ.0) GO TO 52
      CALL EXIT
   52 READ (5,1010) INTRY, KARD, (HED(I), I=1,12)
      IF(KARD.NE.MARK) GO TO 52
      WRITE (6,2020) (AJA(I), I=1,9), (HED(I), I=1,12)
      READ (5,1011) JPT,JPL
      IF (JPT .EQ. 0) GO TO 53
      READ (5,1013) ((JPLOT(I,J), J=1,7), I=1,JPT)
      N=6*JPT
      READ (5,1012) (JCOMNT(I), I=1,N)
   53 READ (5,1011) KEL,KPL
      JKPL=JPL+KPL
      JKPL1=JKPL+1
      IF (KEL .EQ. 0) GO TO 54
      READ (5,1014) ((KPLOT(I,J), J=1,6), I=1,KEL)
      N=6*KEL
      READ (5,1012) (KCOMNT(I), I=1,N)
   54 READ (5,1000) NUMNP,NUMEL,NUMMAT,NT,NPRINT,NP,ALFA,BETA,DELT
      WRITE (6,2000) NUMNP,NUMEL,NUMMAT,DELT,NT,NPRINT,ALFA,BETA
      IF (JKPL.EQ.0) GO TO 56
```

```
      REWIND NTAPE
      WRITE (NTAPE) NT,JPT,JPL,((JPLOT(I,J),J=1,7),I=1,JPT),KEL,KPL,
     1 ((KPLOT(I,J),J=1,6),I=1,KEL),(B(I),I=1,637)
   56 DO 59 M=1,NUMMAT
      READ (5,1001) I,BLK(I),SHR(I),RO(I),ALPHA(I),CELL(I)
      READ (5,1001) I,B11(I),B22(I),B33(I),U11(I),U22(I)
      WRITE (6,2011) I,BLK(I),SHR(I),RO(I),ALPHA(I),CELL(I),B11(I),
     1 B22(I),B33(I),U11(I),U22(I)
   59 CONTINUE
C
C     READ AND PRINT OF NODAL POINT DATA
C
      WRITE (6,2020) (AJA(I), I=1,9), (HED(I), I=1,12)
      WRITE (6,2004)
      L=0
   60 READ (5,1002) N,KODE(N),R(N),Z(N),CH(N),CV(N),T(N),Q
      R(N)=12.0*R(N)
      Z(N)=12.0*Z(N)
      CH(N)=12.0*CH(N)
      CV(N)=12.0*CV(N)
      IF (Q) 65,62,65
   62 X0(2*N-1)=0.0
      X0(2*N)=0.0
      X1(2*N-1)=0.0
      X1(2*N)=0.0
      GO TO 67
   65 READ (5,1006) X0(2*N-1),X0(2*N),X1(2*N-1),X1(2*N)
   67 NL=L+1
      ZX=N-L
      DR=(R(N)-R(L))/ZX
      DZ=(Z(N)-Z(L))/ZX
   70 L=L+1
      IF(N-L) 100,90,80
   80 KODE(L)=KODE(L-1)
      R(L)=R(L-1)+DR
      Z(L)=Z(L-1)+DZ
      X0(2*L-1)=0.0
      X0(2*L)=0.0
      X1(2*L-1)=0.0
      X1(2*L)=0.0
      T(L)=0.0
      CH(L)=CH(L-1)
      CV(L)=CV(L-1)
      GO TO 70
   90 WRITE (6,2002) (K,KODE(K),R(K),Z(K),X0(2*K-1),X0(2*K),X1(2*K-1),
     1X1(2*K),T(K),CH(K),CV(K),K=NL,N)
      IF(NUMNP-N) 100,110,60
  100 WRITE (6,2009) N
      CALL EXIT
  110 CONTINUE
C
```

```
C       READ AND PRINT OF LOAD DATA
C
      IF (NP.EQ.0) GO TO 125
      WRITE (6,2020) (AJA(I), I=1,9), (HED(I), I=1,12)
      WRITE (6,2007)
      DO 120 M=1,NP
  120 READ(5,1004) (P(K,M),K=1,3)
      WRITE (6,2005) ((P(K,M),K=1,3),M=1,NP)
C
C       READ AND PRINT OF ELEMENT PROPERTIES
C
  125 WRITE (6,2020) (AJA(I), I=1,9), (HED(I), I=1,12)
      WRITE (6,2001)
      N=0
  130 READ (5,1003) M,(IX(M,I),I=1,5)
  140 N=N+1
      IF (M-N) 170,170,150
  150 IX(N,1)=IX(N-1,1)+1
      IX(N,2)=IX(N-1,2)+1
      IX(N,3)=IX(N-1,3)+1
      IX(N,4)=IX(N-1,4)+1
      IX(N,5)=IX(N-1,5)
  170 WRITE (6,2003) N,(IX(N,I),I=1,5)
      IF (M-N) 180,180,140
  180 IF (NUMEL-N) 190,190,130
  190 CONTINUE
C
C     CALCULATE CONSTANTS FOR THE STEP-BY-STEP SOLUTION
C
      C1=3.0*(ALFA+2.0/DELT)
      C2=3.0+ALFA*DELT*0.5
      C3=1.0+3.0*BETA/DELT
      C3I=1.0/C3
      C4=C1*C3I/DELT
      DELT2=DELT*DELT
      DT1=3.0/DELT
      DT2=0.5*DELT
      DT3=3.0/DELT2
C
C     DETERMINE BAND WIDTH
C
      J=0
      DO 340 N=1,NUMEL
      DO 340 I=1,3
      II1=I+1
      DO 325 L=II1,4
      KK=IABS(IX(N,I)-IX(N,L))
      IF (KK-J) 325,325,320
  320 J=KK
      NELE=N
  325 CONTINUE
  340 CONTINUE
```

```
      MBAND=2*J+2
      NEQ=2*NUMNP
      IF (MBAND-36) 348,348,344
  344 WRITE (6,2012) MBAND,NELE
      CALL EXIT
  348 WRITE (6,2013) MBAND,NELE
C
C     FORM INITIAL STIFFNESS MATRIX
C
      NNN=0
      CALL STIFF
C
C     SAVE PLOT DATA AT T=0
C
      IF (JKPL .EQ. 0) GO TO 353
      LSHIFT=0
      IF (JPT .EQ. 0) GO TO 351
      TT=0.0
      CALL SAVEPD (JPLOT,JPT,7,JPL,50)
  351 IF (KEL .EQ. 0) GO TO 353
      PLD(1,1)=0.0
      M=JPL+2
      MJ=M+KPL-1
      DO 352 I=M,MJ
      PLD(1,I)=0.0
  352 CONTINUE
C
C     CHECK FOR KINEMATIC INPUT
C
  353 READ (5,1011) KBP
      WRITE (6,2020) (AJA(I), I=1,9), (HED(I), I=1,12)
      WRITE (6,2021) KBP
      IF (KBP .EQ. 0) GO TO 360
      READ (5,1015) (KBNP(I), I=1,KBP)
C
      DO 358 I=1,KBP
      IF (KBNP(I) .LT. 0) GO TO 356
      IV(I)=1
      GO TO 358
  356 IV(I)=0
      KBNP(I)=-KBNP(I)
  358 CONTINUE
C
      READ (5,1011) NTIME
      WRITE (6,2022) (KBNP(I), I=1,KBP)
      WRITE (6,2023) NTIME
C
C     READ IN AND PRINT OUT VELOCITIES AND TIMES
C
      IF (NTIME .EQ. 0) GO TO 359
      READ (5,1020) ((V(I,J), J=1,3), I=1,NTIME)
C
```

```
      WRITE (6,2020) (AJA(I), I=1,9), (HED(I), I=1,12)
      WRITE (6,2040)
      WRITE (6,2041) ((V(I,J), J=1,3), I=1,NTIME)
C
C     CHECK FOR NODAL POINT TO BE QUIETED
C
  359 READ (5,1011) NQ
      WRITE (6,2020) (AJA(I), I=1,9), (HED(I), I=1,12)
      WRITE (6,2024) NQ
      IF (NQ .EQ. 0) GO TO 360
      READ (5,1021) ((IQ(I,J), J=1,5), I=1,NQ)
      WRITE (6,2025)
      WRITE (6,2026) ((IQ(I,J), J=1,5), I=1,NQ)
C
  360 LL=1
      TT=0.0
C
      DO 365 I=1,NUMEL
      DO 365 J=1,4
      SIG(I,J)=0.0
      EPS(I,J)=0.0
  365 CONTINUE
C
      DO 680 NNN=1,NT
C
      IF (NNN.EQ.1) GO TO 375
C
C     REFORM STIFFNESS MATRIX AND (H) MATRICES
C
      CALL STIFF
C
  375 TT=TT+DELT
      MMM=NNN-LL*NPRINT
      CALL LOAD
C
      DO 380 I=1,NEQ
      DELB = B(I)-B0(I)
      B0(I)=B(I)
      B(I) = DELB
  380 CONTINUE
C
C     FORM EFFECTIVE LOAD VECTOR
C
      DO 390 I=1,NEQ
      II = (I+1)/2
      B(I) = B(I) + MASS(II) * (C1 * X1(I) + C2 * X2(I))
     1            +A(I,1)*(3.0*X1(I)+0.5*DELT*X2(I))*BETA
      DO 385 J=2, MBAND
      J1= J-1
      IMJ1 = I-J1
      IF (IMJ1 .LT. 1) GO TO 382
      B(I)=B(I)+A(IMJ1,J)*(3.0*X1(IMJ1)+0.5*DELT*X2(IMJ1))*BETA
```

```
  382 IPJ1 = I+J1
      IF (IPJ1 .GT. NEQ) GO TO 385
      B(I)=B(I)+A(I,J)*(3.0*X1(IPJ1)+0.5*DELT*X2(IPJ1))*BETA
  385 CONTINUE
  390 CONTINUE
C
      DO 395 I=1,NEQ
      B(I) = C3I *B(I)
  395 CONTINUE
C
C     FORM EFFECTIVE STIFFNESS MATRIX
C
      DO 400 I=1,NEQ
      II = (I+1)/2
      A(I,1) = A(I,1) + C4 * MASS(II)
  400 CONTINUE
C
      IF (KBP .EQ. 0) GO TO 410
      CALL VELOAD (X0,X1,X2,R,BLK,SHR,RO,TT,DELT,NNN,NUMNP,NUMMAT,
     1 BETA,MBAND,B,NEQ,KODE,A)
C
C     CALCULATE DISPL. INCREMENTS THROUGH T=T+2*DELT
C
  410 CALL SYMSOL (1)
      CALL SYMSOL (2)
C
C     OBTAIN SOLUTION AT T=T+DELT
C
      DO 500 I=1,NEQ
      X0(I)=X0(I)+B(I)
      X1(I)=DT1*B(I)-2.0*X1(I)-DT2*X2(I)
      X2(I)=-DT3*B(I)+DT1*X1(I)-0.5*X2(I)
  500 CONTINUE
C
      DO 510 I=1,NUMNP
      I2=I+I
      R(I)=R(I)+B(I2-1)
      Z(I)=Z(I)+B(I2)
  510 CONTINUE
C
C     SAVE DISPL., VELO. AND ACC. FOR PLOTTING TIME-HISTORY
C
      IF (JPT .EQ. 0) GO TO 520
      CALL SAVEPD (JPLOT,JPT,7,JPL,50)
C
C     PRIND DISPL., VELO. AND ACC. AT SPECIFIED INTERVAL
C
  520 IF (MMM.NE.0) GO TO 580
  540 LL=LL+1
      NSTART=-49
      NSTOP=0
  560 NSTART=NSTART+50
```

```
      NSTOP=NSTOP+50
      IF (NSTOP .GT. NUMNP) NSTOP=NUMNP
      WRITE (6,2020) (AJA(I), I=1,9), (HED(I), I=1,12)
      WRITE (6,2006) TT
      WRITE (6,2008) ((N,X0(2*N-1),X0(2*N),X1(2*N-1),X1(2*N),X2(2*N-1),
     1 X2(2*N),N), N=NSTART,NSTOP)
      IF (NSTOP .LT. NUMNP) GO TO 560
C
C     COMPUTE, PRINT AND SAVE STRESSES
C
  580 CALL STRESS (XC,YC)
      IF (KEL.EQ.0) GO TO 590
      CALL SAVEPD (KPLOT,KEL,6,JPL,50)
  590 IF (MMM.NE.0) GO TO 660
C
      NSTART = - 49
      NSTOP = 0
  600 NSTART = NSTART + 50
      NSTOP = NSTOP + 50
      IF (NSTOP .GT. NUMEL)  NSTOP = NUMEL
      WRITE (6, 2020)  (AJA(I), I= 1, 9), (HED(I), I= 1, 12)
      WRITE (6, 2030)  TT
      WRITE (6,2031) ((N,XC(N),YC(N),SIG(N,1),SIG(N,2),SIG(N,4),
     1 SIG(N,5),SIG(N,6),SIG(N,7)), N=NSTART,NSTOP)
      IF (NSTOP .LT. NUMEL)  GO TO 600
  660 CONTINUE
  680 CONTINUE
C
      IF (JKPL.EQ.0) GO TO 900
      NT1=NT+1
      M=MOD(NT1,50)
      IF (M.EQ.0) GO TO 900
      WRITE (NTAPE) ((PLD(I,J), J=1,JKPL1), I=1,50)
C
  900 GO TO 50
C
 1000 FORMAT (6I5, 3F10.0)
 1001 FORMAT (I5,5F15.0)
 1002 FORMAT (2I5,6F10.0)
 1003 FORMAT (6I5)
 1004 FORMAT (3F10.0)
 1006 FORMAT (4E20.10)
 1010 FORMAT (I1,A1,12A6)
 1011 FORMAT (2I3)
 1012 FORMAT (6A6)
 1013 FORMAT (I3,1X,6I1)
 1014 FORMAT (I3,1X,5I1)
 1015 FORMAT (10I5)
 1020 FORMAT (3E20.0)
 1021 FORMAT (5I5)
 2000 FORMAT
     1(30H0 NUMBER OF NODAL POINTS------ I4 /
```

```
     2 30H0 NUMBER OF ELEMENTS---------- I4 /
     3 30H0 NUMBER OF DIFF. MATERIALS--- I4 /
     4 30H0 TIME INCREMENT-------------- F7.5/
     5 30H0 NUMBER OF CYCLES------------ I4 /
     6 30H0 PRINTING INTERVALS---------- I4/
     7 30H0 DAMPING COEFFICIENT ALFA---- F7.4/
     8 30H0 DAMPING COEFFICIENT BETA---- F7.4///
     9 27H0 MATERIAL PROPERTIES TABLE//
     1 1X, 8HMATERIAL, 5X, 4HBULK, 7X, 5HSHEAR, 6X, 4HMASS, 29X,
     2 27HELASTO-PLASTIC COEFFICIENTS/2X, 6HNUMBER, 5X, 7HMODULUS, 4X,
     3 7HMODULUS, 4X, 7HDENSITY, 5X, 4HALFA, 8X, 3HCEE, 8X, 2HB1, 9X,
     4 2HB2, 9X, 2HB3, 9X, 3HMU1, 8X, 3HMU2/)
2001 FORMAT (8X, 44HEL NO     I     J     K     L    MATERIAL NO/)
2002 FORMAT (I6, I8, 2F12.2, 2F13.5, 2F14.5, 3F13.5)
2003 FORMAT (I13, 4I6, I10)
2004 FORMAT (43X, 22HINITIAL  DISPLACEMENTS, 8X,
    1 19HINITIAL  VELOCITIES/1X, 8HNODAL PT, 2X, 4HTYPE, 5X, 5HX-ORD,
    2 7X, 5HY-ORD,10X, 2HXO,11X, 2HYO, 12X, 3HX10, 11X, 3HY10,7X,
    3 9HARRIVAL T, 7X, 2HCH, 11X, 2HCV/13X, 2(8X, 4H(IN)),
    4 2(9X, 4H(IN)), 2X, 2(6X, 8H(IN/SEC)), 7X, 5H(SEC)/)
2005 FORMAT (F15.5, 2F20.2)
2006 FORMAT (8H TIME T=F7.5//1X, 9HNODAL PT., 4X,
    1 8HX-DISPL., 8X, 8HY-DISPL., 7X, 10HX-VELOCITY,
    2 6X, 10HY-VELOCITY, 8X, 6HX-ACC., 10X, 6HY-ACC., 7X, 9HNODAL PT./
    3 4X, 2(12X, 4H(IN)), 2X, 2(8X, 8H(IN/SEC)), 1X,
    4 2(7X, 9H(IN/SEC2))/)
2007 FORMAT (10X, 4HTIME, 13X, 6HX-LOAD, 14X, 6HY-LOAD/10X, 5H(SEC),
    1 13X, 5H(PSI), 15X, 5H(PSI)/)
2008 FORMAT (I6, 6F16.5, I12)
2009 FORMAT (26H0NODAL POINT CARD ERROR N= I5)
2011 FORMAT (I5, 4X, 10E11.4)
2012 FORMAT (22H0BAND WIDTH EXCEEDED =, I4, 9H, ELEMENT, I4)
2013 FORMAT (13H0BAND WIDTH =, I3, 9H, ELEMENT, I4)
2020 FORMAT (1H1, 20X, 9A6//1X, 12A6/)
2021 FORMAT (64H0TOTAL NUMBER OF POINTS QUIETED AND POINTS WITH VELOCIT
    1Y INPUT =, I3/)
2022 FORMAT (20H0NODAL POINT NUMBERS//(10I8))
2023 FORMAT (/32H0NUMBER OF VELOCITY-TIME CARDS =, I4)
2024 FORMAT (33H TOTAL NUMBER OF POINTS QUIETED =, I3/)
2025 FORMAT (9H0TYPE  OF, 6X, 9HCORRECTOR, 7X, 6HSENSOR,9X, 8HMATERIAL,
    1 4X, 11HSEQUENCE NO/9H BOUNDARY, 8X, 4HNODE, 11X, 4HNODE, 11X,
    2 5HINDEX, 7X, 9HIN (KBNP)/)
2026 FORMAT (I5, 4I15)
2030 FORMAT (8H TIME T=F7.5//3X, 6HEL.NO., 6X, 1HX, 11X, 1HY, 11X,
    1 7HSIGMA-X, 8X, 7HSIGMA-Y, 9X, 6HTAU-XY, 6X, 10HMAX-STRESS, 5X,
    2 10HMIN-STRESS, 5X, 5HANGLE/6X, 2(8X, 4H(IN)),10X, 5H(PSI),
    3 4(10X, 5H(PSI)), 8X, 5H(DEG)/)
2031 FORMAT (I7, 2F12.2, 5F15.5, F11.2)
2040 FORMAT(15H VELOCITY INPUT///1X,10HTIME (SEC),10X,19HX-VELOCITY (IN
    1/SEC),6X,19HY-VELOCITY (IN/SEC)/)
2041 FORMAT (F10.6,14X,F10.6,14X,F10.6)
C
      END
```

```
      SUBROUTINE SAVEPD (JK, II, JJ, JPL, NR)
C
      REAL MASS
      COMMON ALFA,BETA,DELT,MBAND,N,NEQ,NNN,NP,NT,NUMNP,NUMEL,NUMMAT,
     1 TT,VOL,DUMMY(5),A(550,36),SIG(250,7),B(550),B0(550),CC(1500),
     2 C(3,3),CH(275),CV(275),EPS(250,4),H(6000),IX(250,5),KODE(275),
     3 MASS(275),P(3,50),R(275),Z(275),S(10,10),T(275),X0(550),X1(550),
     4 X2(550)
      COMMON/PLDATA/PLD(50,51),JKPL1,KEL,LSHIFT,NTAPE
      DIMENSION JK(NR,1)
C
      NN1 = NNN + 1 - LSHIFT
      PLD (NN1, 1) = TT
      IF (JJ - 6) 100, 200, 100
C
C     DISPLACEMENT, VELOCITY OR ACCELERATION TO BE SAVED
C
  100 M = 2
      DO 120  I= 1, II
      L = JK(I, 1)
      L2 = 2 * L
      L1 = L2 - 1
      DO 110  J= 2, 7
      IF (JK(I, J) .EQ. 0)  GO TO 110
      J1 = J - 1
      GO TO (101,102,103,104,105,106),J1
  101 PLD (NN1, M) = X0(L1)
      GO TO 109
  102 PLD(NN1, M) = X0(L2)
      GO TO 109
  103 PLD(NN1, M) = X1(L1)
      GO TO 109
  104 PLD(NN1, M) = X1(L2)
      GO TO 109
  105 PLD(NN1, M) = X2(L1)
      GO TO 109
  106 PLD(NN1, M) = X2(L2)
  109 M = M + 1
  110 CONTINUE
  120 CONTINUE
      IF (KEL .EQ. 0) GO TO 400
      GO TO 500
C
C     STRESSES TO BE SAVED
C
  200 M = JPL + 2
      DO 220  I= 1, II
      N = JK(I, 1)
      DO 210  J= 2, 6
      IF (JK(I, J) .EQ. 0)  GO TO 210
      J1 = J - 1
      GO TO (201,202,203,204,205), J1
```

```
  201 PLD(NN1,M)=SIG(N,1)
      GO TO 209
  202 PLD(NN1,M)=SIG(N,2)
      GO TO 209
  203 PLD(NN1,M)=SIG(N,4)
      GO TO 209
  204 PLD(NN1,M)=SIG(N,5)
      GO TO 209
  205 PLD(NN1,M)=SIG(N,6)
  209 M=M+1
  210 CONTINUE
  220 CONTINUE
C
  400 IF (NN1 .LT. 50) GO TO 500
      WRITE (NTAPE)  ((PLD(I,J), J=1,JKPL1), I=1,50)
      LSHIFT=LSHIFT+50
C
  500 RETURN
C
      END
      SUBROUTINE STIFF
C
      REAL MASS
      COMMON ALFA,BETA,DELT,MBAND,N,NEQ,NNN,NP,NT,NUMNP,NUMEL,NUMMAT,
     1 TT,VOL,DUMMY(5),A(550,36),SIG(250,7),B(550),B0(550),CC(1500),
     2 C(3,3),CH(275),CV(275),EPS(250,4),H(6000),IX(250,5),KODE(275),
     3 MASS(275),P(3,50),R(275),Z(275),S(10,10),T(275),X0(550),X1(550),
     4 X2(550)
      COMMON/MATARG/BLK(12),SHR(12),RO(12),ALPHA(12),CELL(12),B11(12),
     1 B22(12),B33(12),U11(12),U22(12)
      DIMENSION LM(4)
C
      IF (NNN.NE.0) GO TO 45
      DO 40 I=1,NUMNP
   40 MASS(I)=0.0
   45 DO 50 I=1,NEQ
      DO 50 J=1,MBAND
   50 A(I,J)=0.0
C
      DO 210 N=1,NUMEL
C
      IF (NNN.EQ.0) GO TO 60
C
      NO=6*(N-1)
      C(1,1)=CC(NO+1)
      C(1,2)=CC(NO+2)
      C(1,3)=CC(NO+3)
      C(2,2)=CC(NO+4)
      C(2,3)=CC(NO+5)
      C(3,3)=CC(NO+6)
      C(2,1)=C(1,2)
      C(3,1)=C(1,3)
```

```
      C(3,2)=C(2,3)
      GO TO 90
C
   60 MTYPE=IX(N,5)
      BM=BLK(MTYPE)
      G=SHR(MTYPE)
      C(1,1)=BM+4.0*G/3.0
      C(2,2)=C(1,1)
      C(1,2)=BM-2.0*G/3.0
      C(2,1)=C(1,2)
      C(3,3)=G
      C(1,3)=0.0
      C(2,3)=0.0
      C(3,1)=0.0
      C(3,2)=0.0
C
C     CST ELEMENT
C
   90 IF (IX(N,3) .NE. IX(N,4)) GO TO 100
      CALL CSTSTF
      NPT=3
      GO TO 120
C
C     QUADRILATERAL ELEMENT
C
  100 CALL QUAD
      NPT=4
C
C     FORM MASS MATRIX
C
  120 IF (NNN.NE.0) GO TO 185
      X=NPT
      MTYPE=IX(N,5)
      ELMASS=VOL*RO(MTYPE)/X
      DO 130 I=1,NPT
      K=IX(N,I)
      MASS(K)=MASS(K)+ELMASS
  130 CONTINUE
C
C     ADD ELEMENT STIFFNESS TO TOTAL STIFFNESS
C
  185 DO 190 I=1,NPT
      LM(I)=2*IX(N,I)-2
  190 CONTINUE
      DO 200 I=1,NPT
      DO 200 K=1,2
      II=LM(I)+K
      KK=2*I-2+K
      DO 200 J=1,NPT
      DO 200 L=1,2
      JJ=LM(J)+L-II+1
      LL=2*J-2+L
```

```
      IF (JJ .LT. 1) GO TO 200
      IF (JJ.LE.36) GO TO 195
      WRITE (6,2000) N
      CALL EXIT
  195 A(II,JJ)=A(II,JJ)+S(KK,LL)
  200 CONTINUE
  210 CONTINUE
C
C     MODIFY STIFFNESS MATRIX FOR ZERO DISPLACEMENTS
C
  250 DO 600 N=1,NUMNP
      KK=KODE(N)
      KD=10
      DO 600 M=1,2
      IF (KK-KD) 580,550,550
  550 NX=2*N-2+M
      DO 575 J=2,MBAND
      A(NX,J)=0.0
      NN=NX-J+1
      IF (NN) 575,575,570
  570 A(NN,J)=0.0
  575 CONTINUE
      A(NX,1)=1.0
      KK=KK-KD
  580 KD=KD/10
  600 CONTINUE
C
      IF (NNN .NE. 0) RETURN
C
C     CALCULATE INITIAL ACCELERATION
C
      DO 700 I=1,NEQ
      X2(I)=0.0
  700 B(I)=X0(I)+BETA*X1(I)
      DO 800 I=1,NEQ
      K=NEQ-I+1
      IF (K-MBAND) 720,720,710
  710 K=MBAND
  720 DO 730 J=1,K
      IJ=I+J-1
  730 X2(I)=X2(I)+A(I,J)*B(IJ)
      IF (I-MBAND) 750,740,740
  740 L=MBAND-1
      GO TO 760
  750 L=I-1
      IF (L) 800,800,760
  760 II=I
      DO 770 J=1,L
      II=II-1
  770 X2(I)=X2(I)+A(II,J+1)*B(II)
  800 CONTINUE
      TT=0.0
```

```
C
      CALL LOAD
C
      DO 810 I=1,NEQ
      B0(I)=B(I)
  810 CONTINUE
C
      DO 850 M=1,NUMNP
      K=2*M
      X2(K-1)=(B(K-1)-X2(K-1))/MASS(M)-ALFA*X1(K-1)
      X2(K)=(B(K)-X2(K))/MASS(M)-ALFA*X1(K)
  850 CONTINUE
C
      RETURN
C
 2000 FORMAT (38H0STIFF COEFF GETS OUT OF BAND, ELEMENT I4)
      END
      SUBROUTINE CSTSTF
C
      REAL MASS
      COMMON ALFA,BETA,DELT,MBAND,N,NEQ,NNN,NP,NT,NUMNP,NUMEL,NUMMAT,
     1 TT,VOL,DUMMY(5),A(550,36),SIG(250,7),B(550),B0(550),CC(1500),
     2 C(3,3),CH(275),CV(275),EPS(250,4),H(6000),IX(250,5),KODE(275),
     3 MASS(275),P(3,50),R(275),Z(275),S(10,10),T(275),X0(550),X1(550),
     4 X2(550)
      DIMENSION X(3),Y(3),CB(3,6)
C
      I=IX(N,1)
      J=IX(N,2)
      K=IX(N,3)
C
      X(1)=R(K)-R(J)
      X(2)=R(I)-R(K)
      X(3)=R(J)-R(I)
      Y(1)=Z(J)-Z(K)
      Y(2)=Z(K)-Z(I)
      Y(3)=Z(I)-Z(J)
      AREA=0.5*(X(3)*Y(2)-X(2)*Y(3))
      IF (AREA.GT.0.0) GO TO 100
      WRITE (6,1000) N
      CALL EXIT
  100 VOL=AREA
C
C     PREPARE (H) MATRICES FOR THE NEXT STEP
C
      A2I = 1.0/(2.0*AREA)
      N0 = (N-1)*24
      N1 = N0 +3
      N2 = N0 +11
      DO 140 I=1,3
      H(N0+I) = A2I*Y(I)
      H(N1+I) = 0.0
```

```
      H(N2+I) = A2I*X(I)
      H(N0+19+I) = H(N0+I)
      H(N1+5+I) =0.0
      H(N2+5+I) = H(N2+I)
  140 CONTINUE
C
C     FORM ELEMENT STIFFNESS MATRIX
C
      COM =0.5*A2I
      DO 180 I=1,3
      DO 180 J=1,3
      CB(I,J) = COM*(C(I,1) * Y(J) + C(I,3)*X(J))
  180 CONTINUE
      DO 200 I=1,3
      DO 200 J=1,3
      CB(I,J+3) = COM*(C(I,2)*X(J)+C(I,3)*Y(J))
  200 CONTINUE
      DO 220 I=1,3
      DO 220 J=1,6
      S(I,J) = CB(1,J) * Y(I) + CB(3,J)*X(I)
  220 CONTINUE
      DO 240 I=1,3
      DO 240 J=1,6
      S(I+3,J) = CB(2,J) * X(I) + CB(3,J) *Y(I)
  240 CONTINUE
C
      RETURN
C
 1000 FORMAT (39H0AREA OF TRIANGLE NEGATIVE, ELEMENT NO. I4)
C
      END
      SUBROUTINE QUAD
C
      REAL MASS
      COMMON ALFA,BETA,DELT,MBAND,N,NEQ,NNN,NP,NT,NUMNP,NUMEL,NUMMAT,
     1 TT,VOL,DUMMY(5),A(550,36),SIG(250,7),B(550),B0(550),CC(1500),
     2 C(3,3),CH(275),CV(275),EPS(250,4),H(6000),IX(250,5),KODE(275),
     3 MASS(275),P(3,50),R(275),Z(275),S(10,10),T(275),X0(550),X1(550),
     4 X2(550)
      DIMENSION ST(3,10)
C
C     FORM QUADRILATERAL STIFFNESS MATRIX
C
      DO 140 J=1,10
      DO 100 I=1,10
  100 S(I,J)=0.0
      DO 120 K=1,3
  120 ST(K,J)=0.0
  140 CONTINUE
C
      VOL=0.0
      I=IX(N,1)
```

```
      J=IX(N,2)
      K=IX(N,4)
      CALL LSTSTF(1,3,7,I,J,K,ST)
      I=IX(N,3)
      J=IX(N,4)
      K=IX(N,2)
      CALL LSTSTF(5,7,3,I,J,K,ST)
C
C     ELIMINATE CENTER POINT
C
      DO 500 K=1,2
      IH=10-K
      ID=IH+1
      DO 500 I=1,IH
      S(ID,I)=S(ID,I)/S(ID,ID)
      DO 490 J=1,3
  490 ST(J,I)=ST(J,I)-ST(J,ID)*S(ID,I)
      DO 500 J=1,IH
  500 S(J,I)=S(J,I)-S(J,ID)*S(ID,I)
C
C     STORE (ST) AS (H) MATRIX
C
      NO=(N-1)*24-8
      DO 600 I=1,3
      NO=NO+8
      DO 600 J=1,8
      H(NO+J)=ST(I,J)
  600 CONTINUE
C
      RETURN
C
      END
      SUBROUTINE LSTSTF(N1,N2,N3,I,J,K,ST)
C
      REAL MASS
      COMMON ALFA,BETA,DELT,MBAND,N,NEQ,NNN,NP,NT,NUMNP,NUMEL,NUMMAT,
     1 TT,VOL,DUMMY(5),A(550,36),SIG(250,7),B(550),B0(550),CC(1500),
     2 C(3,3),CH(275),CV(275),EPS(250,4),H(6000),IX(250,5),KODE(275),
     3 MASS(275),P(3,50),R(275),Z(275),S(10,10),T(275),X0(550),X1(550),
     4 X2(550)
      DIMENSION BA(3,2),U(3,4),V(3,4),UV(3,4,2),LM(4),ST(3,10)
      EQUIVALENCE (UV(1),U(1)),(UV(13),V(1))
C
      BA(1,1)=Z(J)-Z(K)
      BA(2,1)=Z(K)-Z(I)
      BA(3,1)=Z(I)-Z(J)
      BA(1,2)=R(K)-R(J)
      BA(2,2)=R(I)-R(K)
      BA(3,2)=R(J)-R(I)
      AREA=0.5*(BA(3,2)*BA(2,1)-BA(2,2)*BA(3,1))
      IF (AREA) 90,90,100
   90 WRITE (6,1000) N
      CALL EXIT
```

```
C
  100 VOL=VOL+AREA
      COMM=1./(48.*AREA)
      C11=C(1,1)*COMM
      C12=C(1,2)*COMM
      C13=C(1,3)*COMM
      C22=C(2,2)*COMM
      C23=C(2,3)*COMM
      C33=C(3,3)*COMM
C
      DO 150 NN=1,2
      D1=BA(1,NN)
      D2=BA(2,NN)
      D3=BA(3,NN)
      UV(1,1,NN)=D1
      UV(2,1,NN)=D1
      UV(3,1,NN)=D1
      UV(1,2,NN)=D2
      UV(2,2,NN)=D2-2.*D3
      UV(3,2,NN)=-D2
      UV(1,3,NN)=D3
      UV(2,3,NN)=-D3
      UV(3,3,NN)=D3-2.*D2
      UV(1,4,NN)=0.
      UV(2,4,NN)=4.*D3
  150 UV(3,4,NN)=4.*D2
      LM(1)=N1
      LM(2)=N2
      LM(3)=N3
      LM(4)=9
C
      COMM=8.*AREA
      DO 310 I=1,4
      II=LM(I)
C
      UU=(U(2,I)+U(3,I))/COMM
      VV=(V(2,I)+V(3,I))/COMM
      ST(1,II)=ST(1,II)+UU
      ST(2,II+1)=ST(2,II+1)+VV
      ST(3,II)=ST(3,II)+VV
      ST(3,II+1)=ST(3,II+1)+UU
C
      SUM=U(1,I)+U(2,I)+U(3,I)
      SUM1=SUM+U(1,I)
      SUM2=SUM+U(2,I)
      SUM3=SUM+U(3,I)
      SUM=V(1,I)+V(2,I)+V(3,I)
      SVM1=SUM+V(1,I)
      SVM2=SUM+V(2,I)
      SVM3=SUM+V(3,I)
      DO 300 J=1,4
```

```
      JJ=LM(J)
      UQU=U(1,J)*SUM1+U(2,J)*SUM2+U(3,J)*SUM3
      VQU=V(1,J)*SUM1+V(2,J)*SUM2+V(3,J)*SUM3
      VQV=V(1,J)*SVM1+V(2,J)*SVM2+V(3,J)*SVM3
      UQV=U(1,J)*SVM1+U(2,J)*SVM2+U(3,J)*SVM3
      S(II,JJ)=S(II,JJ)+ C11*UQU+C13*(VQU+UQV)+C33*VQV
      S(II+1,JJ+1)=S(II+1,JJ+1)+ C22*VQV+C23*(VQU+UQV)+C33*UQU
      S(II,JJ+1)=S(II,JJ+1)+ C23*VQV+C13*UQU+VQU*C12+C33*UQV
  300 S(JJ+1,II)=S(II,JJ+1)
  310 CONTINUE
C
  400 RETURN
C
 1000 FORMAT (39H0AREA OF TRIANGLE NEGATIVE, ELEMENT NO. I4)
C
      END
      SUBROUTINE LOAD
C
      REAL MASS
      COMMON ALFA,BETA,DELT,MBAND,N,NEQ,NNN,NP,NT,NUMNP,NUMEL,NUMMAT,
     1 TT,VOL,DUMMY(5),A(550,36),SIG(250,7),B(550),B0(550),CC(1500),
     2 C(3,3),CH(275),CV(275),EPS(250,4),H(6000),IX(250,5),KODE(275),
     3 MASS(275),P(3,50),R(275),Z(275),S(10,10),T(275),X0(550),X1(550),
     4 X2(550)
C
      IF (NP.NE.0) GO TO 20
      DO 10 I=1,NEQ
      B(I)=0.0
   10 CONTINUE
      GO TO 270
C
   20 N=1
  100 TAU=TT-T(N)
      IF (TAU) 50,150,150
  150 K=1
   60 IF(TAU.GE.P(1,K).AND.TAU.LT.P(1,K+1)) GO TO 200
      K=K+1
      GO TO 60
  200 D=P(1,K+1)-P(1,K)
      DH=P(2,K+1)-P(2,K)
      DV=P(3,K+1)-P(3,K)
      DT=TAU-P(1,K)
      FH=P(2,K)+DT*DH/D
      FV=P(3,K)+DT*DV/D
  160 IF(CH(N).EQ.0.0.AND.CV(N).EQ.0.0) GO TO 50
      IF(CH(N)) 300,250,300
  250 B(2*N-1)=0.0
  350 B(2*N)=CV(N)*FV
      GO TO 500
  300 B(2*N-1)=CH(N)*FH
      IF(CV(N)) 350,400,350
   50 B(2*N-1)=0.0
```

```
  400 B(2*N)=0.0
  500 N=N+1
      IF (NUMNP-N) 270,120,120
  120 IF(T(N)-T(N-1)) 100,140,100
  140 IF (TAU) 50,160,160
C
  270 RETURN
C
      END
      SUBROUTINE VELOAD (X0,X1,X2,R,BLK,SHR,RO,TT,DELT,NNN,NUMNP,NUMMAT
     1,BETA,MBAND,B,NEQ,KODE,A)
C
      COMMON/KINBC/KBP,KBNP(60),NTIME,NQ,IQ(60,5),DV(120),V(150,3),
     1 IV(60)
      DIMENSION X0(1),X1(1),X2(1),R(1),BLK(1),SHR(1),RO(1),B(1),KODE(1)
     1,CPS(15,2),VJ(2),A(550,1)
C
      KBP2=2*KBP
      DO 100 I=1,KBP2
      DV(I)=0.0
  100 CONTINUE
C
      IF (NQ .EQ. 0) GO TO 500
      IF (NNN .NE. 1) GO TO 240
C
C     CALCULATE P- AND S-WAVE SPEED
C
      DO 120 I=1,NUMMAT
      BLKM=BLK(I)
      SHRM=SHR(I)
      YMOD=9.0*BLKM*SHRM/(3.0*BLKM+SHRM)
      U=(3.0*BLKM-2.0*SHRM)/(6.0*BLKM+2.0*SHRM)
      CPS(I,1)=SQRT(YMOD*(1.-U)/(RO(I)*(1.+U)*(1.-2.*U)))
      CPS(I,2)=SQRT(YMOD/(2.*RO(I)*(1.+U)))
  120 CONTINUE
C
C     CALCULATE CORRECTIONS TO PRESCRIBED VELOCITIES
C
  240 IF (NTIME .EQ. 0) GO TO 260
      T=TT-DELT
      VJ(1)=VELINT(T,2,V,1,150)
      VJ(2)=VELINT(T,3,V,0,150)
C
  260 DO 490 I=1,NQ
      I1=IQ(I,1)
      I2=IQ(I,2)
      I3=IQ(I,3)
      I4=IQ(I,4)
      I5=IQ(I,5)
C
C     I1=TYPE OF BOUNDARY (1 OR 2)
C     I2= NODE NUMBER OF CORRECTOR
```

```
C       I3= NODE NUMBER OF SENSOR
C       I4= MATERIAL PROPERTY INDEX
C       I5= SEQUENCE NUMBER IN KBNP ARRAY
C
        IF (I1 .EQ. 1) I0=0
        IF (I1 .NE. 1) I0=275
C
        DO 480 J=1,2
        DEL=ABS(R(I2+I0)-R(I3+I0))/CPS(I4,J)
        T=TT-DELT-DEL
        IF(T .LE. 0.0) GO TO 480
        IF(I1 .EQ. 1) N=J
        IF(I1 .NE. 1) N=3-J
        DUM1=X1(2*I3-2+N)
        DUM2=X1(2*I2-2+N)
        IF (NTIME .EQ. 0) GO TO 460
        IF (IV(I5) .EQ. 0) GO TO 460
        DUM1=DUM1-VELINT(T,N+1,V,1,150)
        DUM2=DUM2-VJ(N)
  460   DV(2*I5-2+N)=(DUM2*(DEL-DELT)+DUM1*DELT)/DEL
  480   CONTINUE
  490   CONTINUE
        IF (NTIME .EQ. 0) GO TO 600
C
C       ADD SPECIFIED VELOCITIES TO THE CORRECTIONS
C
  500   T=TT
        VI1=VELINT(T,2,V,1,150)
        VI2=VELINT(T,3,V,0,150)
        DO 520 I=1,KBP
        IF (IV(I) .EQ. 0) GO TO 520
        I2=2*I
        I1=I2-1
        DV(I1)=DV(I1)+VI1
        DV(I2)=DV(I2)+VI2
  520   CONTINUE
C
C       CALCULATE THE INCREMENTAL DISPLACEMENTS CORRESPONDING TO THE
C       SPECIFIED INCREMENTAL VELOCITIES
C
  600   CONST=DELT/3.0
        DO 620 I=1,KBP
        N=KBNP(I)
        I2=2*I
        I1=I2-1
        N2=2*N
        N1=N2-1
        DV(I1)=CONST*(DV(I1)+2.0*X1(N1)+0.5*DELT*X2(N1))
        DV(I2)=CONST*(DV(I2)+2.0*X1(N2)+0.5*DELT*X2(N2))
  620   CONTINUE
C
C       MODIFY LOAD VECTOR FOR KINEMATIC INPUT (VELOCITY)
```

```
C
      DO 820 I=1,KBP
      N=KBNP(I)
      N2=2*N
      N1=N2-1
      A(N1,1)=1.0
      A(N2,1)=1.0
      DO 760 J=2,MBAND
      J1=J-1
      N11=N1+J1
      N22=N2+J1
      B(N11)=B(N11)-A(N1,J)*DV(2*I-1)
      A(N1,J)=0.0
      IF (N22.GT.NEQ) GO TO 780
      B(N22)=B(N22)-A(N2,J)*DV(2*I)
  760 A(N2,J)=0.0
  780 CONTINUE
      DO 800 J=2,MBAND
      J1=J-1
      N3=N1-J1
      N4=N2-J1
      B(N4)=B(N4)-A(N4,J)*DV(2*I)
      A(N4,J)=0.0
      IF (N3.LT.1) GO TO 820
      B(N3)=B(N3)-A(N3,J)*DV(2*I-1)
  800 A(N3,J)=0.0
  820 CONTINUE
C
C     SET LOADS CORRESP. TO CONSTRAINED POINTS TO SPECIFIC VALUES
C
  840 DO 890 N=1,NUMNP
      KK=KODE(N)
      IF (KK.EQ.0) GO TO 890
      IF (KK-10) 870,880,860
  860 B(2*N-1)=0.
  870 B(2*N)=0.
      GO TO 890
  880 B(2*N-1)=0.
  890 CONTINUE
C
      DO 900 I=1,KBP
      N=KBNP(I)
      B(2*N-1)=DV(2*I-1)
      B(2*N)=DV(2*I)
  900 CONTINUE
C
      RETURN
C
      END
      FUNCTION VELINT(T,N,V,K,NTIME)
```

```
C
      DIMENSION V(NTIME,1)
C
      IF(K.NE.1) GO TO 30
      J=1
   10 IF (T.GE.V(J,1).AND.T.LT.V(J+1,1)) GO TO 20
      J=J+1
      GO TO 10
   20 DT1=V(J+1,1)-V(J,1)
      DT2=T-V(J,1)
   30 DV=V(J+1,N)-V(J,N)
      VELINT=V(J,N)+DV*DT2/DT1
C
      RETURN
C
      END
@ ELT STRESS,1,690919, 52167
@ EOF @
      SUBROUTINE STRESS (XC,YC)
C
      REAL MASS
      COMMON ALFA,BETA,DELT,MBAND,N,NEQ,NNN,NP,NT,NUMNP,NUMEL,NUMMAT,
     1 TT,VOL,DUMMY(5),A(550,36),SIG(250,7),B(550),B0(550),CC(1500),
     2 C(3,3),CH(275),CV(275),EPS(250,4),H(6000),IX(250,5),KODE(275),
     3 MASS(275),P(3,50),R(275),Z(275),S(10,10),T(275),X0(550),X1(550),
     4 X2(550)
      COMMON/ELPLS/STRESS(4),STRAIN(4),STRINC(4),BM,G,ALPH,CEE,
     1 B11,B2,B3,U1,U2
      DIMENSION XC(1),YC(1)
C
C     COMPUTE ELEMENT STRESSES
C
      DO 500 N=1,NUMEL
C
      CALL CANDDE (B,H,N,IX,NUMEL,SIG,EPS,CC)
C
      DO 100 J=1,4
      SIG(N,J)=STRESS(J)
      EPS(N,J)=STRAIN(J)
  100 CONTINUE
C
      J=IX(N,2)
      K=IX(N,3)
      L=IX(N,4)
      IF (K.NE.L) GO TO 200
      I=IX(N,1)
      XC(N)=(R(I)+R(J)+R(K))*0.33333
      YC(N)=(Z(I)+Z(J)+Z(K))*0.33333
      GO TO 300
  200 XC(N)=(R(J)+R(L))*0.5
      YC(N)=(Z(J)+Z(L))*0.5
C
```

```
C     CALCULATE PRINCIPAL STRESSES
C
  300 CB=(SIG(N,1)+SIG(N,2))*0.5
      BC=(SIG(N,1)-SIG(N,2))*0.5
      CR=SQRT(BC**2+SIG(N,4)**2)
      SIG(N,5)=CB+CR
      SIG(N,6)=CB-CR
      IF ((BC.EQ.0.0).AND.(SIG(N,4).EQ.0.0)) GO TO 400
      ANGLE=ATAN2(SIG(N,4),BC)*0.5
      SIG(N,7)=57.296*ANGLE
      GO TO 500
  400 SIG(N,7)=0.0
  500 CONTINUE
C
      RETURN
C
      END
      SUBROUTINE SYMSOL (KKK)
C
      COMMON ALFA,BETA,DELT,MBAND,N,NEQ,NNN,NP,NT,NUMNP,NUMEL,NUMMAT,
     1 TT,VOL,DUMMY(5),A(550,36),SIG(250,7),B(550),B0(550),CC(1500),
     2 C(3,3),CH(275),CV(275),EPS(250,4),H(6000),IX(250,5),KODE(275),
     3 MASS(275),P(3,50),R(275),Z(275),S(10,10),T(275),X0(550),X1(550),
     4 X2(550)
C
      GO TO (1000,2000),KKK
C
C     REDUCE MATRIX
C
 1000 DO 280 N=1,NEQ
      DO 260 L=2,MBAND
      CONST=A(N,L)/A(N,1)
      I = N+L-1
      IF(NEQ-I) 260,240,240
  240 J=0
      DO 250 K=L,MBAND
      J=J+1
  250 A(I,J)=A(I,J)-CONST*A(N,K)
  260 A(N,L)=CONST
  280 CONTINUE
      GO TO 500
C
C     REDUCE VECTOR
C
 2000 DO 290 N=1,NEQ
      DO 285 L=2,MBAND
      I=N+L-1
      IF(NEQ-I) 290,285,285
  285 B(I)=B(I)-A(N,L)*B(N)
  290 B(N)=B(N)/A(N,1)
C
C     BACK SUBSTITUTION
```

```
C
      N=NEQ
  300 N = N-1
      IF(N) 350,500,350
  350 DO 400 K=2,MBAND
      L=N+K-1
      IF(NEQ-L) 400,370,370
  370 B(N) = B(N) - A(N,K) * B(L)
  400 CONTINUE
      GO TO 300
C
  500 RETURN
C
      END
      SUBROUTINE ELFUN(B,G,B1,B2,B3,U1,U2,STRAIN,NE,B0)
      DIMENSION UELMAX(250),STRAIN(4)
      EQUIVALENCE(DUM,UCRNT)
      E1=STRAIN(1)
      E2=STRAIN(2)
      E3=STRAIN(3)
      E4=STRAIN(4)
C
      UCRNT=ABS((1.+E1+E2+E1*E2-E4*E4)*(1.+E3)-1.)
C
      UMAX=UELMAX(NE)
      IF(UCRNT.GE.UMAX) GO TO 10
C UNLOADING/RELOADING HYDROSTAT
      BP=B2+(B1-B2)*UMAX/U1
      IF(BP.GE.B1) BP=B1
      B=BP+(B1-BP)*DUM/U1
      GO TO 100
C  VIRGIN HYDROSTAT
   10 B=B1-(B1-B2)*EXP(-DUM/U2)
      UELMAX(NE)=UCRNT
  100 CONTINUE
  300 CONTINUE
      B=B0
      RETURN
      END
      SUBROUTINE ELAST(B,G,C)
      DIMENSION C(4,4)
      C(1,1) = B +1.333*G
      C(1,2) = B-.6667*G
      C(4,4)=G
C
      C(1,3)=C(1,2)
      C(1,4)=0.
      C(2,1)=C(1,2)
      C(2,2) =C(1,1)
      C(2,3)=C(1,2)
      C(2,4)=0.
      C(3,1)=C(1,2)
```

```
      C(3,2)=C(1,2)
      C(3,3)=C(1,1)
      C(3,4)=0.
      C(4,1)=0.
      C(4,2)    =0.
      C(4,3)=0.
      RETURN
      END
      SUBROUTINE YLDFUN(S,COEFF,B,G,ALPHA,CEE,IREG)
      DIMENSION S(4),COEFF(4,4)
      DIMENSION F(4)
      DUM=.1667*((S(1)-S(2))**2+(S(2)-S(3))**2+(S(3)-S(1))**2)+S(4)**2
      DUM=SQRT(ABS(DUM))
      F(1)=(.1667*(2.*S(1)-S(2)-S(3))/DUM)-ALPHA
      F(2)=(.1667*(2.*S(2)-S(1)-S(3))/DUM)-ALPHA
      F(3)=(.1667*(2.*S(3)-S(1)-S(2))/DUM)-ALPHA
      F(4)=S(4)/DUM
C
      CALL PLAST(F(1),B,G,COEFF(1,1))
C
      RETURN
      END
      SUBROUTINE COMPUT(COEFF,STRINC,STRESS,STRSIN)
      DIMENSION COEFF(4,4),STRINC(4),STRESS(4),STRSIN(4)
   35 DO 50 I=1,4
      DUM=0.
      DO 40 J=1,4
      DUM=COEFF(I,J)*STRINC(J)+DUM
   40 CONTINUE
      STRSIN(I)=DUM
   50 CONTINUE
C
      DO 60 I=1,4
      STRESS(I)=STRESS(I)+STRSIN(I)
   60 CONTINUE
      RETURN
      END
```

```
@ ELT CANDDE,1,691121, 64671
@ EOF @
      SUBROUTINE CANDDE (B,H,N,IX,NEL,SIG,EPS,CC)
C
      COMMON/MATARG/BLK(12),SHR(12),RO(12),ALPHA(12),CELL(12),B11(12),
     1 B22(12),B33(12),U11(12),U22(12)
      COMMON/ELPLS/STRESS(4),STRAIN(4),STRINC(4),BM,G,ALPH,CEE,
     1 B1,B2,B3,U1,U2
      DIMENSION B(1),H(1),IX(250,1),BB(8),EPS(250,1),C(4,4),CC(1),
     1 SIG(250,1)
C
C     READY INCREMENTAL CORNER DISPLACEMENTS
C
      DO 100 I=1,3
      I2=I+I
      J2=2*IX(N,I)
      BB(I2-1)=B(J2-1)
      BB(I2)=B(J2)
  100 CONTINUE
      J24=2*IX(N,4)
      IF(J24 .EQ. J2) GO TO 120
      BB(7) = B(J24-1)
      BB(8) = B(J24)
      NF=8
      GO TO 140
  120 NF=6
C
C     COMPUTE INCREMENTAL STRAINS
C
  140 DO 160 I=1,3
      STRINC(I) = 0.0
  160 CONTINUE
C
      NO = N*24-32
      DO 200 I=1,3
      NO = NO+8
      DO 180 J=1,NF
      K = NO+J
      STRINC(I) = STRINC(I) + H(K)*BB(J)
  180 CONTINUE
  200 CONTINUE
      STRINC(4) = STRINC(3)
      STRINC(3) = 0.0
C
C     PREPARE TO GO TO ELPL
C
      DO 220 I=1,4
      STRESS(I) = SIG(N,I)
      STRAIN(I) = EPS(N,I)
```

```
  220 CONTINUE
      MTYPE = IX(N,5)
      BM = BLK(MTYPE)
      G = SHR(MTYPE)
      ALPH = ALPHA(MTYPE)
      CEE = CELL(MTYPE)
      B1 = B11(MTYPE)
      B2 = B22(MTYPE)
      B3 = B33(MTYPE)
      U1=U11(MTYPE)
      U2=U22(MTYPE)
C
      CALL ELPL(C,N)
C
C     STORE (C) MATRIX
C
      NO=6*(N-1)
      CC(NO+1)=C(1,1)
      CC(NO+2)=C(1,2)
      CC(NO+3)=C(1,4)
      CC(NO+4)=C(2,2)
      CC(NO+5)=C(2,4)
      CC(NO+6)=C(4,4)
C
      RETURN
C
      END
```

```
@ ELT ELPL,1,691121, 64672
@ EOF @
      SUBROUTINE ELPL (COEFF,NE)
      DIMENSION COEFF(4,4),DS(4),DE(4),STROLD(4),STRSIN(4)
      COMMON/ELPLS/STRESS(4),STRAIN(4),STRINC(4),
     1B0,G,ALPHA,CEE,B1,B2,B3,U1,U2
      IREG=1
      DO 1 I=1,4
      STROLD(I)=STRESS(I)
    1 CONTINUE
      CALL ELFUN(B,G,B1,B2,B3,U1,U2,STRAIN(1),NE,B0)
      CALL ELAST(B,G,COEFF(1,1))
      CALL COMPUT(COEFF(1,1),STRINC(1),STRESS(1),STRSIN(1))
      CALL TSTYLD(IREG,STRESS(1),1,ALPHA,CEE)
      IF(IREG.EQ.1) GO TO 30
      DO 20 I=1,4
      STRESS(I)=STRESS(I)-STRSIN(I)
   20 CONTINUE
      CALL YLDFUN(STRESS(1),COEFF(1,1),B,G,ALPHA,CEE,IREG)
      CALL COMPUT(COEFF(1,1),STRINC(1),STRESS(1),STRSIN(1))
C    THIS CALL TO TSTYLD ADJUSTS THE DEVIATORS SO THAT STRESS EX ACTLY
C   SATISFIES THE YIELD CONDITION
C
      CALL TSTYLD(IREG,STRESS(1),2,ALPHA,CEE)
      IF (IREG.EQ.1) CALL ELAST(B,G,COEFF(1,1))
   30 CONTINUE
      DO 40 I=1,4
      DS(I)=STRESS(I)-STROLD(I)
   40 CONTINUE
C
      DP=(DS(1)+DS(2)+DS(3))*.33333
C
      DO 50 I=1,3
      DE(I)=(.3333*DP/B)+(.5*(DS(I)-DP)/G)
      STRAIN(I)=STRAIN(I)+DE(I)
   50 CONTINUE
      STRAIN(4)=STRAIN(4) + (DS(4)/G)
      END
```

```
@ ELT TSTYLD,1,691121, 64673
@ EOF @
      SUBROUTINE TSTYLD(IREG,STRESS,I,ALPHA,CEE)
      DIMENSION STRESS(4)
C
C
      S1=STRESS(1)
      S2=STRESS(2)
      S3=STRESS(3)
      S4=STRESS(4)
C
C
      DUM1=.1667*((S1-S2)**2+(S2-S3)**2+(S3-S1)**2)+S4*S4
      DUM2=S1+S2+S3
      DUM1=SQRT(DUM1)
      P=ABS(DUM2/3.)
   40 CONTINUE
      IF(I.EQ.2)GO TO 20
      F=DUM1-0.95*(ALPHA*DUM2+CEE)
      IF(F.LE.0.)GO TO 10
C
C  PLASTIC DEFORMATION
C
      IREG=2
      IF(I.EQ.1) RETURN
C   STRESS HAS PROPERLY BEEN COMPUTED BY YLDFUN
   20 DMAX=DUM2
      IF(ALPHA.EQ.0.0)GO TO 50
      DD=-.95*CEE/ALPHA
      IF(DUM2.LT.DD) GO TO 50
      DMAX=DD
      IREG=1
   50 FACTOR=0.
      IF(DUM1.NE.0.)FACTOR=ABS(ALPHA*DMAX+CEE)/DUM1
      IF(FACTOR.EQ.0.) IREG=1
      DO 30 J=1,3
   30 STRESS(J)=(STRESS(J)-DUM2/3.)*FACTOR+DMAX/3.
      STRESS(4)=STRESS(4)*FACTOR
      RETURN
   10 IREG=1
      RETURN
      END
```

```
@ ELT PLAST,1,691121, 64674
@ EOF @
      SUBROUTINE PLAST(F,B,G,C)
      DIMENSION F(4),C(4,4)
      F1=F(1)
      F2=F(2)
      F3=F(3)
      F4=F(4)
C
C  LAME S PARAMETER
      X=B-.667*G
C
C
      FF=F1 + F2 + F3
      S=F1*F1 + F2*F2 + F3*F3 + 2.*F4*F4
      D=X*FF*FF + 2.*G*S
      A1=X*FF+2.*G*F1
      A2=X*FF+ 2.*G*F2
      A3= X*FF+ 2.*G*F3
C
      C(1,1)= (X+2.*G) -(A1*A1/D)
      C(1,2) = X-(A1*A2/D)
      C(1,3) = X-(A1*A3/D)
      C(1,4) = -2.*G*F4*A1/D
C
      C(2,2) = X+2.*G-(A2*A2/D)
      C(2,3) = X-(A2*A3/D)
      C(2,4) = -2.*G*F4*A2/D
C
      C(3,3) = X+2.*G-(A3*A3/D)
      C(3,4) = -2.*G*F4*A3/D
C
      C(4,4) = G-(4.*G*G*F4*F4/D)
C
      C(2,1)=C(1,2)
      C(3,1)=C(1,3)
      C(3,2)=C(2,3)
      C(4,1) =C(1,4)
      C(4,2)=C(2,4)
      C(4,3)=C(3,4)
   20 RETURN
      END
```

APPENDIX I

EXAMPLE OF COMPLETE ANALYSIS--CASE 5

In Case 5, the soil is represented as being homogeneous with C_p = 2500 fps and C_s = 1440 fps, as illustrated in Figure I-1. The structure is the same as is used in Cases 3 and 4. The input is the first four seconds of the east-west Golden Gate record. One calculation with a structure and one calculation of free field response were performed.

The main results of the calculation are shown in Tables I-1 and I-2 in terms of acceleration spectra in the free field and at the foundation. Pseudo-velocity spectra for the same points are shown in Figures I-2 and I-3. The spectra of the foundation lie below those of the free field in the horizontal direction, and mainly above the free field in the vertical direction. The structural spectra may be regarded as suppressed relative to the free field in the horizontal direction and partly amplified in the vertical direction. The horizontal suppression is similar to that observed in Case 3 and less that that observed in Case 4. The vertical spectra of the structure are amplified over those of the free field by a greater amount than in Cases 3 and 4. The reason for amplification in the vertical direction is presently unknown. The oscillators having transverse frequencies of 4 cps and 5 cps also have fundamental modes of vertical vibration at approximately 21 cps and 38 cps, respectively. These frequencies are too high to affect the frequency range shown in Tables I-1 and I-2.

Selected acceleration/time histories of free-field and structure foundation are shown in Figures I-4 through I-7. The angular acceleration of the base and its shock spectra are shown in Figures I-8 and I-9. There are peaks in the angular velocity spectra at 2.5 cps and at 4 cps. These are apparently related to the transverse frequencies of the oscillators. The fixed base frequencies of these oscillators are 4 cps and 5 cps within ±2 percent. However, the base of the structure is sufficiently flexible

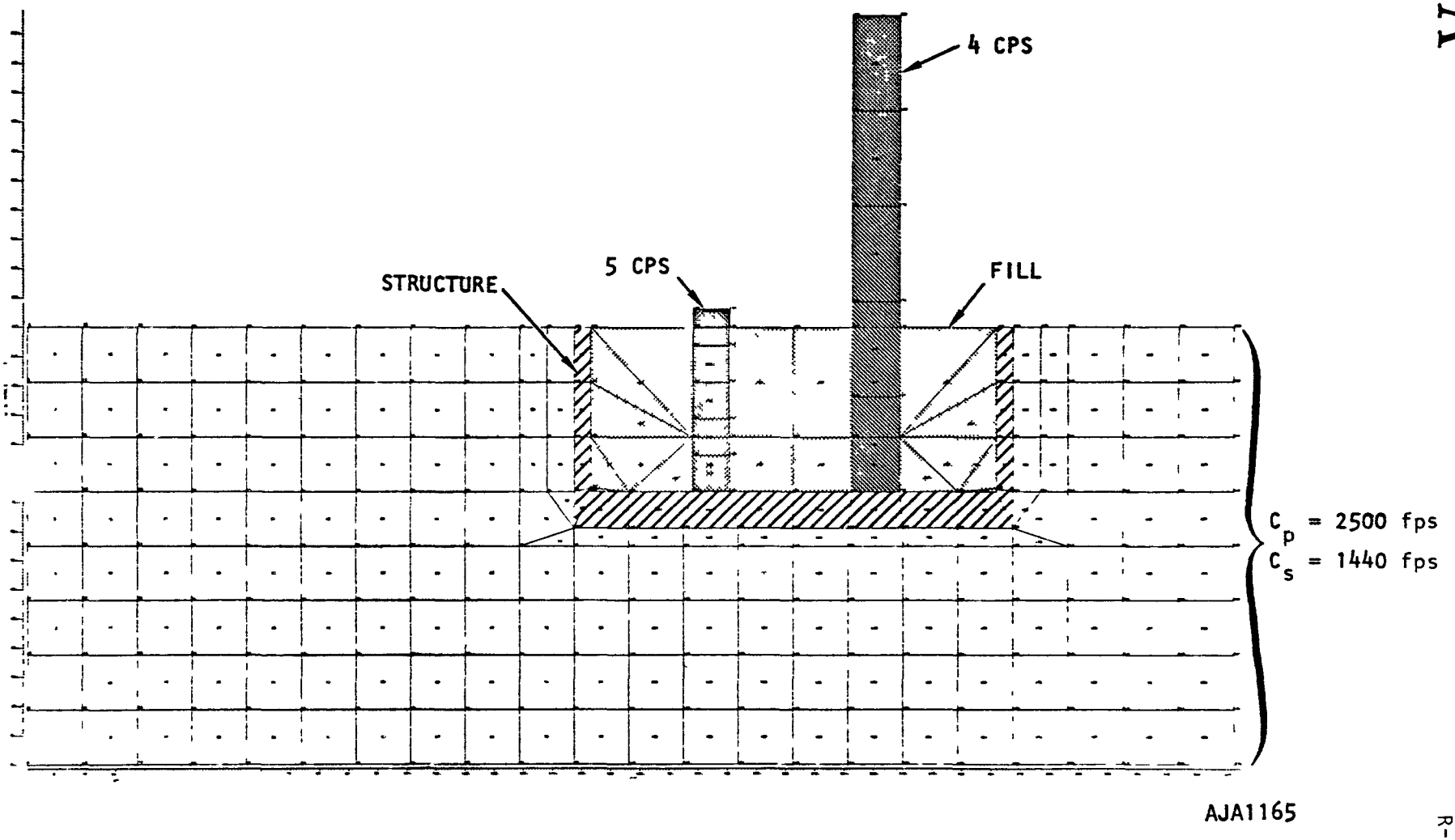

FIGURE 1-1. FINITE ELEMENT REPRESENTATION OF EMBEDDED NUCLEAR REACTOR STRUCTURE--CASE 5

TABLE I-1. SUPPRESSION OF HORIZONTAL ACCELERATION SPECTRA BY STRUCTURE--CASE 5

Horizontal Acceleration Spectra

Frequency, cps	Without Structure		With Structure	Ratio, $\frac{\text{With structure}}{\text{Without structure}}$	
	a_{140}, g	a_{144}, g	a_{150}, g	$\frac{a_{150}}{a_{144}}$	$\frac{a_{150}}{a_{140}}$
1	0.035	0.035	0.038	1.09	1.09
2	0.056	0.058	0.063	1.09	1.12
2.5	0.18	0.21	0.16	0.76	0.89
3	0.075	0.094	0.071	0.76	0.95
4	0.23	0.29	0.17	0.59	0.74
5	0.14	0.18	0.092	0.51	0.66
6	0.26	0.31	0.19	0.61	0.73
8	0.33	0.37	0.32	0.84	0.97
10	0.20	0.28	0.14	0.50	0.7

Subscripts refer to nodal point numbers

Case	Node	Depth Below Surface
Without structure	140	55 ft
Without structure	144	0 ft
With structure	150	55 ft

TABLE I-2. SUPPRESSION OF VERTICAL ACCELERATION SPECTRA BY STRUCTURE--CASE 5

Vertical Acceleration Spectra

Frequency, cps	Without Structure		With Structure	Ratio, $\frac{\text{With structure}}{\text{Without structure}}$	
	a_{140}, g	a_{144}, g	a_{150}, g	$\frac{a_{150}}{a_{144}}$	$\frac{a_{150}}{a_{140}}$
1	0.017	0.016	0.017	1.06	1.00
2	0.027	0.024	0.040	1.67	1.48
2.5	0.088	0.071	0.11	1.55	1.25
3	0.041	0.030	0.039	1.30	0.95
4	0.093	0.049	0.045	0.92	0.48
5	0.054	0.025	0.036	1.44	0.67
6	0.067	0.064	0.066	1.03	0.99
8	0.053	0.12	0.075	0.62	1.41
10	0.063	0.12	0.035	0.29	0.56

Subscripts refer to nodal point numbers

Case	Node	Depth Below Surface
Without structure	140	55 ft
Without structure	144	0 ft
With structure	150	55 ft

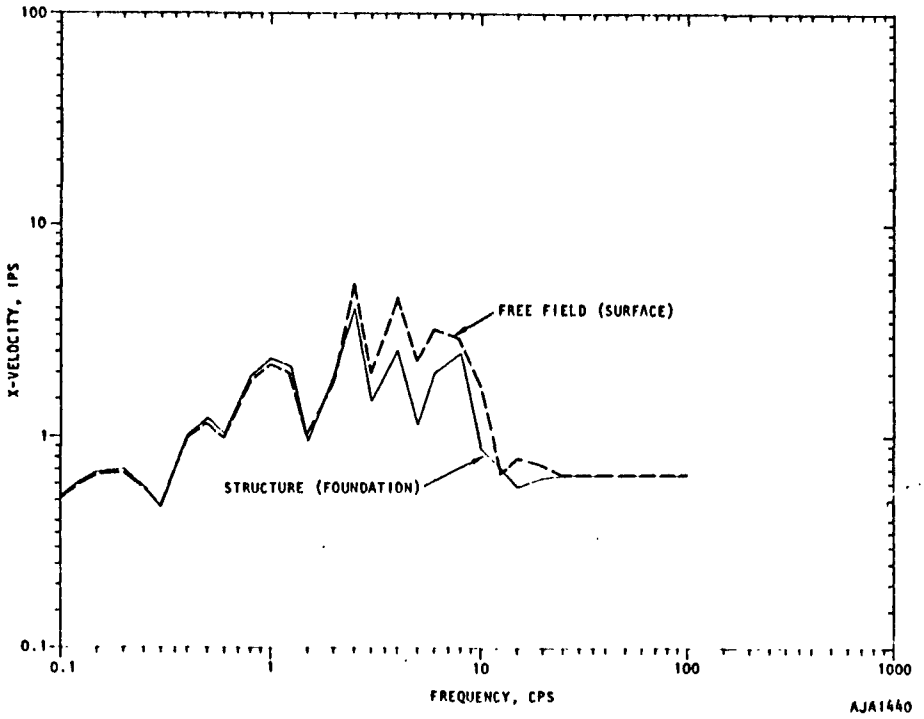

FIGURE I-2. HORIZONTAL SPECTRA, CASE 5

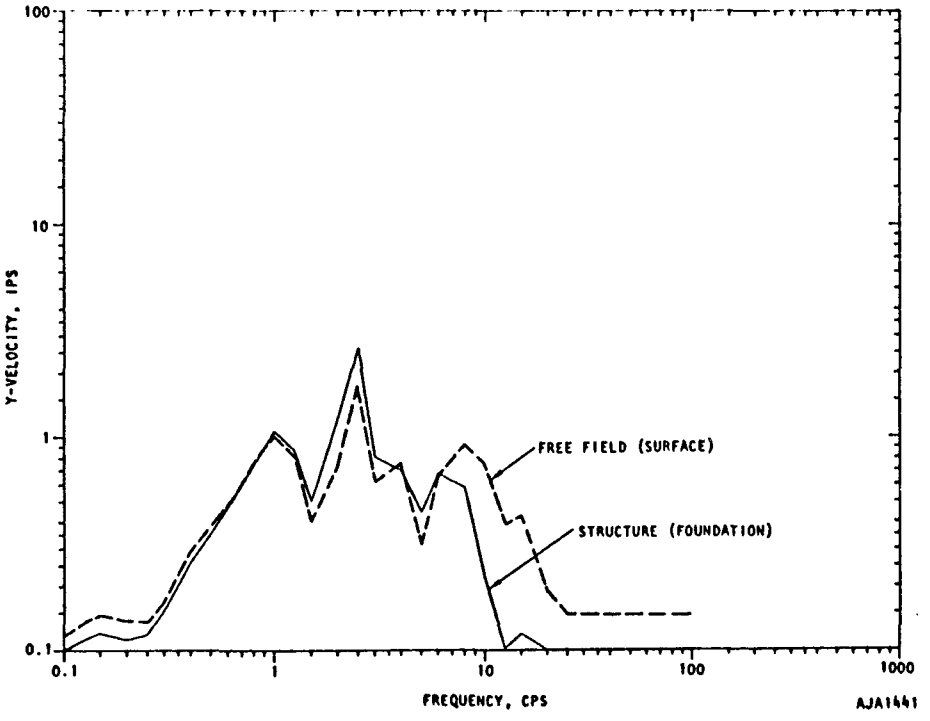

FIGURE I-3. VERTICAL SPECTRA, CASE 5

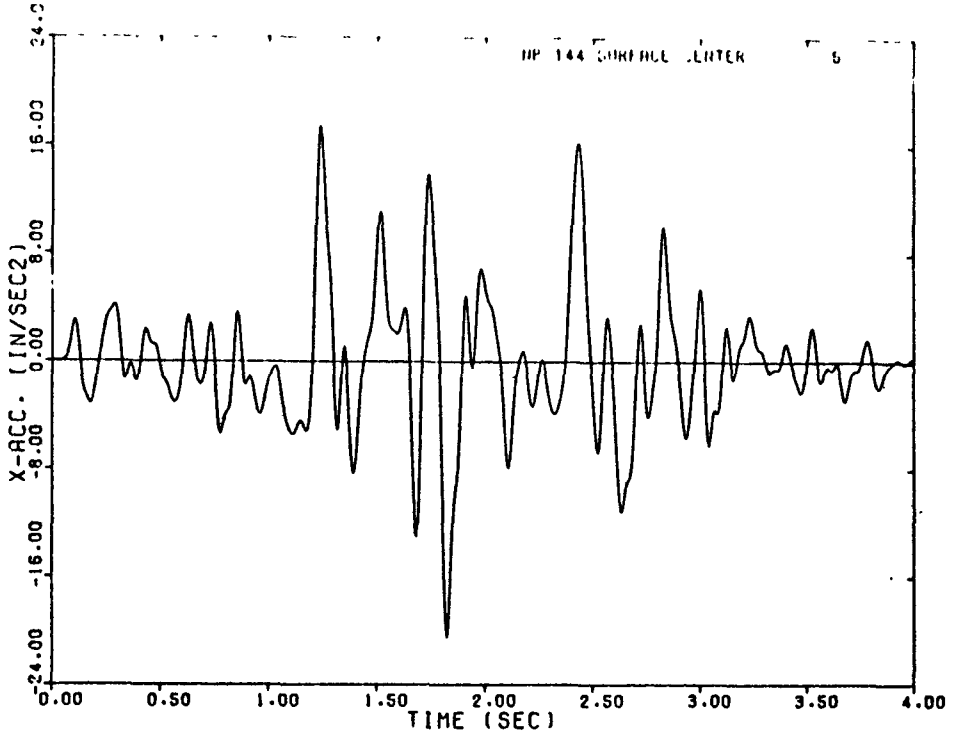

FIGURE I-4. HORIZONTAL ACCELERATION OF FREE-FIELD SURFACE

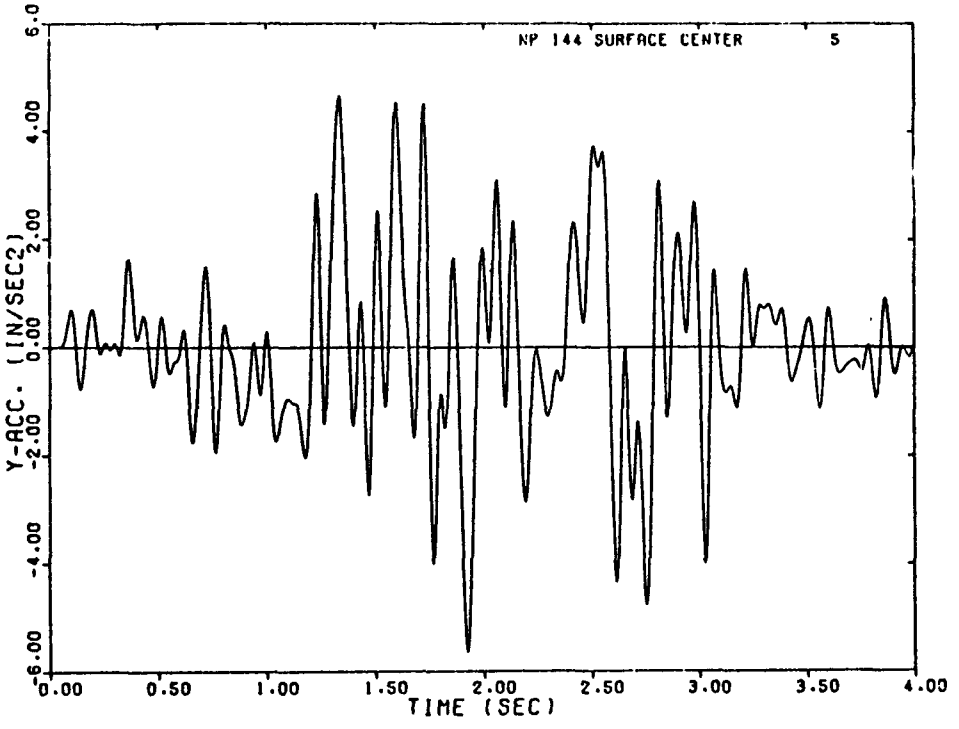

FIGURE I-5. VERTICAL ACCELERATION OF FREE-FIELD SURFACE

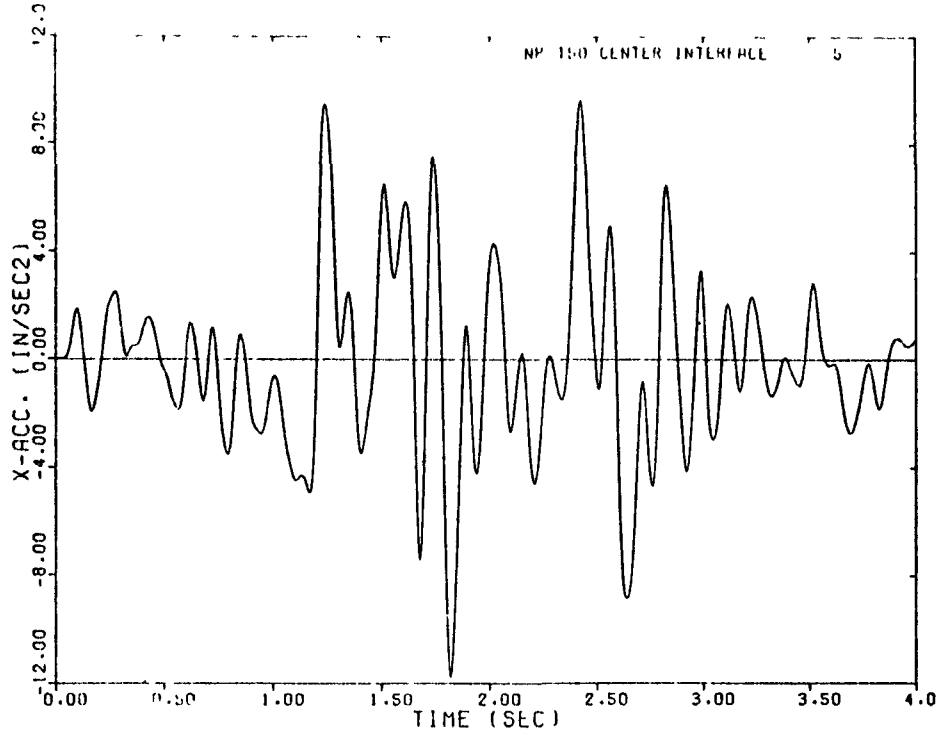

FIGURE I-6. HORIZONTAL ACCELERATION OF STRUCTURE FOUNDATION

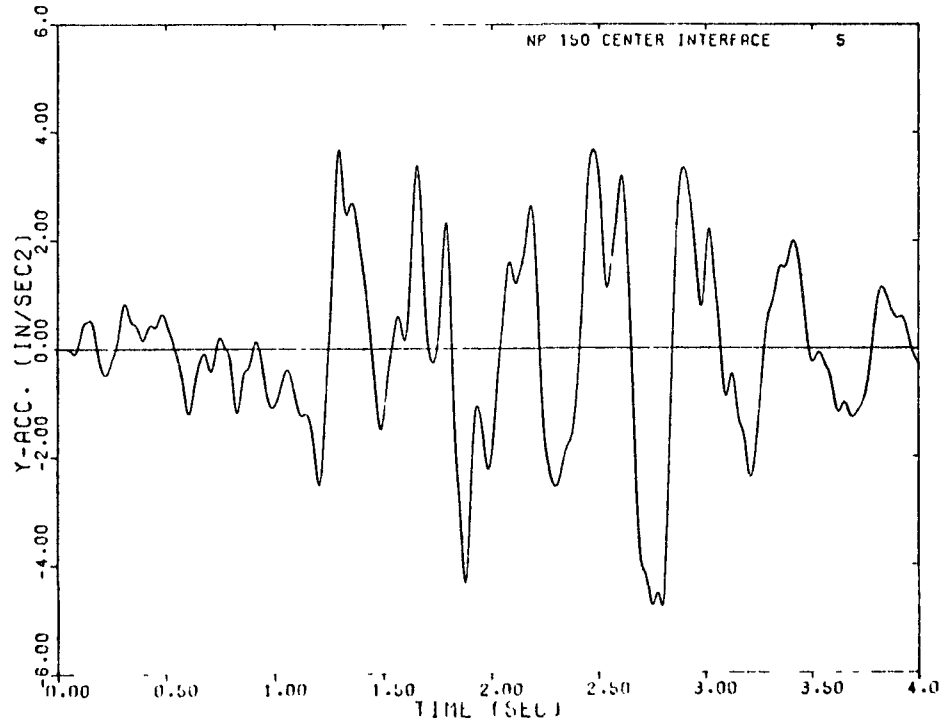

FIGURE I-7. VERTICAL ACCELERATION OF STRUCTURE FOUNDATION

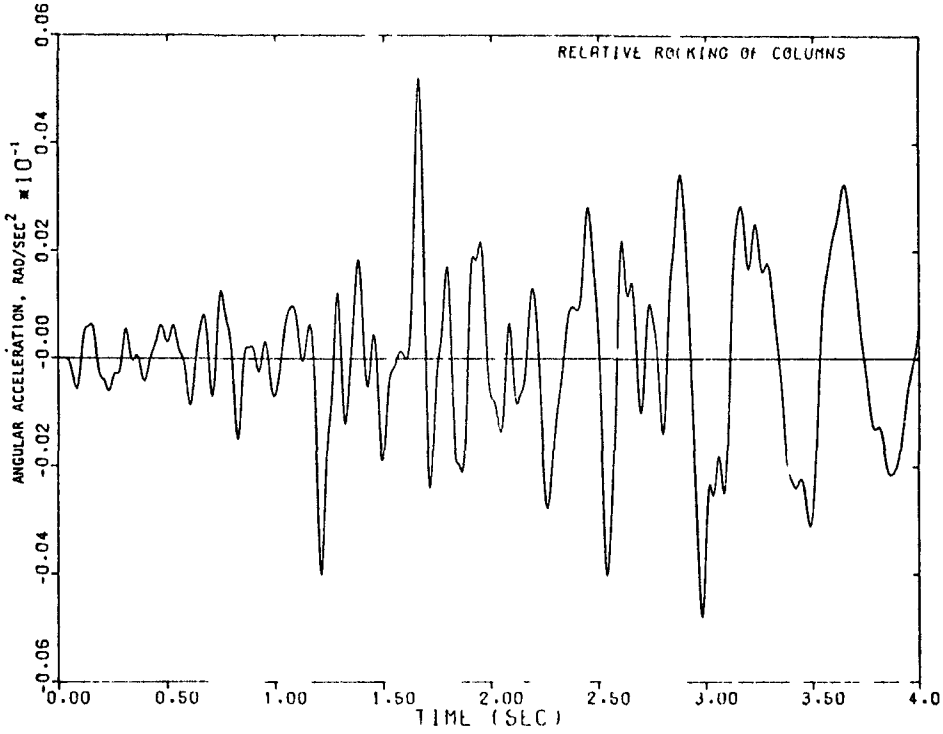

FIGURE I-8. ANGULAR ACCELERATION OF STRUCTURE BASE

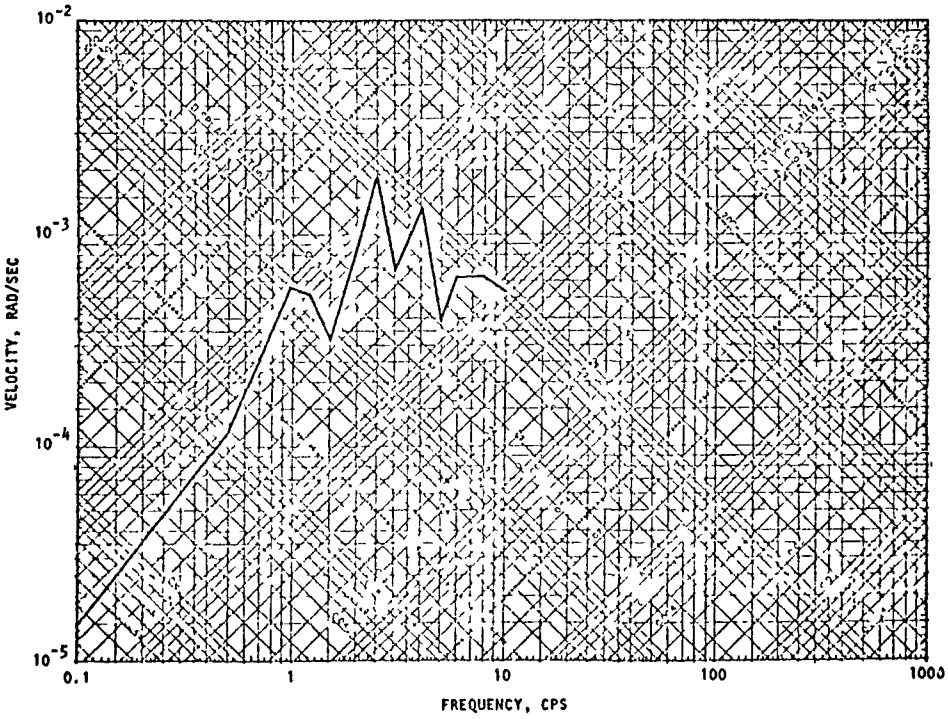

FIGURE I-9. ANGULAR VELOCITY SPECTRA FOR BASE OF STRUCTURE

that, under dynamic response conditions the natural frequencies are reduced to about 2.5 cps and 4 cps, respectively. This is illustrated in Figures I-10 and I-11, which show the oscillators vibrating at frequencies close to the natural ones for the conditions of fixity used in the calculations.

The stress/time histories in Figures I-12 through I-17 are for a point directly below the center of the foundation and for the corresponding point in the free field. The structure suppresses horizontal stresses and increases vertical stresses relative to the free field values. The stresses are predominatly tensile (positive in present sign convention).

Comparison of vertical and horizontal free-field shock spectra from Cases 3, 4 and 5 indicates the relative responses for hard, soft and layered sites. Figures I-18 through I-21 show the spectra from the three types of sites at the surface and at 55 ft depth, equal to the depth of the foundation. The most remarkable feature of these spectra is in Figure I-19, where the vertical spectra of the layered site is greatly amplified while that of the hard site is slightly depressed at 5 to 6 cps. The reason for this behavior is presently under study. That it is related to the interface between hard and soft layers is more clearly shown in Figures I-22 through I-24, where the vertical spectra from each case at two different depths are plotted on the same graph. Cases 3 and 5 (homogeneous) are similar, but there is a remarkable amplification in Case 4 (layered) between the interface at 55 ft and the surface.

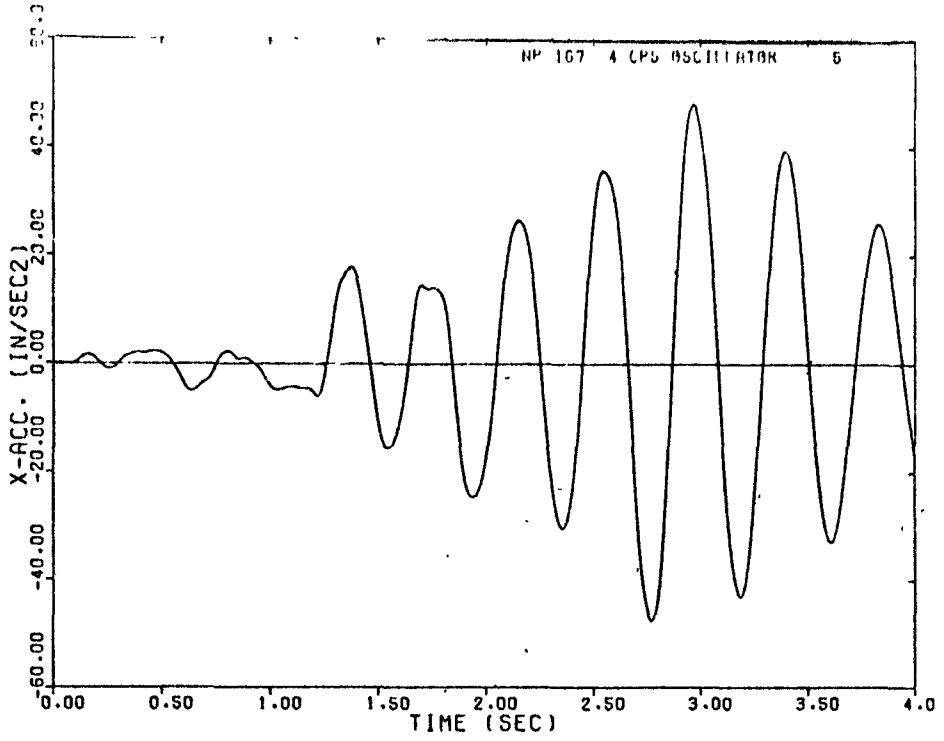

FIGURE I-10. TRANSVERSE ACCELERATION OF 4-CPS OSCILLATOR

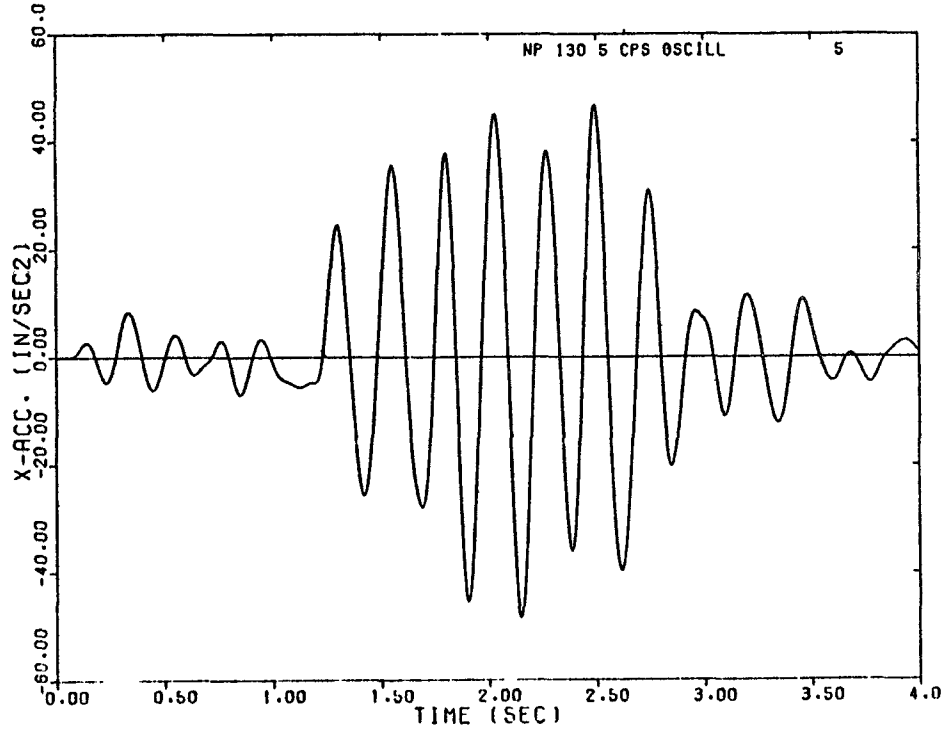

FIGURE I-11. TRANSVERSE ACCELERATION OF 5-CPS OSCILLATOR

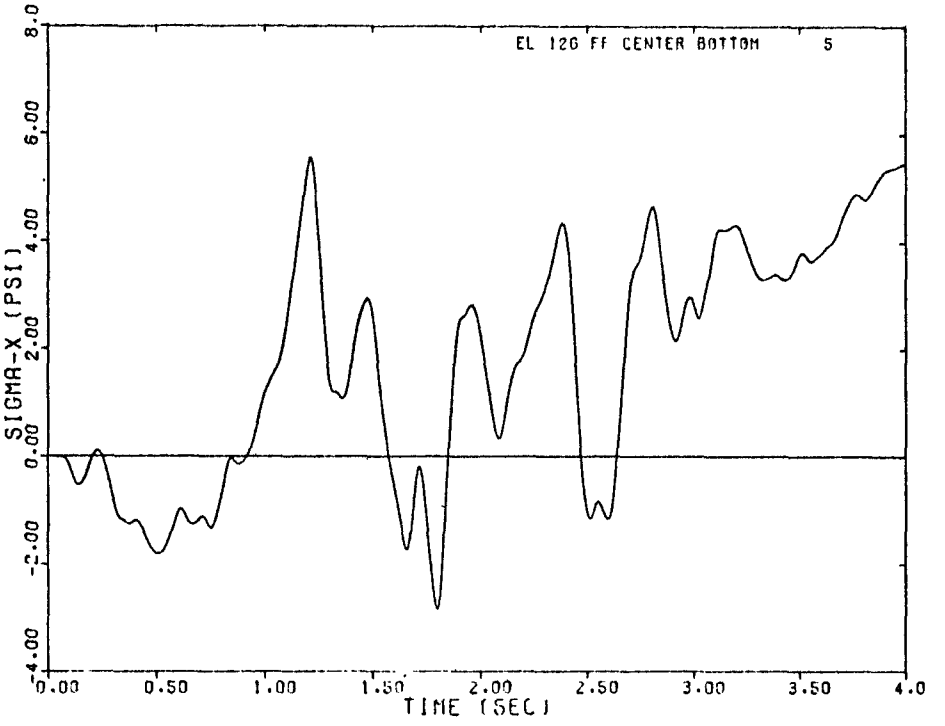

FIGURE I-12. HORIZONTAL STRESS IN FREE FIELD

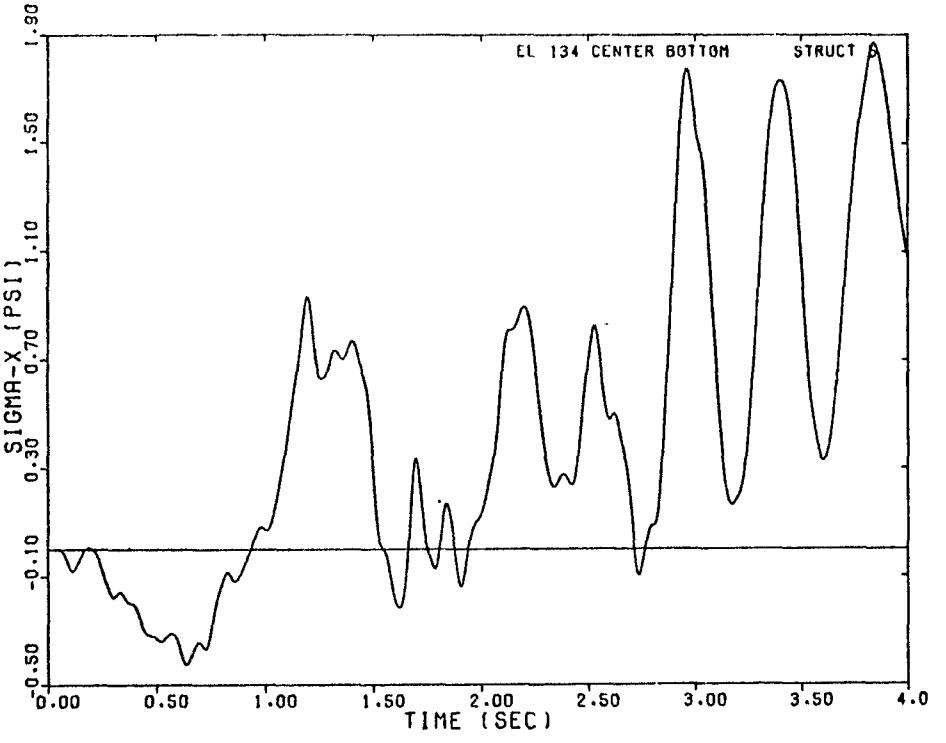

FIGURE I-13. HORIZONTAL STRESS BENEATH FOUNDATION

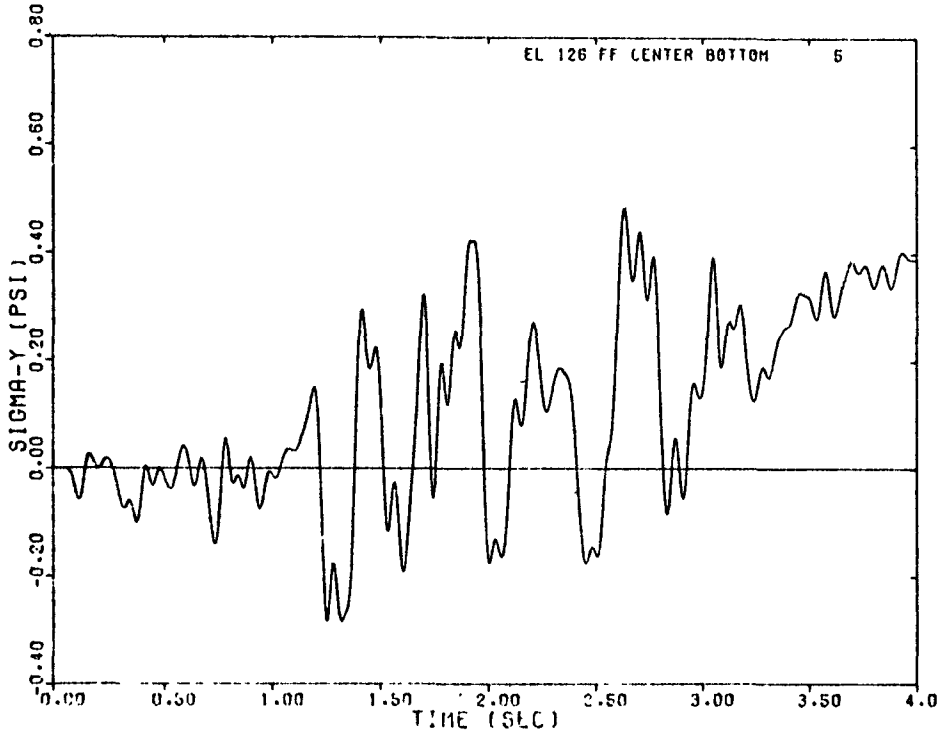

FIGURE I-14. VERTICAL STRESS IN FREE FIELD

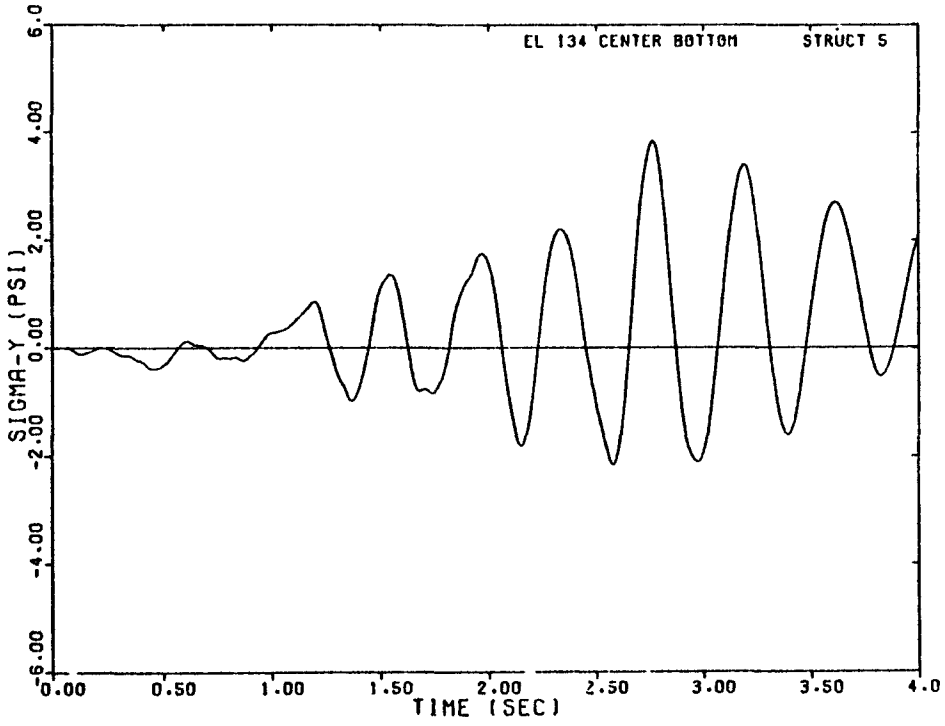

FIGURE I-15. VERTICAL STRESS BENEATH FOUNDATION

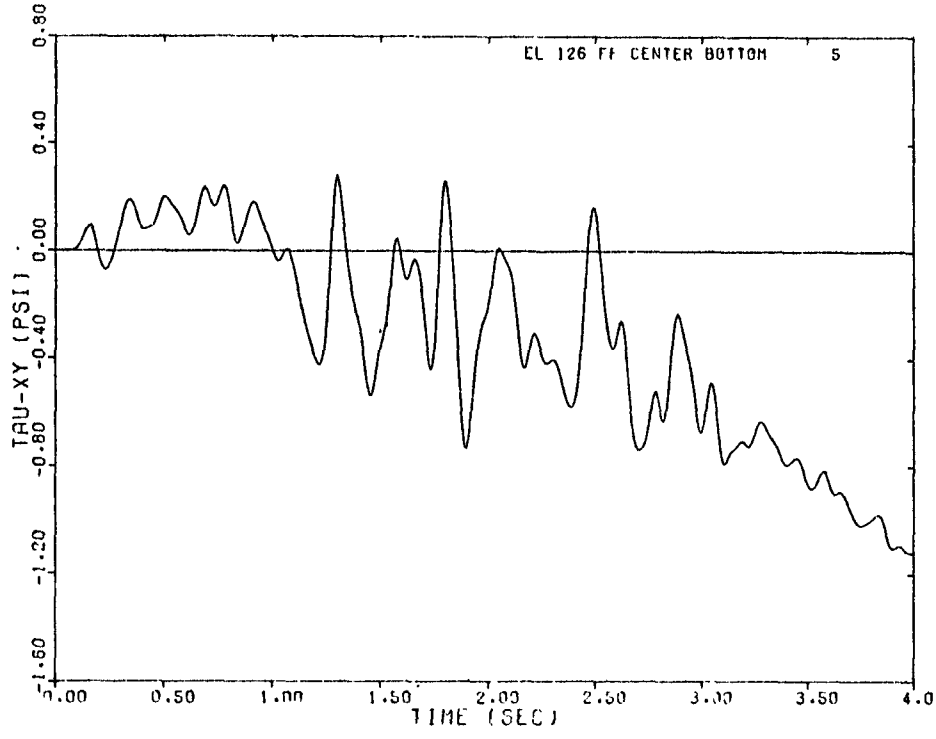

FIGURE I-16. SHEAR STRESS IN FREE FIELD

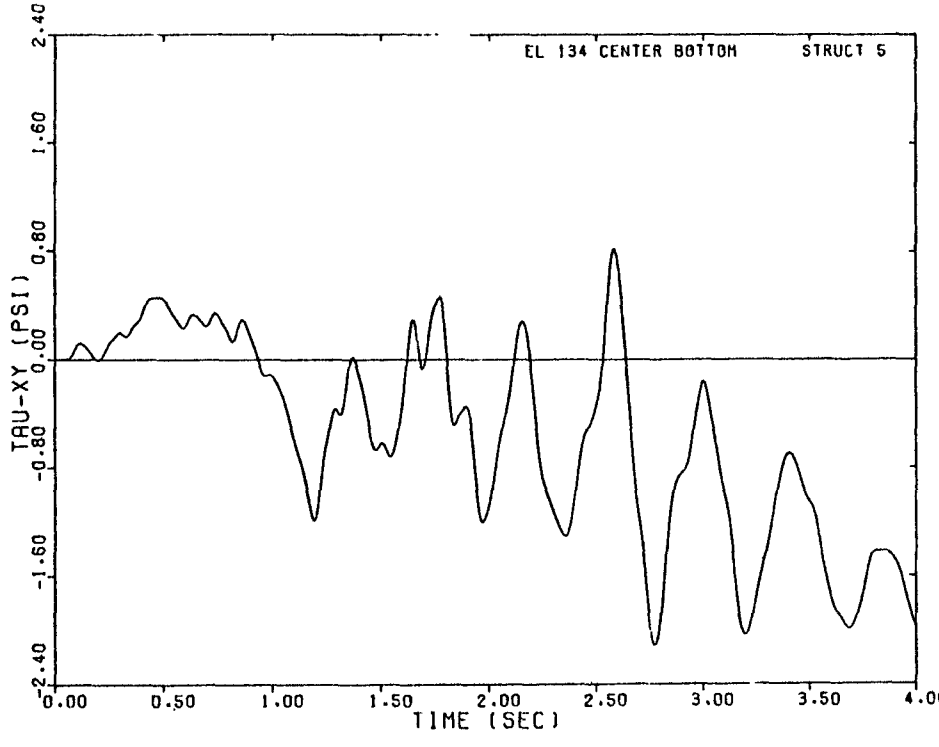

FIGURE I-17. SHEAR STRESS BENEATH FOUNDATION

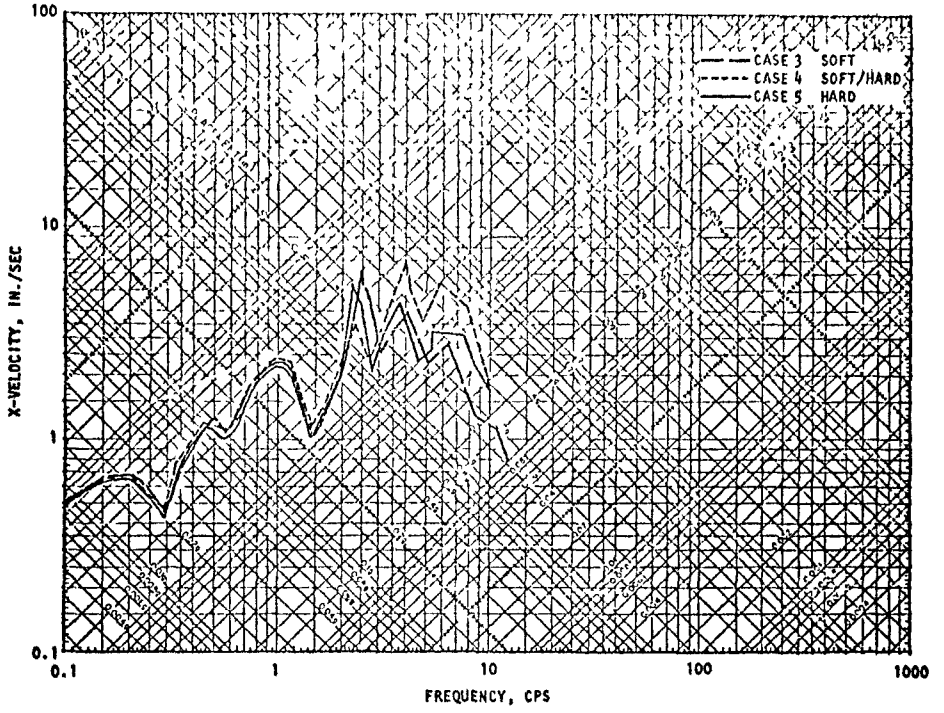

FIGURE I-18. HORIZONTAL SPECTRA AT SURFACE OF THREE SITES

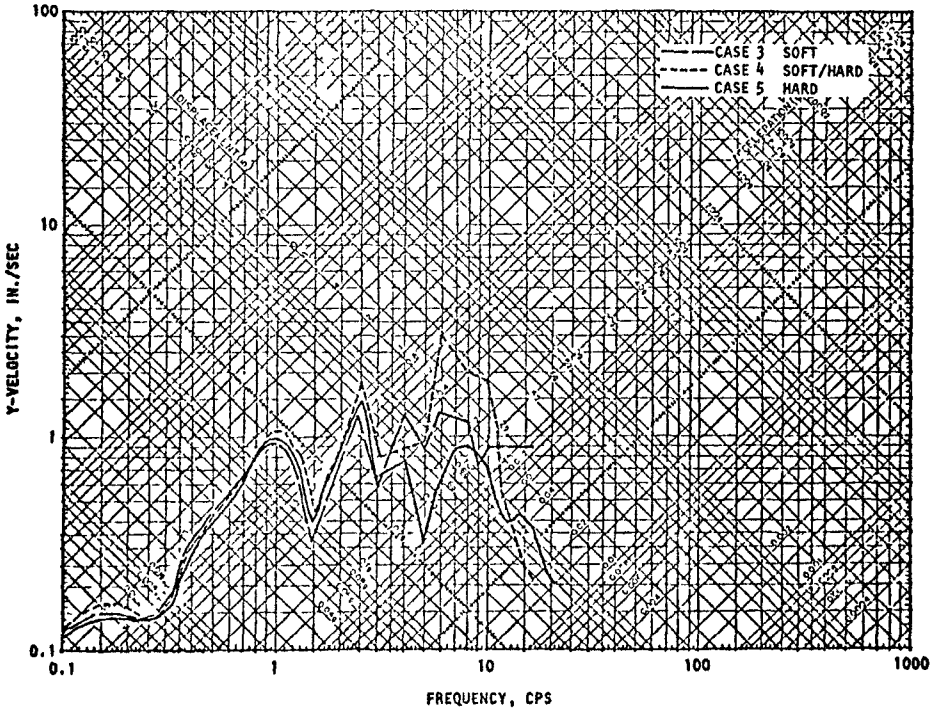

FIGURE I-19. VERTICAL SPECTRA AT SURFACE OF THREE SITES

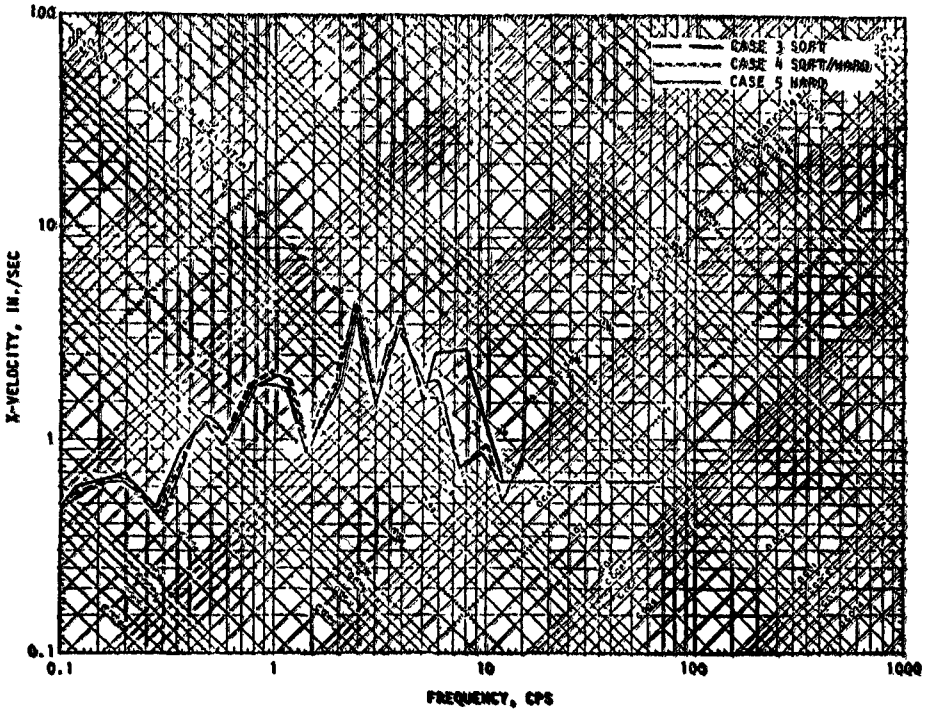

FIGURE I-20. HORIZONTAL SPECTRA AT 55-FT DEPTH OF THREE SITES

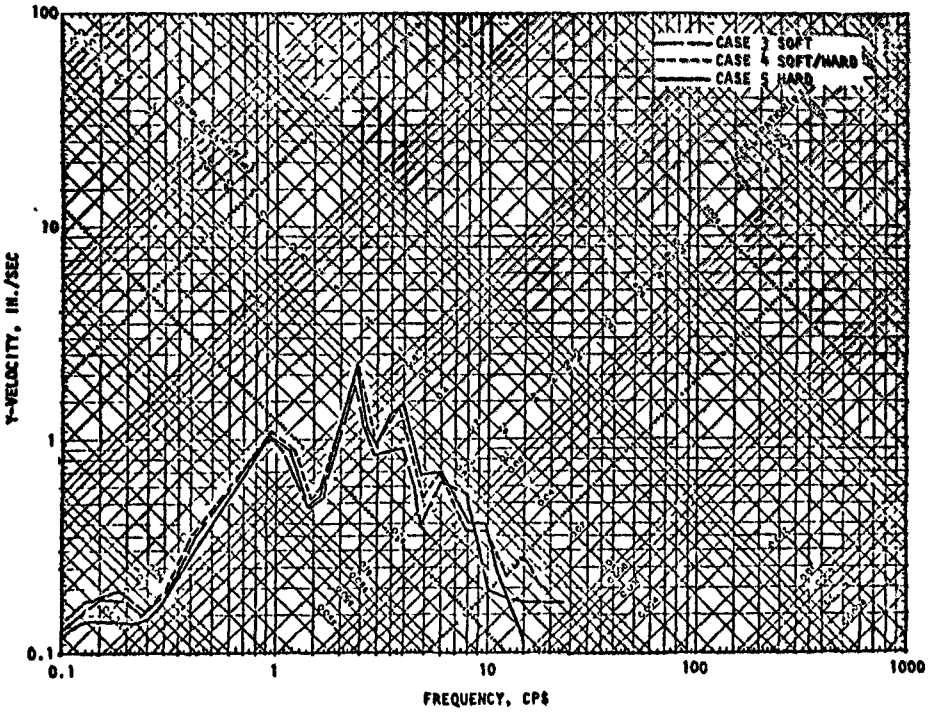

FIGURE I-21. VERTICAL SPECTRA AT 55-FT DEPTH OF THREE SITES

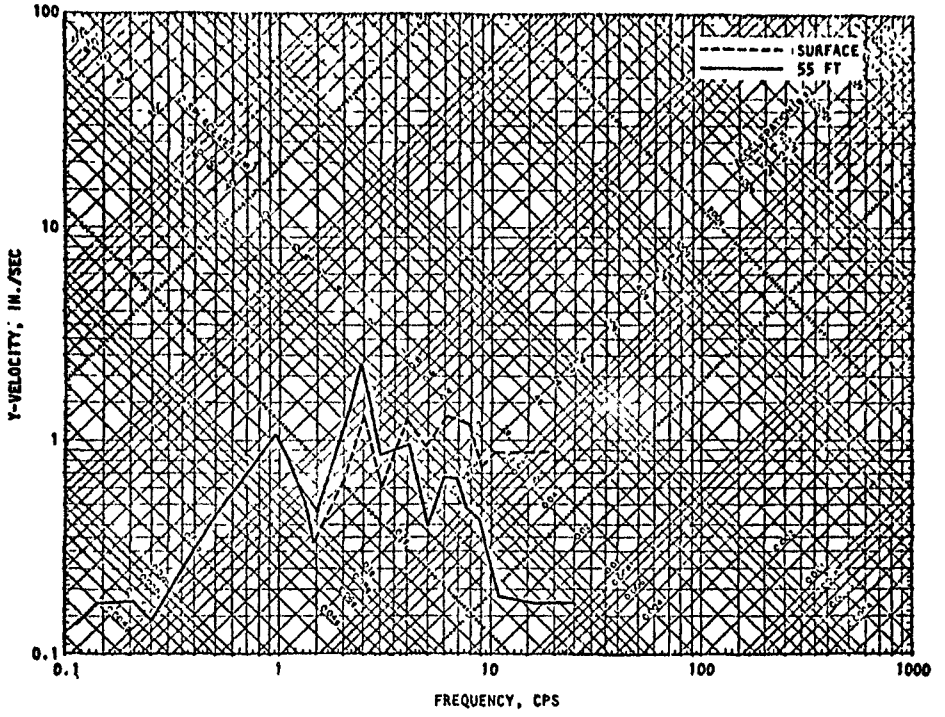

FIGURE I-22. VERTICAL SPECTRA, SOFT SITE, CASE 3

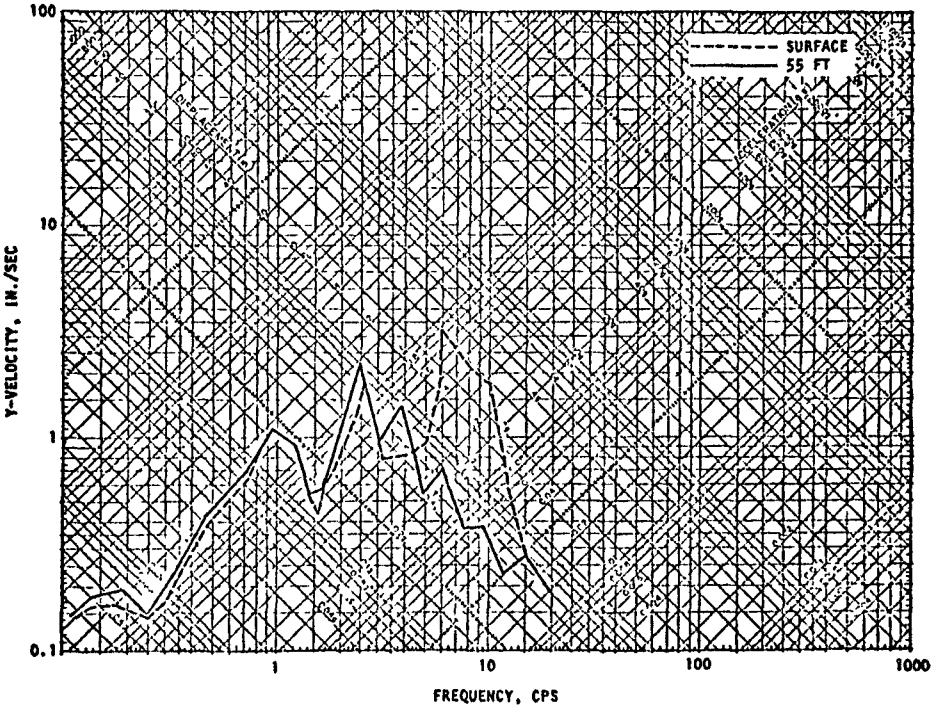

FIGURE I-23. VERTICAL SPECTRA LAYERED SITE, CASE 4

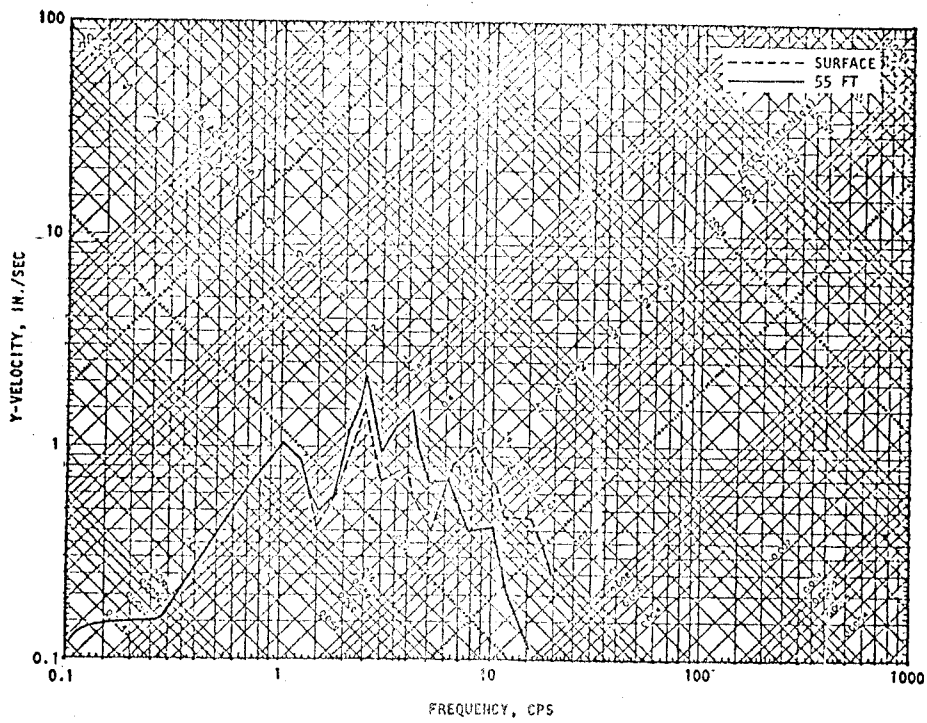

FIGURE I-24. VERTICAL SPECTRA HARD SITE, CASE 5